Safety Report

15-Foot Bubble Chamber

15-Foot Bubble Chamber

Safety Report

July 1972

Volume 1

National Accelerator Laboratory
Batavia, Illinois

Safety report 1, 15-foot bubble chamber, July 1972.

Operated by Universities Research Association Inc.
Under Contract of the United States Atomic Energy Commission

TABLE OF CONTENTS

VOL. I

	Title	Page
I.	INTRODUCTION	1
II.	RESPONSIBILITIES	1
III.	SAFETY CRITERIA	2
IV.	EQUIPMENT	
	A. Special Report by Battelle Memorial Institute on Stress Analysis of the 15-Foot Vacuum Tank	6
	B. Failure Mode Analysis: LARGE RUPTURE OF THE BUBBLE CHAMBER WITH SPILLAGE OF LIQUID INTO THE VACUUM VESSEL	48
	C. Chamber Vessel	
	1. User's Design Specification	60
	2. Special Report by Battelle Memorial Institute on Stress Analysis of the 30,000 Liter Bubble Chamber	95
	Chicago Bridge & Iron Company Review of Battelle Stress Report, and Certification	226
	3. National Accelerator Laboratory Specification for Stainless Steel Weldment for the NAL 30,000 Liter Hydrogen Bubble Chamber	230
	4. Chicago Bridge & Iron Company Quality Assurance Program	244
	5. Report of Inspection Trip to Fabricator's Plant	294
	6. Special Report by Battelle Memorial Institute on Charpy Impact Testing	298
	7. Chemical Analysis of Component Parts	313
	D. Failure Mode Analysis: CHAMBER AND CHAMBER PIPING	316

LIST OF DRAWINGS

VOL. I

2627.ME-25002	Vacuum Chamber - Lower Half
2621.ME-25134	30 K Liter Hydrogen Bubble Chamber Bubble Chamber/Chamber Head
2621.ME-25305	30 K Liter Hydrogen Bubble Chamber Beam Window Assembly
2621.ME-25486	30 K Liter Hydrogen Bubble Chamber Chamber Support Assembly
2621.ME-25172	30 K Liter Hydrogen Bubble Chamber Stainless Steel Weldment/Chamber
2625.MD-33445	Vacuum Sphere 12" Vent Stack & 18" Manway

TABLE OF CONTENTS

VOL. II

Title

IV. EQUIPMENT (Cont'd)

E. Expansion System Actuator

F. Failure Mode Analysis: EXPANSION SYSTEM ACTUATOR

G. Piston and Seals

1. Design

2. A Detailed Stress Analysis of NAL Chamber Expansion Piston Assembly by Battelle Memorial Institute

3. Stress Analysis Report on Chamber Expansion Piston for NAL 30,000 Liter Hydrogen Bubble Chamber by Brunswick Corporation

H. Failure Mode Analysis: PISTON AND SEALS

I. Optics

J. Failure Mode Analysis: OPTICS

K. Magnet

1. Superconducting Magnet for the 15-foot NAL Bubble Chamber - Design Report

2. Investigation of the Stability and Quench Characteristics of the Conductor for the NAL Bubble Chamber Magnet/Summary of Calculations

3. Voids in Solder Bond

4. Magnetic and Thermal Stresses in the Windings/ Summary of Calculations

5. Status Reports

L. Failure Mode Analysis: MAGNET

M. Main Vacuum

TABLE OF CONTENTS

VOL. III

Title

V. CRYOGENIC SYSTEMS

A. Hydrogen System

B. Cooling Loops

C. Failure Mode Analysis: HYDROGEN SYSTEM FOR A SINGLE FAILURE

D. Failure Mode Analysis: HYDROGEN SYSTEM FOR TWO UNRELATED FAILURES

E. Helium System

F. Failure Mode Analysis: HELIUM SYSTEM

G. Vent System

H. Chamber Warm-Up

VI. INSTRUMENTATION

A. Source Failure Provisions - Pneumatic, Electrical

B. Device Instrumentation

C. Process Instrumentation

D. Interlocked Instrumentation

VII. MISCELLANEOUS

A. Tests

1. Vacuum Tank
2. Chamber
3. Magnet Vacuum
4. Magnet Cryostat
5. Optics
6. Piston
7. Piston Seals
8. Liquid H_2 Pump
9. Piping
10. High Pressure Gas Storage

TABLE OF CONTENTS

VOL. III (Cont'd)

Title

VII. MISCELLANEOUS (Cont'd)

A. Tests (Cont'd)

11. Low Pressure Gas Storage

12. Expansion System

13. Helium Refrigerator

14. Hydrogen Refrigerator

B. Operation

1. Organization of Crews

2. Training Program

3. Procedures Associated With the Magnetic Field

4. Procedures Associated With Hydrogen Areas

5. Documents Available to Crew

SAFETY REPORT
15-FOOT HYDROGEN BUBBLE CHAMBER

I. INTRODUCTION

The purpose of this document is to show that the National Accelerator Laboratory's 15-foot hydrogen bubble chamber is safe for operation. The hazards associated with the facility have been considered and provisions incorporated into the design to insure a minimum risk to equipment and operators.

This report is to be issued in two versions. The first version (Nov 1970) covers the material necessary for the final design of the buildings and facilities, as well as descriptions of all the equipment which plays an important role in the layout and arrangement of the area. Also included is a detailed stress analysis report on the 22-foot diameter vacuum tank, a failure mode analysis of a large rupture of the bubble chamber with spillage of liquid into the vacuum vessel, and a cryogenic systems safety report.

The second version, entitled "Safety Report -- July 1972", will be issued in July 1972 one month before the scheduled first hydrogen operation of the chamber in order to allow time for review.

II. RESPONSIBILITIES

Safety at the National Accelerator Laboratory is the responsibility of the Director. He relies on individual staff members who supervise the design and later the operation of the bubble chamber to follow procedures which minimize the risk of damage to laboratory property or injury of personnel. These scientists at the laboratory have available much knowledge and experience gained over the years at other acceleratory laboratories and universities, as well as in industry and at other government agencies. The bubble chamber staff has applied this information to the 15-foot hydrogen bubble chamber during it's design and in planning it's operation while at the same time assuring the Director that:

1. The organization of the work includes implementing safety requirements.

2. The buildings and facilities will in use provide an environment for the safe conduct of bubble chamber experiments.

3. Safety considerations have been incorporated from the beginning and that an independent review of the safety features has been carried out.

4. There exist multiple and/or sequential safeguards which provide for protection of life and property.

III. SAFETY CRITERIA

Efforts to make the NAL 15-foot bubble chamber complex safe are directed toward minimizing the probability that energy will be released into the environment in a manner that will cause injury to persons or equipment. The major source of energy release which must be considered here is the chemical reaction of hydrogen with oxygen. However, other sources can cause significant damage and must therefore be considered (e.g., energy stored as the result of pressure in compressible fluids and energy stored in the magnetic and electric fields). Because of the cryogenic aspects of the bubble chamber complex, additional factors become important. The environment itself, being at a relatively high temperature, is a source of thermal energy which, if permitted to enter the low temperature regions at an excessive rate, can lead to failure of low temperature components. Conversely, the draining of energy from components at ambient temperatures can degrade their characteristics and induce conditions that will cause their failure.

It is therefore convenient to consider that a safe system is obtained by preventing energy transfer from one region to another in a manner which causes damage. This is done by placing barriers or lines of defense to block or direct such transfers.

The following material in this section is aimed at defining basic safety criteria used in the chamber design.

Because of the large inventory of some of the components of the system, a rupture in various parts may release very large quantities of hydrogen or deuterium into the atmosphere or bubble chamber building. A large quantity of hydrogen more or less thoroughly mixed with air will generate a destructive pressure wave when ignited. This pressure wave will be the source of extensive damage to the facility and will cause injury or death to personnel in the area. A fundamental safety criterion to be used in the design of the system is the prevention of the release of large quantities of hydrogen or deuterium when a line of defense fails. The system is designed to limit the leakage into the chamber building or environment in accordance with:

(a) The failure of a line of defense shall not permit the introduction of more than 2 g/sec. (50 scfm) of hydrogen into the bubble chamber building or H_2 compressor room. The instantaneous rate of 2 g/sec. is the rate tolerated over an extended period of time. If time of the release is short, the criterion will be that no more than a total of 1,000 scft will be released in any single occurrence inside the bubble chamber building or H_2 compressor room.

(b) In areas outside the bubble chamber building and H_2 compressor room, the failure of a single line of defense shall not permit the release of hydrogen into the environment at a rate larger than 10 g/sec. (250 scfm) on a continuous basis. For a short duration release, the total quantity released shall not exceed 15,000 scft of hydrogen gas or equivalent.

The quantities and rates mentioned under (a) are based on the chamber building volume and anticipated rate of venting or dispersal of the gas in the building.

The quantities and rates mentioned under (b) are for areas outside buildings where adequate ventilation and dispersal of the spilled gas or liquid is available.

Other safety criteria to be used are the following:

1. Except where specified, pressure vessels and piping will be designed in accordance with either the ASME Code for Unfired Pressure Vessels, Section VIII, or the ASME Code for Nuclear Vessels, Section III, and ASA Piping Code, Section B31.3, for Petroleum Refinery Piping.

2. Relief valves will be sized to handle the maximum flow rate which may be anticipated from loss of insulation, etc. without exceeding the design limits of vessels and piping.

3. Instrumentation and other electrical equipment will be designed in accordance with procedures in effect at other bubble chamber installations.

4. The chamber vent system will be designed similar to those at other large volume bubble chambers. Other vent systems will be designed to receive the discharge from relief valves and other control valves used to discharge hydrogen to the atmosphere. These vent systems will be equipped with N_2 purge connections and weather covers.

5. The layout of the buildings and equipment is based on experience at other bubble chamber installations and the Compressed Gas Association's Standard for Liquified Hydrogen Systems at consumer sites. The three goals here are (1) limit damage to only the equipment that fails, (2) prevent escalation of a bubble chamber accident; i.e., protect other laboratory facilities, (3) protect the bubble chamber equipment from accidents that might originate in experiments in the vicinity of the bubble chamber.

6. Detailed procedures shall cover initial start-up, normal operation and maintenance, and emergency conditions. These procedures are being developed during the design phase to insure that the design accommodates all requirements and contingencies for safe operation.

7. Systematic "failure mode analysis" are made as soon as sufficient design details are available. This insures that all reasonable possibilities have been considered.

8. The chamber is to be manned by well-trained crews at a force level to insure safe operation.

9. Controls are in effect to follow the safety philosophy outlined above throughout the test and operation of the bubble chamber.

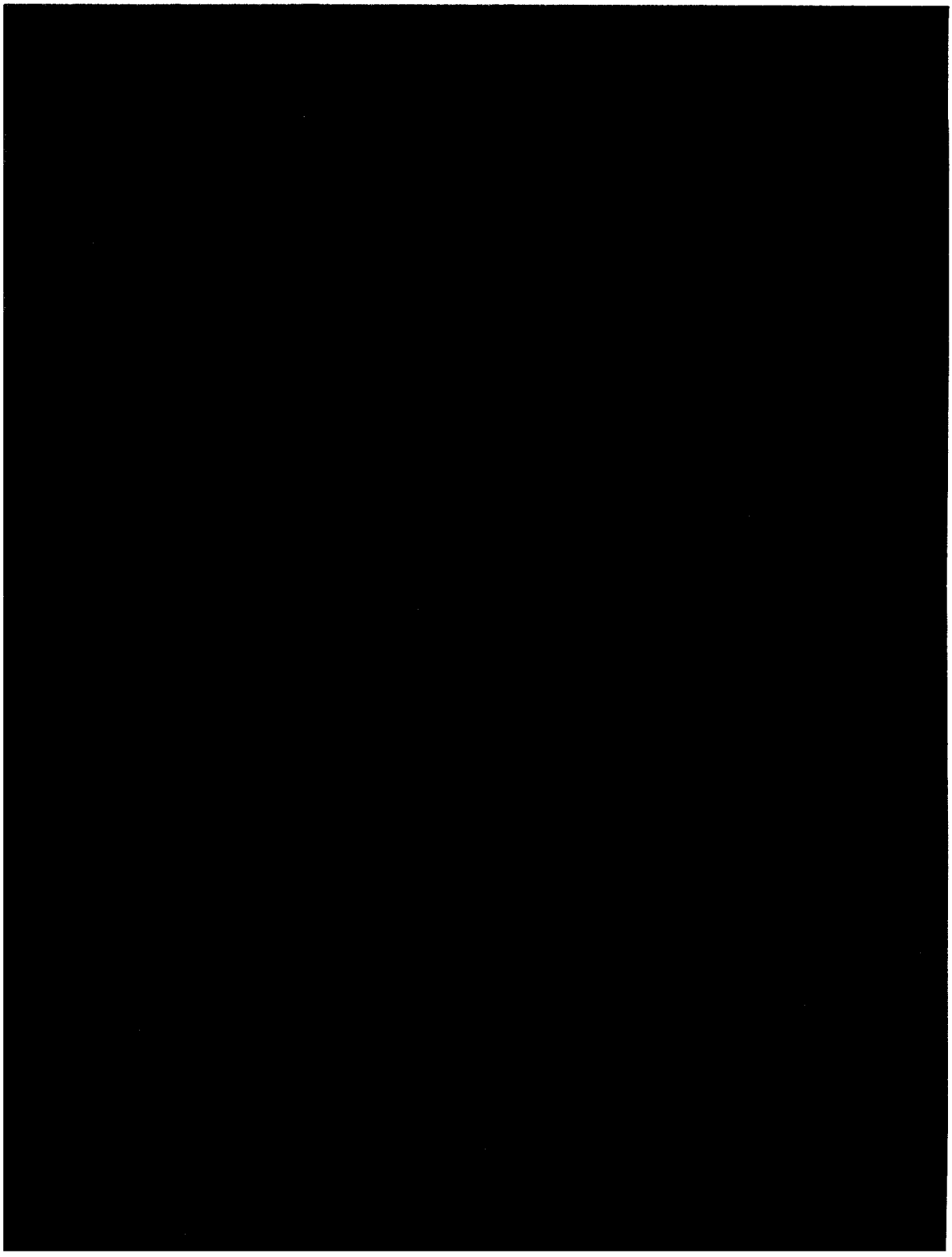

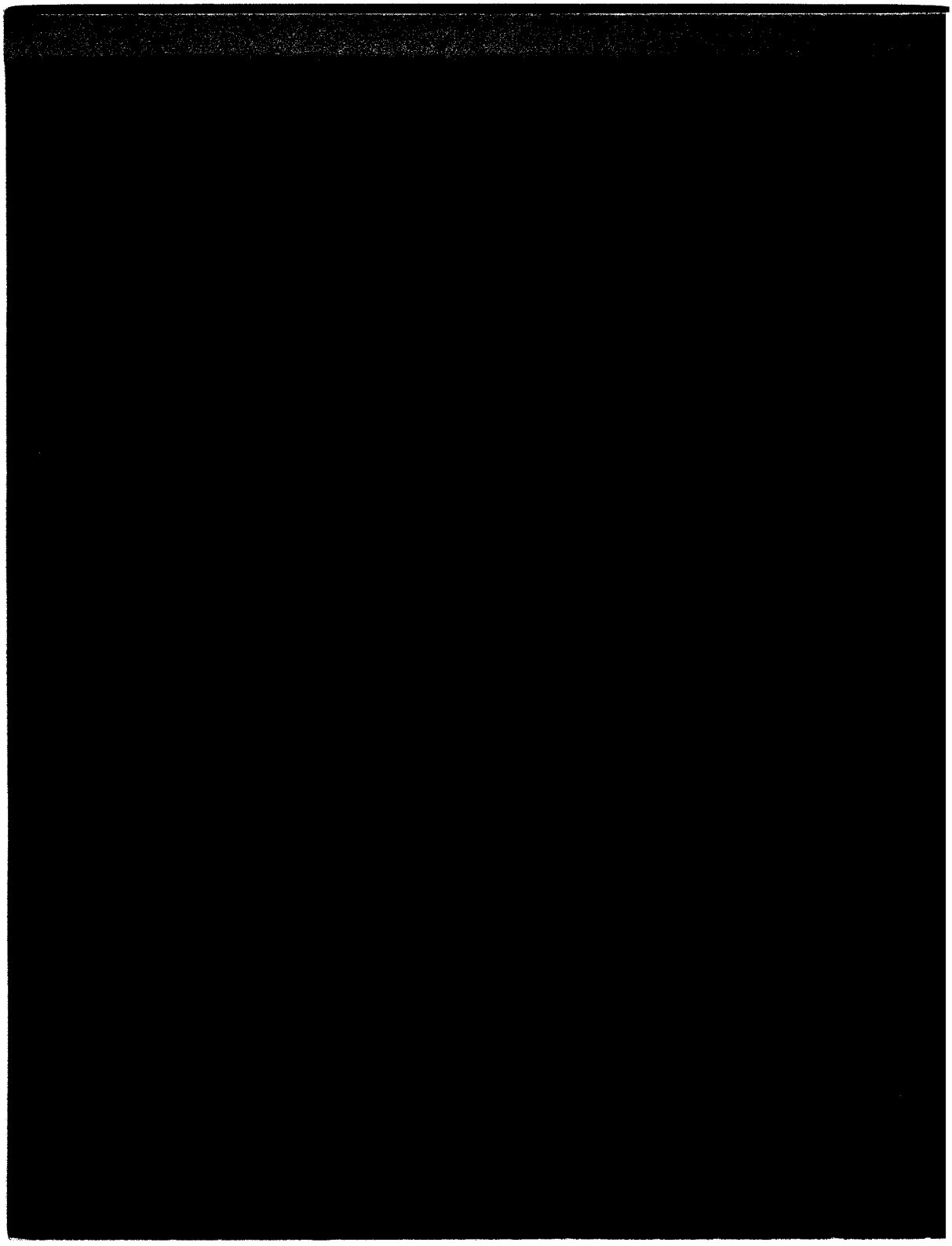

IV. EQUIPMENT

A. Special Report by Battelle Memorial Institute on Stress Analysis of the 15-foot Vacuum Tank

Prepared by

M. Vagins

TABLE OF CONTENTS

IV. EQUIPMENT		Page
A.	Special Report by Battelle Memorial Institute on Stress Analysis of the 15-Foot Vacuum Tank	
(1)	Introduction	8
(2)	Emergency-Pressure Stress Criteria	9
(3)	General Procedure	16
(4)	Conclusions and Recommendations	17
(5)	The Vacuum Tank Subjected to the Emergency-Pressure Condition	18
(6)	Welding and Inspection Requirements	41
(7)	A Check of the Adequacy of the Vacuum Tank to Sustain a Vacuum Loading	41
(8)	Appendix A-1:Beam Window Reinforcement Analysis	44

LIST OF FIGURES

FIGURE 1.	STRESS CATEGORIES AND LIMITS OF STRESS INTENSITIES	12
FIGURE 2	INITIAL GEOMETRIC MODEL FOR INPUT TO MONSA-S	10
FIGURE 3.	NOMINAL STRESS OUTPUT FOR FIRST MODEL OF VACUUM TANK	21
FIGURE 4.	NOMINAL STRESS OUTPUT FOR FINAL MODEL OF VACUUM TANK	23
FIGURE 5.	CB&I RECOMMENDED MAIN FLANGE CONFIGURATION	25
FIGURE 6.	ACCEPTABLE ALTERNATE BOTTOM FLANGE CONFIGURATION	26
FIGURE 7.	ACCEPTABLE BOTTOM MATING FLANGE CONFIGURATION	28
FIGURE 8.	PROPOSED ACCESS PORT AND MANWAY CONFIGURATION	29
FIGURE 9.	MAXIMUM STRESSES IN PROPOSED TOP ACCESS PORT CONFIGURATION	30
FIGURE 10.	CB&I PROPOSED BEAM WINDOW DESIGN	33
FIGURE 11.	MONSA-S MODEL OF MIDSPAN WINDOW POSITION	34
FIGURE 12.	CALCULATED MAXIMUM STRESSES IN CB&I PROPOSED BEAM WINDOW CONFIGURATION	35
FIGURE 13.	CALCULATED MAXIMUM STRESSES IN MODIFIED PROPOSED BEAM WINDOW CONFIGURATION	37

LIST OF FIGURES (cont'd)

Page

FIGURE 14. PROPOSED MODIFIED BEAM WINDOW DESIGN 39

LIST OF TABLES

TABLE 1. CLASSIFICATION OF STRESSES FOR SOME TYPICAL CASES 14

IV. A. A STRESS ANALYSIS OF NATIONAL ACCELERATOR LABORATORY'S PROPOSED 30,000 LITER BUBBLE CHAMBER VACUUM TANK

(1) INTRODUCTION

National Accelerator Laboratory, Bubble Chamber Group, is presently in the design stage of the building of a 30,000 liter bubble chamber complex. This chamber which will operate at cryogenic temperatures and which will undergo cyclic pressure loadings for long periods of time, is a large and highly complex structure. It is basically composed of a 22 foot diameter spherical vacuum tank and a 12-1/2 foot diameter spherical bubble chamber. The bubble chamber is presently envisioned as being supported on three sets of two adjacent legs each and is positioned within and concentric to the vacuum can. The bubble chamber, during operation will be filled with liquid hydrogen, deuterium, or a mixture of liquid hydrogen and neon. The fluids, which will be maintained at temperatures as low as -423 F, will undergo pressure oscillations where the peak pressure may be as high as 130 psia and the minimum pressure during operation may reach 10 psia.

The vacuum tank which is supported on three evenly spaced legs will normally be subjected to a vacuum loading, the vacuum being sustained between the vacuum tank and the bubble chamber. However, the vacuum tank has an additional mission which it may be called upon to carry out once in its operational lifetime. In the event that a leak occurs in the bubble chamber proper the vacuum tank must be capable of sustaining and containing the pressure and the liquid gas which was originally contained by the bubble chamber. Such an occurrence should, of course, not take place. However, the possibility of such an emergency occurring must be accepted and the vacuum tank should be designed to act as a containment vessel in such a contingency.

National Accelerator Laboratory has asked Battelle to render design assistance for the bubble chamber complex. The first task for Battelle was to critically analyze the proposed vacuum tank geometry to determine its adequacy to sustain the emergency condition. This condition was defined by National Accelerator Laboratory (NAL) as the application of a 150 psig internal pressure to the vacuum tank, with no leakage of pressurized gas ensuing. The responsibility for designing the vacuum tank to sustain the operational vacuum load was given to Chicago Bridge and Iron Co. The initial stress analysis for the emergency-pressure condition was carried out on CB&I's original design.

This report deals with the philosophy and details of the design analysis of the vacuum tank carried out by Battelle.

(2) EMERGENCY-PRESSURE STRESS CRITERIA

Initially NAL proposed that the stress criterion to be met when the vacuum tank is subjected to the emergency-pressure condition of 150 psig internal pressure is that the stress at any point in the structrue is not to exceed 90% of the minimum specified yield strength of the material comprising the structure. It is believed by the author of this report that such a criterion is extremely conservative and that to meet it a large penalty would have to be paid in the required increase in wall thickness and hence cost of the tank. This belief is based upon the author's and others' experience in the design and analysis of containment vessels under emergency loading conditions and is reflected in the specifications of the American Society of Mechanical Engineers Boiler and Pressure Vessel Code, Section III, "Nuclear Vessels". In that code in Article 4, "Design", Paragraph N-412(t)-(3), found in the Summer, 1968 Addenda, an emergency condition is defined as,

> "Any deviation from normal conditions which require shutdown for correction of the conditions or repair of damage in the system. The conditions have a low probability of occurrence but are included to provide assurance that no gross loss of

structural integrity will result as a concommitant effect of any damage developed in the system. The total number of postulated occurrences for such events shall not exceed twenty-five (25)."

Further, Figure N-414 of this code as shown in The Summer, 1970 Addenda (shown in this report as Figure 1) specifies what stress limits should be imposed on a pressure vessel undergoing an emergency condition. This figure specifies that if an elastic stress analysis is used then three criteria should be met. These deal only with primary stresses and are:

- The general membrane stress must not exceed the minimum specified yield strength of the material, S_y.
- The local membrane stress must not exceed 1.5 times S_y.
- The primary bending stress must not exceed 1.5 times S_y.

Note from this figure that no evaluation is required for an emergency condition for types of stress that fall into the Q (secondary stresses) and F (peak stresses) categories. To further clarify these types of stress Table N-413, "Classification of Stresses for Some Typical Cases", has been extracted from Section III and is shown here as Table 1. In this table P_m means primary general membrane stress, P_L means primary local membrane stress, P_b means primary bending stress, and Q and F are defined as above. This table is quite self-explanatory with one amplification. In the consideration of primary local membrane stress, a stressed region may be considered local if the distance over which the stress exceeds 1.1 S_Y does not extend in the meridional direction more than $0.5\sqrt{Rt}$ and if it is not closer in the meridional direction than $2.5\sqrt{Rt}$ where the limits of general primary membrane stress are exceeded. Here R is the mean radius of the vessel and t is the wall thickness at the location of concern. Note also, that in Table 1, P_b, primary bending stress in a pressure vessel under internal

pressure, occurs in only three conditions: in the crown of a dished or conical head, in the center region of a flat head, and in a typical ligament (closely spaced penetrations) in a perforated head or shell.

Thus from the above it is quite clear that the code stress requirements are much less stringent than those NAL has initially proposed. Further, the code, by not requiring a stress evaluation for Q type stresses under emergency conditions, recognizes that such stresses can be quite in excess of the yield stress without destroying the structural integrity of the vessel.

As an example of the success of applying the code reasoning to a vessel undergoing emergency conditions the author's experience with the design analysis of Argonne National Laboratory's vacuum tank component of their bubble chamber can be cited. In that case an elastic analysis determined that in certain components of the vacuum can the Q stresses, in this case secondary stresses, were as high as 3 and 4 times the yield stress of the material. Subsequent hydrostatic testing of the vessel at 1.25 times the anticipated emergency pressure proved the adequacy of the structure and did show some local deformations at the positions predicated by the elastic analysis.

Based on all the above, the emergency pressure stress criteria followed in this study were those specified by Section III except in those areas where the addition of sufficient material to bring the peak stress down to 90% of S_Y did not impose a severe wall thickness increase requirement. For the purposes of this analysis and as specified in Section III, for 304 stainless steel the following stress values were used

$$S_Y = 30{,}000 \text{ psi}$$

$$P_m \leq S_Y \text{ psi}$$

$$P_L \leq 1.5\ S_Y\ (45{,}000) \text{ psi}$$

$$P_b \leq 1.5\ S_Y\ (45{,}000) \text{ psi}$$

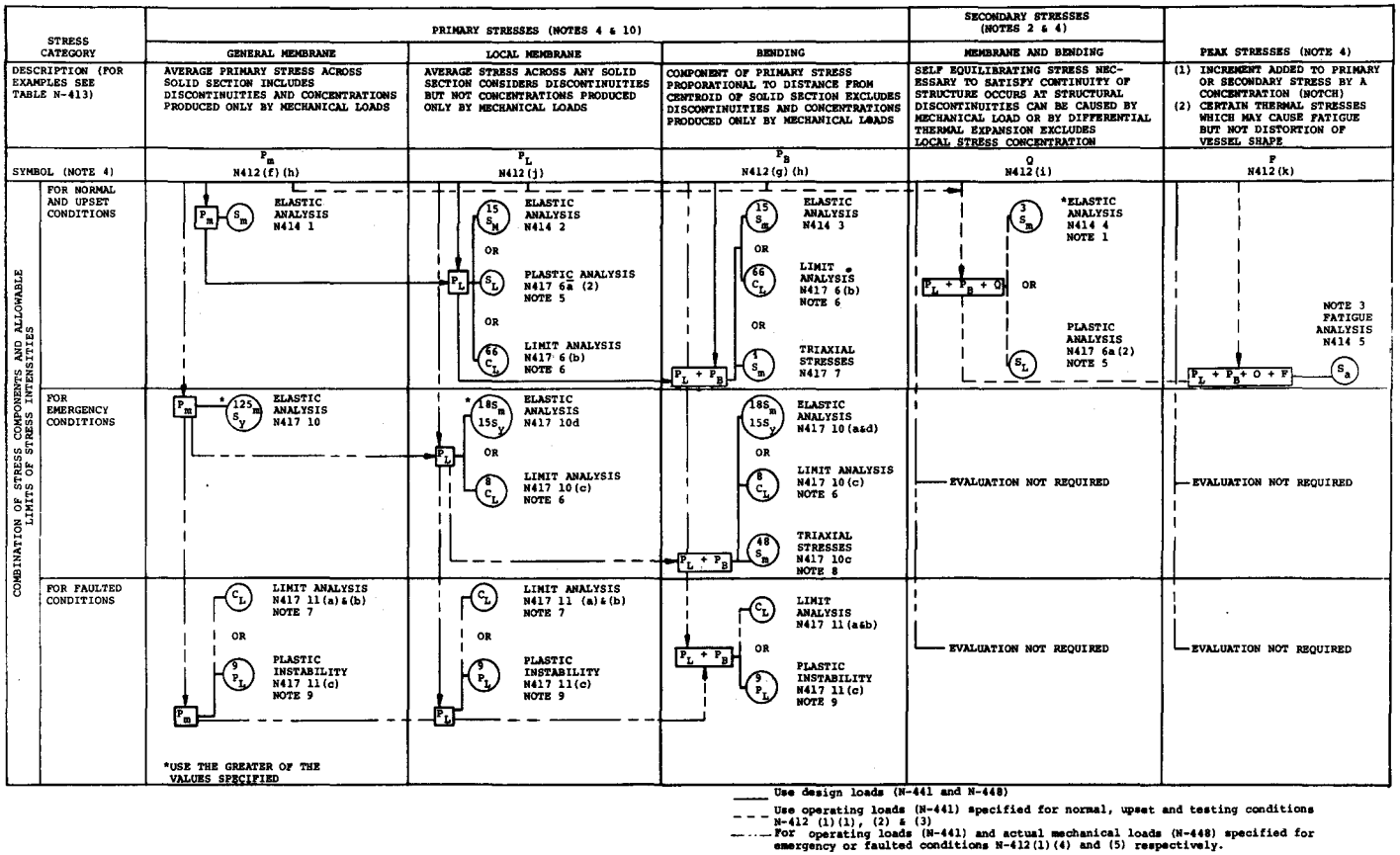

Use design loads (N-441 and N-448)

Use operating loads (N-441) specified for normal, upset and testing conditions N-412 (1)(1), (2) & (3)

For operating loads (N-441) and actual mechanical loads (N-448) specified for emergency or faulted conditions N-412(1)(4) and (5) respectively.

FIG. N-414
STRESS CATEGORIES AND LIMITS OF STRESS INTENSITY

NOTE 1 - This limitation applies to the range of stress intensity, When the secondary stress is due to a temperature excursion at the point at which the stresses are being analyzed, the value of S_m shall be taken as the average of the S_m values tabulated in Tables N-421, N-422, and N-423 for the highest and the lowest temperature of the metal during the transient. When part or all of the secondary stress is due to mechanical load, the value of S_m shall be taken as the S_m value for the highest temperature of the metal during the transient.

NOTE 2 - The stresses in Category Q are those parts of the total stress which are produced by thermal gradients, structural discontinuities, etc., and do not include primary stresses which may also exist at the same point. It should be noted, however, that a detailed stress analysis frequently gives the combination of primary and secondary stresses directly and, when appropriate, this calculated value represents the total of $P_L + P_b + Q$ and not Q alone. Similarly, if the stress in Category F is produced by a stress concentration, the quantity F is the additional stress produced by the notch, over and above the nominal stress. For example, if a plate has a nominal stress intensity, $P_m = S$, $P_b = O$, $Q = O$ and a notch with a stress concentration K is introduced, then $F = P_m (K - 1)$ and the peak stress intensity equal $P_m + P_m (K - 1) = KP_m$. However P_L is the total membrane stress which results from mechanical loads including discontinuity effects, rather than a stress increment. Therefore the P_L value always includes the P_m contribution.

NOTE 3 - S_α is obtained from the fatigue curves, Fig. N-415. The allowable stress intensity for the full range of fluctuation is $2S_\alpha$.

NOTE 4 - The symbols P_m, P_L, P_b, Q, and F do not represent single quantities, but rather sets of six quantities representing the six stress components σ_t, σ_l, σ_r, τ_{tl}, τ_{lr}, and τ_{rt}.

NOTE 5 - S_L denotes the structural action of shakedown load as defined in N-412 (q) calculated on a plastic basis as applied to a specific location on vessel

NOTE 6 - C_L denotes the collapse load calculated on the basis of the lower bound theorem of limit analysis and yield strength values specified in Table N-424 (as defined in N-412(s).

NOTE 7 - C_L denotes the collapse load calculated on the basis of the lower bound theorem of limit analysis and yield strength whose value is the greater of 1.5 S_m and 1.2 S_y.

NOTE 8 - The triaxial stresses represent the algebraic sum of the three primary principal stresses $(\sigma_1+\sigma_2+\sigma_3)$ for the combination of stress components.

NOTE 9 - PL denotes the plastic instability load calculated on the basis of plasticity analysis, and which is defined by the instability condition in which true stress in the material increases faster than the strain hardening can accomodate.

NOTE 10 - For configurations where compressive stresses occur, the stress limits shall be revised to take into account critical buckling stresses. (See Par. N-410(c)).

FIGURE 1 STRESS CATEGORIES AND LIMITS OF STRESS INTENSITIES

TABLE 1. (Extracted from Section III)

TABLE N-413 CLASSIFICATION OF STRESSES FOR SOME TYPICAL CASES

VESSEL COMPONENT	LOCATION	ORIGIN OF STRESS	TYPE OF STRESS	CLASSIFICATION
Cylindrical or spherical shell	Shell plate remote from discontinuities	Internal pressure	General membrane Gradient through plate thickness	P_m Q
		Axial thermal gradient	Membrane Bending	Q Q
	Junction with head or flange	Internal pressure	Membrane Bending	P_L Q
Any shell or head	Any section across entire vessel	External load or moment, or internal pressure	General membrane averaged across full section. Stress component perpendicular to cross section	P_m
		External load or moment	Bending across full section. Stress component perpendicular to cross section	P_m
	Near nozzle or other opening	External load moment, or internal pressure	Local membrane Bending Peak (fillet or corner)	P_L Q F
	Any location	Temp. diff. between shell and head	Membrane Bending	Q Q
Dished head or conical head	Crown	Internal pressure	Membrane Bending	P_m P_b
	Knuckle or junction to shell	Internal pressure	Membrane Bending	P_L* Q
Flat head	Center region	Internal pressure	Membrane Bending	P_m P_b
	Junction to shell	Internal pressure	Membrane Bending	P_L Q

TABLE 1. (Extracted from Section III)(contd.)

VESSEL COMPONENT	LOCATION	ORIGIN OF STRESS	TYPE OF STRESS	CLASSIFICATION
Perforated head or shell	Typical ligament in a uniform pattern	Pressure	Membrane (Av. thru cross section)	P_m
			Bending (Av. thru width of lig., but gradient thru plate)	P_b
			Peak	F
	Isolated or atypical ligament	Pressure	Membrane	Q
			Bending	F
			Peak	F
Nozzle	Cross section perpendicular to nozzle axis	Internal Pressure or external load or moment	General membrane av. across full section. Stress component perpendicular to section	P_m (See N-417.9)
		External load or moment	Bending across nozzle section	P_m (See N-417.9)
	Nozzle wall	Internal pressure	General membrane	P_m (See N-417.9)
			Local Membrane	P_L
			Bending	Q
			Peak	F
		Differential expansion	Membrane	Q
			Bending	Q
			Peak	F
Cladding	Any	Differential expansion	Membrane	F
			Bending	F
Any	Any	Thermal Gradient thru plate thickness	Bending	F**
Any	Any	Any	Stress Concentration (notch effect)	F

* Consideration must also be given to the possibility of wrinkling and excessive deformation in vessels with large diameter-to-thickness ratio.

** Consider possibility of thermal stress ratchet (see N-417.3).

(3) GENERAL PROCEDURE

This work consists of a detailed stress analysis of the proposed vacuum can subjected to an internal emergency pressure condition of 150 psig. Working with the preliminary sizing of the vacuum tank components as recommended by CB&I the analysis indicated the correct wall thickness required to meet the emergency-pressure stress criteria. This analysis also established the sizing and spacing of bolts in certain flanges and the design of one flange connection. Though not the primary responsibility of Battelle, some analytic checks were made to assure that configuration change recommendations did not damage the ability of the structure to sustain the normal operational vacuum load.

In general the vacuum tank is a shell of revolution. As such, it lends itself well to the basic analytic tool used by Battelle in this work. This tool is MONSA, a digital computer program for the stress and displacement analysis of shells of revolution loaded by symmetric or nonsymmetric loads. It is based upon A. Kalnin's work as described in a paper in the Journal of Applied Mechanics, Vol 3, September, 1964, pp 467-476, titled, "Analysis of Shells of Revolution Subjected to Symmettrical and Nonsymmetrical Loads". Though continually modified and amplified over the years, the basic program has been used extensively by Battelle personnel since mid-1965. In its present form, it is based on the multisegment numerical integration method for the analysis of the general shell of revolution boundary value problem. It has two components, MONSA-S and MONSA-V. MONSA-S will determine the displacements, forces, and stresses for a composite shell. Such a shell may be composed of a number of distinct parts which may have the following shapes: cylindrical, spheroidal, ellipsoidal, paraboloidal, conical, and toroidal. The shell wall may be composed of four different layers of orthotropic materials. The thicknesses of these layers can vary along the meridional generator.

Mechanical and temperature loadings can be applied to the shell.

For nonsymmetric loadings, the loads must be broken into their Fourier harmonics, each harmonic requiring a computer run, though as many as 15 harmonics can be run consecutively at one machine run. Temperatures can vary meridionally as well as through the shell thickness. Further, this program allows the analysis of a shell spinning about its axis as well as analysis of a shell subjected to harmonically (time dependence) varying mechanical and temperature loads.

MONSA-V will determine the natural frequencies and mode shapes of the composite shells of revolution described above.

Where the configuration of the vacuum tank deviates from a shell of revolution, as in the beam window area and at non-radial penetrations, other suitable analytic techniques were employed.

(4) CONCLUSIONS AND RECOMMENDATIONS

The work carried out as detailed in this report showed that some modifications of the originally proposed vacuum tank geometry must be made if the structure is to adequately sustain the emergency-pressure condition of an internal pressure of 150 psig. These changes dealt with the thickness of the bottom half of the vacuum tank and the configuration of the beam window reinforcement and are incorporated in the present design. Also developed in this report is an acceptable alternate flange geometry for the bottom of the cylindrical portion of the tank and the design of its mating flange.

A brief check of the critical buckling pressures showed that the tank is structurally adequate to sustain its operational one atmosphere vacuum load.

This work also showed the importance of proper welding techniques as it affects the structural integrity of the vessel. Further, since the camera penetrations in the top half of the tank have not as yet been specified it is pointed out that an analysis of their configurations must be eventually carried out before a complete judgment as to the vessel's structural adequacy to sustain emergency-pressure condition can be made.

(5) THE VACUUM TANK SUBJECTED TO THE EMERGENCY-PRESSURE CONDITION

Method of Analysis

Vacuum Tank Nominal Stresses

Working from the preliminary drawing of the vacuum tank supplied by NAL the vacuum tank was initially modeled for input to MONSA-S as a body revolution as shown in Figure 2. At this stage all penetrations and local discontinuities were omitted. Referring to Figure 2 the parts of the shell and their thickness were as follows.

Part No.	Type of Shell	Thickness
1	Cylinder	0.5 inch
2	Sphere	0.625 inch
3	Sphere	Variable thickness (geometrically a rectangular section ring)
4	Sphere	0.5
5	Sphere	0.5 inch
6	Torus	0.5 inch
7	Cylinder	Variable Thickness
8	Flat plate (cone of 0° angle)	1.0 inch
9	Sphere	0.625 inch
10	Cylinder	0.5 inch
11	Sphere	0.625 inch
12	Cylinder	Variable thickness (main length - 0.75 inch thick)
13	Cylinder	5.0 inches
14	Flat plate	2.0 inches
15	Sphere	0.625 inch
16	Cylinder	1.0 inch

Parts 1 and 10 do not model any real parts of the structure. They

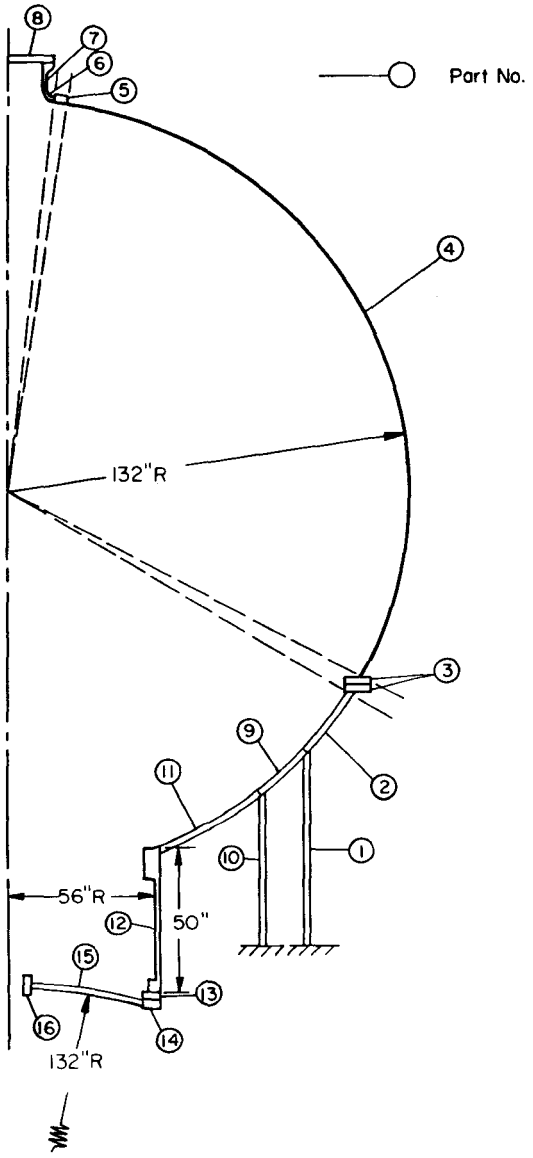

FIGURE 2. INITIAL GEOMETRIC MODEL FOR INPUT TO MONSA-S

are used as convenient anchors for the tank model and are placed on radial lines equal to the radial distances from the axis of rotation to the inner and outer edges of the cylinders supporting the tank. Part 12 was modeled as a cylinder of variable thickness to allow rapid thickness variation studies in this area. Initially, as shown in Figure 2, the top of the cylinder had a reinforced section such that the thickness (cylinder and reinforcement combined) was 2.75 inches for a length of 3 inches. Part 12 was then connected to Part 13 which was modeled as a cylinder with a thickness of 2 inches and a length of 4.0 inches. This part represents the reinforcement at the bottom of the cylinder. This in turn was connected to Part 14 which is an annular flat plate which models the flange of the spherical bottom piece.

This model when input to MONSA-S rendered stresses acting on the vessel when modeled as above. These stresses are identified in keeping with Section III nomenclature as P_m, primary membrane stress, P_L, local membrane stress, P_b, primary bending stress, and Q, secondary stress. (σ_ϕ) means that the stress is in the meridional direction while (σ_θ) means that the stress is in the circumferential or hoop direction

Examination of Figure 3 shows that NAL's initial emergency-pressure criteria of 90% of yield or 27,000 psi peak stress is violated in many places throughout the vessel. This is even further magnified by the knowledge that the stresses shown are nominal stresses and must be modified by local stress concentration factors and gross stress intensifiers at the positions where penetrations will be put in the vessel.

Based on these figures, the only stress that violates the Section III criteria is the one between Parts 6 and 7 at the top access port. This of course clearly indicates that this area must be reinforced, which was anticipated. However, the presence of penetrations in the bottom spherical part of the tank, particularly those for the bubble chamber legs, require that this section must see lower nominal stresses

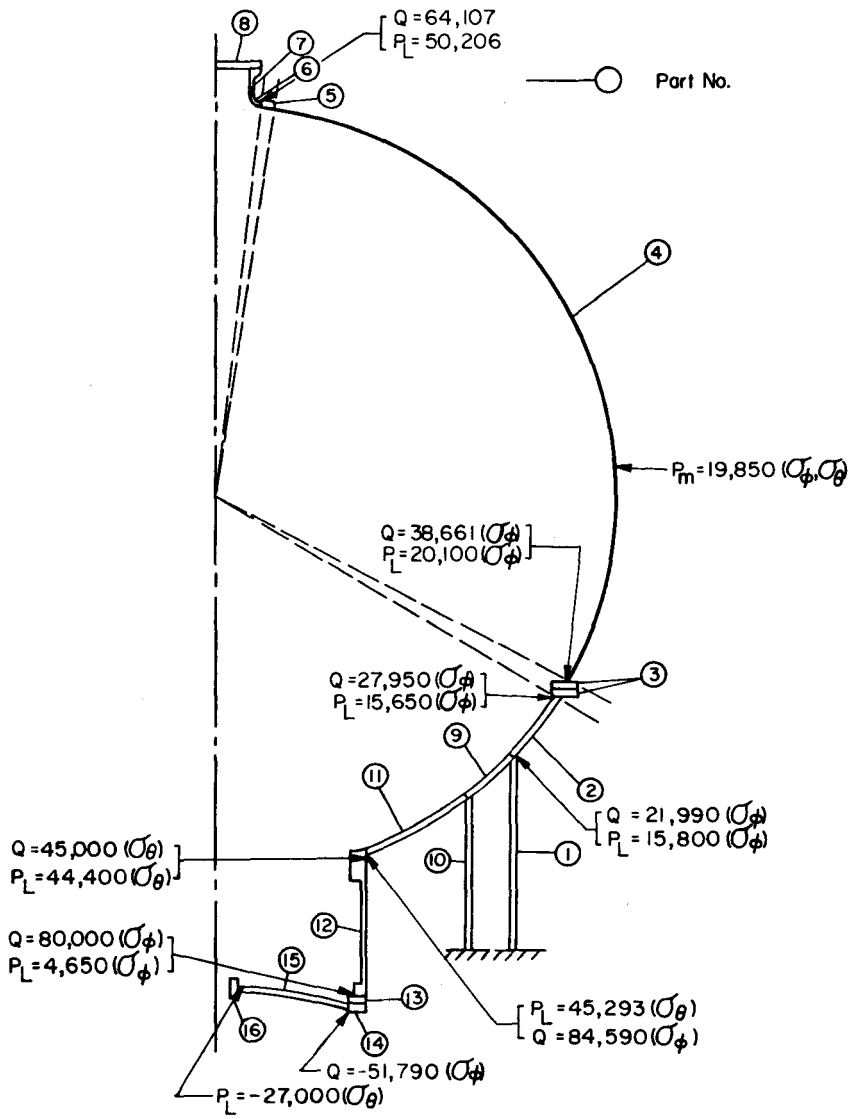

FIGURE 3. NOMINAL STRESS OUTPUT FOR FIRST MODEL OF VACUUM TANK

than those indicated by Figure 3.

Various geometry changes were applied to the geometric model and the stresses were examined until the stress levels were reduced at positions where the presence of large penetrations could be accepted.

The changes from the initial geometry were as follows.

Part No.	Type of Shell	Thickness Change
5	Sphere	From 0.5 to 1.0 inches
2,9,11	Sphere	From 0.625 to 1.0 inch
12	Cylinder	Variable thickness, main length thickness from 0.75 to 0.5 inch
15	Sphere	From 0.625 to 1.0 inch

Part 12 was modeled to conform to the geometry for this part shown in NAL drawing No. 2627.ME-25002, Rev F. The most important change made was to set the bottom spherical part of the tank equal to 1.0 inch. The nominal stress output for this model is shown in Figure 4. Note here that even with these changes NAL's requirement of peak stresses being less than 90% of yield stress is violated in several places. Again when one considers local stress concentrations these violations become more severe. However, from the Section III viewpoint, all critical stresses are considerably below code requirements and here local stress concentrations need not be evaluated since they fall into the Q category.

Main Closure Flange

The main closure flange, between the top 1/2 inch thick spherical portion and the bottom 1 inch thick spherical portion of the vacuum tank was not analyzed in detail for the following reason. This element was modeled as a 4 x 4 inch cross section ring denoted as Part 3 in the original and final MONSA-S model. This represented two flanges, each 2 x 4 inch, tightly bolted together. In a flange of such thickness the stresses induced by the 150 psig internal pressure are small. The large stresses occur in the shells in the junction of the shells to the flanges and of course in the bolts securing them. As can be seen from Figure 4,

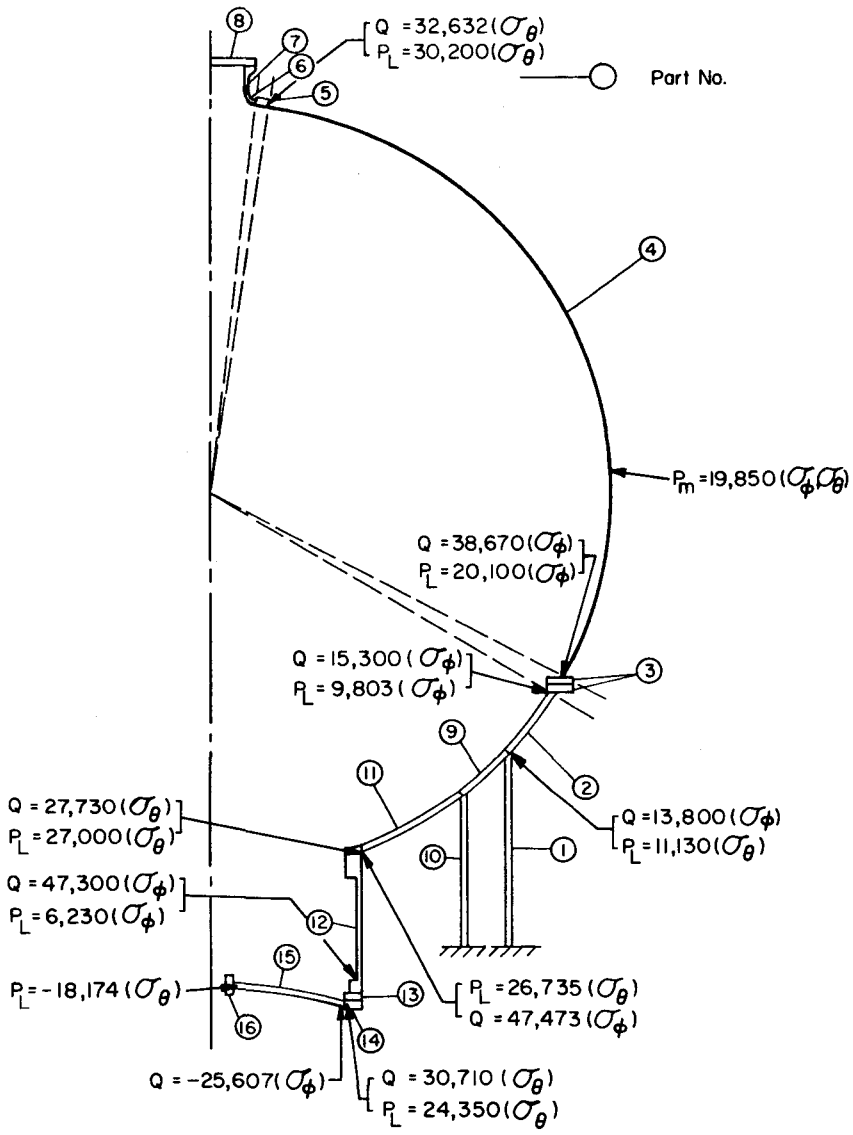

FIGURE 4. NOMINAL STRESS OUTPUT FOR FINAL MODEL OF VACUUM TANK

P_L, the stress of primary concern in both the top and bottom shells at their intersection with the flange are well below the limit of 45,000 psi set by Section III. This being the case, the CB&I recommended flange configuration as shown in Figure 5 is quite satisfactory. The main members of the flange are of slightly greater section than those analyzed and the reinforcing gussets and "L" bars would lower the stresses in the vicinity of the flange below those calculated by MONSA-S.

To secure the flanges it is recommended that 240 1-inch root diameter bolts be used, positioned as shown on NAL drawing No. 2627.ME-25002, Rev F. These bolts should be 18 chromium, 8 nickel type bolts conforming to ASTM Specification A193-66. They should be strain hardened to surface Brinell hardness of 320, maximum. They must have minimum specified yield and tensile strengths of 65,000 and 105,000 psi, respectively. The pressure loading of these bolts will result in a stress per bolt of approximately 35,000 psi.

Bottom Flange

The bottom flange of the vacuum tank, in the cylindrical portion was modeled for MONSA-S in conformity with the NAL drawing quoted above. This flange was "L" shape in cross section with the minimum thickness given as 3 inches. This flange configuration is quite adequate with one exception. In the crotch of the "L" section a fillet radius of at least 1 inch is required. This will prevent any appreciable notch effect in this location.

If this flange configuration is deemed too expensive to machine or is rejected for some other reason an alternate configuration can be used. This configuration is shown in Figure 6, and is composed of a built-up flange of 2 rings and 36 gussets. The maximum stress which occurs in this configuration during the emergency-pressure condition is approximately 41,000 psi in the toe of each gusset plate. This stress is categorized as P_b and is limited by Section III to 45,000 psi.

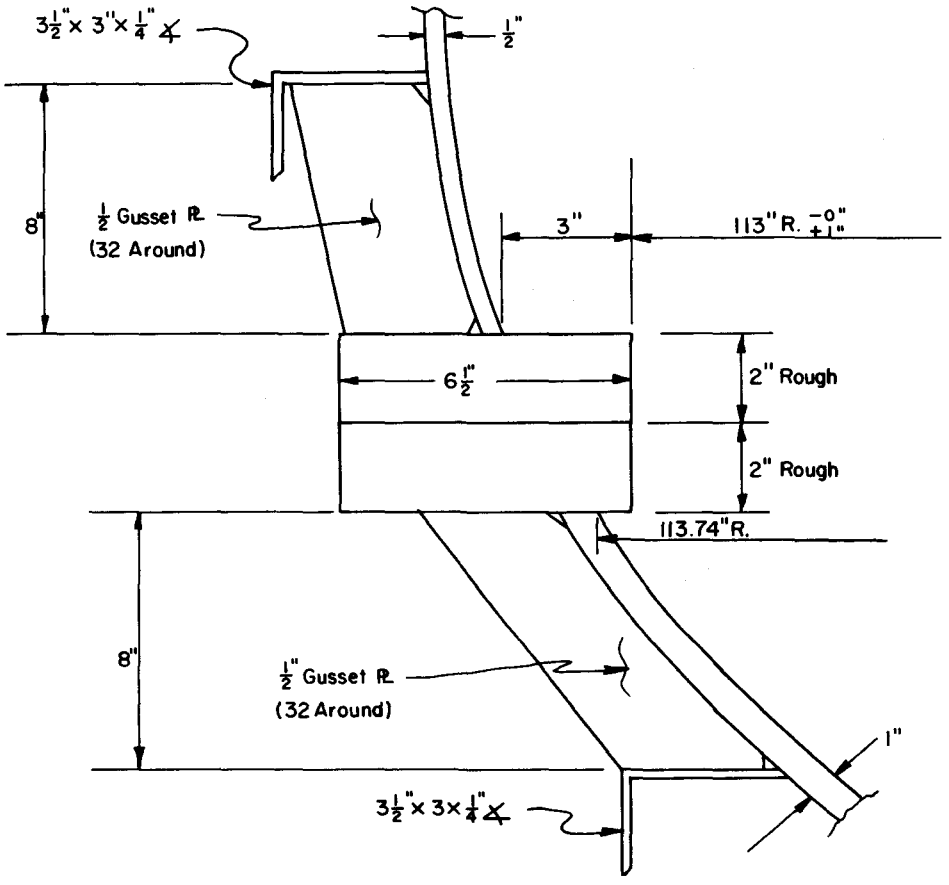

FIGURE 5. CB&I RECOMMENDED MAIN FLANGE CONFIGURATION

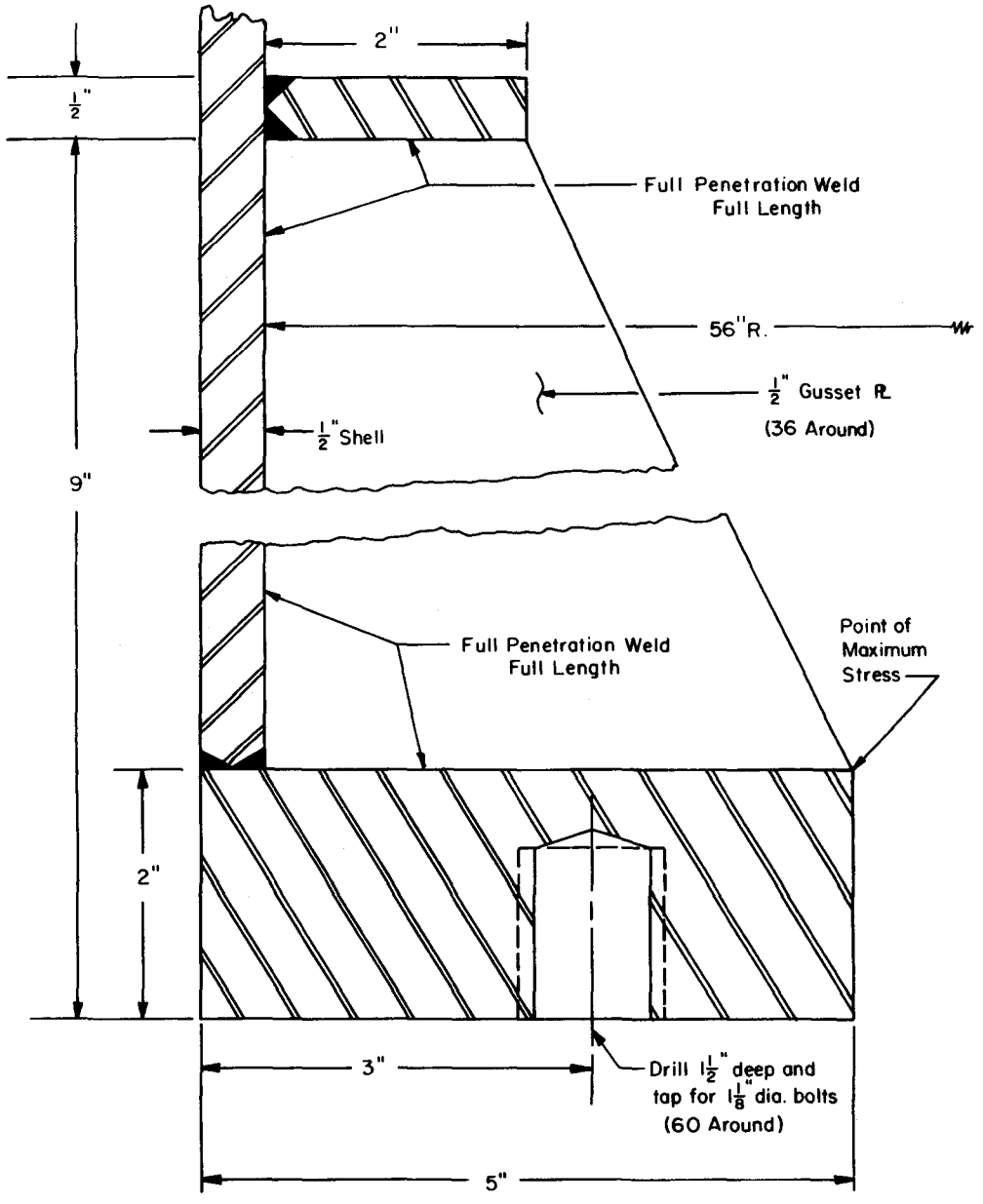

FIGURE 6. ACCEPTABLE ALTERNATE BOTTOM FLANGE CONFIGURATION

This configuration and stress was arrived at by considering each gusset as part of an inverted "T" section, where the gusset formed the stem and the shell between gussets formed the flange. The moment and axial load applied to this section was derived from the MONSA-S output for the previously described flange model. These parameters when converted for use with the "T" section were an axial load per "T" of 31,900 lbs and a bending moment of 126,730 in-lb per "T". The geometry of this acceptable alternate bottom flange configuration is shown in Figure 6. For this flange 60, 1-1/8 inch diameter bolts of the same material and specification as those called for in the main flange are required.

The mating flange for the one detailed above is shown in Figure 7. This flange configuration was almost exactly modeled in the final MONSA-S model and the maximum stress of concern is as shown in Figure 4, P_L = 24,350 psi.

Top Access Port and 18-Inch Diameter Manway

CB&I submitted proposed configurations for a 26-inch diameter access port and an 18-inch diameter manway. These configurations are shown in Figure 8. The top access port was analyzed using MONSA-S by considering it as a central penetration in the top of a 132 inch hemispherical shell 1/2 inch thick. This was done to ensure that only the stresses induced by the penetration were developed and that no extraneous edge effects were introduced. The maximum stresses found in the top access port configuration are shown in Figure 9.

The manway was not analyzed. As can be seen from Figure 8 the manway is effectively more reinforced than the top access port. Thus lower stresses can be expected to occur in this structure than were found above.

It is emphasized that the Q stress shown, 60,300 psi (σ_c) is a local bending stress and thus does not violate the Section III emergency condition requirement. However, if it is desired to reduce this stress then either the cylinder wall can be increased to a 1/2 inch thickness

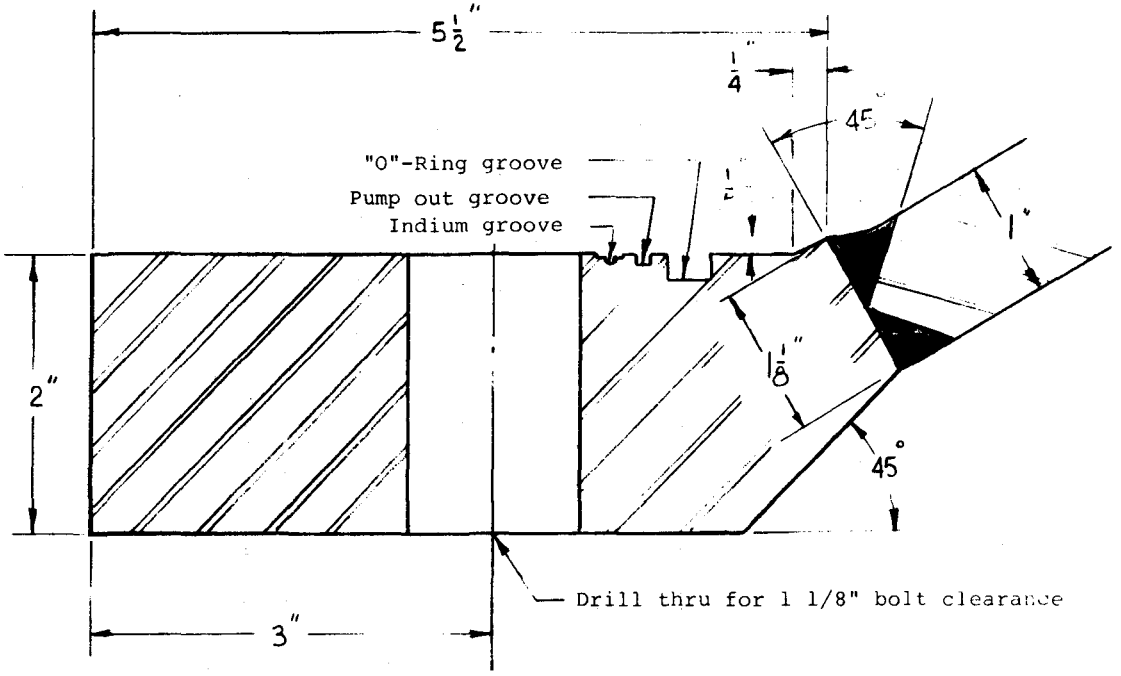

FIGURE 7. ACCEPTABLE BOTTOM MATING FLANGE CONFIGURATION

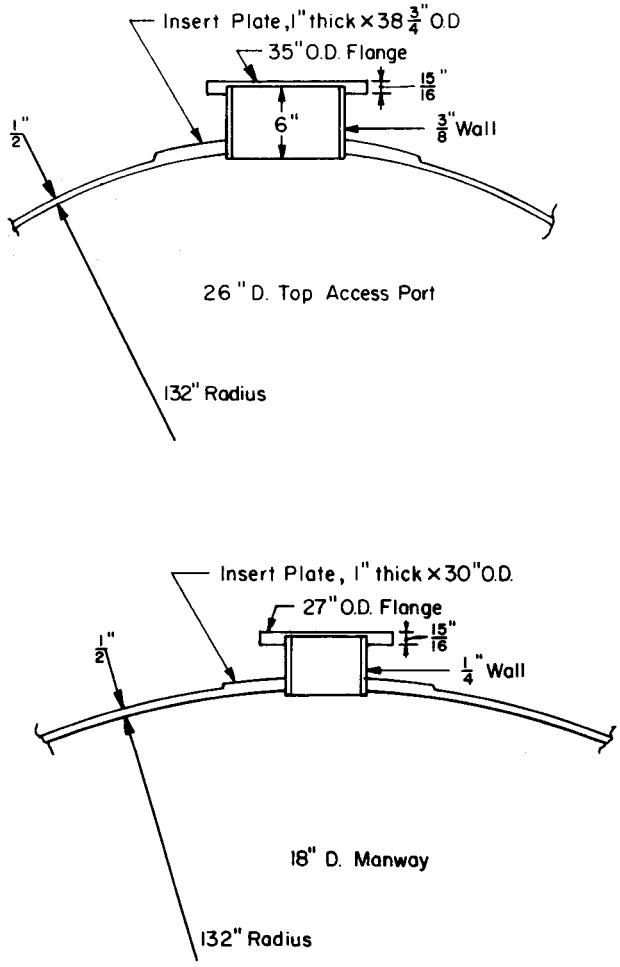

E 8. PROPOSED ACCESS PORT AND MANWAY CONFIGURATION

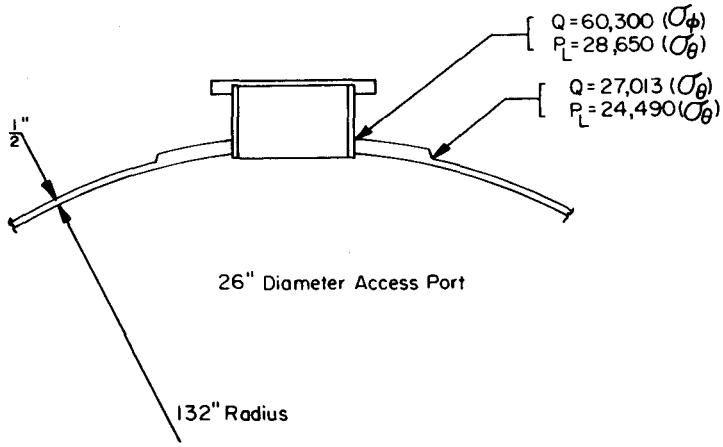

FIGURE 9. MAXIMUM STRESSES IN PROPOSED TOP ACCESS PORT CONFIGURATION

or the OD of the plate insert can be increased to 52 inches. Either change will reduce the peak stress at this point to approximately 34,000 psi.

The cover plate for the top access port must be at least 1.0 inch thick and must be secured to the port flange by 16 evenly spaced 5/8 inch root diameter stainless steel bolts of the type previously discussed. The manway top plate must be at least 3/4 inch thick and secured by 10 evenly spaced 5/8 inch diameter stainless steel bolts. This will ensure a stress level of approximately 25,000 psi in each bolt under emergency-pressure condition.

At the time this report was written, the exact location of these penetrations in the top of the vacuum tank had as yet not been established. However if they are placed so that the centerline of the penetration approaches no closer than a certain distance D to the center line of an adjacent penetration then each penetration can be considered as being isolated. Here the distance D which is measured along the surface of the shell is given as

$$D = (d_1 + d_2) \text{ inches}$$

where $d_{1,2}$ = diameters of adjacent penetrations.

This means that adjacent penetrations meeting this distance requirement need no more additional reinforcement than would be required if they were each the only penetration in the shell. This distance requirement is modified to treat the contingency of a penetration close to a large discontinuity (such as the leg penetration and the sphere-cylinder intersection in the bottom of the vacuum tank). In this case a good guide would be

$$D = 2d ,$$

where

D = distance along surface of shell from the centerline of the penetration to the edge of the discontinuity

d_1 = the diameter of the penetration close to the large discontinuity.

If these spacing requirements are not met, additional reinforcement will be required.

Beam Window

CB&I proposed beam window design is shown in Figure 10. This configuration is not in any sense a body of revolution, thus not applicable for direct analysis by MONSA-S. An approximate analysis was developed as follows. The reinforcing bar configuration was treated as a frame composed of "I" bars. The "I" bars were composed of the outer 3 x 3/4 inch bar as the top flange, the 5 x 1 inch bar as the bottom flange, and the 1/2 inch shell as the web connecting the flanges. This elliptical frame was then assumed to be acted upon by a uniform load along the flat outer sections of the ellipse. The uniform load was determined by the membrane force acting in the sphere at this location.

Costigliano's theorm was then applied to this model to determine the maximum spreading deflection which would occur at the midspan window position. Such an analysis is shown in Appendix A.

Another model was structured for input to MONSA-S as shown in Figure 11. This model was a body of revolution composed of two cylindrical stub sections between which the 1/8 inch thick beam window was represented as a toroidal segment. The loads applied to this model were edge displacements δ_u and δ_w, and the internal pressure of 150 psig. δ_u was developed from the frame analysis. δ_w was developed from calculated radial displacement of a 132 inch radius sphere with a 1/2 inch wall thickness acted upon by a 150 psig internal pressure. This model renders stresses which are only applicable to the beam window in midspan. However, since the maximum stresses in the window are expected to occur at this position such an analysis is sufficient.

For the proposed CB&I configuration, δ_u was calculated from the frame analysis as approximately 0.3 inch, while δ_w was determined to be 0.09 inch. With these values as input, MONSA-S calculated the stresses in the window model. The maximum stresses found are shown in Figure 12.

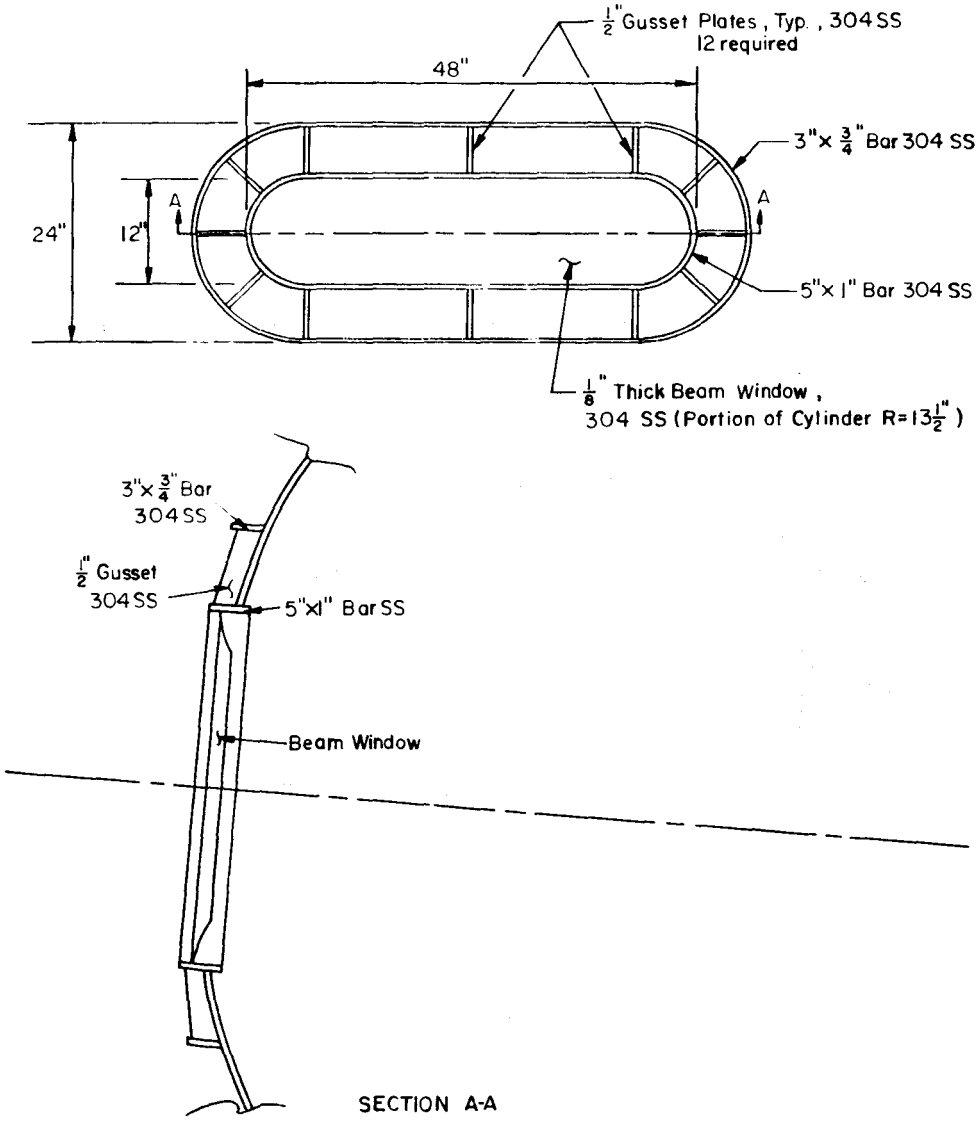

FIGURE 10. CB&I PROPOSED BEAM WINDOW DESIGN

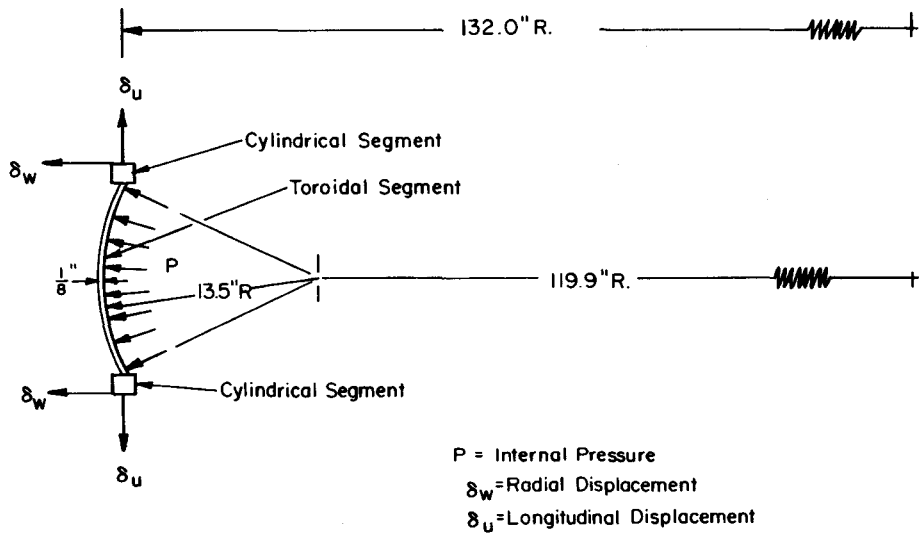

FIGURE 11. MONSA-S MODEL OF MIDSPAN WINDOW POSITION

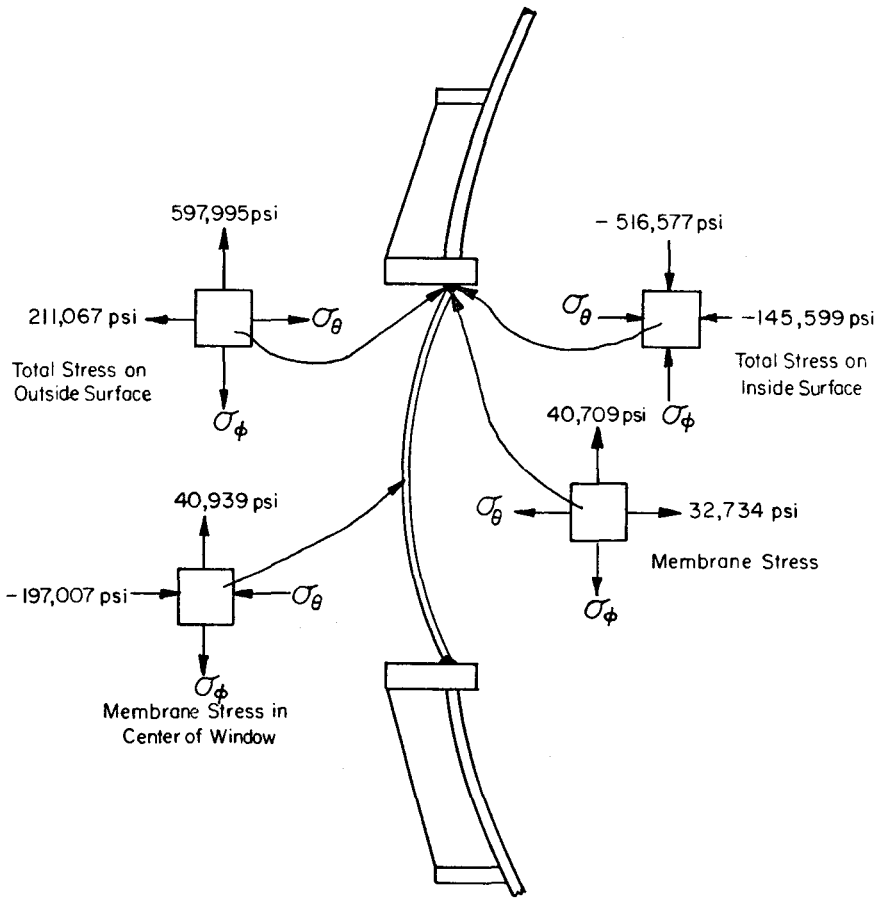

FIGURE 12. CALCULATED MAXIMUM STRESSES IN CB&I PROPOSED BEAM WINDOW CONFIGURATION

As can be seen from the figure the stresses are quite unacceptable even acknowledging that this analysis is rather conservative.

To reduce these stresses the frame dimensions were increased as follows. The 5 x 1 inch bar was increased to a 5 x 1-1/2 inch bar. The 3 x 3/4 inch bar was increased to a 3 x 1 inch bar and the two bars were spread apart from 6 inches to 10 inches. This frame configuration is the one shown analyzed in Appendix A. For such a geometry δ_u was calculated as 0.063 inch. The MONSA-S model of the window was rerun using this new value for δ_u and the results are shown in Figure 13. Though these stresses are still high this reinforcement configuration is deemed adequate for the following reasons.

As can be seen from Figure 13 the high stresses are fundamentally bending stresses, the average membrane stresses being relatively small. These high stresses are not accurate since they are above yield and to determine them accurately an elastic-plastic analysis would have to be carried out. However in linear theory, though the stresses are not accurate, the strains in highly localized areas as calculated from those stresses should be correct. Thus for the maximum strain condition in the modified window design,

$$\varepsilon_{\phi_{max}} = \frac{1}{E} [\sigma_\phi - \nu\sigma_\theta]$$

where

$\varepsilon_{\phi_{max}}$ = maximum meridional strain

σ_ϕ = meridional stress

σ_θ = tangential or hoop stress

ν = Poisson's ratio

E = Modulus of Elasticity

thus $$\varepsilon_{\phi_{max}} = \frac{1}{28 \times 10^6} [134{,}200 - (0.32)(62{,}696)]$$

$$\varepsilon_{\phi_{max}} = 0.00408 \text{ inches/inch},$$

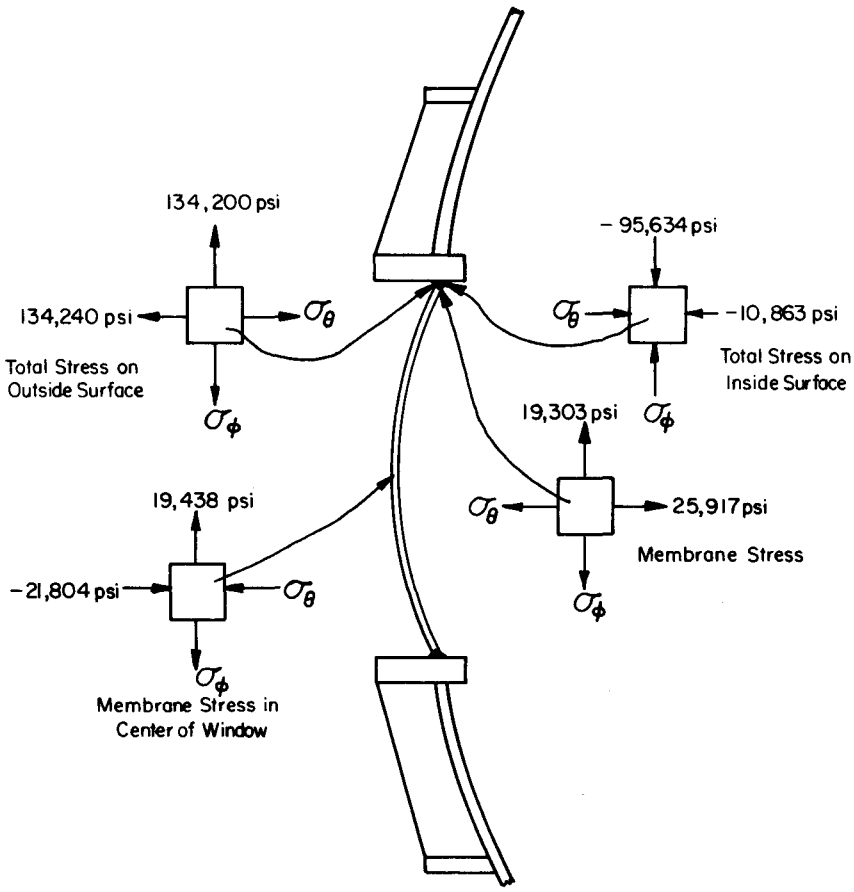

FIGURE 13. CALCULATED MAXIMUM STRESSES IN MODIFIED CB&I PROPOSED BEAM WINDOW CONFIGURATION

thus a total elongation of 0.4%. Considering that annealed 304 stainless steel exhibits a maximum total elongation at room temperature of at least 50 percent, an elongation of 0.4 percent caused by highly localized bending stresses does not constitute a structural inadequacy.

The above reasoning demonstrates the justification for neglecting such localized bending stresses from Section III's emergency criteria. Such stresses under the Code would be classified as Q stresses and not require evaluation. Note also that the local membrane stresses, P_L, for this case are less than the Code required 45,000 psi. When this reasoning is coupled with the inherent conservative nature of the approximate frame analysis developed to determine δ_u, the judged adequacy of the modified beam window design is reinforced. Based on the above, then, the recommended beam window configuration is shown in Figure 14.

Penetrations in Bottom of Vacuum Tank

The minimum thickness spherical shell of 132 inch radius required to sustain a 150 psig internal pressure is given by Section III, Appendix I as

$$t = \frac{PR_o}{2S_m}$$

where

t = required thickness

P = internal pressure

R_o = mean radius

S_m = design stress intensity.

For the vacuum tank and 304 stainless steel we have

$$t = \frac{150(132)}{2(20,000)} = 0.495 \text{ inches}$$

The bottom half of the vacuum tank has a wall thickness already established as 1.0 inch. What this means is that the excess thickness, or 0.505 inch, can be considered as reinforcement for any isolated

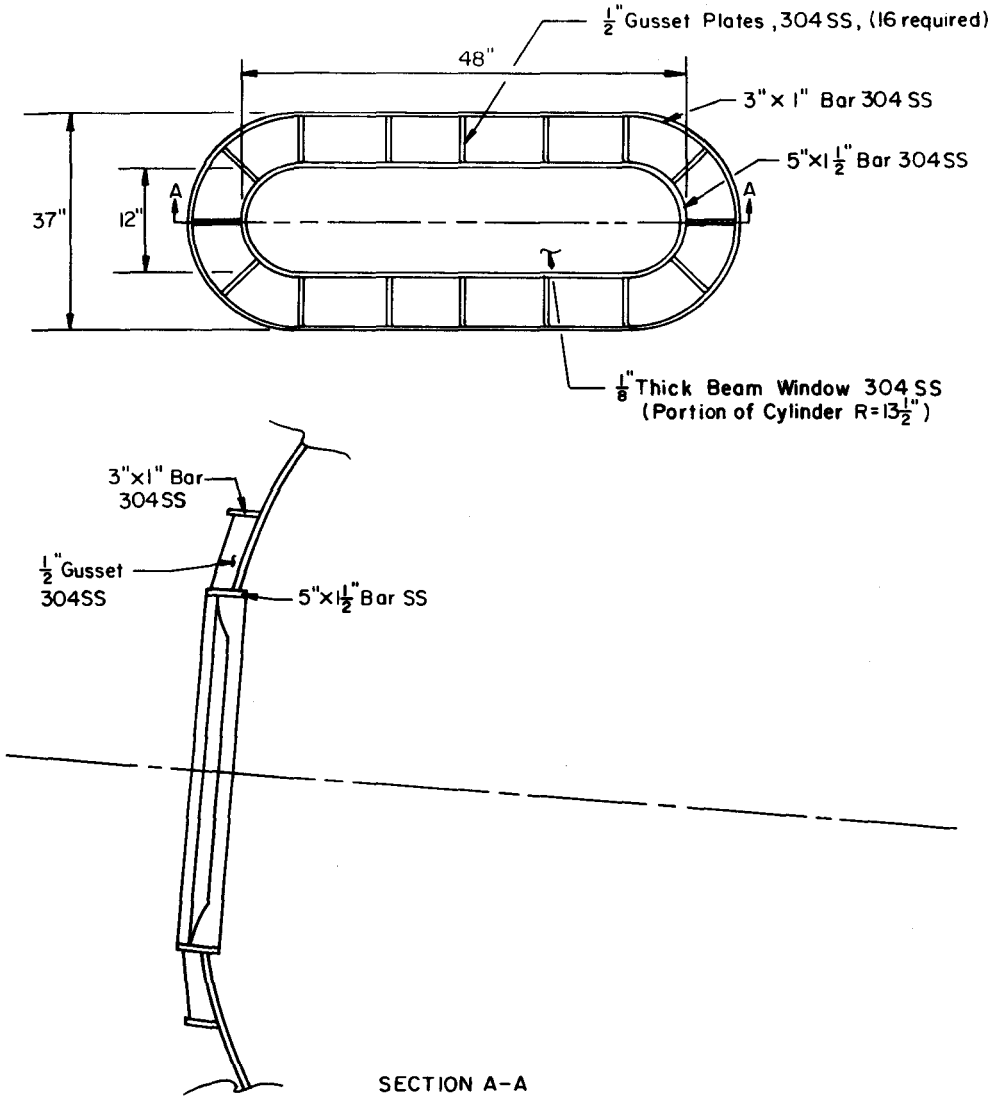

FIGURE 14. PROPOSED MODIFIED BEAM WINDOW DESIGN

penetration of this shell. Further, it means, by the provisions of Section III, that every isolated penetration in this portion of the vacuum can is in fact fully reinforced.

However, there are several penetrations in this area which violate the spacing requirements necessary for them to be considered isolated. In particular those sets of penetrations for the legs supporting both the vacuum can and the bubble chamber, and the manway penetration. NAL drawing No. 2627.ME-25002, Rev K., shows that these particular areas have been additionally reinforced. Though no specific mathematical analysis was carried out the placement of the reinforcement as shown in the quoted drawing does meet the intent and specifications of Section III, with one exception. Section III does not accept added reinforcement in the form of pads. All reinforcement must be integral in nature. However, such a requirement is based upon the knowledge that higher local stress concentrations exist at the welds on added reinforcement than exist at these same locations for integral reinforcements. Where cyclic loading is anticipated such a situation may lead to a premature fatigue failure. In the case of the bubble chamber, if the emergency-pressure condition occurs, it will occur only once. Such local high stress levels, as have been discussed previously, do not affect the adequacy of the vessel to sustain these loads. Thus it is within the intent though not the specifications of the code to allow such local added reinforcements in this case.

Camera and Other Penetrations in The Top of the Vacuum

At this time the size and locations of the camera and other types of penetrations in the top of the vacuum can have not been determined. Since the top half of the vacuum tank has a wall thickness of only 1/2 inch all isolated penetrations must be reinforced. For these penetrations the provisions of Article N-450, "Openings and Compensation", subsections N-451 through N-457 of Section III should be adhered to. The reinforcement should be integral in form and all welding should be

of the full penetration type. Where the spacing of adjacent penetrations do not meet minimum requirements each situation must be individually analyzed so as to determine the correct form of the needed reinforcement.

(6) WELDING AND INSPECTION REQUIREMENTS

This paragraph is not intended to be all inclusive but is included in this report to emphasize the importance of good weld procedure to the structural adequacy of the vacuum tank.

The stresses in the vicinity of all welds in the vacuum tank during the emergency-pressure condition would be quite high. Under such a condition a poor or faulty weld, or a significant amount of residual stress induced in the weld and parent materials as a result of the welds, may lead to a rupture of the structure at such localities. It is for this reason that great care must be taken in the welding procedure. All welds, except those few positions on the OD of an added pad reinforcement, must be full penetration. All specifications of the ASME Boiler and Pressure Vessel Code Section IX, "Welding Specifications", and of Article 5, "Fabrication", of Section III must be adhered to as closely as possible. All specifications of Article 6, "Inspection", of Section III, should also be adhered to.

(7) A CHECK OF THE ADEQUACY OF THE VACUUM TANK TO SUSTAIN A VACUUM LOADING

The following paragraphs describe some brief checks made to ensure the adequacy of the vacuum tank to sustain the operational vacuum load.

Spherical Portion of the Vacuum Tank

The critical buckling pressure for a thin-shelled sphere is given as [1]

$$P_{cr} = \frac{0.365\ Et^2}{r^2}$$

where

P_{cr} = critical buckling pressure

E = Young's Modulus

t = wall thickness

r = mean radius of sphere

Thus for the vacuum tank,

$$P_{cr} = \frac{0.365(28 \times 10^6)(0.5)^2}{(132)^2}$$

Such a high pressure indicates that small eccentricities in the spheroidalness of this section of the tank should not affect its vacuum sustaining capability.

Cylindrical Portion of the Vacuum Tank

The critical buckling pressure for a thin-shelled short cylinder is given as [2]

$$P_{cr} = 0.807 \frac{Et^2}{\ell r} \sqrt[4]{\frac{1}{1-\nu^2}^3 \frac{t^2}{r^2}}$$

(1) R. J. Roark, Formulas for Stress and Strain, 4th Ed., p 354, McGraw-Hill, New York, 1965.

(2) Ibid, p 354.

where in addition to those terms defined above

ℓ = the length of the tube

ν = Poisson's ratio

For the vacuum tank,

$$P_{cr} = 0.807 \frac{(28 \times 10^6)(0.5)^2}{} \sqrt[4]{\frac{1}{1-(0.32)^2}^3 \frac{0.5}{56}^2}$$

$$P_{cr} = 207 \text{ psi}$$

Again quite adequate.

The Beam Window

A conservative estimate of the critical buckling pressure for the 1/8 inch wall section of the beam window can be attained by treating it as a curved panel with its straight edges fixed and its curved edges free. This pressure is given by [3]

$$P_{cr} = \frac{Et^3(k^2-1)}{12^3(1-\nu^2)}$$

(3) Ibid, p 354

where k^2 = factor dependent upon the half angle of the cylindrical section.

For the beam window,

$$P_{cr} = \frac{(28 \times 10^6)(0.125)^3(81 - 1)}{12(13.5)^3(1 - (0.32)^2)} = 165 \text{ psi}$$

Again adequate.

Thus, from the above the vacuum tank in its proposed configuration is structurally adequate to sustain a one atmosphere vacuum operational loading.

(8) APPENDIX A-1

BEAM WINDOW REINFORCEMENT

Treated as an "I" frame to determine the deflection at the center of the opening.

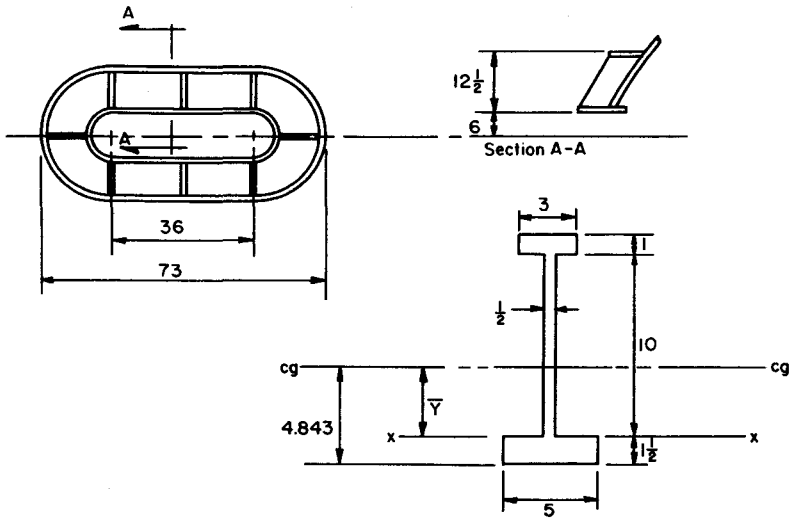

$$A = 5 + 3 + 7\frac{1}{2} = 15.5 \text{ in}^2$$

$$\bar{Y} = \frac{25 + 31.5 - 0.625 * 7.5}{15.5} = \frac{51.8}{15.5} = 3.343 \text{ in}$$

$$I_{cg} = I_{xx} - A\bar{Y}^2 = \frac{5 * 1.5^3}{3} + \frac{0.5 * 10^3}{3} + \frac{3 * 1^3}{12} + 3 * 10.5^2 - A\bar{Y}^2$$

$$= 503.3 - 173.2 = 330 \text{ in}^4$$

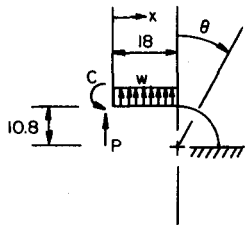

Using Castigliano's Theorem

$0 \leq x \leq 18, \quad d\ell = dx$ $\qquad$ $0 \leq \theta \leq \frac{\pi}{2}, \quad d\ell = 10.8\, d\theta$

$$M \begin{cases} Px \\ \frac{wx^2}{2} \\ C \end{cases} \qquad M \begin{cases} P(18 + 10.8 \sin\theta) \\ 18w(9 + 10.8 \sin\theta) \\ C \end{cases}$$

$$\frac{\partial M}{\partial P} \begin{cases} x \\ 0 \\ 0 \end{cases} \qquad \frac{\partial M}{\partial P} \begin{cases} 18 + 10.8 \sin\theta \\ 0 \\ 0 \end{cases}$$

$$\delta_p = \int_0^{18} \frac{\frac{\partial M}{\partial P} M\, d\ell}{EI} + \int_0^{\frac{\pi}{2}} \frac{\frac{\partial M}{\partial P} M\, d\ell}{EI}$$

Since, for symmetric loading, P = 0

$$\delta_p = \int_0^{18} \left(\frac{wx^3}{2} + Cx\right)\frac{dx}{EI} + \int_0^{\frac{\pi}{2}} (18+10.8\sin\theta)(162w + 18 * 10.8w\sin\theta + C)\frac{10.8d\theta}{EI}$$

$$18 * 10.8 = 194.4$$

$$10.8^2 = 116.64$$

$$194.4 * 162w + 194.4^2 w \sin\theta + 194.4C + 116.64 * 162w \sin\theta$$

$$+ 116.64 * 194.4w \sin^2\theta + 116.64C \sin\theta$$

$$EI\ \delta_p = \int_0^{18} \frac{wx^4}{8} + \frac{Cx^2}{2}$$

$$+ \int_0^{\frac{\pi}{2}} 194.4 * 162W\,\theta - 194.4^2 w \cos\theta + 194.4C\,\theta$$

$$- 116.64 * 162w \cos\theta - \frac{116.64 * 194.4w \sin\theta \cos\theta}{2}$$

$$+ \frac{116.64 * 194.4w\,\theta}{2} - 116.64C \cos\theta$$

$$EI\ \delta_p = \frac{w18^4}{8} + C\,162 + 194.4 * 81\pi w + 194.4^2 w + \frac{194.4}{2} C$$

$$+ 116.64 * 162w + \frac{116.64 * 194.4w}{4} + 116.64C$$

$$EI\ \delta_p = 124947w + 376C$$

$$\frac{\partial M}{\partial C} \begin{cases} 0 \\ 0 \\ 1 \end{cases} \qquad \frac{\partial M}{\partial C} \begin{cases} 0 \\ 0 \\ 1 \end{cases}$$

$$\theta_c = \int_0^{18} \left(\frac{wx^2}{2} + C\right)\frac{dx}{EI} + \int_0^{\frac{\pi}{2}} (162W + 194.4w \sin\theta + C)10.8\,\frac{d\theta}{EI}$$

$$EI\ \theta_c = \int_0^{18} \frac{wx^3}{6} + Cx + \int_0^{\frac{\pi}{2}} 10.8 * 162w\,\theta - 10.8 * 194.4w \cos\theta + 10.8C\,\theta$$

$$EI\ \theta_c = 972w + 18C + 2748w + 2099.5w + 16.96C$$

with symmetry $\theta_c = 0$

$$\therefore \quad 0 = 5819.5w + 34.96C$$

Assuming a sphere radius of 132 inches and an internal pressure of 150 psi

$$w = \frac{Prt}{2T} = \frac{Pr}{2} = \frac{150 * 132}{2} = 9900\ \text{lb/in}$$

Then from the above equation,

$$C = -1.647971 * 10^6$$

The previous equation then becomes

$$\delta_p = \frac{1236.975300 - 376 * 1.647971}{29.5 * 330} = 0.063\ \text{in.}$$

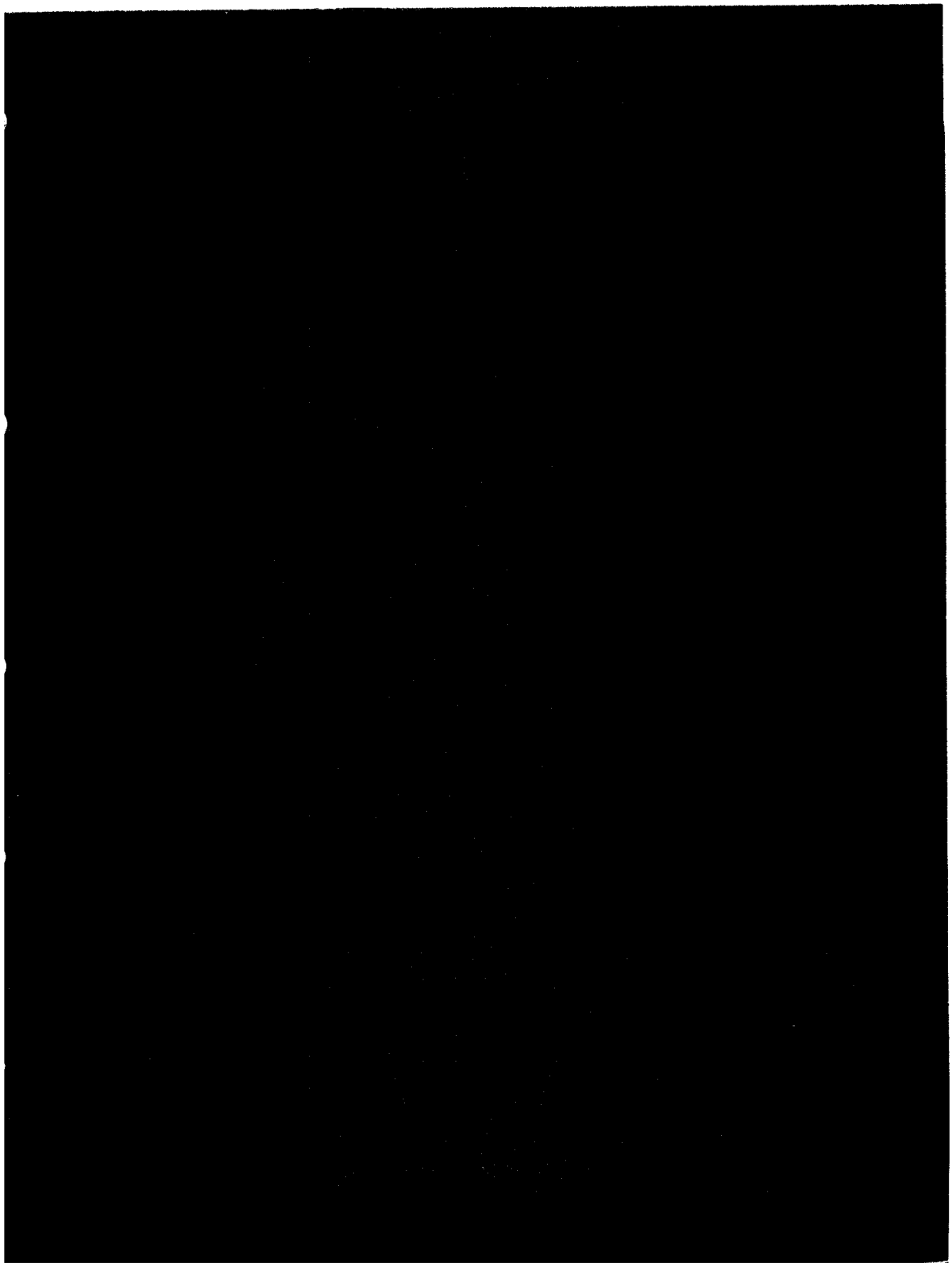

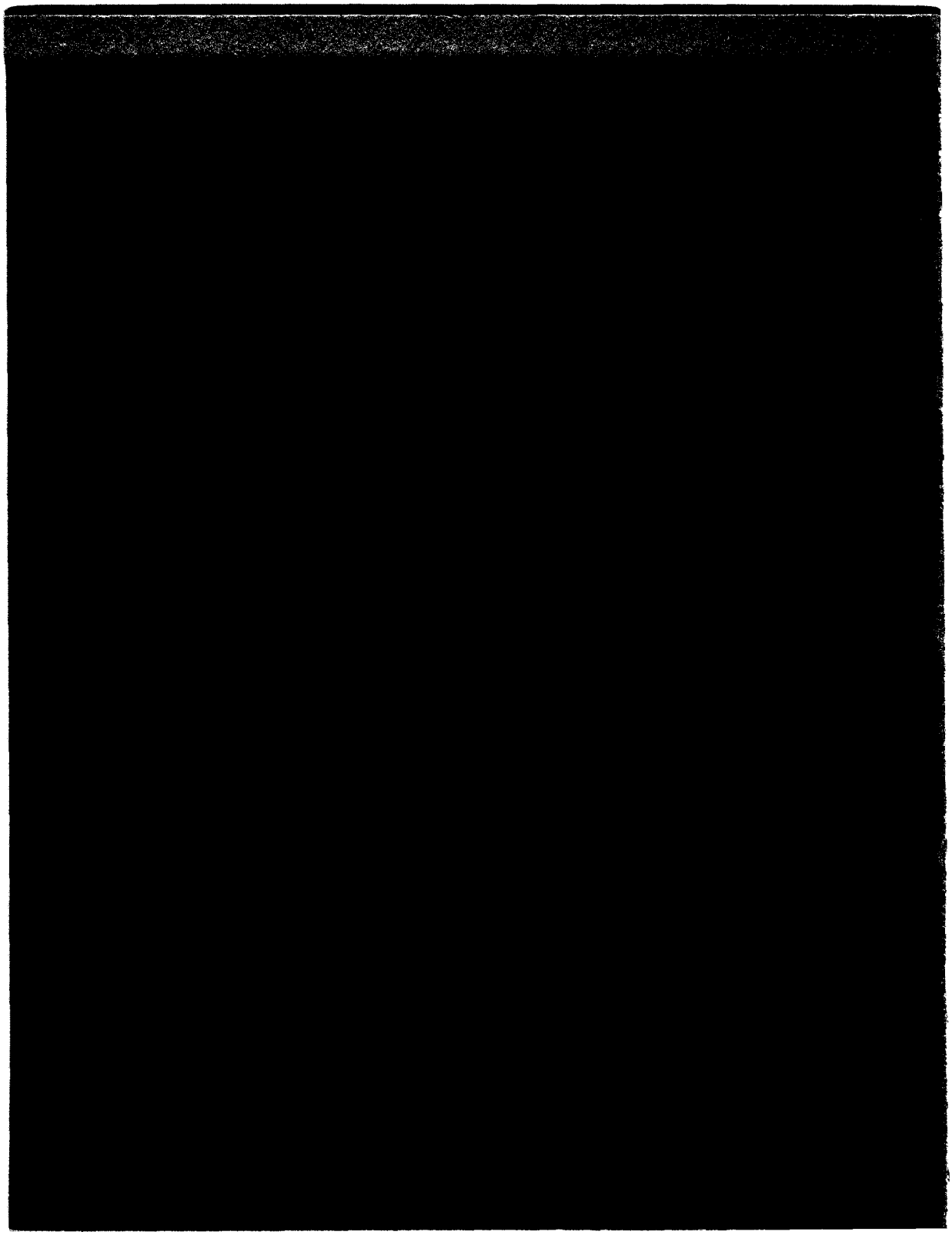

IV. EQUIPMENT

B. Failure Mode Analysis: LARGE RUPTURE OF BUBBLE CHAMBER WITH SPILLAGE OF LIQUID INTO THE VACUUM VESSEL

Prepared by

P. C. Vander Arend

TABLE OF CONTENTS

IV. EQUIPMENT

B. Failure Mode Analysis: Large Rupture of Bubble Chamber with Spillage of Liquid into the Vacuum Vessel

		Page
(1)	Introduction	49
(2)	Parameters Controlling Rate of Pressure Rise	50
(3)	Calculations	51
(4)	Conclusions and Recommendations	58

IV. B. FAILURE MODE ANALYSIS

LARGE RUPTURE OF THE BUBBLE CHAMBER WITH SPILLAGE OF LIQUID INTO THE VACUUM VESSEL

(1) INTRODUCTION

Consider a constant flow rate of 1,000 liters per second from the chamber through a large hole in the vicinity of the mid plane of the chamber. Liquid will continue to flow into the vacuum space for a period of some 20 seconds after which the chamber contains a mixture of liquid and gas equivalent to 10,000 liters or one-third of the original mass in the chamber.

Obviously the pressure in the vacuum vessel will increase. The question is how fast and at what rate does gas have to be released in order to prevent overpressurization of the vacuum vessel. There are three different cases to be evaluated, as follows:

a. The chamber is filled with liquid hydrogen at a temperature of 25.7°K and a static pressure of 65 psig.

b. The chamber is filled with liquid deuterium at a temperature of 31.7°K and a static pressure of 100 psig.

c. The chamber is filled with a mixture of hydrogen and neon with a vapor pressure of 100 psig and a static pressure of 120 psig.

In each case the same basic parameters determine the rate of liquid vaporization and pressure increase in the vacuum vessel. Section II of the report discusses these parameters and their relative importance.

Section III contains the results of a crude analysis for the case of pure deuterium. The analysis lends itself to a computer program in which the important and controlling parameters may be varied.

Section IV contains conclusions drawn from the crude analysis and recommendations for the design of the bubble chamber system to enhance the overall safety of the system and prevent overpressurization and major damage to components of the bubble chamber.

(2) PARAMETERS CONTROLLING RATE OF PRESSURE RISE

In general, the following events occur when a large hole connects the bubble chamber volume with the vacuum vessel surrounding the chamber:

1. The pressure in the chamber immediately decreases to the vapor pressure of the liquid.

2. At a spillage rate of 1,000 liters/sec., the rate of increase of the specific volume of the liquid mass is approximately ten times slower than the rate of increase during the expansion cycle of the chamber. Boiling will take place, and for lack of data, it has been assumed that the rate of gas generation is fast enough to maintain the liquid in the chamber at the saturation point. Throughout the first 10-20 seconds the pressure in the chamber will decay little and it has been assumed that the liquid spilling into the vacuum space has a temperature of 31.7°K (deuterium) and is saturated.

3. The rate of spillage into the vacuum space has been assumed to be constant over a period of 20 seconds, since calculations indicate that the pressure in the vacuum space after 20 seconds is still low relative to chamber pressure.

4. Liquid, upon entering the vacuum space, flashes to equilibrium conditions. Initially liquid flashes to vacuum and in the process the remaining liquid will be very cold.

5. Liquid, upon entering the vacuum space, sprays on warm walls of vacuum vessel and magnet reservoir. Wherever liquid contacts these walls, heat transfer resulting in further evaporation of liquid takes place. The rate of heat transfer has been assumed to be 12 W/cm^2. This is the film boiling rate of liquid hydrogen on warm surfaces (International Advances in Cryogenic Engineering, Vol. 10B, Page 325). The total sprayed surface area has been chosen arbitrarily and may be varied during future studies. The surface area chosen for this analysis is 250 $feet^2$.

6. Liquid sprayed in the vacuum vessel will run off warm walls of vacuum and magnet vessel into the lower part of the vacuum chamber. The

surface thus wetted will give up heat to the liquid at a rate of 12 W/cm^2. The surface area involved is a function of the spray pattern of the hole in the bubble chamber and may be varied in future studies. The surface area chosen for this analysis is 140 $feet^2$.

7. Liquid accumulated in the bottom of the vacuum vessel. The wetted surface area increases with time and transfers heat to the liquid at a rate of 12 W/cm^2.

8. Heat transfer between gas and liquid droplets in the vacuum vessel is assumed to be negligible because the temperature of the gas surrounding the droplets rises at a very low rate.

9. Heat transfer between gas and warm walls of vacuum vessel and magnet reservoir has been assumed to take place at a rate of .5 W/cm^2. This rate may be varied in future studies. Heat transfer between environment and the wall of the vacuum vessel is negligible for event taking place in the first 20-30 seconds. The rate of cooling of the walls is of the order of .05 °K/sec. for heat transfer to gas and 3 °K/sec. for heat transfer to liquid (1/2-inch thick plate).

10. The gas present in the vacuum space is compressed when more liquid is spilled and flashed. The compression is adiabatic and the temperature rise and specific volume is calculated on this basis.

A crude step wise calculation has been made using the criteria set forth to determine qualitatively which parameters are important in controlling the rate of pressure rise in the vacuum chamber and the rate at which gas needs to be vented in order to maintain a constant pressure.

(3) CALCULATIONS

1. Assumptions: Chamber volume is 30,000 liters. Vacuum chamber void volume is 100,000 liters. Surface area of magnet vessel exposed to chamber vacuum vessel is 1,160 $feet^2$. Surface area of chamber vacuum vessel at ambient temperature is 1,520 $feet^2$.

2. Cooling of warm walls in liquid contact: The wall opposite the postulated break in the chamber consists, in general, of a 1/2-inch thick

stainless steel plate. At ambient temperature, the specific heat of the steel is .44 Joules/g °K. The weight of the plate is 10 g/cm^2. Rate of cooling of plate is 2.7 °K/sec. at 300°K and is essentially constant for the first 50°K. Consequently, rate of heat transfer is constant for a period of 20 seconds. Rate of cooling of thicker plates is slower and rate of heat transfer is also constant for a period of 20 seconds.

3. Cooling of warm walls in gas contact: The rate of cooling has been assumed to be .5 W/cm^2. The rate of temperature decrease of a 1/2-inch thick plate is .11 °K/sec. For the duration of the event, the wall will be assumed to be at a constant temperature and the rate of heat transfer to the gas constant.

4. From 2 and 3 above it is evident that heat transfer between environment (air) and the vacuum wall is negligible.

5. Heat transfer to chamber during the spill: The chamber consists of a 1-inch thick stainless steel vessel. With loss of vacuum due to a liquid spill, the vacuum space will be filled with a gas of a temperature of 20-40°K. If we assume that the outside of the chamber wall would be at 30°K, the rate of heat transfer through the wall will be $\frac{.03 \times 10}{2.54} = .12$ W/cm^2. Total heat flux to the chamber fluid is then 130 KW. To maintain chamber pressure at a constant value of 6 atm, rate of vapor generation during the spill needs to be 13,600 g/sec. Heat required to vaporize this is 300 KW, considerably in excess of the heat supplied through the wall of the chamber. Consequently, pressure will decay slowly.

6. Pressure in vacuum chamber rises from 0 to .2 atm: During this period, the following happens:

a. Rate of flashing of liquid from chamber is 31.4 percent or 10,720 gmol/sec.

b. Rate of vapor generation from splashing on warm walls is 3,400 gmol/sec.

c. Rate of vapor generation from sump is 560 gmol/sec.

d. Total rate of vapor generation is 14, 680 gmol/sec.

e. Rate of liquid accumulation in bottom is 19,500 gmol/sec.

f. Rate of heat transfer to gas is 1.07×10^6 watts.

g. Rate of enthalpy rise of gas is 72.4 Joules/gmol.

After .75 seconds, total amount of vapor is 11,000 gmol. Density of this vapor is .110 gmol/liter. Temperature of gas is 22.5°K. From heat transfer to gas from walls gas temperature rises from 19 to 23.3°K. Liquid accumulated in bottom of vacuum vessel is 14,600 gmol (340 liters at .2 atm). Depth of liquid is approximately 2-inches.

7. Pressure in vacuum chamber rises from .2 to .4 atm: During this period, the following happens:

a. Rate of flashing of liquid from chamber is 28 percent or 9,600 gmol/sec.

b. Rate of vapor generation from splashing on warm walls is 3,400 gmol/sec.

c. Rate of vapor generation from sump is 600 gmol/sec.

d. Total rate of vapor generation is 13,600 gmol/sec.

e. Rate of liquid accumulation is 20,500 gmol/sec.

f. Rate of heat transfer to gas is 1.07×10^6 W.

g. Enthalpy gain of gas from compression is 160 Joules/gmol.

Time to reach .4 atm from .2 atm is approximately .45 seconds. After 1.2 Seconds, total amount of vapor is 17,100 gmol. Density of this vapor is .171 gmol/liter. Temperature of gas is 28.5°K. Liquid accumulated in bottom of vacuum vessel is 24,000 gmol. Depth of liquid is approximately 4-inches (570 liters).

8. Pressure in vacuum chamber rises from .4 to .6 atm: During this period, the following happens:

a. Rate of flashing of liquid from chamber is 25.5 percent or 8,700 gmol/sec.

b. Rate of vapor generation from splashing on warm walls is 3,400 gmol/sec.

c. Rate of vapor generation from sump is 660 gmol/sec.

d. Total rate of vapor generation is 12,760 gmol/sec.

e. Rate of liquid accumulation is 21,380 gmol/sec.

f. Enthalpy gain of gas from compression (.4 to .6 atm) is 90 Joules/gmol.

Time to reach .6 atm from .4 atm is approximately .5 seconds. After 1.7 seconds, total amount of vapor is 23,500 gmoles. Density of this vapor is .235 gmol/liter. Temperature of gas is 31.5°K. Liquid accumulated in bottom of vacuum vessel is 34,500 gmol. Depth of liquid is approximately 6-inches (830 liters).

9. Pressure in vacuum chamber rises from .6 to .8 atm: During this period, the following happens:

a. Rate of flashing of liquid from chamber is 23.5 percent or 8,050 gmol/sec.

b. Rate of vapor generation from splashing on warm walls is 3,400 gmol/sec.

c. Rate of vapor generation from sump is 725 gmol/sec.

d. Total rate of vapor generation is 12,175 gmol/sec.

e. Rate of liquid accumulation is 22,000 gmol/sec.

f. Enthalpy gain of gas from compression (.6 to .8 atm) is 80 Joules/gmol.

Time to reach .8 atm from .6 atm is approximately .5 seconds. After 2.2 seconds, total amount of vapor is 29,600 gmol. Density of this vapor is .296 gmol/liter. Temperature of the gas is 34°K. Liquid accumulated in bottom of vacuum vessel is 45,400 gmol. Depth of liquid is approximately 7.5-inches (1,100 liters).

10. Pressure in vacuum chamber rises from .8 to 1.0 atm. During this period the following happens:

a. Rate of flashing of liquid from chamber is 22 percent or 7,500 gmol/sec.

b. Rate of vapor generation from splashing on warm walls is 3,400 gmol/sec.

c. Rate of vapor generation from sump is 800 gmol/sec.

d. Total rate of vapor generation is 11,700 gmol/sec.

e. Rate of liquid accumulation is 22,450 gmol/sec.

f. Enthalpy gain of gas from compression (.8 to 1.0 atm) is 65 Joules/gmol.

Time to reach 1.0 atm from .8 is approximately .5 seconds. After 2.7 seconds, total amount of vapor is 35,500 gmol/liter. Temperature of the gas is 35.5°K. Liquid accumulated in bottom of vacuum vessel is 56,600 gmol. Depth of liquid is approximately 9.5-inches (1,400 liters).

11. Pressure in vacuum chamber rises from 1.0 to 1.5 atm. During this period, the following happens:

a. Rate of flashing of liquid from chamber is 19 percent or 6,500 gmol/sec.

b. Rate of vapor generation from splashing on warm walls is 3,400 gmol/sec.

c. Rate of vapor generation from sump is 880 gmol/sec.

d. Total rate of vapor generation is 10,780 gmol/sec.

e. Rate of liquid accumulation is 23,400 gmol/sec.

f. Enthalpy gain of gas from compression (1.0 to 1.5 atm) is 160 Joules/gmol.

Time to reach 1.5 atm from 1.0 atm is approximately 1.3 seconds. After 4.0 seconds, total amount of vapor is 44,000 gmol. Density of this vapor is .44 gmol/liter. Temperature of the gas is 42.5°K. Liquid accumulated in bottom of vacuum vessel is 92,600 gmol. Depth of liquid is approximately 15-inches (2,300 liters).

12. Pressure in vacuum chamber rises from 1.5 to 2.0 atm. During this period the following happens:

a. Rate of flashing of liquid from chamber is 16.5 percent or 5,630 gmol/sec.

b. Rate of vapor generation from splashing on warm walls is 3,400 gmol/sec.

c. Rate of vapor generation from sump is 950 gmol/sec.

d. Total rate of vapor generation is 9,980 gmol/sec.

e. Rate of liquid accumulation is 24,200 gmol/sec.

f. Enthalpy gain of gas from compression (1.5 to 2.0 atm) is 84 Joules/gmol.

Time to reach 2.0 atm from 1.5 atm is approximately 1.2 seconds. After 5.2 seconds, total amount of vapor is 56,000 gmol. Density of this vapor is .56 gmol/liter. Temperature of the gas is 45°K. Liquid accumulated in bottom of vacuum vessel is 121,500 gmol. Depth of liquid is approximately 24.5-inches (3,150 liters).

13. If we decide to hold the pressure constant from this time on, vapor must leave the system at the rate it is generated. This rate is of the order of 10,000 to 11,000 gmol/sec., dependent on the total wetted surface area in the bottom of the vacuum tank. The temperature of the gas leaving the system is determined from a heat balance. Rate of heat transfer to the gas is 1.07×10^6 W.

Enthalpy gain of gas is approximately 100 Joules/gmol. Gas is generated at 26.3°K and H = 707 J/gmol. Gas leaves at 30.5°K and H = 807 J/gmol.

This rate of venting continues until the liquid level in the chamber drops below the hole in the chamber wall. If the hole is in the area of the beam window, some 15,000 liters will have spilled and elapsed time is 15 seconds. For some 10 seconds the rate of venting is approximately 10,000 to 11,000 gmol/sec.

14. When liquid stops spilling into the vacuum space, pressure in the chamber starts decaying. If we assume sonic velocity and a hole in the chamber equivalent to 50 cm^2 cross-sectional area, the flow rate from the chamber at time 15 seconds will be $\frac{50 \times 4 \times 10^4 \times 1.64}{1000} = 3,280$ gmol/sec. The rate of vaporization in the vacuum vessel at this time will be some 2,460 gmol/sec. (250 $ft.^2$ of wetted surface area total). The rate of vapor addition to the system is then 5,740 gmol/sec. The vent system now handles this flow rate at a somewhat higher temperature of 34°K. From time= 15 seconds the flow rate in the vent system will

decrease and the pressure in the vacuum system will decay.

15. Vent duct: Maximum flow rate handles is 11,000 gmol/sec. Inlet pressure is 2 atm. Temperature is 30.5°K. Density is .88 gmol/liter.

Use a 16-inch pipe with an internal diameter of 16-inches. Velocity at entrance of pipe is 9,600 cm/sec., if the pipe is contoured slightly to prevent constriction of flow due to sharp edge. This pressure drop is 4.7 psig. Steady state pressure drop in duct.

Mass flow rate $g = 250{,}000$ lbs./hr. ft.^{2}

$\mu = .4 \times 10^{-2}$ lbs./ft.hr.

$d_h = 1.33$ ft.

$Re = 8.1 \times 10^7$

$f = .0012$

$j = .0006$

$$\frac{\Delta P}{L} = \frac{.0012 \times (69.5)^2}{193 \times .18 \times 16} = .0105 \text{ psig}$$

Heat transfer coefficient in duct is:

$$H = \frac{J \; cp \; g}{Pr^{2/3}} = \frac{.0006 \times 1.4 \times 250000}{.8} =$$

$= 260$ Btu/hr.ft.^{2} °F

The temperature of the gas emerging from the vent duct is determined by $\ln K = \frac{h \; A}{cp \; W}$ where

$K = \frac{Tw - T \text{ in}}{Tw - T \text{ out}}$

Tw = Wall Temperature

T in = Gas Temperature at Inlet

T out = Gas Temperature at Outlet

A = Surface Area of Pipe in Ft.^{2}

W = Weight Flow Through Pipe in lbs./hr.

cp = Spec. Heat of Gas in Btu/lb. °F

h = Heat transfer Coefficient in Btu/hr. ft.^{2} °F

For 100 feet of pipe:

$$\ln K = \frac{210 \times 100 \times 4.17}{1.4 \times 349000} = .18$$

$K = 1.2$

At the end of 100 feet of pipe, the gas temperature will be 75°K. The amount of heat transfer is: 11,000 x (1993 - 800) = 1.32×10^7 W. The total amount of heat to be removed from 100 feet of pipe (1/4-inch wall) is 1.5×10^8 Joules.

It takes some 10-15 seconds to cool the pipe and pressure drop will be approximately .02 psig/ft.

(4) CONCLUSIONS AND RECOMMENDATIONS

Conclusions

The calculations indicate the following:

1. Initially gas is generated primarily from flashing of relatively warm liquid. After some liquid accumulates in the vacuum space, the rate of gas generation decreases, but the fraction due to vaporization of liquid in the vacuum space increases. With a pressure of approximately 2 atm, the fraction of gas generated from flashing is .6.

2. Heat transfer to the liquid in the vacuum space is large and is a linear function of the wetted surface area. Heat capacity of the walls is large, and for a period of 30-40 seconds, the reduction in temperature of the walls does not result in a significant decrease of the rate of vaporization.

3. The rate of pressure rise will be nearly proportional to the rate of spillage. However, the final pressure reached is practically independent of the rate of spillage and is determined by the total quantity of liquid spilled from the chamber. With some 15,000-16,000 liters spilled, a pressure of approximately 5 atm will be reached.

4. If the leak is at the mid plane of the chamber, the rate of pressure rise will slow down, after some 15,000 liters have been spilled and will decay with time. The time constant needs to be determined when more accurate calculations are made.

5. The vacuum vessel wall will cool rather slowly and frost will appear only at places when liquid is in direct contact with the wall. Parts of the wall in contact with cold gas will only show frost after minutes, except for the area directly around the emergency relief vent system.

6. A relatively small emergency relief system will be adequate to protect the vacuum vessel and magnet reservoir from damage. The relief valve needs to be a spring-loaded swing check which will reseat after the venting subsides to prevent air from entering.

7. Liquid remaining in the chamber will be evaporating at a low rate and a large fraction of it may be transferred to the storage dewar.

Recommendations

1. Carry out more exact calculations with the help of a computer.

2. Provide the chamber vacuum vessel with a relief system, consisting of a pipe of 16-inch minimum diameter and swing check-relief valve. This system will be capable of maintaining a pressure of 15 psig or less in the vacuum vessel.

3. To reduce the rate at which pressure increases, some warm walls opposite potential large leaks might be covered with a material of low thermal conductivity and diffusivity. This material needs to be installed inside the vacuum vessel. In lieu of a low thermal conductivity material, thin gauge metal sheets in poor thermal contact with the warm walls may be used.

4. Liquid will accumulate in the bottom cylinder of the vacuum vessel. All O-rings in this area need to be backed with metal rings which will not lose their ductility at low temperature. To reduce the rate of vapor generation from this area, a thin metal liner with vapor trap will effectively reduce the rate of heat transfer and the generation of large quantities of liquid air or the outside surface of the cylinder after the cylinder has been cooled to 80°K.

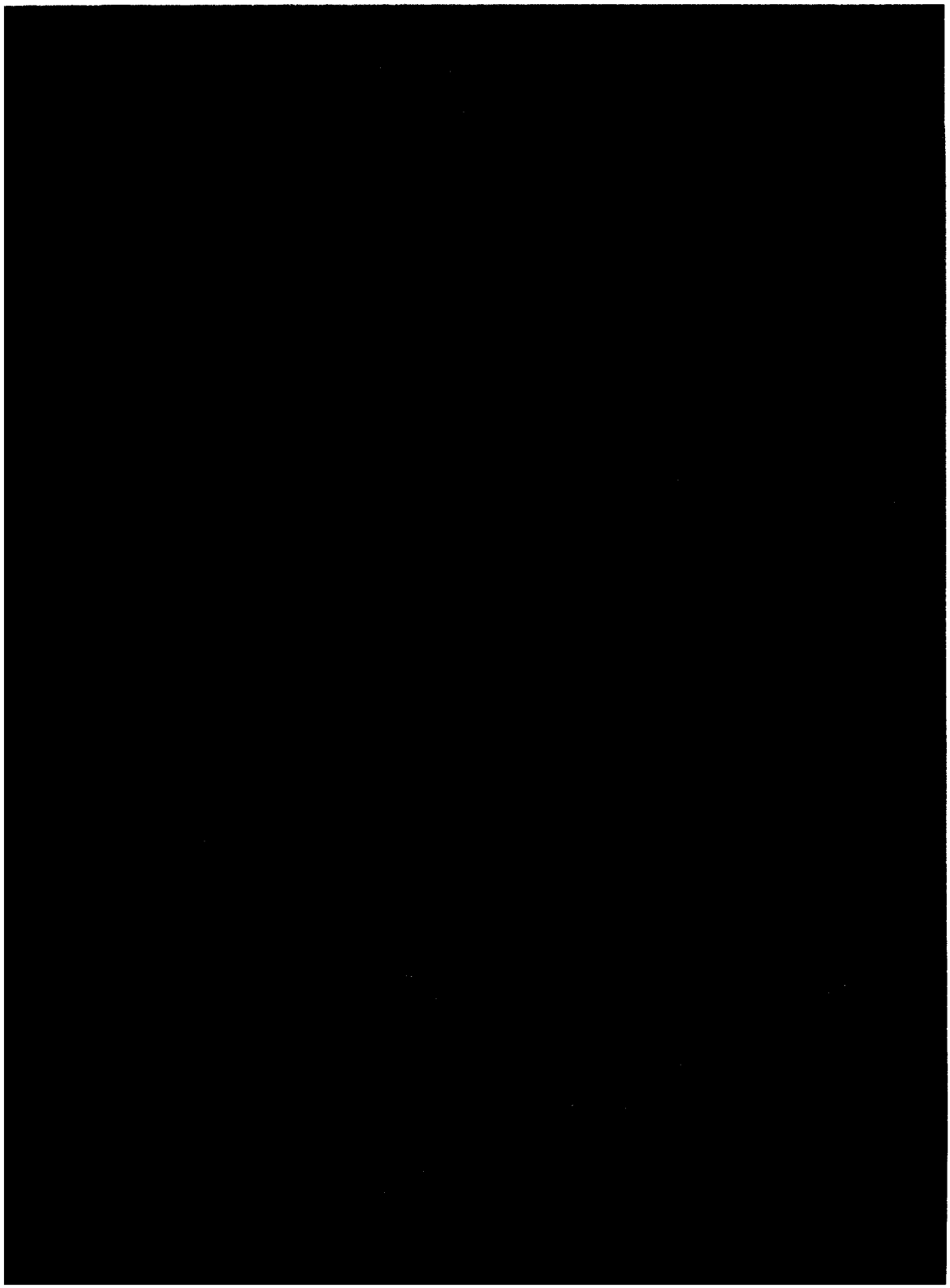

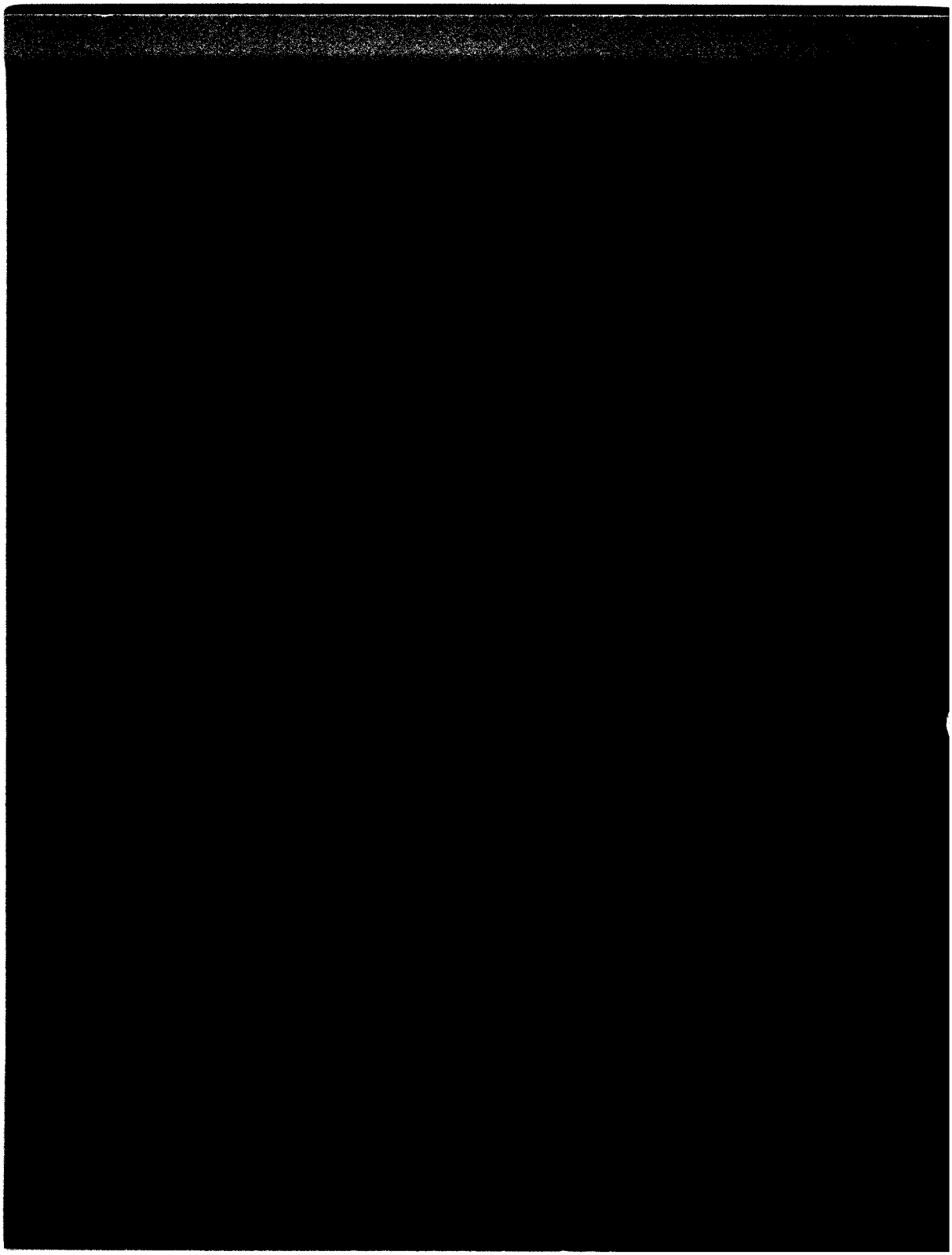

IV. EQUIPMENT

C. Chamber Vessel

1. User's Design Specification

Prepared by

Battelle Memorial Institute
and National Accelerator Laboratory

TABLE OF CONTENTS

IV. EQUIPMENT

C. Chamber Vessel

1. User's Design Report

		Page
1.0	General - Certification	61
2.0	Function	62
3.0	Design	63
4.0	Materials	67
5.0	Fatigue Analysis Requirement	67
Attachments:		
A.	Schematic Drawing of Bubble Chamber	69
B.	Time-Pressure History for Both Zones for Liquid Hydrogen Operation	70
C.	Time-Pressure History for Both Zones for Liquid Deuterium Operation	71
D.	Time-Pressure History for Both Zones for Liquid Neon Operation	72
E.	Extract of Pertinent Sections of the Uniform Building Code Regarding Earthquake Loadings	73
F.	Extract of Paper: Cryogenic Fasteners	85
	Extract of Data Sheet: Allegheny Ludlum Steel Corporation	89

1.0 GENERAL

1.1 This document constitutes the User's Design Specification required by Paragraphs A-301.1 (a), (b), (c) and A-301.2 of the ASME Boiler and Pressure Vessel Code, Section VIII, Pressure Vessels, Division 2 - Alternate Rules, for the 30,000 Liter capacity bubble chamber to be installed as part of a bubble chamber complex at the National Accelerator Laboratory, Batavia, Illinois.

1.2 Certification (A-301.2): The undersigned, a registered Professional Engineer competent in the field of design of pressure vessels and related systems, certifies that this User's Design Specification complies with the requirements of Paragraphs A-301.1 (a), (b), and (c) of the ASME Boiler and Pressure Vessel Code, Section VIII, Pressure Vessels, Division 2 - Alternative Rules, as detailed in the 1971 edition and is correct and complete with respect to functions and operating conditions as required to provide a complete basis for design, construction, and certification inspection in accordance with the aforesaid code.

Joseph Lastinger
Signature

State of Ohio E-032243
Registration, State and Number

2.0 FUNCTION

2.1 General Description: The vessel to be fabricated, inspected and tested in compliance with this User's Design Specification comprises the central, main pressure containing vessel as shown in the attached schematic drawing. This pressure vessel, is to contain, at different times, liquid hydrogen, liquid deuterium and liquid neon. The liquids in the chamber are initially under a sufficient pressure to keep them at the saturated fluid state. A piston at the bottom of the chamber, as shown in the aforementioned drawing, controls this pressure and during operation periodically reduces the pressure to a point at which the fluid becomes super heated liquid. At this time the particles emitted from a particle accelerator enter the chamber and cause the fluid to locally boil on the paths that they have followed. This boiling leaves a discernible track of tiny bubbles. By recording the particle tracks analysis of the type of particle and particle interactions with the fluid is possible. During the pulsing period, which varies dependent upon the fluid being employed but could be as low as 0.040 seconds duration, the pressure changes impose severe dynamic loads on the system.

This pressure system must be capable of sustaining many millions of pressure cycles during its design life expectancy.

Because of the large amounts of liquid hydrogen contained by the vessel, prevention of a significant leak in the vessel becomes of prime importance.

2.2 Design Basis: The design, material, fabrication, inspection and testing of this vessel shall be in accordance with the following:

2.2.1 This specification with the attachments detailed herein.

2.2.2 The ASME Code, Section VIII, Division 2, including those paragraphs referenced in AD-110 (loadings).

2.2.3 The ASME Code, Section IX, Welding Qualifications.

2.2.4 This vessel shall bear the ASME Code stamp as required by ASME Code, Section VIII, Division 2, Part AS.

3.0 DESIGN

3.1 General: This vessel is to be designed in accordance with the ASME Boiler and Pressure Vessel Code, Section VIII, Division 2, as supplemented by this User's Design Specification.

3.2 Mechanical Design Details.

3.2.1 All butt welds, nozzle welds, and boss welds shall be of full penetration design.

3.2.2 All welds in critical areas which are to be determined by a detailed stress analysis are to be ground smooth, flush and imperfections removed. Welds in all other areas shall be ground smooth.

3.2.3 All points along the line of intersection of plates of different thicknesses must have machined or ground fillets of generous radii, or be designed with tapered transitions so as to minimize areas of local stress concentration.

3.2.4 All reentrant corners must have machined fillets of generous radii so as to minimize areas of local stress concentration.

3.2.5 Samples of all base materials and welds must be subjected to Charpy impact tests as specified by Paragraphs AM-204, AM-211, and AM-213, of the ASME Code Section VIII, Division 2, and must meet the minimum standards set therein.

3.3 Loadings, Operational: The following details the loadings to which the vessel shall be subjected.

3.3.1 Temperature - No significant thermal gradients through the wall of the vessel or along the meridional generator of the vessel should exist.

3.3.1.1 The steady state temperature of the vessel material for operation with liquid hydrogen as the pressurized fluid is $\sim -415^{\circ}$ F.

3.3.1.2 The steady state temperature of the vessel material for operation with liquid deterium as the pressurized fluid is $\sim -405^{\circ}$ F.

3.3.1.3 The steady state temperature of the vessel material for operation with liquid neon as the pressurized fluid is $\sim -400^{\circ}$ F.

3.3.1.4 The actual chamber and liquid temperature may vary by as much as $\pm 5^{\circ}$F during operation.

3.3.2 The basic weight of the vessel, empty of the pressurizing fluid is approximately 56,000 lbs.

3.3.3 The density of pressurizing fluids under their maximum design pressures are as follows:

3.3.3.1 Liquid hydrogen - 4.4 lbs/ft^3

3.3.3.2 Liquid deuterium - 8.8 lbs/ft^3

3.3.3.3 Liquid neon - 75 lbs/ft^3

3.3.4 The dead weight of the piston is supported by a structure outside of the vessel and thus poses no such load on the vessel proper.

3.3.5 The dead weight of each of the six camera nozzles, shown in the attached schematic drawing, plus the weight of the nozzle internals, plus the weight effect of the magnetic field acting upon them totals approximately 6,500 pounds for each nozzle.

3.3.6 Pressure loadings - The pressure loadings for each type of pressurizing fluid are cyclic in nature and the vessel is expected to undergo at least 10^7 cycles of operation during its lifetime. The exact number of cycles of operation for each pressurizing fluid are unknown except that they number in the millions for each type. Because the piston is the pressure activation device there will be two (2) pressure zones in the vessel during pulsing operation, above the piston and below the piston. For each pressurizing fluid the piston is initially maintained in an equilibrium position such that the pressure in the two volumes are equal. The piston is pulled downward, lowering the pressure in the volume above the piston and raising it in the volume below it. The piston is then returned to the equilibrium position. The time-pressure history for one cycle of pressure variations in both pressure zones are:

3.3.6.1 Time-pressure history for liquid hydrogen operation; see Attachment B.

3.3.6.2 Time-pressure history for liquid deuterium operation; see Attachment C.

3.3.6.3 Time-pressure history for liquid neon operation; see Attachment D.

3.3.6.4 During operation the outside of the vessel will be a 0 psia pressure, effectively. All time-pressure histories shown in Attachments B, C, and D are in terms of absolute pressure.

3.3.7 All piping and external fixtures are to be connected to the vessel by flexible fittings or bellows, thus no external loads need be considered.

3.3.8 The vessel is to be supported by three (3) sets of two (2) closely spaced legs, the sets spaced 120° apart. This nonuniform and nonsymmetric sypport system must be analyzed in detail to ensure its adequacy from both the viewpoints of its support ability and its effect on the local stresses in the support ring and skirt of the vessel.

3.3.9 The vessel shall at all times during its operational life be housed inside a building. Thus snow and wind loadings need not be considered.

3.4 Loadings, Upset: The only upset loading condition that need be considered is that caused by the event of an earthquake. There is no requirement that the system remain operational during earthquake; the only requirement being that the main pressure boundary is not significantly broached.

The buildings and other structures to be erected at Batavia, Illinois, as part of the National Accelerator Laboratory, are being designed and constructed in accordance with the "Uniform Building Code", 1970 Edition, Volume I which contains the pertinent requirements as regards earthquake loadings. These pertinent sections are shown extracted in Attachment E. Applying these requirements to the design of the main pressure vessel of the bubble chamber and its support system it is determined that a separate seismic analysis is not required. This is based on the opinion that the dynamic loads to be imposed on the bubble chamber during operation are in excess of those which may be induced by the type of earthquake which may occur in the geographic zone in which the vessel is to be installed.

4.0 MATERIALS

4.1 Main Body of Vessel: The main body of the vessel shall be fabricated from 316L stainless steel, ASME Code Section II, Part A-Ferrous, Specification No. SA-240, unless otherwise noted by user.

4.2 The camera nozzles of the vessel shall be fabricated from CF-3M, Specification No. SA-351.

4.3 The bolts to be used in the vessel shall be fabricated from A-286 stainless steel, ASME Code Section II, Part A-Ferrous, Specification No. SA-453, Grade 660.

4.4 The weld rod and welding techniques are to be specified by the fabricator and agreed to by the user on the basis of achieving a sound weld and meeting the impact test requirements described in paragraph 3.2.5 above.

4.5 Additional available material data for the metals specified above, particularly when subjected to a cryogenic temperature environment, are shown in Attachment F. These and other data, such as that contained in National Bureau of Standards Monograph 13, "Mechanical Properties of Structural Materials at Low Temperatures", (not shown here), indicate that these materials exhibit improved strength, including fatigue properties, along with an increase in ductility and elongation, at the anticipated bubble chamber operation temperatures. However for the design of the bubble chamber, these property improvements shall not be used and the chamber shall be designed to meet the stress intensity requirements specified for these materials at room temperature as defined by Section VIII, Division 2.

5.0 FATIGUE ANALYSIS REQUIREMENT

5.1 Paragraph AD-160.2 "Rules to Determine Need for Fatigue Analysis of Integral Parts of Vessels", of ASME Code Section

VIII, Division 2, states that "A fatigue analysis need not be made provided all of Condition A or all of Condition B is met". The first part of Condition A is not met. This part requires that the number of expected pressure cycles where the full range of pressure variation exceeds 20 percent of the design pressure, together with other types of pressure variations, such as startup and shutdown, does not exceed 1000 cycles. As can be seen from Attachment D, in the liquid neon operation alone the pressure range exceeds 20 percent of the design pressure and millions of cycles are anticipated.

Condition B, (a) states that a fatigue analysis is not required if "The expected design number of full range pressure cycles, including startup and shutdown, does not exceed the number of cycles in the applicable fatigue curve of Appendix 5 corresponding to an S_a value of 3 times the S_m value found in the tables of design stress intensity values in Article M-6 for the material at the operating temperatures". First there are no applicable curves or tables for 316L at -423°F. Thus assuming room temperature, S_m for 316L from Article M-6 is 16,600 psi, 3 S_m thus equals 49,800 psi. From Figure 5-110.2 it can be seen that the allowable number of cycles for such an S_a (49,800 psi) is approximately 60,000 cycles. In excess of 10^7 cycles of actual operation are anticipated; thus Condition B is not met.

From the above it is concluded that a full fatigue evaluation of this vessel is required and must be made in accordance with Appendix 5 of Section VIII, Division 2. Sufficient information when coupled with the design details to be developed by the manufacturer, have been supplied in this User's Design Specification to allow such an analysis to be conducted.

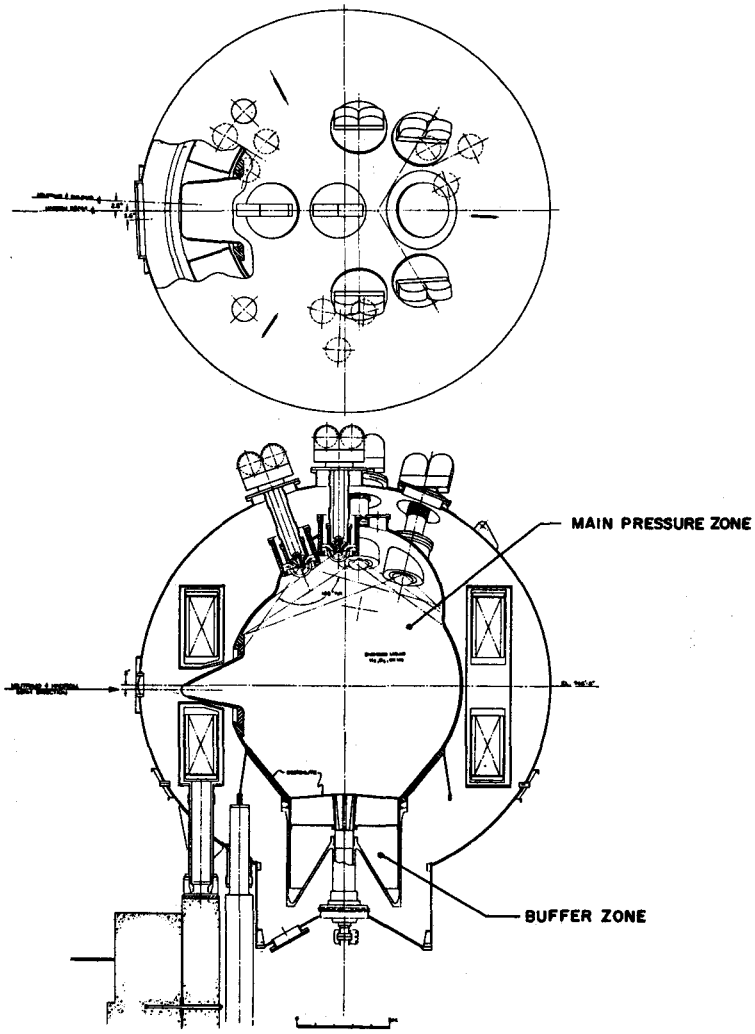

Attachment "A": Schematic Drawing of Bubble Chamber

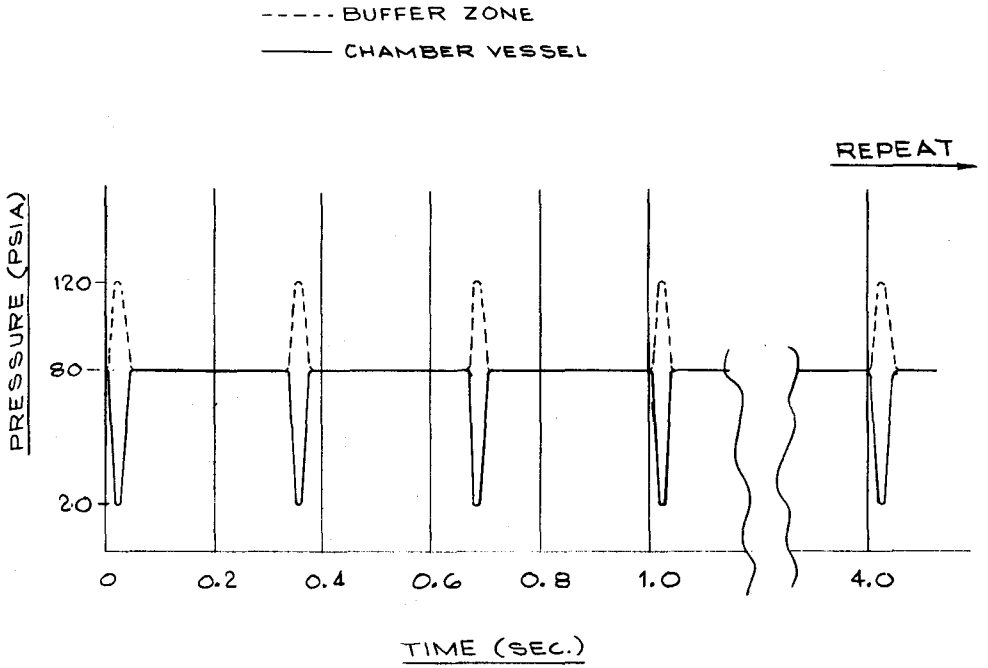

Attachment "B": Time-Pressure History For Both Zones For Liquid Hydrogen Operation

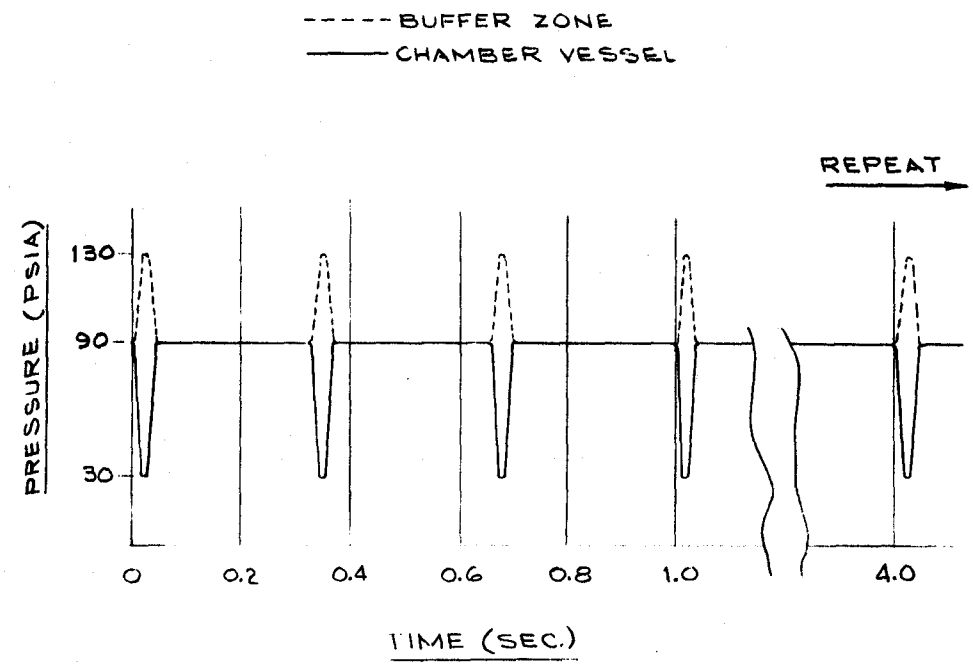

Attachment "C": Time-Pressure History For Both Zones For Liquid Deuterium Operation

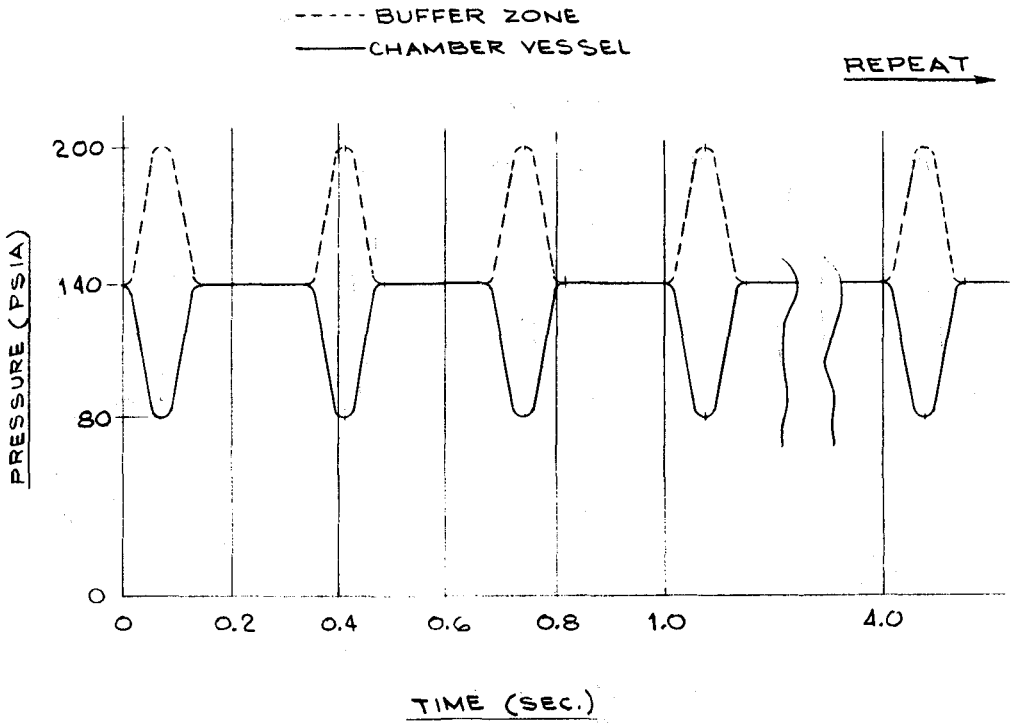

Attachment "D": Time-Pressure History For Both Zones For Liquid Neon Operation

ATTACHMENT "E"

Extract of Pertinent Sections of the

Uniform Building Code Regarding Earthquake Loadings

EARTHQUAKE REGULATIONS

Sec. 2314. (a) General. Every building or structure and every portion thereof shall be designed and constructed to resist stresses produced by lateral forces as provided in this Section. Stresses shall be calculated as the effect of a force applied horizontally at each floor or roof level above the foundation. The force shall be assumed to come from any horizontal direction.

The provisions of this Section apply to the structure as a unit and also to all parts thereof, including the structural frame or walls, floor and roof systems, and other structural features.

(b) Definitions. The following definitions apply only to the provisions of this Section:

BOX SYSTEM is a structural system without a complete vertical load-carrying space frame. In this system the required lateral forces are resisted by shear walls as hereinafter defined.

LATERAL FORCE RESISTING SYSTEM is that part of the structural system to which the lateral forces prescribed in Section 2314 (d) 1 are assigned.

SHEAR WALL is a wall designed to resist lateral forces parallel to the wall. Braced frames subjected primarily to axial stress shall be considered as shear walls for the purpose of this definition.

SPACE FRAME is a three-dimensional structural system composed of interconnected members, other than bearing walls, laterally supported so as to function as a complete self-contained unit with or without the aid of horizontal diaphragms or floor bracing systems.

SPACE FRAME-DUCTILE MOMENT RESISTING is a space frame-moment resisting complying with the requirements for a ductile moment resisting space frame as given in Section 2314 (j).

SPACE FRAME-MOMENT RESISTING is a vertical load carrying space frame in which the members and joints are capable of resisting design lateral forces by bending moments.

SPACE FRAME-VERTICAL LOAD-CARRYING is a space frame designed to carry all vertical loads.

(c) Symbols and Notations. The following symbols and notations apply only to the provisions of this Section.

C = Numerical coefficient for base shear as specified in Section 2314 (d) 1.

C_p = Numerical coefficient as specified in Section 2314 (d) 2 and as set forth in Table No. 23-I.

D = The dimension of the building in feet in a direction parallel to the applied forces.

D_s = The plan dimension of the vertical lateral force resisting system in feet.

F_i, F_n, F_x = Lateral force applied to level "i", "n", or "x", respectively

F_p = Lateral forces on the part of the structure and in the d direction under consideration.

F_t = That portion of "V" considered concentrated at the top of the structure, at the level "n". The remaining portion of the

total base shear "V" shall be distributed over the height of the structure including level "n" according to Formula (14-5).

h_i, h_n, h_x = Height in feet above the base to level "i", "n", or "x", respectively.

J = Numerical coefficient for base moment as specified in Section 2314 (h).

J_x = Numerical coefficient for overturning moment at level "x".

K = Numerical coefficient as set forth in Table No. 23-H.

Level i = Level of the structure referred to by the subscript "i".

Level n = That level which is uppermost in the main portion of the structure.

Level x = That level which is under design consideration.

M = Overturning moment at the base of the building or structure.

M_x = The overturning moment at level "x".

N = Total number of stories above exterior grade.

T = Fundamental period of vibration of the building or structure in seconds in the direction under consideration.

V = Total lateral load or shear at the base.

$$V = F_t + \sum_{i=1}^{n} F_i$$

where i = 1 designates first level above the base.

W = Total dead load including partitions using the actual weight of the partitions or the partition loading specified in Section 2302 (b).

$$W = \sum_{i=1}^{n} w_i$$

EXCEPTION: "W" shall be equal to the total dead load plus 25 percent of the floor live load in storage and warehouse occupancies.

w_i, w_x = That portion of "W" which is located at or is assigned to level "i" or "x" respectively.

W_p = The weight of a part or portion of a structure.

Z = Numerical coefficient dependent upon the zone as determined by the map on the inside back cover. For locations in Zone No. 1 "Z" shall be equal to one-fourth. For locations in Zone No. 2 "Z" shall be equal to one-half. For locations in Zone No. 3 "Z" shall be equal to one.

(d) Minimum Earthquake Forces for Structures. 1. Total lateral force and distribution of lateral force. Every structure shall be designed and constructed to withstand minimum total lateral seismic forces assumed to act nonconcurrently in the direction of each of the main axes of the structure in accordance with the following formula:

$$V = ZKCW \qquad (14\text{-}1)$$

The value of "K" shall be not less than that set forth in Table No. 23-H. The value of "C" shall be determined in accordance with the following formula:

$$C = \frac{0.05}{\sqrt[3]{D}} \qquad (14\text{-}2)$$

Except as provided in Table No. 23-I, the maximum value of "C" need not exceed 0.10. For all one- and two-story buildings the value of "C" shall be considered as 0.10.

"T" is the fundamental period of vibration of the structure in seconds in the direction under consideration. Properly substantiated

technical data for establishing the period "T" may be submitted. In the absence of such data, the value of "T" for buildings shall be determined by the following formula:

$$T = \frac{0.05h_n}{\sqrt{D}} \qquad (14\text{-}3)$$

EXCEPTION: In all buildings in which the lateral force resisting system consists of a moment-resisting space frame which resists 100 percent of the required lateral forces and which frame is not enclosed by or adjoined by more rigid elements which would tend to prevent the frame from resisting lateral forces:

$$T = 0.10N \qquad (14\text{-}3A)$$

The total lateral force "V" shall be distributed in the height of the structure in the following manner:

$$F_t = .004V\left(\frac{h_n}{D_s}\right)^2 \qquad (14\text{-}4)$$

"F_t" need not exceed 0.15 "V" and may be considered as 0 for values of $\left(\frac{h_n}{D_s}\right)$ 3 or less, and

$$F_s = \frac{(V - F_t)w_s h_s}{\sum_{i=1}^{n} w_i h_i} \qquad (14\text{-}5)$$

EXCEPTION: One- and two-story buildings shall have uniform distribution.

At each level designated as "x", the force "F" shall be applied over the area of the building in accordance with the mass distribution on that level.

2. Lateral force on parts or portions of buildings or other structures. Parts or portions of buildings or structures and their anchorage shall be designed for lateral forces in accordance with the following formula:

$$F_p = ZC_pW_p \qquad (14\text{-}6)$$

The values of "C_p" are set forth in Table No. 23-I. The distribution of these forces shall be according to the gravity loads pertaining thereto.

3. Pile foundations. Individual pile or caisson footings of every building or structure shall be interconnected by ties each of which can carry by tension and compression a horizontal force equal to 10 percent of the larger pile cap loading unless it can be demonstrated that equivalent restraint can be provided by other approved methods.

(e) Distribution of Horizontal Shear. Total shear in any horizontal plane shall be distributed to the various elements of the lateral force resisting system in proportion to their rigidities considering the rigidity of the horizontal bracing system or diaphragm.

Rigid elements that are assumed not to be part of the lateral force resisting system may be incorporated into buildings provided that their effect on the action of the system is considered and provided for in the design.

(f) Drift. Lateral deflections or drift of a story relative to its adjacent stories shall be considered in accordance with accepted engineering practice.

(g) Horizontal Torsional Moments. Provisions shall be made for the increase in shear resulting from the horizontal torsion due to an eccentricity between the center of mass and the center of rigidity. Negative torsional shears shall be neglected. Where the vertical resisting elements depend on diaphragm action for shear distribution at any level, the shear-resisting elements shall be capable of resisting a torsional moment assumed to be equivalent to the story shear acting with an eccentricity of not less than five percent of the maximum building dimension at that level.

(h) Overturning. Every building or structure shall be designed to resist the overturning effects caused by the wind forces and related requirements specified in Section 2308, or the earthquake forces specified in this Section, whichever governs.

EXCEPTION: The axial loads from earthquake forces on vertical elements and footings in every building or structure may be modified in accordance with the following provisions:

1. The overturning moment, "M", at the base of the building or structure shall be determined in accordance with the following formula:

$$M = J(F_t h_n + \sum_{i=1}^{n} F_i h_i) \qquad (14\text{-}7)$$

WHERE:

$$J = \frac{0.6}{\sqrt[3]{T}} \qquad (14\text{-}8)$$

The value of "J" need not be more than 1.00. For structures other than buildings the value of "J" shall be not less than 0.45.

2. The overturning moment, "M_x", at any level designated as "x" shall be determined in accordance with the following:

$$M_x = J_x[F_t(h_n - h_x) + \sum_{i=x}^{n} F_i(h_i - h_x)] \qquad (14\text{-}9)$$

WHERE:

$$J_x = J + (1-J)\left(\frac{h_x}{h_n}\right)^3 \qquad (14\text{-}10)$$

At any level the incremental changes of the design overturning moment, in the story under consideration, shall be distributed to the various resisting elements in the same proportion as the distribution of the shears in the resisting system. Where other vertical members are provided which are capable of partially resisting the overturning moments, a redistribution may be made to these members if framing members of sufficient strength and stiffness to transmit the required loads are provided.

Where a vertical resisting element is discontinuous, the overturning moment carried by the lowest story of that element shall be carried down as loads to the foundation.

(i) Setbacks. Buildings having setbacks wherein the plan dimension of the tower in each direction is at least 75 percent of the corresponding plan dimension of the lower part may be considered as a uniform building without setbacks for the purpose of determining seismic forces.

For other conditions of setbacks the tower shall be designed as a separate building using the larger of the seismic coefficients at the base of the tower determined by considering the tower as either a separate building for its own height or as part of the over-all structure. The resulting total shear from the tower shall be applied at the top of the lower part of the building which shall be otherwise considered separately for its own height.

EXCEPTION: Nothing in this subsection shall be deemed to prohibit the submission of properly substantiated technical data for establishing the lateral design forces by a dynamic analysis.

(j) Structural Systems. 1. Design requirements. Buildings more than 160 feet in height shall have a ductile moment-resisting space frame capable of resisting not less than 25 percent of the required seismic force for the structure as a whole. All buildings designed with a horizontal force factor "K" of 0.67 or 0.80 shall have a ductile moment-resisting space frame of structural steel (complying with Section 2722 for buildings in Seismic Zones No. 2 and No. 3 or Section 2723 for buildings in Seismic Zone No. 1) or of reinforced concrete (complying with Section 2630 for buildings in Seismic Zones No. 2 and No. 3 or Section 2631 for buildings in Seismic Zone No. 1).

EXCEPTIONS: 1. Buildings more than 160 feet in height in Seismic Zone No. 1 may have concrete shear walls designed in conformance with Section 2632 of this Code in lieu of a ductile moment-resisting space frame, provided a "K" value of 1.00 or 1.33 is utilized in the design.

2. Other structural concepts may be approved by the Building Official when evidence is submitted showing that equivalent ductility and energy absorption are provided.

Moment-resisting space frames and ductile moment-resisting space frames may be enclosed by or adjoined by more rigid elements which would tend to prevent the space frame from resisting lateral forces where it can be shown that the action or failure of the more rigid elements will not impair the vertical and lateral load-resisting ability of the space frame.

2. Construction. The necessary ductility for a ductile moment-resisting space frame shall be provided by a frame of structural steel with moment-resisting connections (complying with Section 2722 for buildings in Seismic Zones No. 2 and No. 3 or Section 2723 for buildings in Seismic Zone No. 1) or by a reinforced concrete frame (complying with Section 2630 for buildings in Seismic Zones No. 2 and No. 3 or Section 2631 for buildings in Seismic Zone No. 1).

Shear walls in buildings where K = 0.80 shall be composed of axially loaded bracing members of A36, A440, A441, A572 (except Grades 60 and 65) or A588 Grades A, B or C structural steel; or reinforced concrete bracing members or walls conforming with the requirements of Section 2632.

Reinforced concrete shear walls and reinforced concrete braced frames for all buildings shall conform to the requirements of Section 2632. In buildings where K = 0.67 and K = 0.80, all-structural elements below the base required to transmit seismic forces to the foundation shall be composed of structural steel (complying with Section 2722 for buildings in Seismic Zones No. 2 and No. 3 or Section 2723 for buildings in Seismic Zone No. 1) or by reinforced concrete (complying with Section 2630 for buildings in Seismic Zones No. 2 and No. 3 or with Section 2631 for buildings in Seismic Zone No. 1 and with Section No. 2632 for buildings in Seismic Zones Nos. 1, 2, and 3).

(k) Design Requirements. 1. Building separations. All portions of structures shall be designed and constructed to act as an integral unit in resisting horizontal forces unless separated structurally by a distance sufficient to avoid contact under deflection from seismic action or wind forces.

2. Minor alterations. Minor structural alterations may be made in existing buildings and other structures, but the resistance to lateral forces shall be not less than that before such alterations were made, unless the building as altered meets the requirements of this Section of the Code.

3. Reinforced masonry or concrete. All elements within the structure which are of masonry or concrete and which resist seismic forces or movement shall be reinforced so as to qualify as reinforced masonry or concrete under the provisions of Chapters 24 and 26. Principal reinforcement in masonry shall be spaced 2 feet maximum or center in buildings using a moment-resisting space frame.

4. Combined vertical and horizontal forces. In computing the effect of seismic force in combination with vertical loads, gravity load stresses induced in members by dead load plus design live load, except roof live load, shall be considered.

5. Exterior elements. Precast, nonbearing, non-shear wall panels or other elements which are attached to, or enclose the exterior, shall accommodate movements of the structure resulting from lateral forces or temperature changes. The concrete panels or other elements shall be supported by means of poured-in-place concrete or by mechanical fasteners in accordance with the following provisions:

A. Connections and panel joints shall allow for a relative movement between stories of not less than two times story drift caused by wind or seismic forces; or 1/4 inch whichever is greater.

B. Connections shall have sufficient ductility and rotation capacity so as to preclude fracture of the concrete or brittle failures at or near welds. Inserts in concrete shall be attached to, or hooked around reinforcing steel, or otherwise terminated so as to effectively transfer forces to the reinforcing steel.

C. Connections to permit movement in the plane of the panel for story drift may be properly designed sliding connections using slotted or oversize holes or may be connections which permit movement by bending of steel.

(l) Earthquake Recording Instrumentations. For earthquake recording instrumentations see Appendix, Section 2314 (l).

TABLE NO. 23-H - HORIZONTAL FORCE FACTOR "K"
FOR BUILDINGS OR OTHER STRUCTURES[1]

Type or Arrangement of Resisting Elements	Value[2] of K
All building framing systems except as hereinafter classified	1.00
Buildings with a box system as specified in Section 2314 (b)	1.33
Buildings with a complete horizontal bracing system capable of resisting all lateral forces, which system includes a moment resisting space frame, which when assumed to act independently is capable of resisting a minimum of 25 percent of the total required lateral force.	0.80
Buildings with a moment resisting space frame which when assumed to act independently of any other more rigid elements is capable of resisting 100 percent of the total required lateral forces in the frame alone.	0.67
Elevated tanks supported with four or more cross-braced columns and not supported by a building	3.00[3]
Structures other than buildings and other than those set forth in Table No. 23-I.	1.50

[1]Where wind load as set forth in Section 2307 would produce higher stresses, this load shall be used in lieu of the loads resulting from earthquake forces.

[2]See map on inside back cover for seismic probability zones and definition of "Z" as set forth in Subsection (c).

[3]The tower shall be designed for an accidental torsion of five percent as set forth in Section 2314 (b). Elevated tanks which are supported by buildings or do not conform to type or arrangement of supporting elements as described above shall be designed in accordance with Section 2314 (d) 2 using "C_p" = .2.

TABLE NO. 23-I - HORIZONTAL FORCE FACTOR "C_p" FOR PARTS OR PORTIONS OF BUILDINGS OR OTHER STRUCTURES

Part or Portion of Buildings	Direction of Force	Value of C_p
Exterior bearing and nonbearing walls, interior bearing and nonbearing walls which extend three-fourths of the height of the room, and masonry and concrete fences over six feet (6') in height.[1]	Normal to flat surface	0.2
Cantilever parapet and other cantilever walls, except retaining walls.	Normal to flat surface	1.00
Exterior and interior ornamentations and appendages.	Any direction	1.00
When connected to or a part of a building; towers, tanks, towers and tanks plus contents, chimneys, smokestacks, and penthouses.	Any direction	0.20[2]
When resting on the ground, tank plus effective mass of its contents.	Any direction	0.10
Floors and roofs acting as diaphragms.[3]	Any direction	0.10

[1]In no case shall horizontal force be less than 10 pounds per square foot. See Section 2313 (b) for limitations on deflection.

[2]When "H/D" of any building is equal to or greater than five to one increase value by 50 percent.

[3]Floors and roofs acting as diaphragms shall be designed for a minimum value of "C_p" of 10 percent applied to loads tributary from that story unless a greater value of "C_p" is required by the basic seismic formula V = ZKCW.

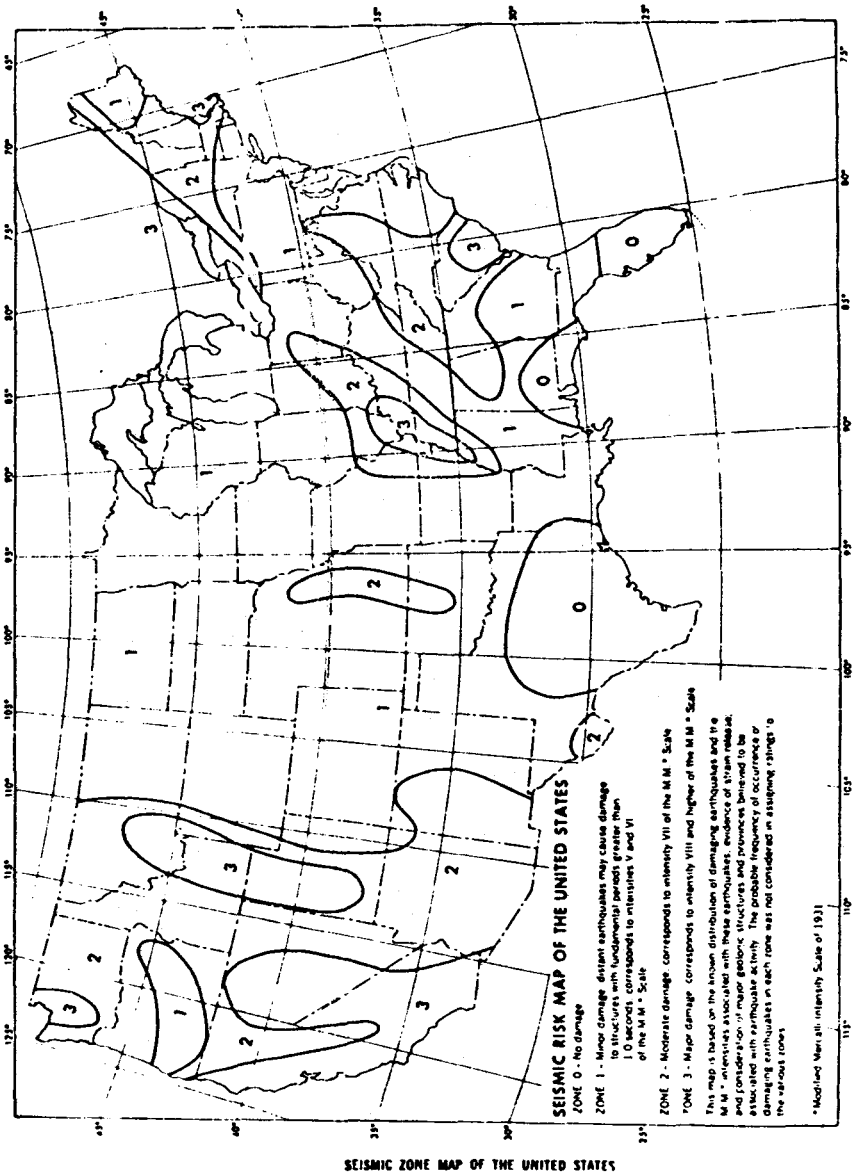

SEISMIC ZONE MAP OF THE UNITED STATES

1970 EDITION SEISMIC RISK MAP

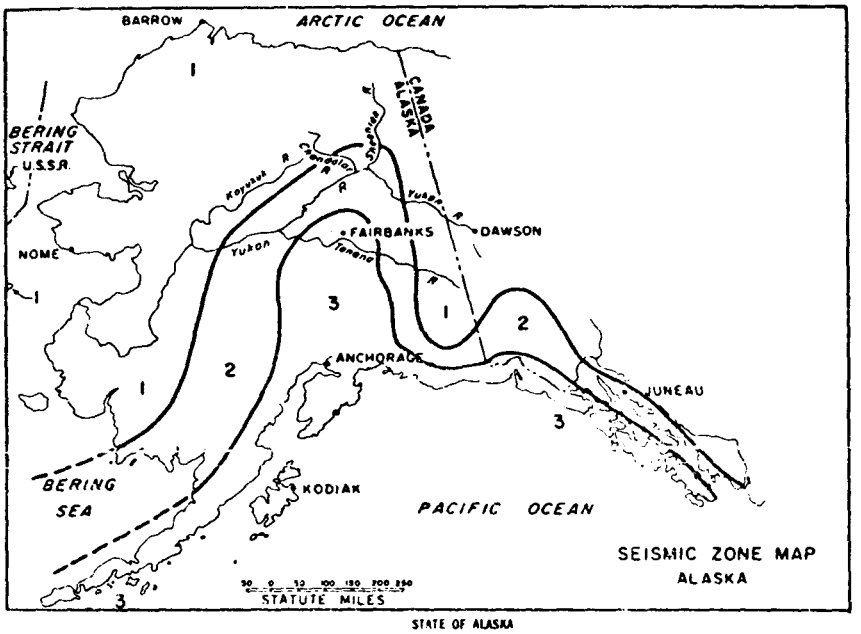

STATE OF ALASKA

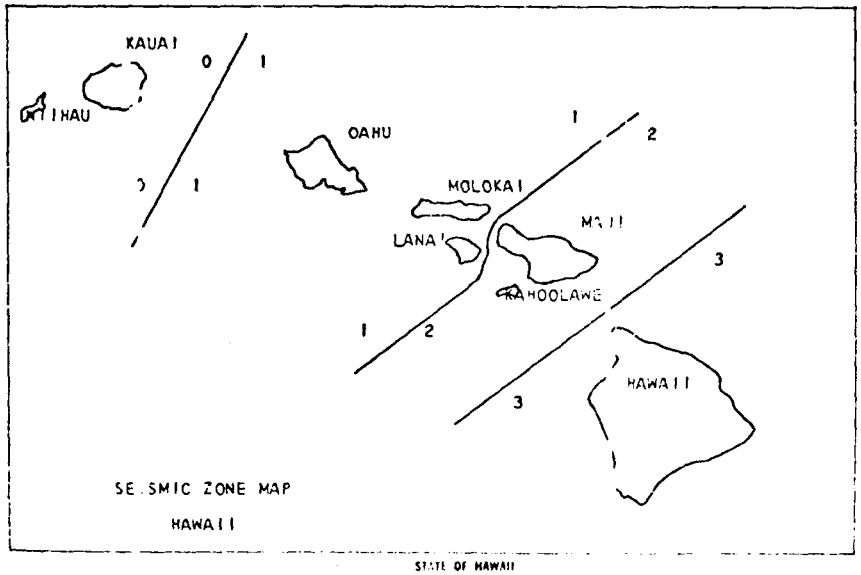

STATE OF HAWAII

ATTACHMENT "F"

Extract of Paper Titled "Cryogenic Fasteners",
From Metals Progress, July, 1966

Extract of Data Sheet Published by
Allegheny Ludlum Steel Corporation

Cryogenic Fasteners

The evaluation of materials for threaded fasteners in cryogenic assemblies indicates that one nickel-base alloy (Inconel 718) and two iron-base alloys (A286 and Unitemp 212) have the needed mechanical properties down to -423 F (the temperature of liquid hydrogen).

Eighteen Materials Examined

In all, 18 iron, nickel, cobalt, titanium, and aluminum-base alloys were investigated. The three alloys discussed here experienced no brittle failure down to -423 F. Further, as shown in Table 1, almost all mechanical properties of A286, Unitemp 212 and Inconel 718 alloys were better at -423 F than at room temperature. Some nickel-base alloys hold promise at this low temperature, but most of the other alloys tested proved unsuitable or inferior for use as fasteners below -320 F. Many exhibited brittle failure either in tension, shear or impact before that temperature was reached. Several alloys became brittle between -320 and -423 F; they might warrant further evaluation for applications down to -320 F.

Other Material Possibilities

Two points of the investigation may apply to all cryogenic fasteners and fastener materials:

First, fasteners must be tested in their finished form. Properties of standard test specimens are not reliable indicators of cryogenic bolt performance. For example, we tested the cobalt-base alloy, L605 (51.5 Co, 20 Cr, 3 Fe max, 15 W, 10 Ni) which had been cold reduced 30% and was in the unaged condition. It had an unsatisfactory notch-to-smooth specimen tensile strength ratio of 0.80. However, as a threaded fastener it proved to have an acceptable bolt-to-material tensile strength ratio of 1.00. Also, the test results showed that properties of 18% Ni maraging steel increased as the temperature was lowered to -423 F, while bolt shear strength fell below that obtained at room temperature.

Second, there is no satisfactory single indicator of over-all cryogenic performance. A complete series of tests on the fastener is still requisite. For example, the impact strength of the titanium alloy (Ti-5Al-5Sn-5Zr) rose as temperature decreased to -423 F, but tensile strength of the bolt dropped sharply.

The three materials reported on here are probably not the only satisfactory bolt materials for cryogenic applications. One promising titanium alloy (Ti-5Al-2.5Sn) is being investigated further. And many nickel-base alloys such as Waspalloy, René 41, and AF 1753 (7.2 Co, 16 Cr, 8.4 W, 3.2 Ti, 9.5 Fe, 1.9 Al, 1.6 Mo) show possibilities. The A286, Unitemp 212 and Inconel 718 alloys, however, were the first proven and available fastener materials with considerable documentation at the critical low temperatures.

Low Temperature Improves Properties

Table 1 shows that the tensile strength of 1/4 in. diameter A286 bolts increased 35% as the temperature decreased to -423 F. Similarly, the tensile strengths of the Unitemp 212 and Inconel 718 bolts rose approximately 30%.

In double shear strength tests the gain at -423 F over room temperature strength for the bolts ranged from 35% for A286 to 25% for

Table 1 - Mechanical Properties of Cryogenic Fastener Materials

Bolt Material	Nominal Composition, %	Test Temp. F	Axial Tensile Strength, psi	3° Angle-Block Tensile Strength, psi	Shear Strength, psi	Tension-Impact Strength, ft-lb.
A286, cold rolled	0.05C,1.35Mn,0.95Si, 15Cr,26Ni,1.25Mo, 2.0Ti,0.20Al,0.30V, bal Fe	-423	291,400	282,300	158,000	36.3
		-320	268,500	270,000	--	41.0
		70	214,400	215,000	116,000	35.0
Unitemp 212	0.08C,16Cr,25Ni, 0.50Cb+Ta,4.0Ti, 0.35Al,0.05Zr,0.06B, bal Fe	-423	277,800	272,000	165,700	43.3
		-320	275,600	275,000	--	47.3
		70	213,600	215,000	132,400	46.4
Inconel 718	0.04C,0.20Mn,0.20Si, 19Cr,52.5Ni,3.0Mo, 0.80Ti,0.60Al,5.20Cb+ Ta,18Fe	-423	291,400	286,300	168,400	23.3
		-320	276,000	284,000	--	23.7
		70	225,600	229,000	138,200	23.7

Inconel 718. By comparison, the shear strength of 18% Ni maraging steel fell from 160,000 psi at 70 F to 130,000 psi at -423 F.

A series of angle-block tensile (or bending) tests formed a critical part of this study. It enabled determination of the effect of high localized stress at cryogenic temperatures on tensile strength. Bolt assemblies were loaded in a conventional tensile testing machine, but with a 3^{o} angle bushing placed under the bearing surface of the nut. The eccentric loading from bending sharply increases stress concentrations, particularly in the bolt thread.

The angle-block tensile properties (Table 1) for the three alloys approximate their axial tensile properties at both 70 and -320 F, and are only slightly below axial properties at -423 F. Even at the latter temperature, the angle-block tensile strengths remain 10% above those at room temperature.

The tension-impact tests at -423 F were probably the first on finished parts in which the entire piece was submerged in liquid hydrogen at impact.

Table 1 shows that the tension-impact properties of the bolts are highest at -320 F and somewhat lower at -423 F. For A286 and Inconel 718, the properties at -423 F still approximately equal or exceed the tension-impact properties at 70 F. The performance of Unitemp 212 at liquid hydrogen temperature is about 7% below that at room temperature.

Effect of Thermal Cycling

Thermal cycling had little effect on the tensile properties of bolts of the three alloys. Typical is cold reduced A286 where both material and bolts were cycled twelve times from 70 to -423 to 70 F, each time being held 5 min. at temperature. Little change occurred in the tensile properties. The material tensile strength after cycling rose 1900 psi to 196,800 psi. The bolt and nut assembly showed a slight change from 213,600 psi in the as-received condition to 212,800 psi after low temperature cycling. In addition, A286 bolt and nut assemblies and the material itself were cycled from 70 to 1200 to 70 F. The tensile strength of the material after this high temperature cycling was 194,300 psi. The bolt and nut assembly exhibited a strength of 213,600 psi. The cycling also had no effect on the locking properties of the locknuts simultaneously tested as part of the investigation.

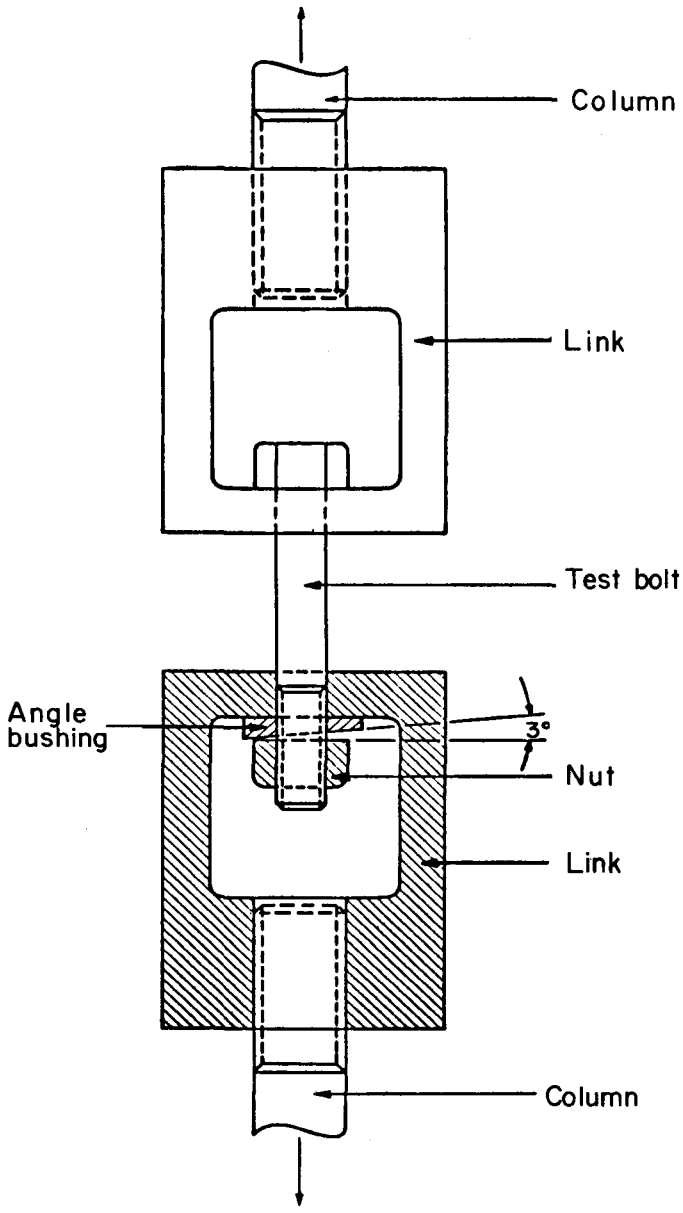

FIGURE 1. THIS 3° ANGLE BUSHING PRODUCED BENDING IN A CRYOGENIC BOLT AND FACILITATED STUDY OF THE EFFECT OF LOCALIZED STRESS ON TENSILE STRENGTH

Allegheny Ludlum Data Sheet

Many new metals are being developed for low temperature service. Allegheny Ludlum itself has several in the research stage. But most of the applications so far have used familiar Allegheny Stainless Steels. Here's why.

The missile age has focused attention on temperatures down to the temperatures of liquid oxygen (-295 F), liquid hydrogen (-423 F) and liquid helium (-456 F). Materials for use at these low temperatures must be ductile, tough and strong. Steels of the face-centered cubic or austenitic structure satisfy these requirements. The austenitic chromium-nickel Allegheny Stainless Steels are a natural for use at temperatures down to -456 F. They not only maintain their toughness and ductility but they also increase in strength as temperatures decrease.

The 300 series Allegheny Stainless Steels are used primarily in the annealed condition. Their most important mechanical properties are the yield strength (.2 percent offset), the tensile strength, the elongation and the impact strength. Since toughness and resistance to impact loading are important at low temperatures, you will be interested in this table.

CHARPY V-NOTCH IMPACT STRENGTH OF
ALLEGHENY LUDLUM STAINLESS STEELS
FROM ROOM TEMPERATURE TO -423 F

Grade	Testing Temperature °F	Foot-pounds
302	+ 70	110-120
	-100	113
	-320	100-120
304	+ 70	110-160
	-100	110-125
	-320	90-110
	-423	85-90
310	+ 70	90-100
	-320	90
	-423	85
316	+ 70	110
	-100	110
	-320	110
321	+ 70	110-125
	-100	120-170
	-320	110
347	+ 70	85-110
	-100	70-125
	-320	85-105
	-423	60

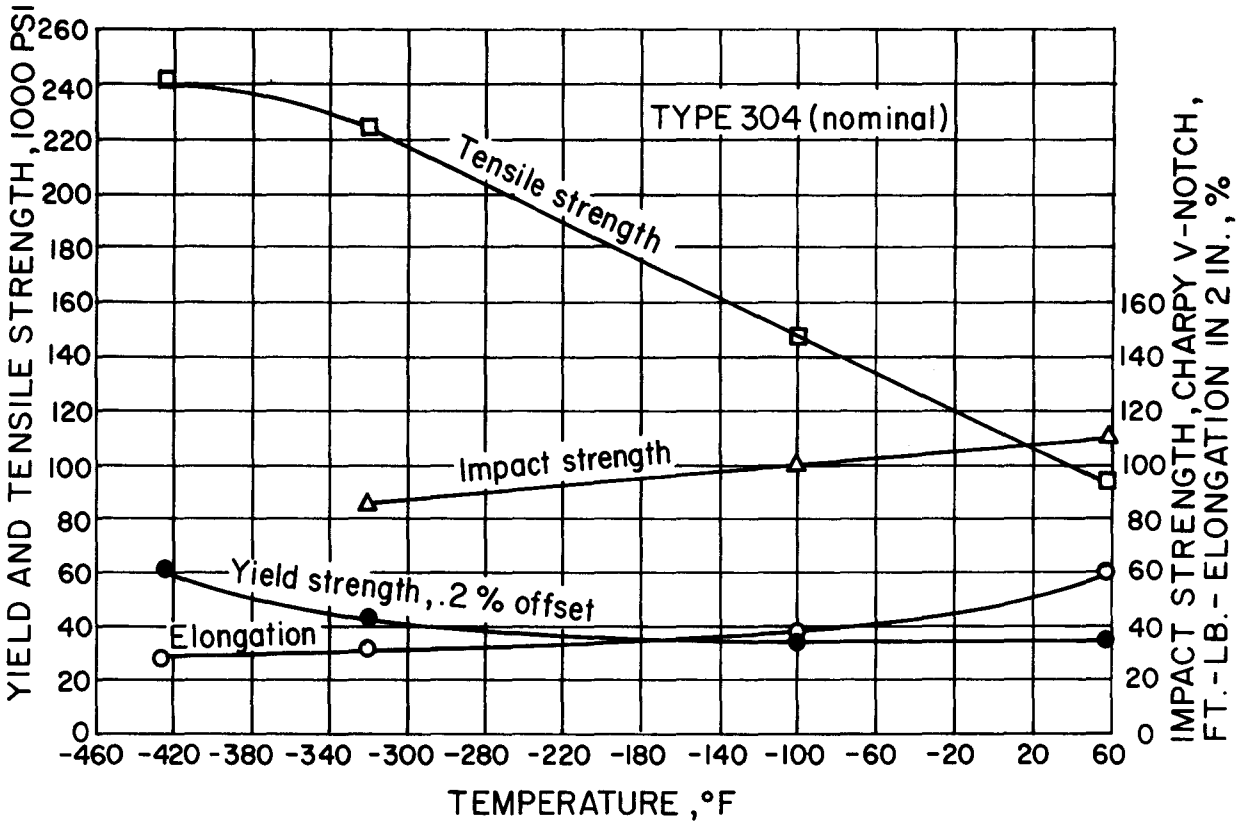

ALLEGHENY STAINLESS TYPE 304 - MECHANICAL PROPERTIES FROM ROOM TEMPERATURE TO -423 F

Impact properties are retained even after long periods of exposure to low temperatures. After one year at -320 F, Type 304 Stainless has a Charpy keyhole impact strength of 77 foot-pounds at -320 F. The yield and tensile strengths of the austenitic Allegheny Stainless are typically higher at sub-zero temperatures than at room temperature. The tensile strength increases at a much more rapid rate than does the yield strength. The yield strength, tensile strength and elongation for some of the chromium-nickel stainless steels are listed below. Also, Type 304 properties are graphically illustrated.

THE EFFECT OF LOW TEMPERATURES ON
THE MECHANICAL PROPERTIES OF ALLEGHENY
CHROMIUM-NICKEL AUSTENITIC STAINLESS

Grade	Testing Temperature °F	Yield Strength .2% Offset ksi	Ultimate Tensile Strength ksi	Elongation in 2 inches percent
302	+ 70	35	95	68
	-100	52	160	53
	-320	80	230	35
	-423	125	268	25
304	+ 70	37	90	65
	-100	45	153	52
	-320	60	230	35
	-423	70	250	31
310	+ 70	35	80	60
	-100	40	100	55
	-320	70	150	54
	-423	95	180	56
316	+ 70	35	84	70
	-100	48	120	65
	-320	75	185	58
	-423	84	210	55
321	+ 70	38	90	60
	-100	50	140	49
	-320	68	210	43
	-423	92	238	35
347	+ 70	38	91	62
	-100	45	140	53
	-320	50	195	42
	-423	65	230	40

Fatigue strength and modulus of elasticity are also higher at sub-zero temperatures than at room temperature.

Missile and rocket applications call for high strength-to-weight ratios. The strength of the Allegheny chromium-nickel Stainless Steels can be enhanced by cold working and in this condition they offer some strength advantages over annealed material, but care must be exercised in choosing the proper steel since embrittlement of the less stable grades may occur at low temperatures.

For applications where strength-to-weight ratios (both at room and cryogenic temperatures) greater than those of regular austenitic stainless steels are desired, corrosion-resistant, heat-treatable, Altemp A-286 is finding usage. Normally thought of as a high temperature material, this precipitation-hardening austenitic iron-nickel chromium steel has tensile strengths such as 150,000 psi at 60 F and 225,000 psi at -423 F. Impact strengths at low temperature are excellent and approach those of Type 302 and 304 Stainless Steel.

Mar-Aging Steels ALMAR 18

Another group of special steels receiving much consideration for non-corrosion-resistant, low-temperature usage are the recently developed Mar-Aging Steels, named the ALMAR group by Allegheny Ludlum. Most of the interest is in the ALMAR 18 steels, containing 18 percent nickel with cobalt and molydbenum.

CRYOGENIC-TEMPERATURE MECHANICAL PROPERTIES OF ALLEGHENY ALMAR 18 (250)

Condition	Direc-tion	Temp. °F	0.2 Percent Offset Yield Strength, ksi	Ultimate Tensile Strength, ksi	Elonga-tion, %	Reduc-tion of Area, %	Matched Tensile Strength, ksi
			Plate				
A1500+M900	T	RT	232	243	10	44	--
A1500+M900	T	-320	292	310	7	29	--
A1500+M900	L	RT	232	243	12	57	--
A1500+M900	L	-320	291	305	9	40	--
			Sheet				
A1500+M900	L	RT	250	262	4.5	--	256
	L	-320	315	329	4.5	--	244
A1500+C50+	L	RT	286	289	3.5	--	265
M900	L	-320	335	338	0	--	266

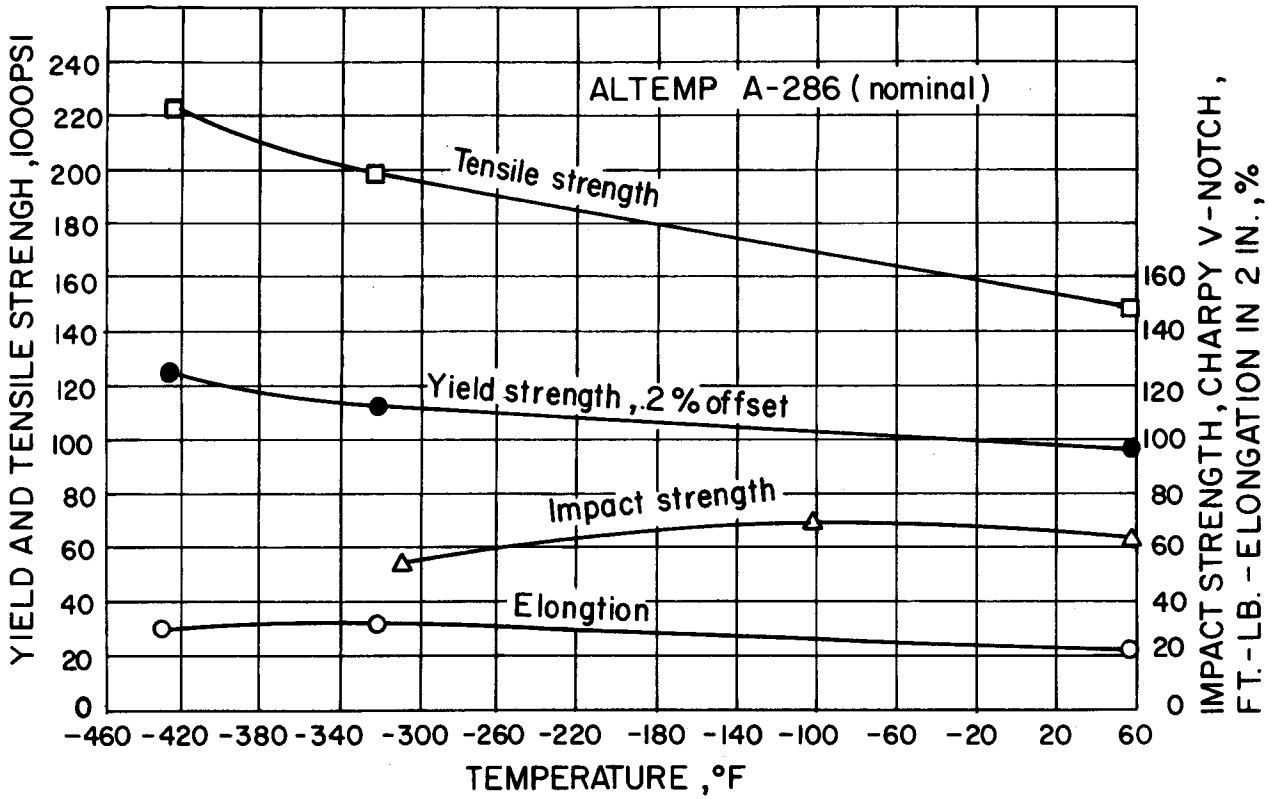

ALTEMP A-286 - LOW TEMPERATURE PROPERTIES FROM ROOM TEMPERATURE TO -423 F

ALMAR 18 combines the ultra-high strength found in the low alloy steels with superior toughness and ductility. While their impact strengths at -320 F are not as good as the austenitic steels such as Type 304 Stainless or Altemp A-286, they are well above that of other ultra-high-strength steels.

CHARPY V-NOTCH IMPACT STRENGTH OF ALLEGHENY ALMAR 18 (250) FROM ROOM TEMPERATURE TO -320 F

Condition	Direction	Temperature °F	Charpy V-Notch Energy, Ft-lb.
A1500	T	Room	42
A1500	L	Room	97
A1500+M900	T	Room	18
A1500+M900	L	Room	24
A1500+M900	--	0	24
A1500+M900	--	-100	21
A1500+M900	--	-175	21
A1500+M900	--	-244	20
A1500+M900	--	-320	20

Allegheny Ludlum specializes in producing, in all product forms, special steels like those just briefly described.

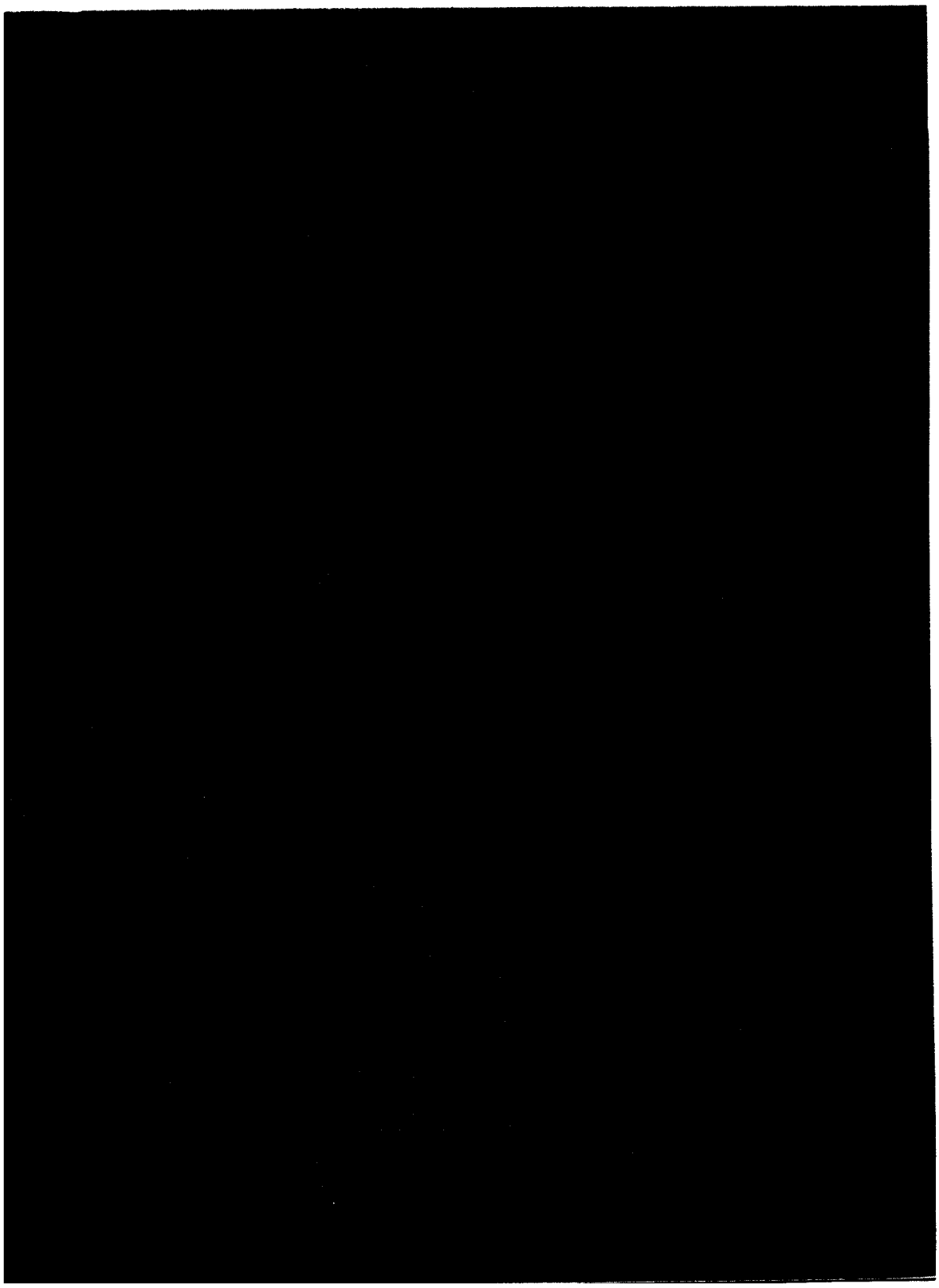

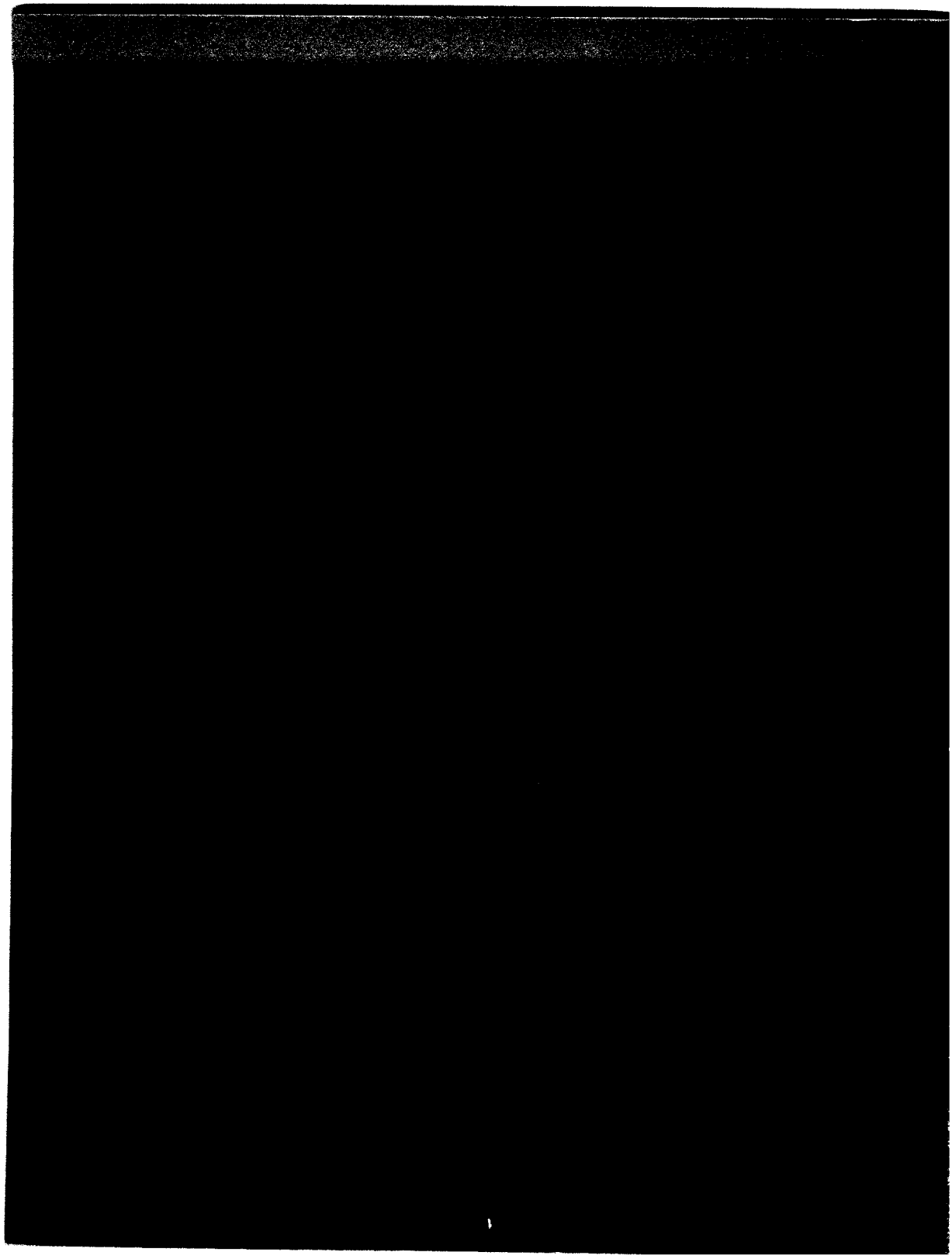

IV. EQUIPMENT

C. Chamber Vessel

2. Special Report by Battelle Memorial Institute on the Stress Analysis of the 30,000 Liter Bubble Chamber

Prepared by

M.Vagins, R.H.Prause, and G.H.Workman

and

Chicago Bridge & Iron Company Review of Battelle Report, and Certification

Prepared by

Jon Hagstrom

IV. C. 2. TABLE OF CONTENTS

		Page
(1)	INTRODUCTION	99
(2)	DESIGN ANALYSIS PHILOSOPHY	101
(3)	GENERAL PROCEDURE	109
(4)	CONCLUSIONS	109
(5)	STATIC STRESS ANALYSIS OF CHAMBER COMPONENTS	110
	The "Beanie"-Chamber Intersection	112
	"Beanie"-Camera Nozzle Configuration	116
	Lower Chamber or "Z" Section	125
	"Z" Section Flange Bolt Requirements	133
	Beam Window Flange	135
	Lower Half of the Main Chamber and the Support Cone	145
	Flange Spacer	161
	Beam Window and Beam Window Protuberance	163
(6)	DYNAMIC ANALYSIS OF BUBBLE CHAMBER COMPLEX	176
	Axisymmetric Shell Analysis	177
	Weight and Moment of Inertia Data	186
	Finite Element Model Analysis	188
	Dynamic Forcing Function	193
	Solution Technique	196
	Natural Frequencies	199
	Single Pulse Response	199
	Multi-Pulse Response	202
	Incorporation of the 33-Ton Target	205
(7)	SUMMARY AND MISCELLANEOUS	219
	"G" Loadings	219

LIST OF FIGURES

FIGURE 1.	STRESS CATEGORIES AND LIMITS OF STRESS INTENSITIES	103
FIGURE 2.	FATIGUE DESIGN CHART FROM ASME BOILER AND PRESSURE VESSEL CODE, SECTION VIII - DIVISION 2	107
FIGURE 3.	GEOMETRIC AND LOADING MODEL OF MODIFIED "BEANIE"-CHAMBER INTERSECTION FOR INPUT TO MONSA-S	114
FIGURE 4.	MAXIMUM STRESSES IN WELDS AND KNUCKLE OF MODIFIED "BEANIE"-CHAMBER INTERSECTION	115
FIGURE 5.	GEOMETRIC AND LOADING MODEL OF "BEANIE"-CAMERA NOZZLE INTERSECTION FOR INPUT TO MONSA-S	117
FIGURE 6.	MAXIMUM STRESSES AND DEFLECTION PATTERN IN MODIFIED "BEANIE"-NOZZLE INTERSECTION	119

		Page
FIGURE 7.	PRELIMINARY GEOMETRIC AND LOADING MODEL OF "Z" SECTION SHOWING CRITICALLY STRESSED REGIONS	126
FIGURE 8.	EXACT GEOMETRY OF MODIFIED BOTTOM JOINT IN "Z" SECTION FOR INPUT TO MONSA-S	128
FIGURE 9.	MAXIMUM STRESSES IN MODIFIED BOTTOM JOINT OF "Z" SECTION UNDER 200 PSI PRESSURE LOADING	129
FIGURE 10.	ACCEPTABLE BOTTOM JOINT CONFIGURATION	130
FIGURE 11.	PROPOSED FLANGE FOR TOP OF "Z" SECTION	131
FIGURE 12.	EXACT GEOMETRIC MODEL OF PROPOSED "Z" SECTION FLANGE FOR INPUT TO MONSA-S	132
FIGURE 13.	CB&I PROPOSED BEAM WINDOW FLANGE FOR MAIN CHAMBER	137
FIGURE 14.	GEOMETRIC MODEL OF CHAMBER BEAM WINDOW FLANGE FOR INPUT TO MONSA-S	138
FIGURE 15.	ASSUMED LOADING - CASE 1	140
FIGURE 16.	MAXIMUM STRESSES IN FLANGE FOR CASE 1	141
FIGURE 17.	ASSUMED LOADING - CASE 2	142
FIGURE 18.	MAXIMUM STRESSES IN FLANGE FOR CASE 2	143
FIGURE 19.	GEOMETRIC MODEL OF LOWER CHAMBER AREA FOR INPUT TO MONSA-S	147
FIGURE 20.	GEOMETRIC MODEL, LOADINGS, AND MAXIMUM STRESSES FOR CONE INNER WALL IN CHAMBER - CASE 1	149
FIGURE 21.	GEOMETRIC MODEL, LOADINGS, AND MAXIMUM STRESSES FOR CONE INNER WALL IN CHAMBER - CASE 2	150
FIGURE 22.	GEOMETRIC MODEL, LOADING, AND MAXIMUM STRESSES FOR CONE INNER WALL IN CHAMBER - CASE 3	151
FIGURE 23.	GEOMETRIC MODEL, LOADINGS, AND MAXIMUM STRESSES FOR CONE INNER WALL IN CHAMBER - CASE 4	152
FIGURE 24.	GEOMETRIC MODEL USED FOR FOURIER HARMONIC LOAD ANALYSIS OF 3-POINT SUPPORT SYSTEM	155
FIGURE 25.	LOAD APPROXIMATION, 7 TERMS n = 0,3,6,9,12,15	158
FIGURE 26.	RELATIVE DEFLECTION PATTERN AND MAXIMUM STRESSES IN SUPPORT CONE UNDER ASSUMED LOAD	159
FIGURE 27.	BASIC CONFIGURATION OF MAIN FLANGE SPACER	162
FIGURE 28.	FINITE ELEMENT MODEL OF CHAMBER BEAM WINDOW ASSEMBLY	165
FIGURE 29.	FRONT VIEW OF FINITE ELEMENT MODEL	166

		Page
FIGURE 30.	TWO-DIMENSIONAL TRUE LENGTH PLOT OF NOSE CONE MODEL	167
FIGURE 31.	FINITE ELEMENT MODEL OF BEAM WINDOW	169
FIGURE 32.	DISPLACEMENT OF NODES ALONG VERTICAL CENTER-LINE OF MODEL UNDER 150 PSI INTERNAL PRESSURE	170
FIGURE 33.	MAXIMUM STRESSES IN MODEL ALONG VERTICAL CENTERLINE	171
FIGURE 34.	DISPLACEMENT OF NODES ALONG BEAM WINDOW END OF MODEL UNDER 150 PSI INTERNAL PRESSURE	172
FIGURE 35.	MAXIMUM STRESSES ALONG BEAM WINDOW END OF MODEL	173
FIGURE 36.	DISPLACEMENT OF NODES ALONG APPROXIMATE HORIZONTAL CENTERLINE OF MODEL UNDER 150 PSI INTERNAL PRESSURE	174
FIGURE 37.	MAXIMUM STRESS ALONG APPROXIMATE HORIZONTAL CENTER-LINE OF MODEL	175
FIGURE 38.	PRESSURE-TIME HISTORY FOR HYDROGEN OPERATION	178
FIGURE 39.	PRESSURE-TIME HISTORY FOR DEUTERIUM OPERATION	179
FIGURE 40.	PRESSURE-TIME HISTORY FOR NEON OPERATION	180
FIGURE 41.	AXISYMMETRIC MODEL FOR MONSA-V SHELL DYNAMIC STUDY	183
FIGURE 42.	FINITE ELEMENT MODEL OF BUBBLE CHAMBER, VACUUM TANK, SUPPORT LEGS, AND CAISSON	189
FIGURE 43.	ENLARGED VIEW OF NODES ABOVE CAISSON	190
FIGURE 44.	DISPLACEMENT FUNCTIONS	195
FIGURE 45.	RADIAL DISPLACEMENT DURING MULTI-PULSING OF UNBRACED MODEL	204
FIGURE 46.	RADIAL DISPLACEMENT DURING MULTI-PULSING OF BRACED MODEL	206
FIGURE 47.	FINITE ELEMENT MODEL OF BRACED CHAMBER WITH TARGET	207
FIGURE 48.	VERTICAL DISPLACEMENT AT SPOOL END FOR TARGET MODEL	210
FIGURE 49.	PRINCIPAL LATERAL DISPLACEMENT AT SPOOL END FOR TARGET MODEL	211
FIGURE 50.	SECONDARY COMPONENT OF LATERAL DISPLACEMENT AT SPOOL END FOR TARGET MODEL	212
FIGURE 51.	VERTICAL DISPLACEMENT AT SPOOL END FOR "FREQUENCY-APART" TARGET MODEL	213
FIGURE 52.	PRINCIPAL LATERAL DISPLACEMENT AT SPOOL END FOR "FREQUENCY-APART" TARGET MODEL	214

Page

FIGURE 53. SECONDARY COMPONENT OF LATERAL DISPLACEMENT AT SPOOL END FOR "FREQUENCY-APART" TARGET MODEL 215

FIGURE 54. VERTICAL DISPLACEMENT AT SPOOL END FOR "FREQUENCY-TOGETHER" TARGET MODEL 216

FIGURE 55. PRINCIPAL LATERAL DISPLACEMENT AT SPOOL END FOR "FREQUENCY-TOGETHER" TARGET MODEL 217

FIGURE 56. SECONDARY COMPONENT OF LATERAL DISPLACEMENT AT SPOOL END FOR "FREQUENCY-TOGETHER" TARGET MODEL 218

LIST OF TABLES

TABLE 1. CLASSIFICATION OF STRESS FOR SOME TYPICAL CASES 104

TABLE 2. DATA FOR MONSA SHELL ANALYSIS MODEL OF BUBBLE CHAMBER 182

TABLE 3. STATIC DEFLECTION OF BUBBLE CHAMBER STRUCTURE RESULTING FROM VERTICAL AND HORIZONTAL LOADS AT THE BOTTOM OF THE ROD AND CYLINDER GUIDE 184

TABLE 4. RESULTS OF SHELL VIBRATION ANALYSIS OF BUBBLE CHAMBER STRUCTURE (NO LIQUID IN CHAMBER) 185

TABLE 5. SUMMARY OF WEIGHT AND MOMENT OF INERTIA DATA FOR BUBBLE CHAMBER, VACUUM TANK, AND CRYOSTAT 187

TABLE 6. ELASTIC PROPERTIES OF EQUIVALENT BEAM ELEMENTS 193

TABLE 7. FORCING FUNCTION PARAMETERS 197

TABLE 8. NATURAL FREQUENCIES AND MODE TYPE 200

TABLE 9. MAXIMUM DISPLACEMENTS IN SINGLE-PULSE OPERATION 201

TABLE 10. NATURAL FREQUENCIES OF THE NEON MODEL WITH 33-TON TARGET 208

TABLE 11. DISPLACEMENT AND ACCELERATION DATA 221

APPENDIX A 222

THE NORMAL MODE METHOD FOR PROPORTIONAL DAMPING 223

CHICAGO BRIDGE & IRON COMPANY REVIEW OF BATTELLE STRESS REPORT, and CERTIFICATION 226

IV. C 2. A STRESS ANALYSIS OF NATIONAL ACCELERATOR LABORATORY'S PROPOSED 30,000 LITER BUBBLE CHAMBER

(1) INTRODUCTION

National Accelerator Laboratory, Bubble Chamber Group is presently in the design and fabrication stages of the building of a 30,000 liter capacity bubble chamber complex. The chamber proper will operate at cryogenic temperatures and will undergo cyclic pressure loadings for long periods of time. At different times it is expected that the chamber will be filled with liquid hydrogen, deuterium, neon, or a mixture of liquid hydrogen and neon. The exact temperature and pressure loadings to which the chamber will be subjected will vary from time to time but it is anticipated that the worst conditions that the chamber will be exposed to will be a steady state temperature of approximately -423° F and cyclic pressure variations in both the top of the chamber (target area above the piston) and the "Z" section of the chamber (buffer volume below the piston). The maximum peak pressures expected in these two volumes are 150 psia in the top and 200 psia in the "Z" or bottom section. There is vacuum outside these volumes. The chamber pressure varies during an expansion by about 70 psi between maximum and minimum pressures. Part of the design criteria has been to provide a structure which will be able to support a heavy plate for muon identification. Also, all important structural features necessary to mount a large internal track-sensitive target are to be included.

The bubble chamber assembly is a large and highly complex structure. It is basically composed of a 22-foot-diameter spherical vacuum tank and a 12-1/2-foot-diameter spherical bubble chamber. There is also a superconducting magnet enclosed in its own dewar placed between the chamber and the vacuum tank. The responsibility for this component has been given to Argonne National Laboratory. In August 1970, National Accelerator Laboratory (NAL) asked Battelle-Columbus to assist in the

design of the vacuum tank and the bubble chamber proper. While the design of the vacuum tank was fairly well detailed at that time, the design of the bubble chamber proper was in a very preliminary form. Battelle's first task was to carry out an accident-pressure analysis of the vacuum tank. This work was carried out and a report* detailing the conclusions reached, recommendations made, and methods of analysis employed was submitted to NAL in October, 1970.

Battelle's second task was to render design assistance to NAL in sizing the bubble chamber components such as the basic shell thickness, the details of the penetrations for the camera optics, the details of the load transfer path for the cone support, and the details of various flange configurations. As the design procedure progressed the bubble chamber configuration underwent several significant changes such as the addition of a 9-foot-diameter hemispherical "beanie" to the top of the chamber. As changes such as this were incorporated into the chamber design Battelle's input to the design analysis of the structure was enlarged. Added to Battelle's task was the design of the beam window nose protuberance, the analysis of the piston structure, and the determination of the bubble chambers' dynamic response characteristics when acted upon by the impulsive loads caused by the piston motion.

This report details the methods of analysis used and the conclusions reached governing the design of the important structural components of the bubble chamber. This document does not treat with the bubble chamber design history in that the reasoning and requirements for configuration changes made leading to the final selected bubble chamber geometry are not discussed. Rather this work presents a comprehensive stress analysis of the finalized bubble chamber geometry.

---

*Battelle Special Report entitled "A Stress Analysis of National Accelerator Laboratory's Proposed 30,000 Liter Bubble Chamber Vacuum Tank", by M. Vagins, dated October 19, 1970.

(2) DESIGN ANALYSIS PHILOSOPHY

The philosophy of analysis employed by Battelle in this work has been based upon two facets, engineering experience and the intent and requirements of the American Society of Mechanical Engineers, Boiler and Pressure Vessel Code, Section VIII, Pressure Vessels, Division 2 - Alternative Rules. Experience has shown that when pressure vessels, particularly those subjected to cyclic loadings, are designed according to the requirements of this code, a safe vessel capable of carrying out its mission is developed.

The design philosophy of Section VIII - Division 2 involves the establishment of stress limits for the material of which the structure is fabricated and in some cases the particular geometric aspects of the structure. These stress limits are given in terms of stress intensities. The term "stress intensity" is defined in Section VIII - Division 2 in Paragraphs 4-112 and 4-120 as follows:

> 4-112(a) "Stress Intensity. The "equivalent intensity of combined stress", or in short the "stress intensity", is defined as twice the maximum shear stress. In other words, the stress intensity is the difference between the algebraically largest principal stress and the algebraically smallest principal stress at a given point. Tension stresses are considered positive and compression stresses are considered negative".
>
> 4-120 "Derivation of Stress Intensities"
>
> "One requirement for the acceptability of a design (see 4-110(a)) is that the calculated stress intensities shall not exceed specified allowable limits. These limits differ depending on the stress category (primary, secondary, etc.) from which the stress intensity is derived. This paragraph describes the procedure for the calculation of the intensities which are subject to specified limits. The steps in the procedure are given in the following paragraphs.
> (a) At the point on the vessel which is being investigated, choose an orthogonal set of coordinates such as tangential, longitudinal, and radial and designate them by the subscripts t, ℓ, and r. The stress components in these directions are then designated σ_t, σ_r, and σ_ℓ for direct stresses and $\tau_{t\ell}$, $\tau_{\ell r}$, and τ_{rt} for shearing stresses.

(b) Calculate the stress components for each type of loading to which the part will be subjected and assign each set of stress values to one or a group of the categories below.

(1) General primary membrane stress, P_m (see 4-112 (f) and (g)).

(2) Local primary membrane stress, P_L (see 4-112 (i)).

(3) Primary bending stress, P_b (see 4-112 (g)).

(4) Secondary stress, Q (see 4-112 (h)).

(5) Peak stress, F (see 4-112 (j)).

(c) Group the stress components in accordance with 4-120 (b). Figure 4-130.1 is to provide assistance in assigning the stress values to the appropriate category. At any rectangular box calculate the algebraic sum of the σ_t's which result from the different types of loadings and which have entered the box, and similarly for the other five stress components. The result is a set of six stress components in each box.

(d) Translate the stress components in the t, ℓ, and r directions into principal stresses, σ_1, σ_2, and σ_3. (In many pressure vessel calculations, the t, ℓ, and r directions may be so chosen that the shearing stress components are zero and σ_1, σ_2, and σ_3 are identical to σ_t, σ_ℓ, and σ_r.)

(e) Calculate the stress differences S_{12}, S_{23}, and S_{31} from the relations

$$S_{12} = \sigma_1 - \sigma_2$$
$$S_{23} = \sigma_2 - \sigma_3$$
$$S_{31} = \sigma_3 - \sigma_1$$

The stress intensity, S, is the largest absolute value of S_{12}, S_{23}, and S_{31}.

(f) The stress intensity calculated as in (e) from the stress components in any rectangle in Figure 4-130.1 shall not exceed the allowable values of 4-130 which are shown in the circle adjacent to the rectangle in Figure 4-130.1.

Figure 4-130.1 of Section VIII - Division 2 has been extracted and is shown here as Figure 1. To further clarify the types of stresses as defined in this figure, Table 4-120.1, "Classification of Stresses for Some Typical Cases", has also been extracted and is shown here as Table 1. This figure and this table are quite self-explanatory with one amplification. In the consideration of primary local stress, a stressed region may be considered local if the distance over which the stresses exceed 1.1 S_m (where S_m is the stress intensity limit) does not extend in the meridional direction more than $0.5\sqrt{Rt}$ and if it is not closer in the meridional direction than $2.5\sqrt{Rt}$ to another region where the limits of the general membrane stress are exceeded. Here R is the

Stress Category	Primary			Secondary	Peak
	General Membrane	Local Membrane	Bending	Membrane plus Bending	
Description (For examples, see Table 4-120.1)	Average primary stress across solid section. Excludes discontinuities and concentrations. Produced only by mechanical loads.	Average stress across any solid section. Considers discontinuities but not concentrations. Produced only by mechanical loads.	Component of primary stress proportional to distance from centroid of solid section. Excludes discontinuities and concentrations. Produced only by mechanical loads.	Self-equilibrating stress necessary to satisfy continuity of structure. Occurs at structural discontinuities. Can be caused by mechanical load or by differential thermal expansion. Excludes local stress concentrations.	(1) Increment added to primary or secondary stress by a concentration (notch). (2) Certain thermal stresses which may cause fatigue but not distortion of vessel shape.
Symbol (Note 4)	P_m	P_L	P_b	Q	F
Combination of stress components and allowable limits of stress intensities.	P_m — S_m P_L — 1.5 S_m $P_L + P_b$ — 1.5 S_m $P_L + P_b + Q$ — 3 S_m (Note 1) $P_L + P_b + Q + F$ — S_a (Note 3) ——— Use design loads – – – – Use operating loads				

NOTE 1 ~ This limitation applies to the range of stress intensity. When the secondary stress is due to a temperature excursion at the point at which the stresses are being analyzed, the value of S_m shall be taken as the average of the S_m values tabulated in Part AM for the highest and the lowest temperature of the metal during the transient. When part or all of the secondary stress is due to mechanical load, the value of S_m shall be taken as the S_m value for the highest temperature of the metal during the transient.

NOTE 2 ~ The stresses in Category Q are those parts of the total stress which are produced by thermal gradients, structural discontinuities, etc., and do not include primary stresses which may also exist at the same point. It should be noted, however, that a detailed stress analysis frequently gives the combination of primary and secondary stresses directly and, when appropriate, this calculated value represents the total of P_m (or P_L) + P_b + Q and not Q alone. Similarly, if the stress in Category F is produced by a stress concentration, the quantity F is the additional stress produced by the notch, over and above the nominal stress. For example, if a plate has a nominal stress intensity, S, and has a notch with a stress concentration factor, K, then $P_m = S$, $P_b = 0$, $Q = 0$, $F = P_m (K-1)$ and the peak stress intensity equals $P_m + P_m (K-1) = KP_m$.

NOTE 3 ~ S_a is obtained from the fatigue curves, Figs. 5-110.1, 5-110.2 and 5-110.3. The allowable stress intensity for the full range of fluctuation is $2 S_a$.

NOTE 4 ~ The symbols P_m, P_L, P_b, Q, and F do not represent single quantities, but rather sets of six quantities representing the six stress components σ_t, σ_l, σ_r, τ_{tl}, τ_{lr}, and τ_{rt}.

FIG. 4-130.1 STRESS CATEGORIES AND LIMITS OF STRESS INTENSITY

FIGURE 1. STRESS CATEGORIES AND LIMITS OF STRESS INTENSITIES

TABLE 1. (Extracted from Section VIII - Division 2)

TABLE 4-120.1
CLASSIFICATION OF STRESSES FOR SOME TYPICAL CASES

Vessel Component	Location	Origin of Stress	Type of Stress	Classification
Cylindrical or spherical shell	Shell plate remote from discontinuities	Internal pressure	General membrane Gradient through plate thickness	P_m Q
		Axial thermal gradient	Membrane Bending	Q Q
	Junction with head or flange	Internal pressure	Membrane Bending	P_L Q
Any shell or head	Any section across entire vessel	External load or moment, or internal pressure	General membrane averaged across full section. Stress component perpendicular to cross section	P_m
		External load or moment	Bending across full section. Stress component perpendicular to cross section	P_m
	Near nozzle or other opening	External load moment, or internal pressure	Local membrane Bending Peak (fillet or corner)	P_L Q F
	Any location	Temp. diff. between shell and head	Membrane Bending	Q Q
Dished head or conical head	Crown	Internal pressure	Membrane Bending	P_m P_b
	Knuckle or junction to shell	Internal pressure	Membrane Bending	P_L [1] Q
Flat head	Center region	Internal pressure	Membrane Bending	P_m P_b
	Junction to shell	Internal pressure	Membrane Bending	P_L Q
Perforated head or shell	Typical ligament in a uniform pattern	Pressure	Membrane (av. thru cross section) Bending (av. thru width of lig., but gradient thru plate) Peak	P_m P_b F
	Isolated or atypical ligament	Pressure	Membrane Bending Peak	Q F F
Nozzle	Cross section perpendicular to nozzle axis	Internal pressure or external load or moment	General membrane (av. across full section). Stress component perpendicular to section	P_m See 4-138
		External load or moment	Bending across nozzle section	P_m See 4-138
	Nozzle wall	Internal pressure	General membrane Local membrane Bending Peak	P_m See 4-138 P_L Q F
		Differential expansion	Membrane Bending Peak	Q Q F
Cladding	Any	Differential expansion	Membrane Bending	F F
Any	Any	Radial temperature distribution [2]	Equivalent linear stress [3] Nonlinear portion of stress distribution	Q F
Any	Any	Any	Stress concentration (notch effect)	F

[1] Consideration must also be given to the possibility of wrinkling and excessive deformation in vessels with large diameter-to-thickness ratio.

[2] Consider possibility of thermal stress ratchet.

[3] Equivalent linear stress is defined as the linear stress distribution which has the same net bending moment as the actual stress distribution.

mean radius of the vessel and t is the wall thickness at the location of concern.

The bubble chamber proper is to be fabricated from 316L stainless steel plate and a cast stainless designated as CF3M. Table AHA-1 of Section VIII - Division 2 gives the design stress intensity values, S_m, for 316L as 16,600 psi and for CF3M as 20,000 psi at temperatures up to 100° F. Thus according to Figure 4-130.1 the following limits were used to govern the design analysis of the bubble chamber.

For 316L components

$$P_m \leq S_m = 16{,}600 \text{ psi}$$

$$P_L \leq 1.5\ S_m = 24{,}900 \text{ psi}$$

$$P_m(\text{or } P_L) + P_b \leq 1.5\ S_m = 24{,}900 \text{ psi}$$

$$P_m(\text{or } P_L) + P_b + Q \leq 3.0\ S_m = 49{,}800 \text{ psi}$$

For CF3M components

$$P_m \leq S_m = 20{,}000 \text{ psi}$$

$$P_L \leq 1.5\ S_m = 30{,}000 \text{ psi}$$

$$P_m(\text{or } P_L) + P_b \leq 1.5\ S_m = 30{,}000 \text{ psi}$$

$$P_m(\text{or } P_L) + P_b + Q \leq 3.0\ S_m = 60{,}000 \text{ psi}$$

The meeting of these stress limits, with of course the pertinent paragraphs of Section VIII - Division 2, dealing with fabrication, inspection and testing, are all that is required to ensure that the vessel will be capable of sustaining a given static load condition. Because the vessel is to undergo cyclic loadings then the stresses induced in the vessel by such loads must also meet the fatigue evaluation requirements of Paragraph AD-160, and Appendix 5. These articles of the code specify in what cases a fatigue evaluation is required and the means of establishing stress limits to be used in such evaluations. In the case that a fatigue evaluation is required then these paragraphs require that one half the stress range, which now includes local stress concentration factors at any point being

investigated, must be equal to or less than the stress intensity amplitude for the number of cycles of life desired, as given by Figure 5-110.2, extracted and shown in this report as Figure 2. What this means is that the total minimum stress intensity (occurring at the minimum loading condition) is subtracted from the total maximum stress intensity (occurring at the maximum loading condition) to establish the cyclic stress intensity range. This figure is divided in half and the resultant is termed the stress intensity amplitude, S_a. As can be seen from Figure 2 (5-110.2), for the material used in the bubble chamber, S_a is about 26,000 psi to ensure 10^6 cycles of operation. Thus from Figure 1 (see note 3) the allowable stress intensity for the full stress range of load fluctuation is 2 S_a, or about 52,000 psi for 10^6 cycles of operation. The requirement for a fatigue evaluation for the bubble chamber is established by the details of Paragraph AD-160.2 "Rules to Determine Need for Fatigue Evaluation of Integral Parts of Vessels". This paragraph states that "A fatigue analysis need not be made provided that all of Condition A or all of Condition B is met." The first part of Condition A is not met. This part requires that the number of expected pressure cycles where the full range of pressure variation exceeds 20 percent of the design pressure, together with other types of pressure variations, such as startup and shutdown, does not exceed 1000 cycles. As described in the Introduction, the design pressure for the chamber is 150 psig while the pressure excursion is to be about 70 psi. This excursion is greater than 20 percent of the design pressure and millions of cycles of such operation are anticipated. Condition B, (a) states that a fatigue evaluation is not required if "the expected design number of full range pressure cycles does not exceed the number of cycles in the applicable fatigue curve of Appendix 5 corresponding to an S_a value of 3 times the S_m value found in the tables of design stress intensity values in Part AM for the material at the operating

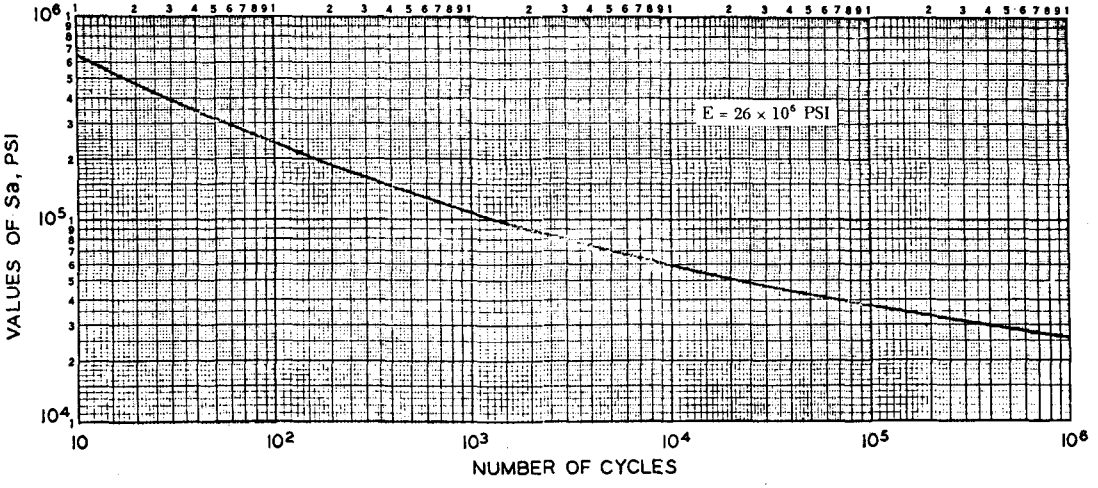

FIG. 5-110.2 DESIGN FATIGUE CURVE FOR SERIES 3XX HIGH-ALLOY STEELS, NICKEL-CHROMIUM IRON ALLOY, NICKEL-IRON-CHROMIUM ALLOY, AND NICKEL-COPPER ALLOY FOR TEMPERATURES NOT EXCEEDING 800 F

FIGURE 2. FATIGUE DESIGN CHART FROM ASME BOILER AND PRESSURE VESSEL CODE, SECTION VIII - DIVISION 2

temperature". As previously discussed the value of 3 S_m for 316L at temperatures up to 100° F is 49,800 psi. From Figure 2 (5-110.2), the number of cycles for such an S_a is approximately 60,000 cycles of operation. Millions of cycles of actual operation are anticipated; thus, Condition B is not met and a fatigue evaluation for the bubble chamber is required.

An anomaly seems to appear in the above discussion. The design basis for the bubble chamber is a cyclic loading condition of in excess of 10^7 cycles of operation at cryogenic temperatures. Yet, Section VIII-Division 2 renders fatigue data only up to 10^6 cycles of operation and only for material temperatures at or above room temperature (standard); and yet this code is being used to set the design requirements for the vessel. In explanation of this situation it should first be pointed out that there is no existing code that explicitly covers cryogenic vessels subjected to cyclic loadings. Secondly, application of the requirements of Section VIII - Division 2 should result in the design of a conservative vessel from the viewpoint of fatigue for the following reasons. The fatigue stress limits as exemplified by Figure 5-110.2 of this code incorporate better than a factor of safety of 2.0 on stress and/or 20.0 on life. Further, the code takes no cognizance of the beneficial effects of extremely low temperatures on the material properties of almost all austenitic steels including 316L. Experimentation* has shown that the fatigue strength of this material more than doubles when operating at liquid hydrogen temperatures.

Based on the above reasoning it is concluded that if the bubble chamber design is governed by the requirements Section VIII-Division 2, then the chamber will be structurally adequate to sustain the

---

*Appendix A of Summary Report to Argonne National Laboratory entitled, "The Study of the Structural Response Characteristics of Argonne's 12-foot-Diameter Hydrogen Bubble Chamber", dated August 9, 1968.

anticipated cyclic loadings through its entire lifetime which should be in excess of 10^7 cycles.

(3) GENERAL PROCEDURE

The general procedure followed in the design analysis of the bubble chamber was, to a large degree, dictated by the operational schedule of NAL. Preliminary analysis, carried out by NAL with Battelle's cooperation, initialized the configuration of various components of the chamber vessel. These components were then critically stress analyzed to ensure their structural adequacy and compliance with the regulations and intent of Section VIII - Division 2. Initially, a static stress analysis was carried out. In this phase the only type of loads considered were the maximum and minimum pressure conditions. Based on these conditions stress intensities were developed and fatigue evaluations were carried out.

To ensure the validity of these findings, the vessel structure was then analyzed for its dynamic response to the actual anticipated time dependent forcing functions. This analysis generated data to enable prediction of the presence of dynamic amplification of stresses in the vessel as calculated on the basis of a static application of loads.

(4) CONCLUSIONS

The components of the bubble chamber analyzed in this report are structurally adequate to sustain the assumed cyclic loadings and meet the intent and specifications of the ASME Boiler and Pressure Vessel Code, Section VIII, Pressure Vessels - Division 2, Alternative Rules. This finding is predicated on the following conditions:

- The loads are as assumed.
- There are no significant, steady-state, thermal gradients in the structure during operation, with the exception of the region of the support cone.
- The as-fabricated condition of the vessel components conform closely to the detail drawings upon which this analysis is based.

- All material and fabrication techniques meet the intent and specification of the pertinent paragraphs of Section VIII - Division 2.

(5) STATIC STRESS ANALYSIS OF CHAMBER COMPONENTS

Most of the bubble chamber components comprise sections of a body of revolution. This being the case they are capable of being stress analyzed by Battelle's thin shell of revolution computer stress analysis code MONSA. MONSA is a digital computer program for the stress and displacement analysis of shells of revolution loaded by symmetric or nonsymmetric loads. It is based upon A. Kalnin's work as described in a paper in the Journal of Applied Mechanics, Vol. 3, September, 1964, pp. 467-476, titled "Analysis of Shells of Revolution Subjected to Symmetrical and Nonsymmetrical Loads". Though continually modified and amplified over the years, the basic program has been used extensively by Battelle personnel since mid-1965. In its present form, it is based on the multi-segment numerical integration method for the analysis of general shell of revolution boundary value problems. It has two components, MONSA-S and MONSA-V. MONSA-S will determine the displacements, forces, and stress for a composite shell. Such a shell may be composed of a number of distinct parts which may have the following shapes: cylindrical, spheroidal, ellipsoidal, paraboloidal, conical, and toroidal. The shell wall may be composed of four different layers of orthotropic materials. The thickness of these layers can vary along the meridional generator. Mechanical and temperature loadings can be applied to the shell. For nonsymmetric loadings, the loads must be broken down into their Fourier harmonics, each harmonic requiring a computer run, though as many as 15 harmonics can be run consecutively at one machine run. Temperatures can vary meridionally as well as through the shell thickness. Further, this program allows the analysis of a shell spinning about its axis as well as the analysis of a shell

subjected to harmonically (time dependence) varying mechanical and temperature loads. MONSA-V will determine the natural frequencies and mode shapes of the composite shells of revolution described above.

MONSA-S was used directly in the analysis of the "beanie"-main shell intersection and the analysis of the complete "Z" section (that part of the chamber below the piston). It was used indirectly in the analysis of the camera penetrations in the "beanie". This program was used to generate "nominal" stresses in the region of the chamber being analyzed. In areas away from local discontinuities and other stress raisers, such as small holes and abrupt changes in wall thickness, these "nominal" stresses can be taken as the total or exact stresses occuring in the part. Where these discontinuities exist the "nominal" stresses must be modified by stress concentration methodology or some other suitable techniques.

The chamber was analyzed under two loading conditions. It was assumed that the target area (above the piston) would be subjected to a maximum internal pressure of 150 psia and a minimum pressure of 0 psia. The "Z" section (below the piston) would be subjected to a maximum internal pressure of 200 psia and a minimum pressure of 0 psia. The outside of the vessel was assumed to be at 0 psia for all cases. It is realized, of course, that while the maximum pressures quoted above are realistic design parameters for the chamber, the minimum pressures will only be seen when the chamber is empty. Ordinarily, a drop in pressure of 70 psi in the target area and somewhat less in the "Z" section is seen during operation. Further the maximum pressures quoted will occur only during operation when the chamber is filled with neon. Further, in normal operation the chamber would be filled with liquid above the piston and with cold gas below it. When the chamber is not pulsing the liquid and the gas are in pressure equilibrium. During the pulse, the piston is forced downward, dropping the pressure in the liquid and increasing the pressure in the gas.

The assumption of the 150-0 psia and the 200-0 psia pressure ranges render conservative stress results. That is the calculated stresses for these pressure conditions should render greater fatigue stresses than those actually expected for the actual pressure cycles that the chamber is expected to sustain. Designing the vessel to meet Section VIII - Division 2 requirements under these assumed loadings should increase the working safety factor for the chamber.

There is one area of analysis where a different set of pressure loadings are applied. The dropping of the pressure in the target area coupled simultaneously with the increase in pressure in the "Z" section will induce a net downward thrust on the support cone. In the analysis of this section, then, it is anticipated that the maximum loading condition will be approximately 70 psia in the target area and 200 psia in the "Z" section while the minimum loading will be 150 psia in both sections. Again, there will be vacuum outside the vessel in all cases. Under these assumed loads, the support cone will see a large net downward and a small net upwards thrust, respectively, such forces constituting the worst design fatigue situation.

The description of the above loadings and the details of the analyses described in the following sections are predicated upon the piston-actuator system being bolted to and supported by the concrete caisson forming the base of the bubble chamber complex. If this design is to be altered such that the piston-actuator system is bolted to the bottom of the "Z" section, then the stresses as calculated and detailed in this report are invalid. Under such a circumstance the structure would have to be reanalyzed before any judgments could be made as to its ability to sustain operational loads.

The "Beanie"-Chamber Intersection

Initially, the basic shape of the bubble chamber was that of a sphere with an inner diameter of 150.0 inches and a wall thickness of 1.0 inch. As the design progressed it was decided to modify the

structure by the addition of a hemispherical shell section having an inner diameter of 108.0 inches and a minimum wall thickness of 1.0 inch. The top of the original sphere was removed and the hemisphere was added. This hemispherical shell, herein called the "beanie", is to contain all the camera nozzles. It was recognized that the line of intersection between the two spherical shell segments would be a region of high stress due to the discontinuity effect of joining the two different diameter sphere sections. To mitigate this stress condition the intersection was designed to incorporate a toroidal knuckle section having a minor radius of 12.0 inches as shown in Figure 3.

The "beanie" is not placed directly on top of the bubble chamber, but rather slightly askew. The center of the "beanie" lies on a vertical line from the center of the main chamber as seen from the location of the beam window. However, as viewed from the side of the chamber, 90° away from that beam window along the equatorial line, the center of the "beanie" lies on a line through the center of the chamber that inclines 10° from the vertical towards the back of the chamber.

For purposes of this analysis, the "beanie"-knuckle-chamber configuration was modeled as a body of revolution as shown in Figure 3. This geometric model, together with the uniform 150 psia internal pressure loading with 0 psia outside pressure, and the boundary conditions shown in Figure 3 were used as input to MONSA-S. The output of MONSA-S showed that the maximum stresses developed in this region are as those depicted in Figure 4. In this figure are depicted stresses occurring at 4 locations; at the midpoint of the toroidal knuckle and in one of the welds, on both the inner and outer surfaces of the shell at each location. Here σ_ϕ represents the meridional and σ_θ represents the circumferential or hoop stress. As shown the maximum stress occurs on the outer surface in the midpoint of the knuckle and is 25,417 psi in the circumferential

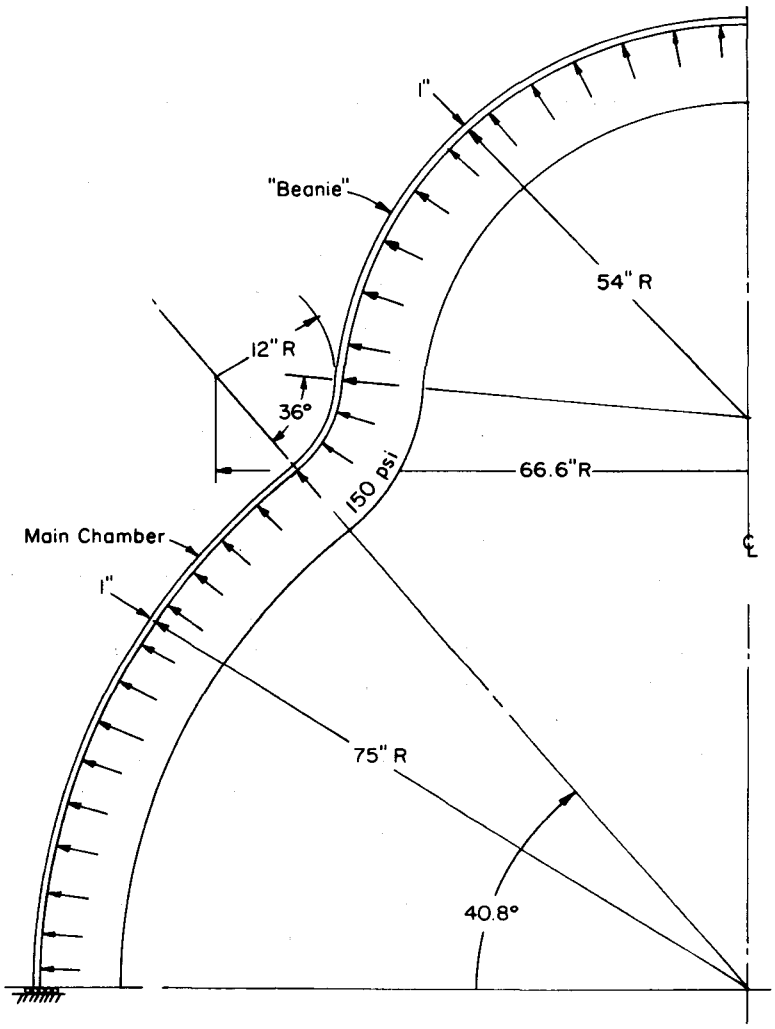

FIGURE 3. GEOMETRIC AND LOADING MODEL OF MODIFIED "BEANIE"-CHAMBER INTERSECTION FOR INPUT TO MONSA-S

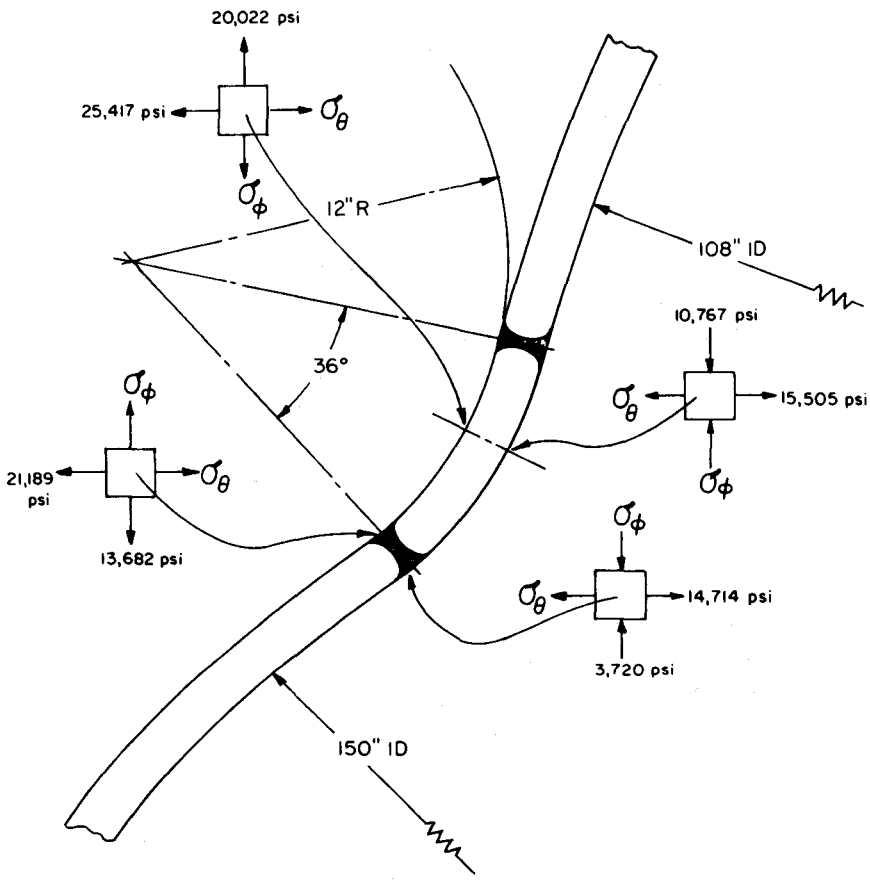

FIGURE 4. MAXIMUM STRESSES IN WELDS AND KNUCKLE OF MODIFIED "BEANIE"-CHAMBER INTERSECTION

direction. The maximum stress intensity at this location is then given by

$$P_L + B_b + Q = |\sigma_\theta - \sigma_r| = |25,417 - (-150)| = 25,567 \text{ psi}$$

This quantity is less than the $3S_m$ limit imposed by the code which is 49,800 psi. Further, considering the smooth nature of the transition in this locality, no stress concentration would be expected to occur there. Thus the peak stress intensity would be the same as determined above or 25,567 psi. This figure is considerably lower than the fatigue limit, $2S_a$, or 52,000 psi, thus meeting the code's fatigue requirement.

"Beanie"-Camera Nozzle Configuration

The "beanie" is to carry 6 camera nozzles in a nonsymmetrical pattern as shown in NAL's drawing No. 2621.ME-25134 (included in this report). These nozzles, which are detailed in NAL's drawing No. 2623.-ME-25001 (not included in this report), have axes which are not coincident and collinear with radial lines taken from the geometric center of the "beanie" shell.

The stress analysis of this section of the chamber was carried out in two parts. The first part dealt with the determination of the stresses induced by a 150 psi internal pressure load acting upon an isolated camera nozzle in a radial penetration orientation in the "beanie" shell. The second part dealt with the effect that the close spacing and lack of radial orientation of the camera nozzles have upon the stress field generated in the first part.

Initially, a model was structured wherein the nozzle-"beanie" assembly formed a body of revolution. This geometric model and the loads acting upon it are shown in Figure 5. The loads on the nozzle are derived from the preloading required to mount and seal the camera-optics package. The "beanie" is fabricated from 316L plate. The nozzles are centrifugal castings of CF3M material. The modulus of

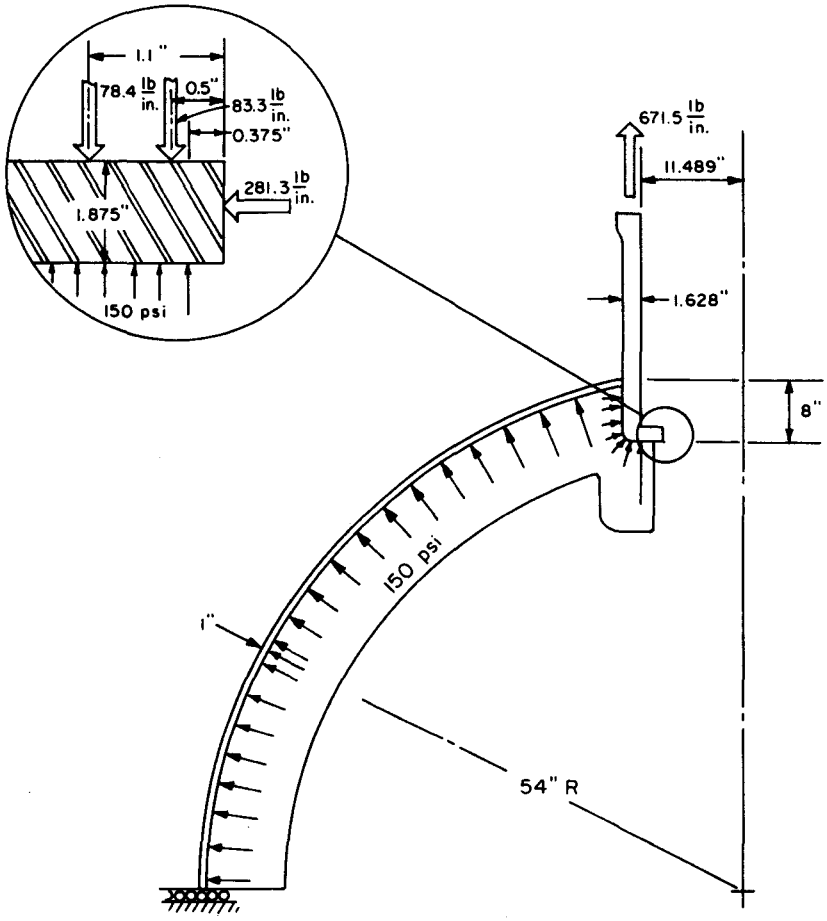

FIGURE 5. GEOMETRIC AND LOADING MODEL OF "BEANIE"-CAMERA NOZZLE INTERSECTION FOR INPUT TO MONSA-S

elasticity used in this analysis for 316L plate is 28 x 10^6 psi. Normally, cast structures fabricated from CF3M would have the same modulus of elasticity as 316L plate. However some recent research carried out by Battelle indicates that the modulus of elasticity of centrifugally cast stainless steel structures may be significantly lower than that of plane or wrought stainless. To determine the effect of such a condition two models of the nozzle-"beanie" configuration were used as input to MONSA-S. Both models had the same geometry and load conditions. The first model used 28 x 10^6 psi as the modulus of elasticity for the "beanie" while 21 x 10^6 psi was used as the modulus of the nozzle material. The second model used 28 x 10^6 psi for the modulus of elasticity for the material of both structures. The output results from MONSA-S showed that the stresses induced in both models by the given load condition were approximately the same. The effect of the reduced modulus for the nozzle was that the maximum stress in the "beanie" was slightly higher while the maximum stress in the nozzle was slightly lower than in the model case where both components had the same modulus. The stress condition and the local deflection pattern for the model employing different modulii of elasticity are shown in Figure 6. The decay length as shown in this figure indicates the distance along the shell to the point at which the maximum stress found in the shell is only 10 percent greater than the stress that would be found in the shell if no discontinuity existed. As can be seen the maximum stresses are quite low. In fact even if an unreasonably high stress concentration factor of 5.0 existed in the high stress location, the ensuing stresses would still be acceptable from the viewpoint of fatigue. A stress concentration greater than 5.0 need not be considered in this application for code purposes for the following reason. Paragraph 5-111 of Section VIII - Division 2 states

"5-111 Local Structural Discontinuities
These effects shall be evaluated by the use of theoretical

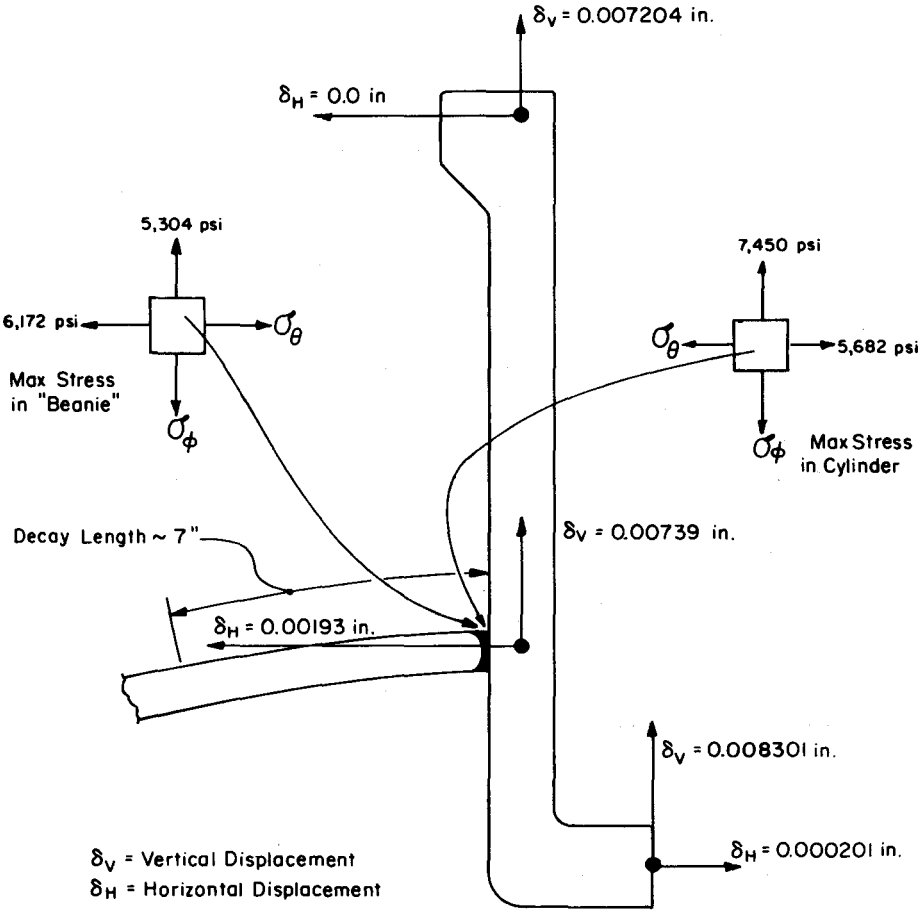

FIGURE 6. MAXIMUM STRESSES AND DEFLECTION PATTERN IN MODIFIED "BEANIE"-NOZZLE INTERSECTION

> stress concentration factors for all conditions, except that experimentally determined fatigue reduction factors may be used when stated herein or when determined in accordance with the procedures of 6-180. Except for the case of crack-like defects, no fatigue strength reduction factor greater than 5.0 need be used."

Experience has shown that with good fabrication procedures and smooth filleting of sharp intersections that eliminate any crack-like defects the stress concentrations that exist in geometries such as the "beanie"-nozzle intersection do not exceed 3.0.

As discussed, the model analyzed above represents an isolated camera in a radial penetration orientation. Such a geometry does not exist in the actual head configuration. Rather the 6 nozzles are grouped in sets of two each. The two nozzles in each set are closely spaced, with the closest spacing being only 2-3/4 inches as measured from the outside of the nozzles along the surface of the "beanie". Further, most of the nozzles are not set in a radial position in respect to the "beanie", but are in a slightly skewed orientation. Such positioning causes the opening in the "beanie" shell to be elliptical in shape rather than circular as would be the case for a radial penetration.

The close spacing of the nozzles and their lack of radial orientation, both cause an increase in the maximum stresses as calculated by MONSA-S for the isolated camera nozzle condition. And, in fact, for unreinforced holes thus closely spaced the stresses actually existing in this region would be unacceptably high. However, these penetrations are reinforced and they do meet code requirements as is shown by the following discussion.

Article D-5, Openings and Their Reinforcement, of Section VIII - Division 2, deals with the problem at hand. The provisions of Paragraph AD-510 merely state that openings of the nature involved in the "beanie"-nozzle configuration must be reinforced. Paragraph AD-520 states

"(a) The total cross-sectional area of reinforcement, A, required in any given plane for a vessel under internal pressure shall not be less than

$$A = dt_rF$$

where

d = the diameter in the given plane of the finished opening in its corroded condition, inches

t_r = the thickness in inches which meets the requirements of Article D-2 in the absence of the opening

F = 1.00 when the plane under consideration is in the spherical portion of a head or when the given plane contains the longitudinal axis of a cylindrical shell. For other planes through a shell, use the value of F determined from Fig. AD-520.1 except that, for reinforcing pads, F = 1.

(b) Not less than half the required material shall be on each side of the centerline of the opening (see also AD-540.1(c))."

Article D-2, Paragraphs AD-201 and AD-202, sets the required thicknesses, t_r, for the nozzle and the "beanie", respectively, as

$$\text{nozzle} \qquad t_r = \frac{PR}{S_m - 0.5P}$$

$$\text{"beanie"} \qquad t_r = \frac{0.5PR}{S_m - 0.25P}$$

where P = the design pressure, psi

R = the inside radius of shell, inches

S_m = the design stress intensity limit for the material, psi

Thus for the nozzle

$$t_r = \frac{(150)(11.489)}{20{,}000 - (0.5)(150)} = 0.087 \text{ inch}$$

and for the "beanie"

$$t_r = \frac{(0.5)(150)(54.0)}{16{,}600 - (0.25)(150)} = 0.245 \text{ inch}$$

The "beanie" has a wall thickness of 1.0 inch and the nozzle has a wall thickness of 1.628 inches. This means that 0.755 inch of the "beanie" wall thickness is available to be considered as reinforcement while the same is true of 1.541 of the nozzle wall. Section A-A of NAL's drawing No. 2621.ME-25134 (included in this report)shows that one nozzle is severely canted and presents the worst case as far as

elliptical penetrations are concerned. The major diameter for this penetration is 30.9 inches. Thus the area of reinforcement required in this plane is

$$A = dt_r(1.0) = (30.9)(0.245)(1.0) = 7.471 \text{ inches}^2$$

half of which, or 3.785 inches^2, must be on either side of the centerline.

Paragraph AD-540, Limits of Reinforcement, sets the boundaries of the cross section in any plane normal to the vessel wall and passing through the center of the opening within which metal shall be located in order to have value as reinforcement. Basically the distance as measured along the shell, on each side of the opening in the plane, is approximately equal to the radius of the opening. The distance normal to the main shell midsurface, both above and below this surface is approximately given by

$$\text{Limit} = 0.5\sqrt{r_m t_n}$$

where r_m = mean radius of nozzle

t_n = nominal nozzle thickness.

From the above it can be seen that the nozzles are more than completely reinforced in those planes not including another nozzle, by the excess material in the "beanie" wall. That is only 3.785 in^2 of reinforcing material are required and

$$0.755 \times (14.0) = 10.5 \text{ in}^2 \text{ are available.}$$

In the region between the nozzles, especially where the nozzles are only 2-3/4 inches apart, only

$$0.755 \times (2.75) \times 0.5 = 1.03 \text{ in}^2$$

are available for each opening.

Thus the remainder of the required reinforcement or 2.755 in^2 for each opening must come from the excess nozzle wall thickness. The distance along the nozzle wherein material may be considered as available for reinforcement is

$$\text{Limit} = 0.5\sqrt{(12.303)(1.628)}$$

$$= 2.40 \text{ inches above and/or below the "beanie" midsurface.}$$

Thus, the area of material in the nozzle available for reinforcement, restricting ourselves to that area above the "beanie" midsurface is equal to

$$(1.541) \times (2.40) = 3.7 \text{ in}^2.$$

This amount of reinforcement is more than enough to meet the code requirements so far as static loads are concerned. To determine the adequacy of the "beanie"-nozzle configuration to sustain cyclic loading the provisions of Article 4-6, Pressure Stresses in Openings for Fatigue Evaluation, were applied. Paragraphs 4-610 through 4-613 deal with the stress index method of evaluating openings for fatigue. This method deals with the analytic establishment of a fatigue concentration factor based on the nominal stresses in the unpenetrated shell for a given family of isolated nozzle configurations. It is not directly applicable to those nozzles in the "beanie" which are closely spaced. However, data generated using this method do give a good indication that the "beanie"-nozzle configuration is acceptable from a fatigue viewpoint.

The nominal stresses, in the 1.0 inch wall thickness "beanie" are given by

$$\sigma_n = \frac{PR}{2t} = \frac{(150)(54)}{2(1)} = 4{,}050 \text{ psi.}$$

Paragraph 4-612 gives the stress index for a radial penetration nozzle of a given type as 2.0. Paragraph 4-613 states

> "(a) The opening is for a circular nozzle whose axis is normal to the vessel wall. If the axis of the nozzle makes an angle, ϕ, with the normal to the vessel wall, an estimate of the σ_n index on the inside may be obtained from the following formula, provided $d/D \leq 0.15$.
>
> For hillside connections in spheres or cylinders
>
> $$K_2 = K_1(1 + 2 \sin^2 \phi)$$

where K_1 = the σ_n inside stress index of 4-612 for a radial connection
K_2 = the estimated σ_n inside stress index for the nonradial penetration."

The greatest angle that any of the nozzle centerlines makes with the normal to the "beanie" shell at each nozzle location is approximately 30 degrees. Thus

$$K_2 = 2.0(1 + 2 \sin^2 30) = 3.0.$$

Thus if these specifications were directly applicable to the nozzle-"beanie" configuration it could be said that the approved estimated peak stress occuring in this area would be

$$S = 3.0(4050) = 12,150 \text{ psi.}$$

This figure is less than 1/4 of the code acceptable value of $2S_a = 52,000$ psi. However, the provisions of Paragraphs 4-611 through 4-613 are not directly applicable for the following reasons.

- The camera nozzle-"beanie" configuration does not exactly match those penetration configurations depicted in Figure 4-613.1 of the code.
- The ratio of the inside nozzle diameter to inside shell diameter, d/D, equals 0.21 and is thus greater than the limit of $d/D \leq 0.15$.
- There are several closely spaced nozzles which cannot be considered isolated.

Regardless of the above variances from code specifications it is the opinion of the authors of this report that the nozzle-"beanie" configuration is adequate to sustain the anticipated cyclic loadings for the mission life of the structure. This opinion is based on the results of the above calculations correlated to the MONSA-S output for the isolated nozzle as shown in Figure 6. The penetration is sufficiently reinforced to reduce the nominal stress concentration in the "beanie" at this location to 1.5. Further, the nominal stress, $\sigma_n = 4050$ psi, is sufficiently low that a total stress concentration of greater than

12.0 would have to occur in this location before the code set fatigue limit of $2S_a$ = 52,000 psi would be surpassed. Again, considering the amount of reinforcement emplaced in this region such a stress intensification is not judged possible.

However, to strictly meet code requirements in this case an experimental evaluation of the stresses in the location of the closest spaced nozzles should be carried out as per the provisions of paragraphs 4-621 and Appendix 6 of Section VIII - Division 2.

Lower Chamber or "Z" Section

The design of the lower chamber or "Z" section was in preliminary design at the start of this analysis. A configuration, primarily based upon the geometric requirements of the piston and the upper chamber was developed. This structure, as shown in Figure 7, is a body of revolution and is thus directly amenable to analysis by use of MONSA-S. The basic structure was modeled as shown in this figure and together with the loads indicated was used as input to the computer program. A slightly more stringent boundary condition than would be anticipated in actual operation was imposed on the upper flange. This boundary condition involved a restriction against rotation of this flange, in the plane of the paper, at the location of the bolt circle, where the bolts are to secure the "Z" section to the upper chamber body. Some rotation of this flange is anticipated in regular operation. The lower portion of the center "spool" cylinder was truncated since this portion was not considered as a structural component so far as the pressure induced stresses are concerned. The 210 pounds per inch of circumference end thrust shown acting on this truncated section is induced by the atmospheric pressure acting on the annular flat plate attached to the bottom of the cone (not shown in this report).

The stresses in this "Z" section, as computed by MONSA-S, are generally quite low and the crude configuration sketched presents a

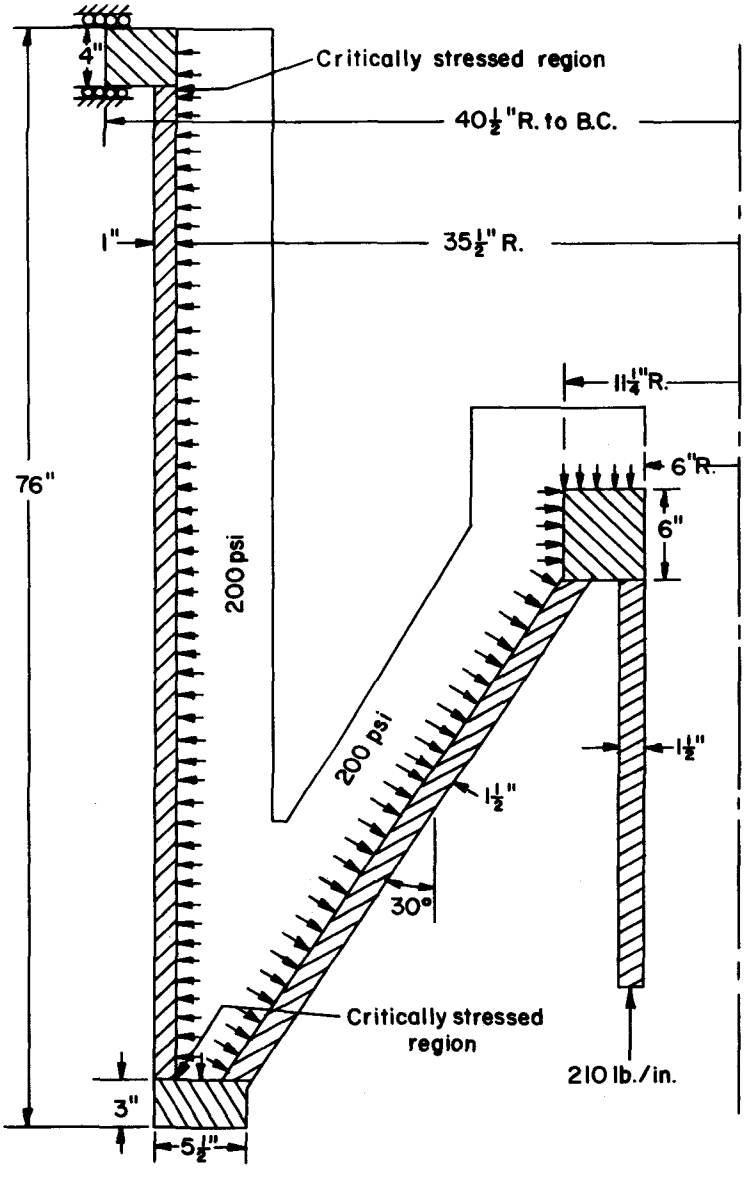

FIGURE 7. PRELIMINARY GEOMETRIC AND LOADING MODEL OF "Z" SECTION SHOWING CRITICALLY STRESSED REGIONS

structurally adequate vessel to sustain the anticipated cyclic loads with but two exceptions. Stresses were calculated to be critically high in the outer cylinder where it joined the upper flange and also where it joined the annular ring connecting it to the inner cone.

The stress condition in the bottom joint was corrected by studying several different joint configurations and evaluating them on the basis of stress reduction, cost and ease of fabrication. The most acceptable configuration is shown in Figure 8. The maximum stresses found in the geometry are shown in Figure 9. These stresses are quite acceptable and the worst condition from the viewpoint of stress intensity occurs in the inner surface of the region where the uniform wall thickness 1.0 inch cylinder joints the tapered transition region. The stress intensity at this point is

$$P_L + P_b + Q = |\sigma_2 - \sigma_3| = |22{,}240 - (-200)| = 22{,}600 \text{ psi.}$$

The code allowable stress, $3S_m$ is 49,800 psi. A working drawing of an acceptable lower joint is shown in Figure 10. In such a configuration one would not reasonably expect a stress concentration factor of greater than 2.0 to exist in this region. Thus the peak stress intensity would become

$$S = 2.0(22{,}600) = 45{,}200 < 2S_a = 52{,}000 \text{ psi.}$$

Thus this joint is acceptable from a fatigue viewpoint.

NAL developed a proposed upper flange and it is shown in Figure 11. This configuration was modeled for input into MONSA-S as shown in Figure 12. As before, the initial boundary condition was assumed to be a restriction against rotation of the flange, in the plane of the paper, at the bolt circle diameter of 77-3/8 inches. The elimination of a portion of the flange as done in this model, as compared to the actual configuration, when coupled with the stringent boundary condition assumed should not introduce any significant errors in the calculated stresses.

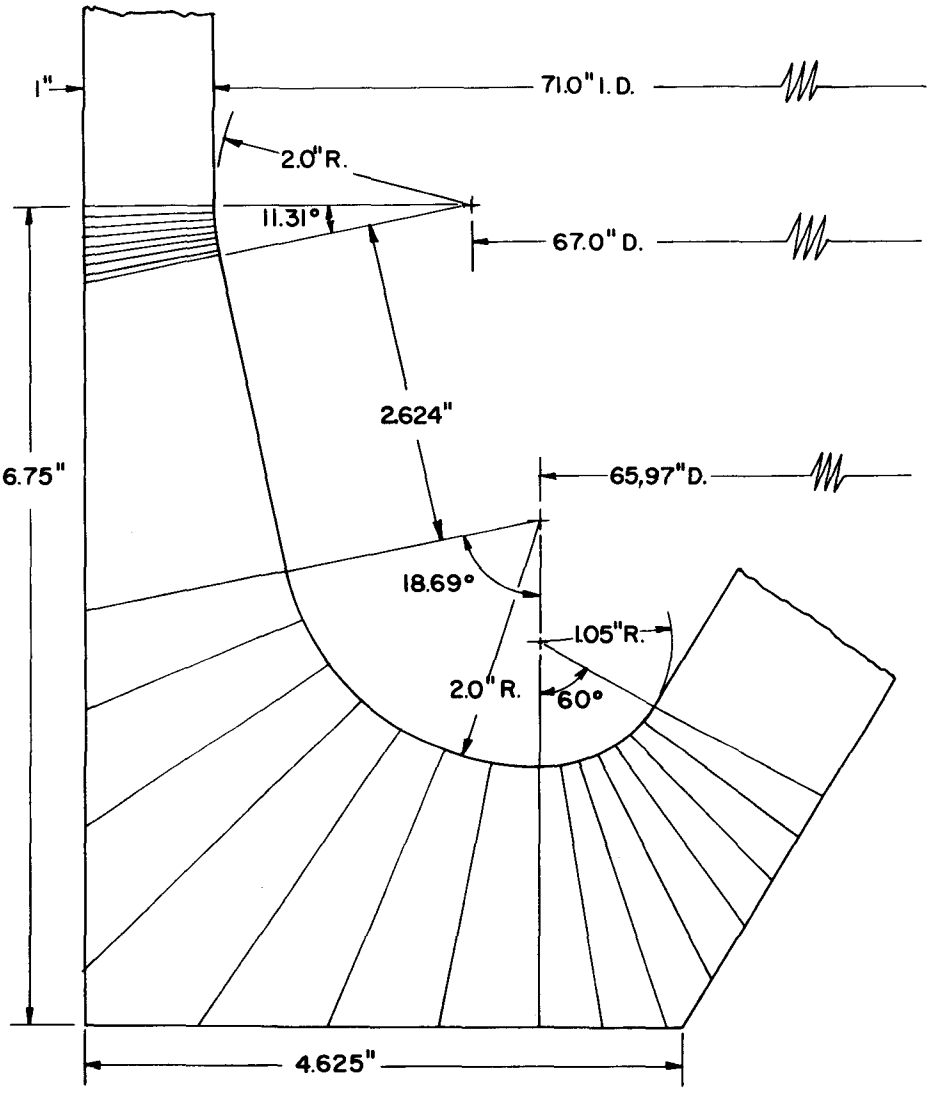

FIGURE 8. EXACT GEOMETRY OF MODIFIED BOTTOM JOINT IN "Z" SECTION FOR INPUT TO MONSA-S

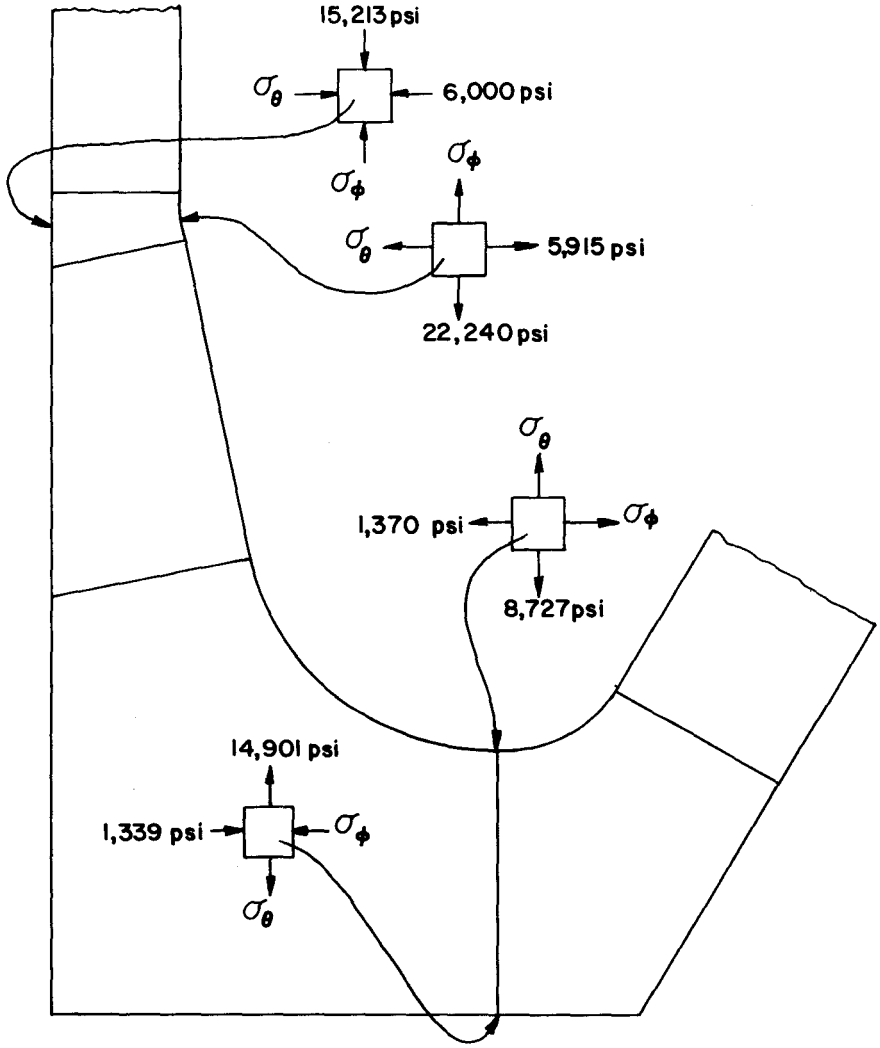

FIGURE 9. MAXIMUM STRESSES IN THE MODIFIED BOTTOM JOINT OF "Z" SECTION UNDER 200 PSI PRESSURE LOADING

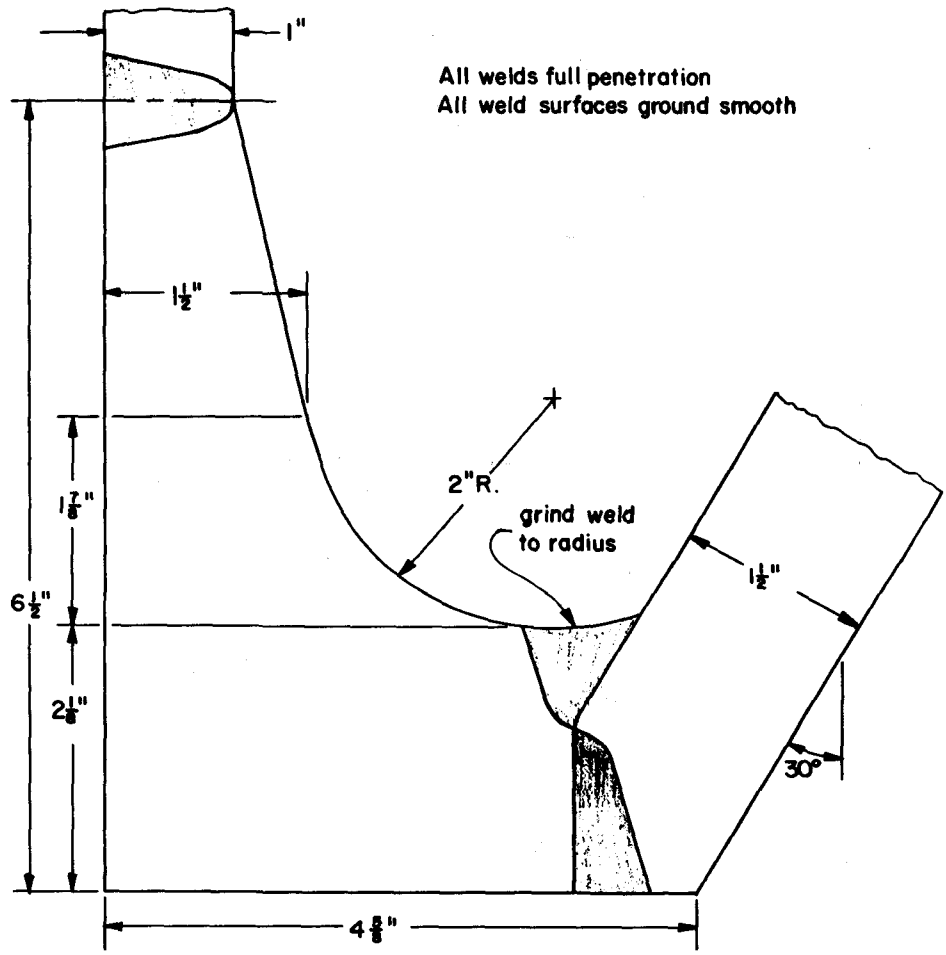

FIGURE 10. ACCEPTABLE BOTTOM JOINT CONFIGURATION

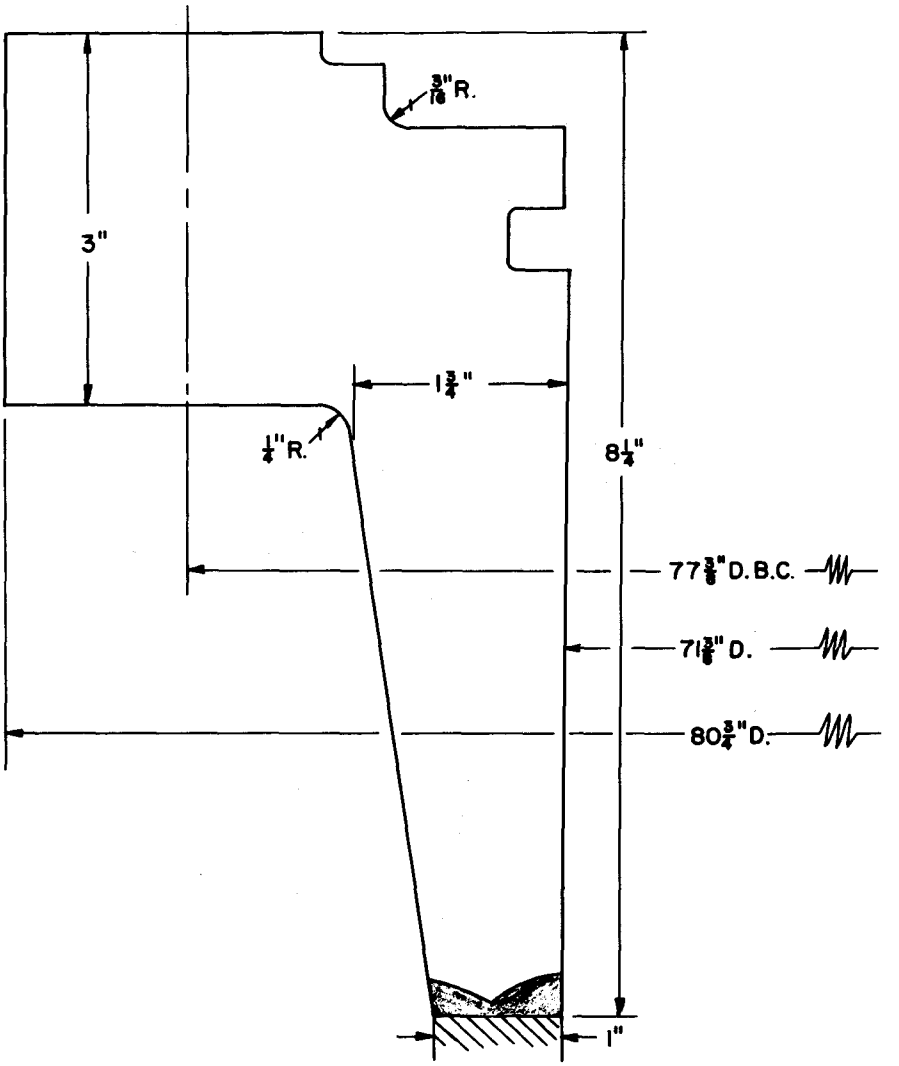

FIGURE 11. PROPOSED FLANGE FOR TOP OF "Z" SECTION

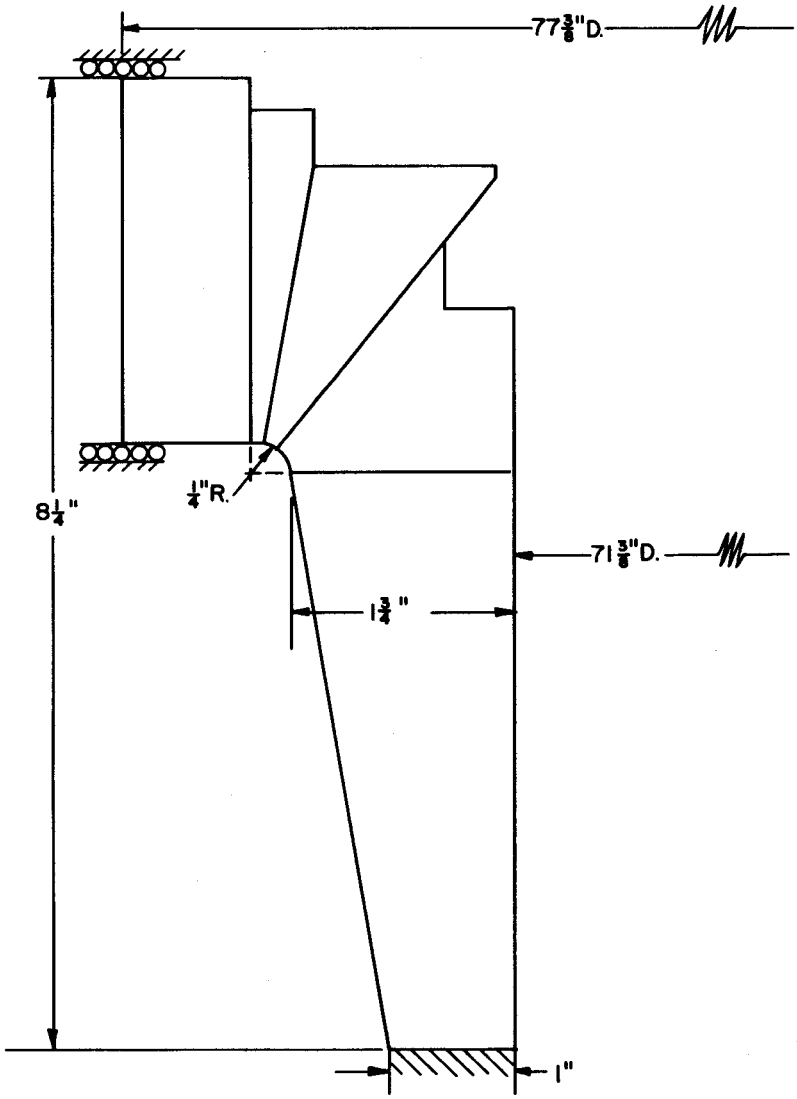

FIGURE 12. EXACT GEOMETRIC MODEL OF PROPOSED "Z" SECTION FLANGE FOR INPUT TO MONSA-S

The stresses induced in this section, as calculated by MONSA-S are quite low. The maximum "nominal" stresses in this flange are lower than the stresses found in the cylinder in regions well removed from the discontinuity. Thus the basic or "nominal" stresses are acceptable from the viewpoint of the code as applies to static loading. For fatigue evaluation, applying the code recommended (Paragraph 5-111) maximum stress concentration factor of 5.0 for local structural discontinuities, to account for the presence of the grooves and cutouts, the peak stresses so generated are still well below the $2S_a$ limit of 52,000 psi.

"Z" Section Flange Bolt Requirements

The analysis carried out on the "Z" section rendered sufficient data to determine the number of bolts required to secure the section to the upper chamber and to establish the amount of preloading of each bolt to ensure prevention of both flange separation and bolt fatigue failure during operation.

Under a 200 psi internal pressure loading of the "Z" section, 3,600 pounds per inch of bolt circle circumference pull-apart-load and 9,300 inch-pounds per inch of circumference moment were calculated as being induced in the flange at the 77-3/8 inch diameter bolt circle location. The 3,600 pounds per inch load can be used directly but the moment load must be converted to a direct tensile load that can be applied to the bolts. For this purpose it will be assumed that this moment is generated by a tensile force acting at the bolts. This tensile force acting through a moment arm equal to the distance fror the bolt circle to the outer radial edge of the flange equals the 9,300 inch-pounds per inch figure. The moment arm distance is 1.5 inches. Thus the equivalent tensile force acting on the bolts due to this moment is 6,200 pounds per inch of bolt circle circumference. This figure, added to the 3,600 pounds per inch tensile force calculated directly, gives a total equivalent tensile force of 9,800 pounds per

inch of bolt circle. The prior application of such a force in compression to the flange by preloading will ensure that no flange separation occurs during operation and that the bolts will undergo, effectively, no alternating loads at all, thus obviating the possibility of fatigue failure therein. To accommodate the required flange bolting load, 80 bolts, spaced 4.5 degrees or approximately 3.04 inches apart have been chosen. With this number of bolts a preload per bolt of 30,000 pounds is required. A 1-1/4-12 UNF bolt having a root area for computing tensile stress of 1.0729 $in.^2$ (ASA B1.1-1960, p.59) will give a prestress of 28,000 psi when loaded to 30,000 pounds.

High strength bolts with expansion coefficients comparable to austenitic steels are available and may be employed. These bolts should comply with ASME Specification SA-453, grade 660. Bolts fabricated from this material should exhibit a minimum tensile strength of 130,000 psi and a minimum yield strength of 85,000 psi, both figures derived at standard room temperature. According to all available literature bolts fabricated from this material have cryogenic behavioral characteristics as good, if not superior, to those bolts conforming to ASME Specification SA-193, grade B8/304, which is code approved for operation at -425 degrees F. Section VIII - Division 2 does not specifically authorize the use of SA-453, grade 660 material for bolting operation. In the opinion of the authors this omission is an oversight on the part of the code committee. This opinion is founded on the fact that ASME Section III, Nuclear Power Plant Components, does include this material and sets the design stress intensity, S_m, at 28,300 psi for temperatures not to exceed 100°F. Thus it is judged that the selection of such material for bolting does meet the intent of Section VIII - Division 2.

Section VIII - Division 2 is rather indefinite when it comes to the specification of design rules for bolt loading. However, Article 3-5, Design Considerations for Bolted Flange Connections, Paragraph 3-500(d) states:

> "..... In any event, it is evident that an initial bolt stress higher than the design value may and, in some cases, must be developed in the tightening operation, and it is the intent of this code that such a practice is permissible, provided it includes necessary and appropriate provision to insure against excessive flange distortion and gross crushing of the gasket."

The NAL flange configuration does not incorporate a gasket and the flange itself is massive enough to preclude any distortion induced by the required preload. Further, Section III, specifically states that the actual service stress in bolts, such as those produced by preload, pressure and differential thermal expansion, may be higher than the listed stress intensity value, S_m, as given for the material. In fact, Paragraph NB-3232.1, of Section III, states

> "The maximum value of service stress, averaged across the bolt cross-section and neglecting stress concentrations, shall not exceed two times the stress values of Table I-1.3."

For this material, this stress value as previously quoted is 28,300 psi. Two times this value is 56,600 psi which is substantially greater than the 38,000 psi maximum average stress calculated previously.

From all the above it is the opinion of the authors of this report that the selection of the bolt material, spacing and preloading, as described in this section completely meets the intent of Section VIII-Division 2.

Beam Window Flange

The beam window flange design was developed by NAL and modified by the fabricator, Chicago Bridge and Iron (CB&I) so as to more adequately conform to the area replacement specification as detailed in Section VIII - Division 2. This flange, shown here in Figure 13, is detailed in CB&I drawing No. 71-2025-4, titled "Beam Window Flange 150" Dia. 30K Liter Weldment". The flange itself does comprise a body of revolution. Its placement in the chamber weldment, however, further causes that structure to deviate from a symmetric geometry. The flange forms one vertical segment of the chamber. Above it is the "beanie" and below it

is the multi-wall cone and support cone components of the chamber. There is a spherical shell section around this flange, between it and both the "beanie" and the bottom cones. Part of this spherical section can be seen in Figure 13.

The flange was analyzed by assuming that it was a part of a body of revolution composed of a uniform-wall-thickness spherical section and two variable-wall-thickness spherical sections. This model and its dimensions are shown in Figure 14. As in the case of the "beanie"-main chamber intersection, the stresses induced in the spherical segment surrounding the flange as a result of the geometric discontinuity are expected to decay in the shell at a relatively small distance from the discontinuity and thus not affect the basic stress conditions at either the cone or the "beanie" intersection.

The maximum loads expected to act on the flange are difficult to determine. These loads are dependent upon the geometry and hence the rigidity of the beam window protuberance. If the beam window protuberance were to be extremely flimsy, as say a membrane, then the only load acting on the flange, other than the direct pressure, would be a ring load of 1,940 pounds per inch. This is determined from the 150 psi pressure acting on an area defined by the 51.75-inch diameter bolt circle. Further, there would be no constraints on the deflections and rotation of the inner diameter surface of the flange. If the beam-window protuberance were to be extremely rigid, as say a thick-flat plate, then the horizontal ring load, as defined above, would still act on the flange but in this instance the meridional deformation and the rotation of the flange at its inner diameter would be restrained. In actuality the nose geometry will be such as to cause a loading on the flange somewhere between those extremes. At the time that this analysis was carried out the design of the beam window protuberance had as yet not been completed. However, some of the preliminary analysis that had

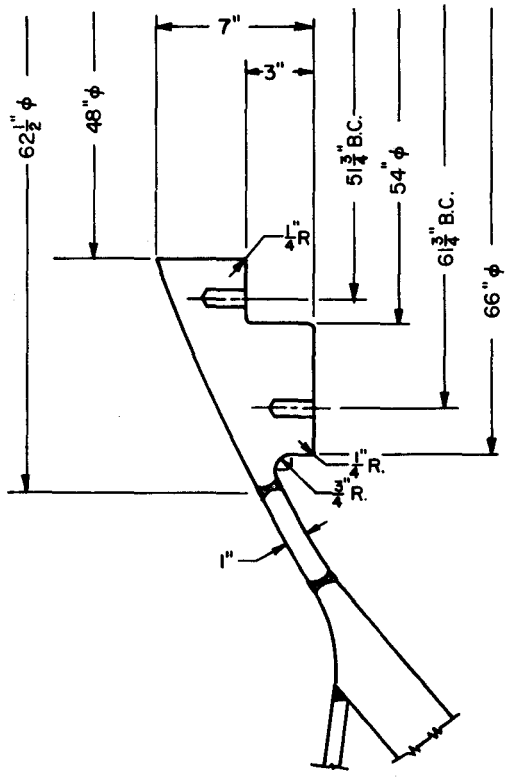

FIGURE 13. CB & I PROPOSED BEAM WINDOW FLANGE FOR MAIN CHAMBER

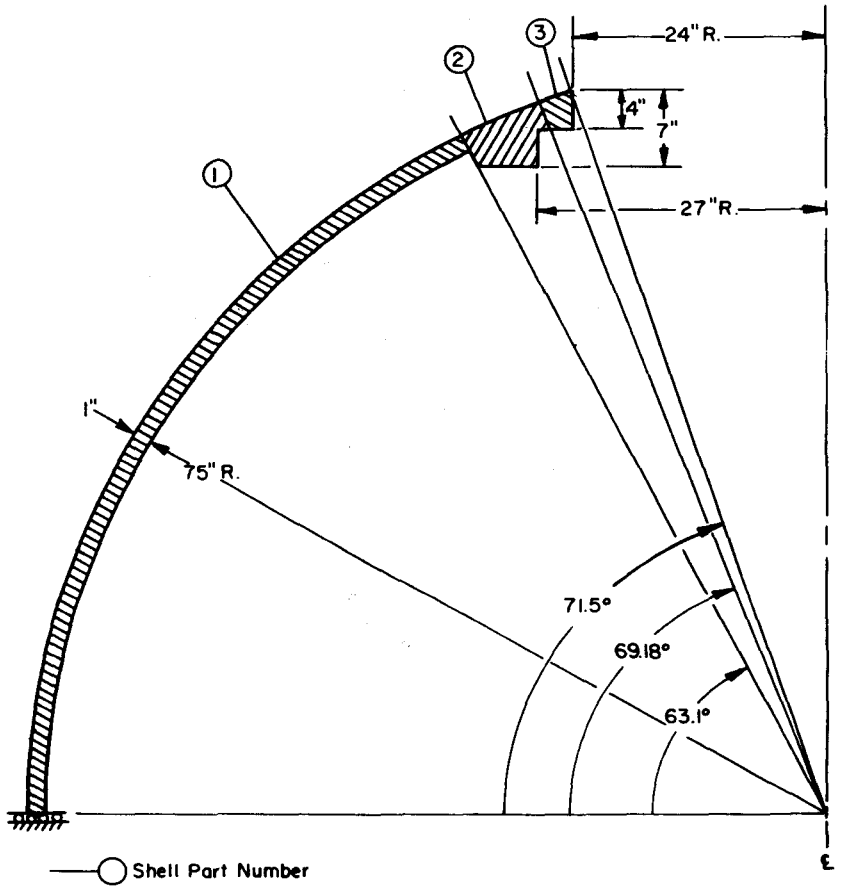

FIGURE 14. GEOMETRIC MODEL OF CHAMBER BEAM WINDOW FLANGE FOR INPUT TO MONSA-S

been conducted to establish the design of that component generated sufficient data to apply to the analysis of the beam window flange.

Considering the lack of definitive data as to the exact loading condition it was decided to consider two loading cases. Case 1, as shown in Figure 15, consists of solely the ring load discussed above. Case 2, as shown in Figure 17, consists of the ring load plus other loads as derived from a worst condition beam window protuberance design. The preliminary beam window protuberance design analysis produced a design that was not satisfactory from the viewpoint of code acceptability of stresses induced in this structure by a 150 psi internal pressure load. This analysis was carried out using a finite-element stress-analysis-computer code. The flange was incorporated in the model analyzed, though not in a form capable of rendering a detailed stress distribution in the flange itself. (The flange was modeled using block elements which represented its overall stiffnesses but which washed out its geometric details.) The loads shown in Figure 17 represent the maximum interaction forces generated between the flange and the beam window protuberance as calculated by the computer program. Because the protuberance is not a body of revolution, these forces occur at only one point on the flange. By assuming that these forces are symmetrically distributed along the bolt circle and the flange inner diameter as shown, a much more severe loading has been applied to the flange than would actually occur. Further, as pointed out above, the load data were generated from a protuberance design that was not satisfactory, as the predicted stresses induced in it were above acceptable levels. This means that the final beam window protuberance design would be stiffer and thus render interaction forces which would be smaller than those shown.

The geometry and the loads for Case 1 and Case 2 were used as input to MONSA-S. The stress outputs are shown in Figures 16 and 18 respectively. The maximum nominal stress intensity occurs for Case 1 and is

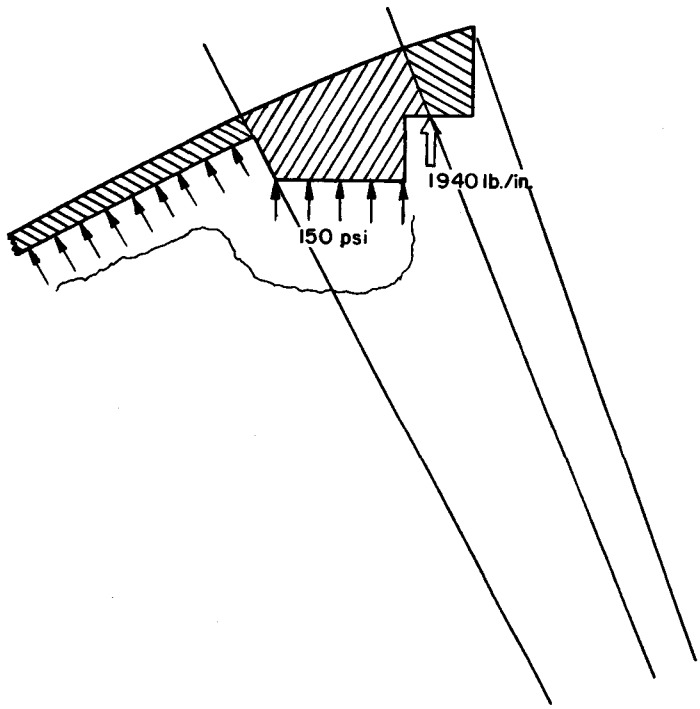

FIGURE 15. ASSUMED LOADING - CASE 1

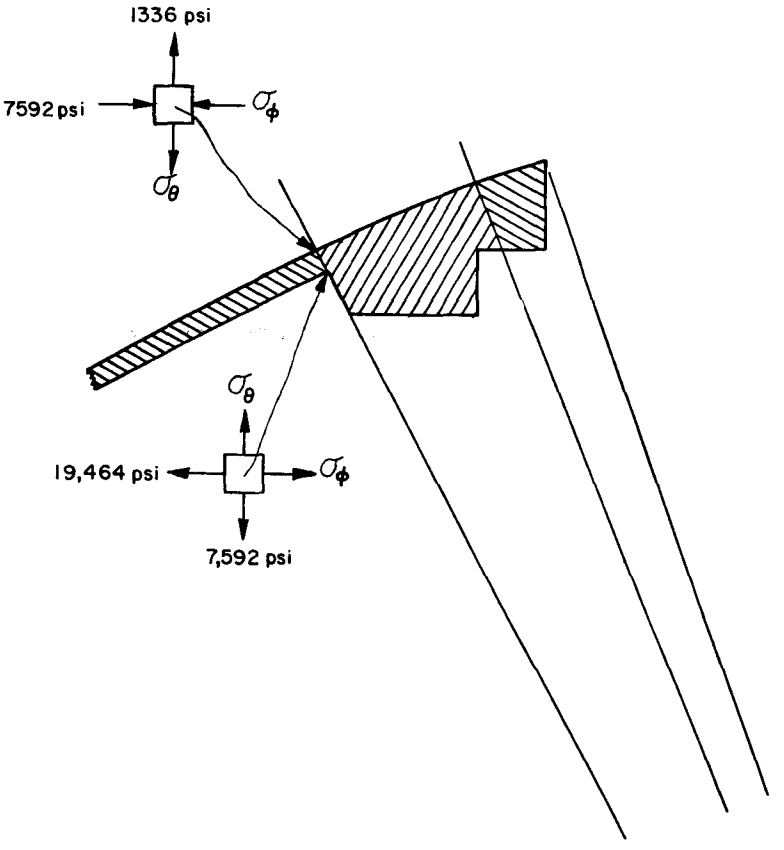

FIGURE 16. MAXIMUM STRESSES IN FLANGE FOR CASE 1

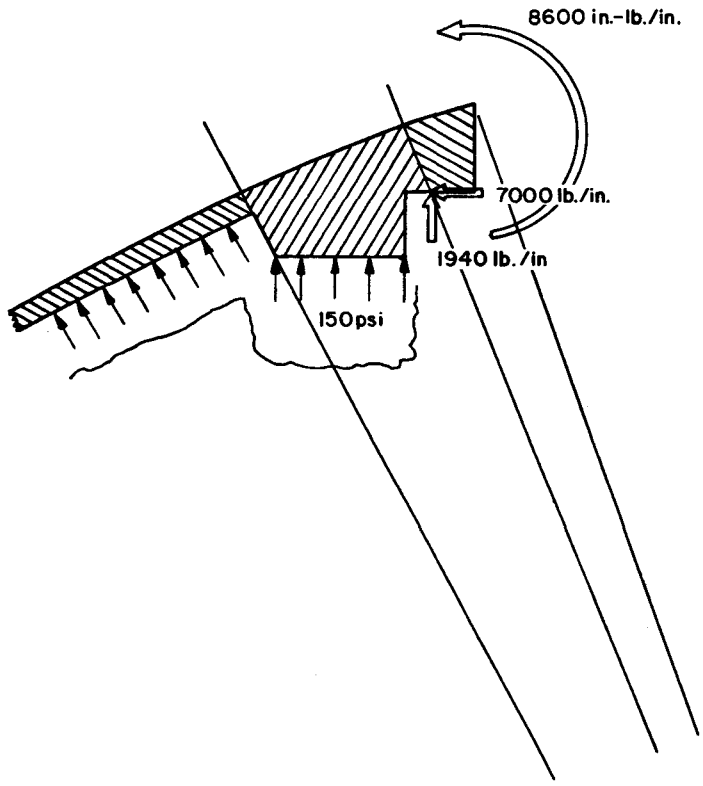

FIGURE 17. ASSUMED LOADING - CASE 2

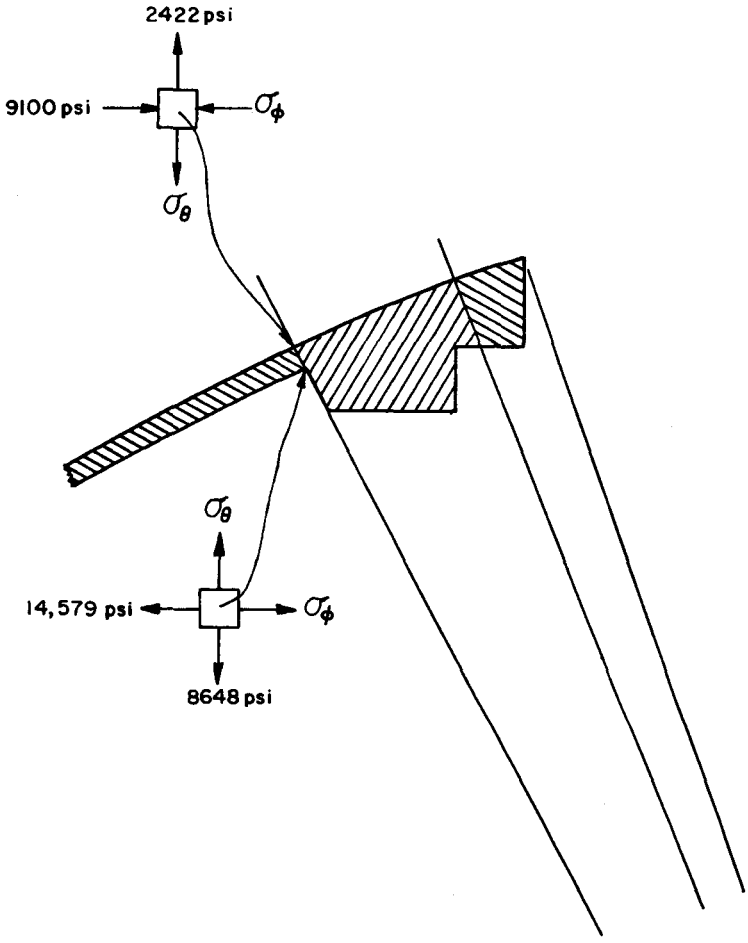

FIGURE 18. MAXIMUM STRESSES IN FLANGE FOR CASE 2.

found on the inner surface of the spherical shell segment at the point of intersection between the flange and the shell. This stress intensity is

$$\sigma_i = |19,464 - (-150)| = 19,614 \text{ psi.}$$

This figure meets the code requirement

$$P_L + P_b + Q \leq 3.0S_m = 49,800 \text{ psi.}$$

To define the adequacy of the flange from the viewpoint of fatigue it is necessary to derive an estimate of the possible stress concentration that may act at the maximum stress location. There does not exist any analytically or experimentally derived data dealing with the stress concentrations that may occur in the exact geometry as presented by the flange configuration. However, extrapolating on some of Peterson's work* and confirming this with experience gained on relatively similar geometries as compared to the flange, there seems to be no plausible reason for assuming that a stress concentration factor of greater than 2.0 should be applied to this geometry. This being the case, the predicted peak stress intensity in the flange would be

$$(2.0)(19,614) = 39,228 \text{ psi.}$$

This figure is less than the code allowable $2S_a$ of 52,000 psi.

The MONSA-S output showed that stresses induced in the spherical shell by the shell-flange thickness discontinuity and edge loads, did decay very rapidly along the shell as measured from the shell-flange intersection. This rapid decay validates the use of the model assumed and indicates that there should be little or no interaction between the discontinuity stresses at the top of the support cone and the "beanie"-main-chamber intersection.

Based on the above, the beam-window flange, including the spherical shell segment surrounding it, is considered structurally adequate to sustain the anticipated loads. However, it must be noted that this

---

*Peterson, R. E., "Stress Concentration Design Factors", John Wiley & Sons, Inc., New York, 1953, Chapter 3, "Shoulder Fillets", pp 59-76.

flange is considered as part of a reinforced opening in the spherical shell and comes under the specifications of Article 4-6 of Section VIII - Division 2, governing fatigue evaluation of openings. For strict compliance with this article it will be necessary to experimentally evaluate the maximum stresses that occur in this structure.

Finally, one note of caution. The beam-window protuberance will load the flange by expanding outwards. As can be seen in Figure 17, a shearing load of 7,000 pounds per inch of flange bolt circle circumference can be generated. This load must not be allowed to act directly on the bolts. This being the case, the space between the inner diameter of the flange and the outer diameter of the beam-window nose protuberance should be shimmed to prevent the shearing load from being applied to the bolts.

Lower Half of the Main Chamber and the Support Cone

The lower half of the main chamber and support cone were analyzed using CB&I drawing No. 71-2025-LO-1, titled "Proposed Construction for 30K Liter Weldment Chamber", to define the geometry of the structure. Continuing the practice of cutting the model of the structure into segments that can be considered independent of each other (with the application of the correct boundary conditions, of course), this section of the vessel was modeled as a body of revolution as shown in Figure 19. The upper half of the "Z" section cylinder including the flange were added to the model to ensure continuity with the heavy flange of the weldment. The upper part of the weldment was considered as a full sphere and cut along a symmetry plane. The base ring of the support cone was initially considered fixed along its entire bottom circumference. Actually, the ring is supported by three sets of two legs each, each set spaced 120 degrees apart. The effect of the discontinuous support system was analyzed and will be discussed in detail later. It was believed that the effect of the three point support

system at the base of the support cone would be dissipated in the cone and the 3.0-inch wall where the cone joins the chamber weldment proper. This being the case then, any stresses induced in the cone because of this support system can be considered as local, affecting only the cone and ring. The other components of the weldment would then see loads, and consequently stresses, that would be generated as if the cone ring was indeed fixed as shown.

The structure was modeled, basically as shown in Figure 19, as an eighteen part shell, for input to MONSA-S. One of the parts, representing the double layered cone containing the cooling space, was modeled as a three-layered shell with the center layer having zero elastic modulii. Because MONSA-S is a shell program, recognizing no stress components normal to the midplane of the shell-wall thickness, the local stresses in this part that are generated by the program are not correct. However, the stiffnesses of this part are correctly modeled and thus the fundamental parameters, such as deflections, rotations, loads and moments, developed at the ends of the part are correct. These fundamental parameters can then be applied to a simple model of the cone wall to determine the local stresses in this part.

Again referring to the model depicted in Figure 19, two pressure loading conditions were assumed. The first condition assumed was that of 150 psi pressure acting in both pressure areas 1 and 2, with $N_{\phi 1}$ and $N_{\phi 2}$ adjusted accordingly. This condition represents the piston in equilibrium condition before the start of an expansion stroke. The second condition assumed was that of 70 psi pressure acting in pressure area 1 and 200 psig pressure acting in pressure area 2, with again the N_{ϕ}'s being adjusted accordingly. This represents the pressure conditions in both the main chamber and "Z" section at the midpoint of the expansion stroke with the piston in its lowermost position. These conditions and the basic geometry were used as input to MONSA-S. The program output

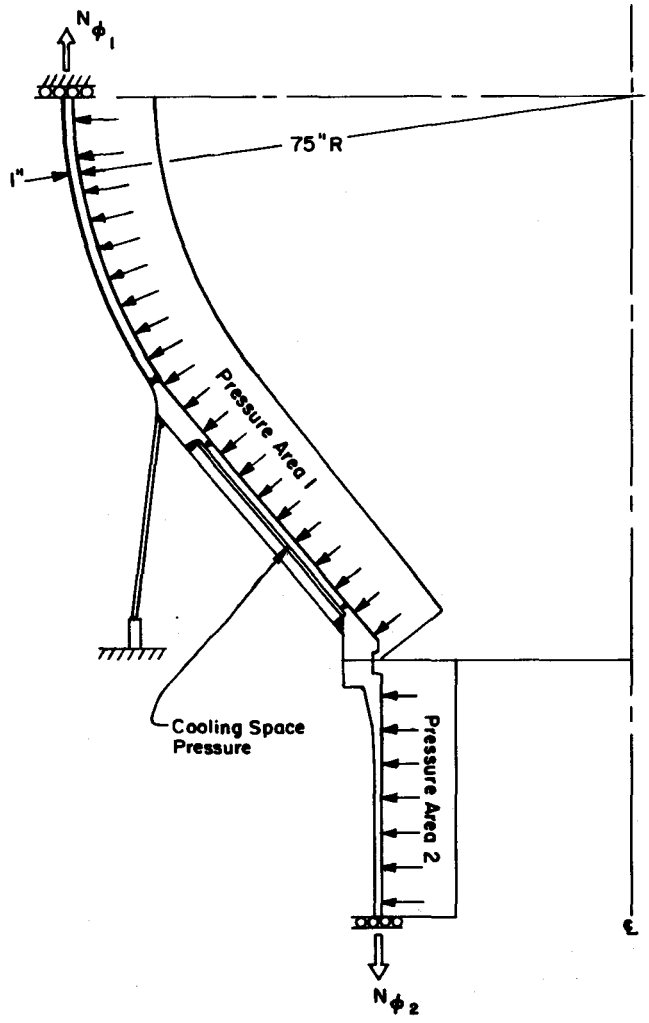

FIGURE 19. GEOMETRIC MODEL OF LOWER CHAMBER AREA FOR INPUT TO MONSA-S

indicated that the nominal stresses throughout the structure, with the exceptions of the multi-walled cone and the support cone, were very low being less than 10,000 psi. The presence of reasonable local stress intensification factors in these areas would not cause the total stresses at any point in the structure modeled to exceed any of the stress intensity limits imposed by Section VIII - Division 2.

The local stresses in the inner 1.0-inch thick wall of the multi-layered cone were calculated for four cases as follows:

- Case 1, 150 psi pressure in both pressure areas 1 and 2 and, 0.0 psi pressure in the cooling space.
- Case 2, 70 psi pressure in pressure area 1, 200 psi pressure in pressure area 2, and 0.0 psi pressure in the cooling space.
- Case 3, 70 psi pressure in pressure area 1, 200 psi pressure in pressure area 2, and 150 psi pressure in the cooling space.
- Case 4, 0.0 psi pressure in both pressure areas 1 and 2 and 150 psi pressure in the cooling space.

The inner 1.0 inch-thick wall was modeled as a cone with a length of approximately 29.0 inches, so that its ends correspond to the weld area locations in the actual structure. The geometry of the model, the boundary conditions and the pressure-loading conditions for the four cases are shown in Figures 20 through 23. The maximum nominal stresses found in the cone wall for the four cases are also shown in these figures. As can be seen, the worst stress condition occurs under loading Case 3 where the maximum stress intensity is

$$P_L + P_B + Q = 15{,}035 - (-150) = 15{,}185 \text{ psi}$$

which is considerably below the code limit of $3.0S_m = 49{,}800$ psi. If the welds at both ends of this conical section are ground smooth on both surfaces of the shell then a conservative estimate of the stress

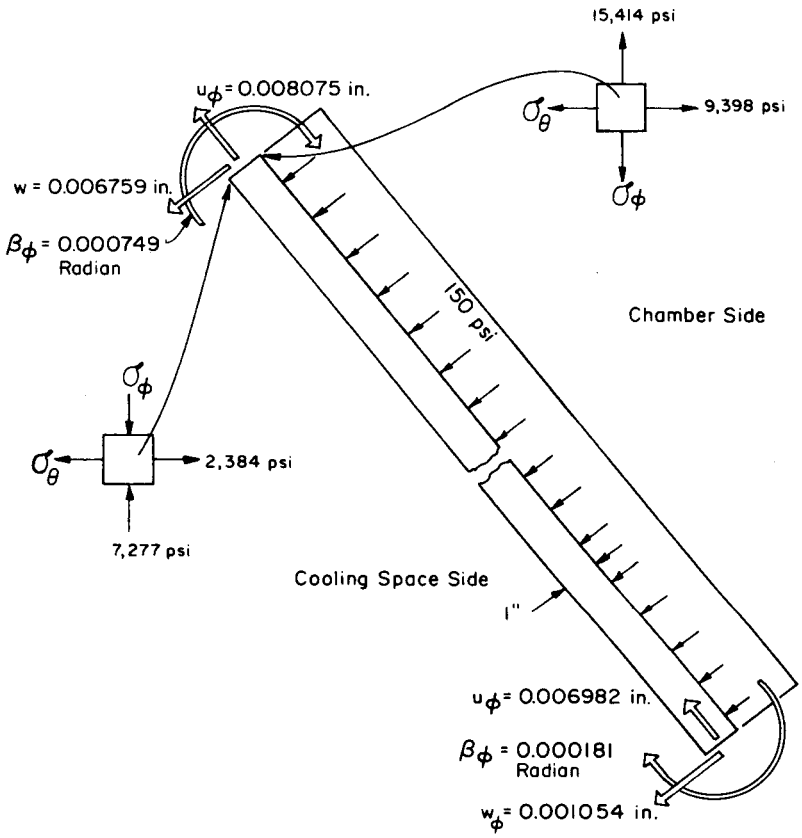

FIGURE 29. GEOMETRIC MODEL, LOADINGS, AND MAXIMUM STRESSES FOR CONE INNER WALL IN CHAMBER - CASE 1

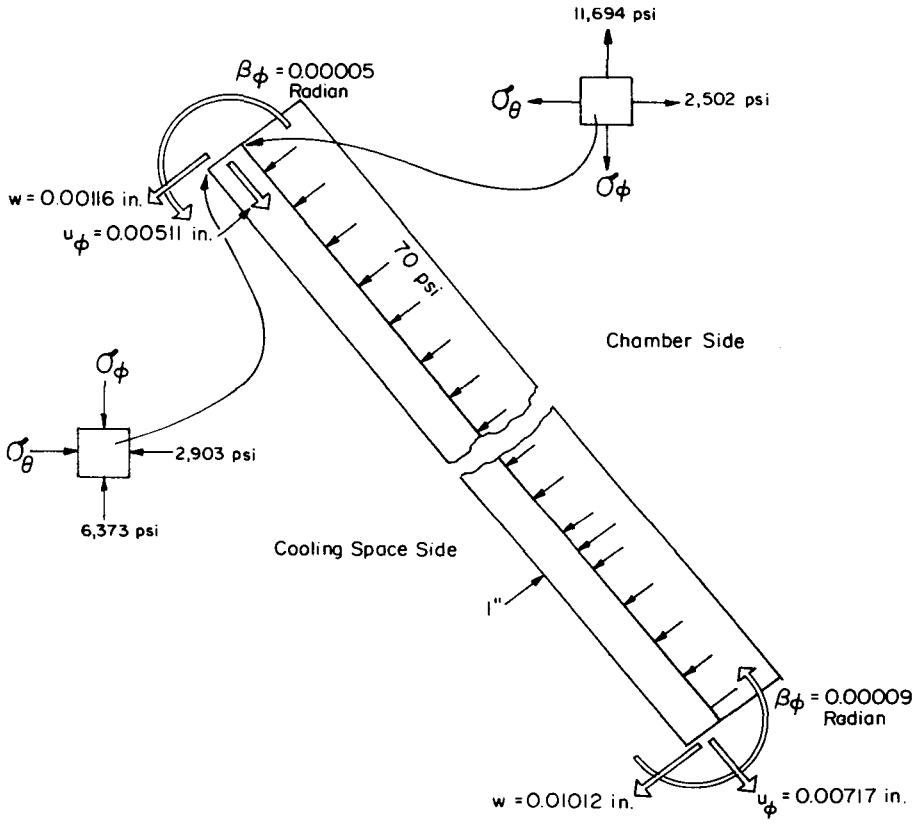

FIGURE 21. GEOMETRIC MODEL, LOADINGS, AND MAXIMUM STRESSES FOR CONE INNER WALL IN CHAMBER - CASE 2

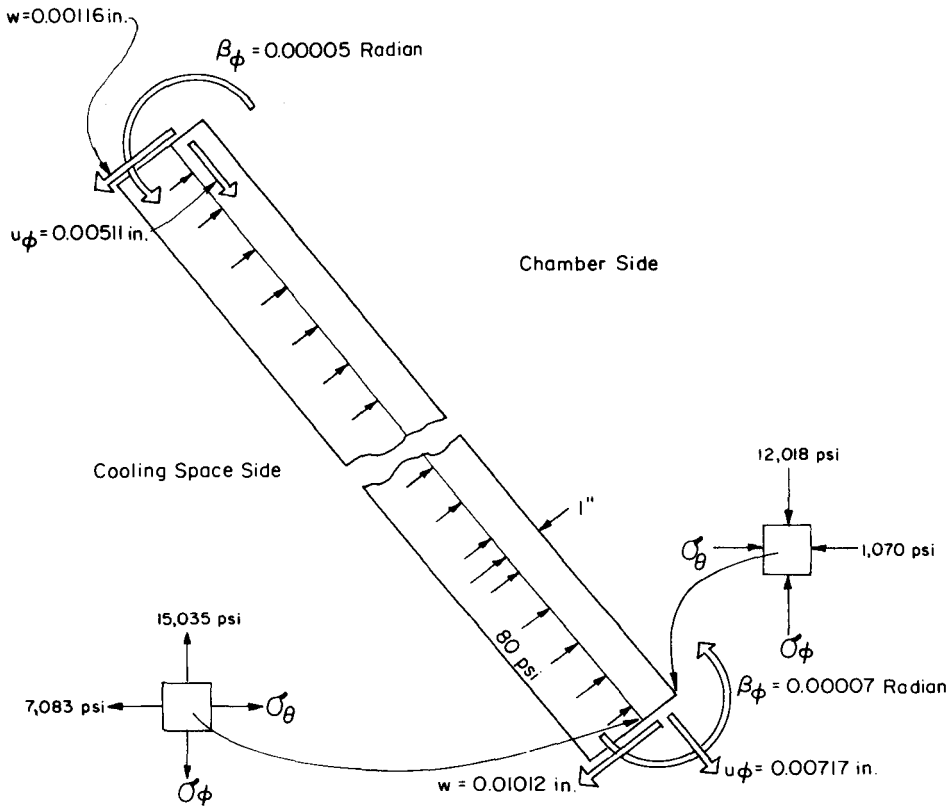

FIGURE 22. GEOMETRIC MODEL, LOADING, AND MAXIMUM STRESSES FOR CONE INNER WALL IN CHAMBER - CASE 3

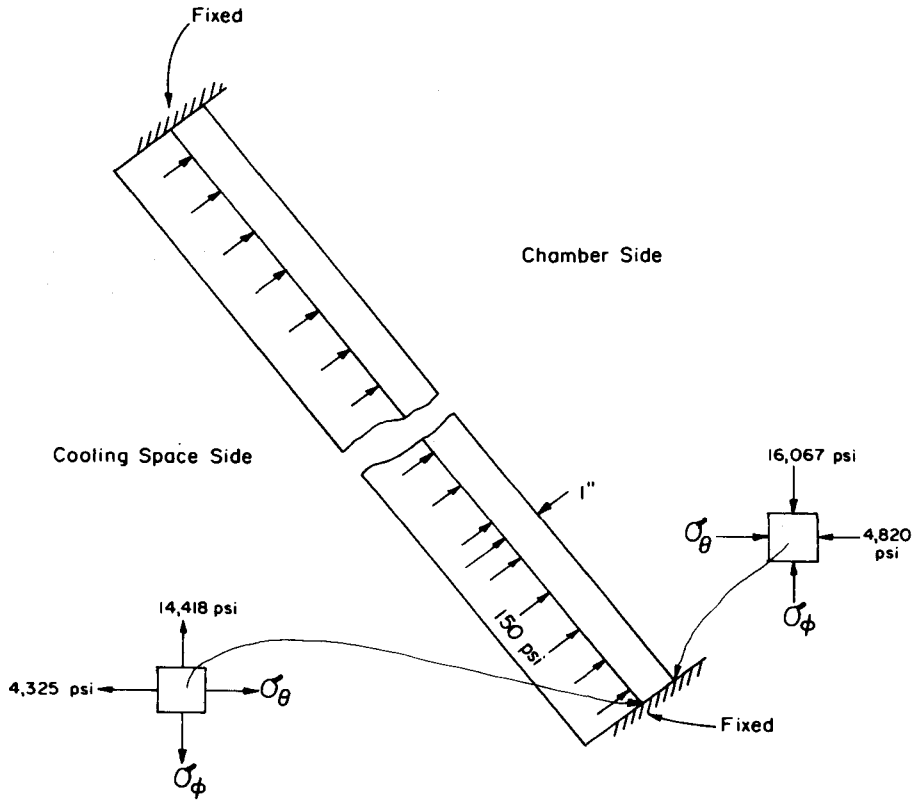

FIGURE 23. GEOMETRIC MODEL, LOADING, AND MAXIMUM STRESSES FOR CONE INNER WALL IN CHAMBER - CASE 4

concentration factor occurring in this location would be 2.0. Thus the anticipated peak stress intensity would be

$$\sigma_i = (2.0)(15,185) = 30,370 \text{ psi.}$$

This figure is below the $2S_a$ limit of 52,000 psi and thus the inner wall configuration is acceptable as far as fatigue is concerned.

The stresses in the outer wall of the multilayer cone were not determined directly but were extrapolated from the results of the analysis carried out for the inner wall.

The purpose of the multi-wall construction is to allow a cooling fluid to be circulated around the base of the main chamber. The fluid, for any given operational cycle of the chamber, is always maintained at a constant pressure while the pressure in the main chamber varies during the expansion period. This being the case, the pressure induced stresses in the outer wall remain constant during operation while a small oscillating stress component is induced by the deflections and rotations of the entire structure. The outer wall is 1.0 inch thick, as is the inner wall. In order to determine the total stress picture in this component is is only necessary to examine Figures 22 and 23, which describe Cases 3 and 4 as discussed above. The worst loading on the outer wall occurs when there is 150 psi in the cooling chamber, 70 psi in area 1 and 200 psi in area 2. This is actually Case 3 and a model of the loading would be similar to Figure 22, except that the pressure loading would be 150 psi and acting in a direction opposite to that shown. In order to separate the pressure stresses from the rotational and deflection induced stresses recourse is made to Case 4 and Figures 22 and 23. By scaling the pressure, and subtracting and adding, the maximum stress occurring in the outer wall is determined to be an 11,970 psi tensile stress located at the bottom joint on the inside surface. The maximum stress intensity at this location becomes

$$\sigma_i = |11,970 - (-150)| = 12,120 \text{ psi}$$

which is lower than the $3.0S_m$ limit of 49,800 psi. From the viewpoint of fatigue, however, the only stress components of concern are those induced by the gross rotations and deflections of the chamber as shown in Figure 22. The maximum oscillating stress component occurs on the outer surface of the outer cone at the bottom joint and equals 7,345 psi. At this location this is the maximum stress intensity of the alternating stress. Conservatively assuming that the minimum stress intensity at this location is zero the full stress range of the maximum alternating stress component becomes 7,345 psi, which compares quite favorably with the code imposed limit of $2S_a$ = 52,000 psi. Because this component of the chamber is to be attached to the chamber weldment by a one-sided, full penetration welding procedure, the exact stress concentration factor to be applied to the joint is difficult to establish. However, this joint will be checked by use of liquid penetrant examination. Any crack-like defects will be repaired. Thus it is reasonable and in keeping with the code intent that a stress concentration factor no greater than 5.0 be applied to the "nominal" stresses calculated to exist at this location. Thus the peak stress intensity at the critical location becomes

$$\sigma_i = (5.0)(7,345) = 36,725 \text{ psi} < 52,000 \text{ psi}.$$

Thus this component is judged adequate for operation under the assumed load conditions as pertains to fatigue considerations.

The local stresses in the support cone induced by the three-point-support system were determined using the nonsymmetric loading capability of MONSA-S. This was done in the following manner.

A body of revolution model was developed as shown in Figure 24. This model is basically similar to that shown in Figure 19, except that an entire sphere and centrally located "beanie" (not shown on drawing) were added to the structure and instead of being supported on the support-cone ring, it was fixed in space by fixing the mid-cylinder point of the "Z" section. The load $N_\phi(\theta)$ shown acting on the bottom of the support-cone ring is not a symmetric load. This $N_\phi(\theta)$ represents an approximation

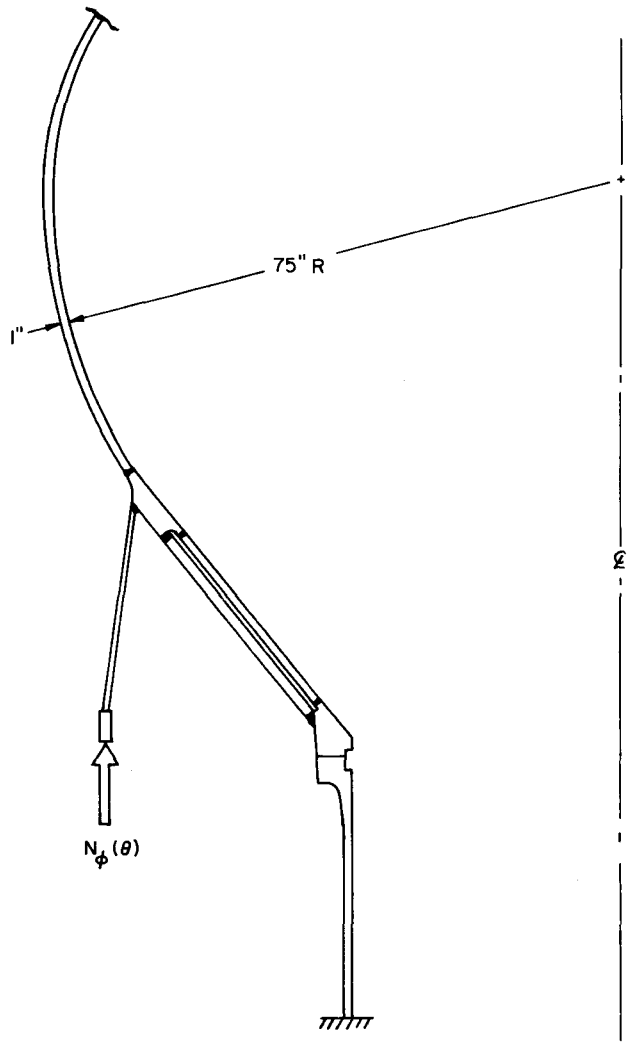

FIGURE 24. GEOMETRIC MODEL USED FOR FOURIER HARMONIC LOAD ANALYSIS OF 3-POINT SUPPORT SYSTEM

of the three localized area loads induced by the leg-support system. The leg-support system is composed of three sets of two legs each, each leg in a set spaced 22.5 inches apart and each set spaced at 120 degrees from each other. Each of these leg set supports two curved plates, one of which has a bend radius of approximately 66.75 inches, while the other has a bend radius of approximately 69.25 inches. The plates stand edgewise on the legs with the direction of the bend radii in towards the center of the chamber. Each plate is 1.0 inch thick, 10.0 inches high and the mean chord of the curved sections is 36.0 inches. These plates are secured to each set of legs and the support cone ring slips between the legs and is securely fastened to the plates.

This support system was replaced by 3-half-sine loads acting over the 36 inch cord length. The loads were such that a net upward thrust was developed at the ring equal to that load induced by the 70 psi pressure condition in the main chamber, the 200 psi pressure in the "Z" section, and a dead-weight load of 125,000 pounds, representing the weight of the chamber proper and the pressurizing fluid.

The manner in which MONSA-S analyzes a nonsymmetric load problem is as follows. The load is broken into its cosine series Fourier harmonic terms. That is, the load can be considered as an infinite summation of cosine terms around the periphery of the shell. At any position θ, measured in radians from the center of one of the leg sets the load can be represented as:

$$P_\theta = P_o + P_1 \cos(\theta) + P_2 \cos(2\theta) + P_3 \cos(3\theta) + \ldots\ldots$$

or,

$$P_\theta = P_o + \sum_{n=1}^{\infty} P_n \cos(n\theta)$$

where,

$$P_o = \frac{1}{\pi} \int_0^{\pi} f(\theta)d\theta, \quad P_n = \frac{2}{\pi} \int_0^{\pi} f(\theta) \cos(n\theta)d\theta, \quad (n=1,2,3,4,\ldots)$$

For the problem being analyzed

$$f(\theta) = 9{,}620 \cos \frac{\pi\theta}{(0.530)} \text{ lbs/in.}, \qquad 0 \leq \theta \leq 0.265$$

$$f(\theta) = 0.0, \qquad 0.265 \leq \theta \leq 1.829$$

$$f(\theta) = 9{,}620 \sin \frac{(\pi[\theta - 1.829])}{(0.530)} \text{ lbs/in.}, \qquad 1.829 \leq \theta \leq 2.359$$

$$f(\theta) = 0.0, \qquad 2.359 \leq \theta \leq 3.1415,$$

where θ given in radians.

Battelle's computer program EXPAND was used to generate the harmonic terms for the cosine series representation of the load function, and the load function was plotted as a function of the number of terms, N, used in the load approximation

$$P_\theta = P_o + \sum_{n=1}^{N} P_n \cos(n\theta).$$

Figure 25 shows the function approximation using only 7 terms, P_o, P_3, P_6, P_9, P_{12}, and P_{15}. As can be seen from this figure, these terms were sufficient to achieve a very good approximation of the complete function. For each of these P's MONSA-S calculates the shell response. A separate computer run must be made in each case. The program prints out the fundamental variables and stresses for each harmonic number as a function of the meridional generators. These quantities must be multiplied by either cos $(n\theta)$ or sin $(n\theta)$ to determine their values at positions of θ other than 0 or 90 degrees. The total shell response at any point of interest then is determined by superposition. This procedure was carried out for the model shown in Figure 24 and for the loads discussed. The resultant maximum stresses occur on a line along the cone defined at a point midway between the legs in each set. These maximum stresses and the predicted vertical and horizontal deflections at the top of the support cone relative to the base ring are shown in Figure 26. As can be seen, all the stresses are compressive. Tensile stresses do occur in the cone at some θ's removed from the leg position. These stresses are lower in magnitude than those shown. The output also confirmed that only the net upward force was transmitted to components of the chamber above the top of the support cone. The harmonics

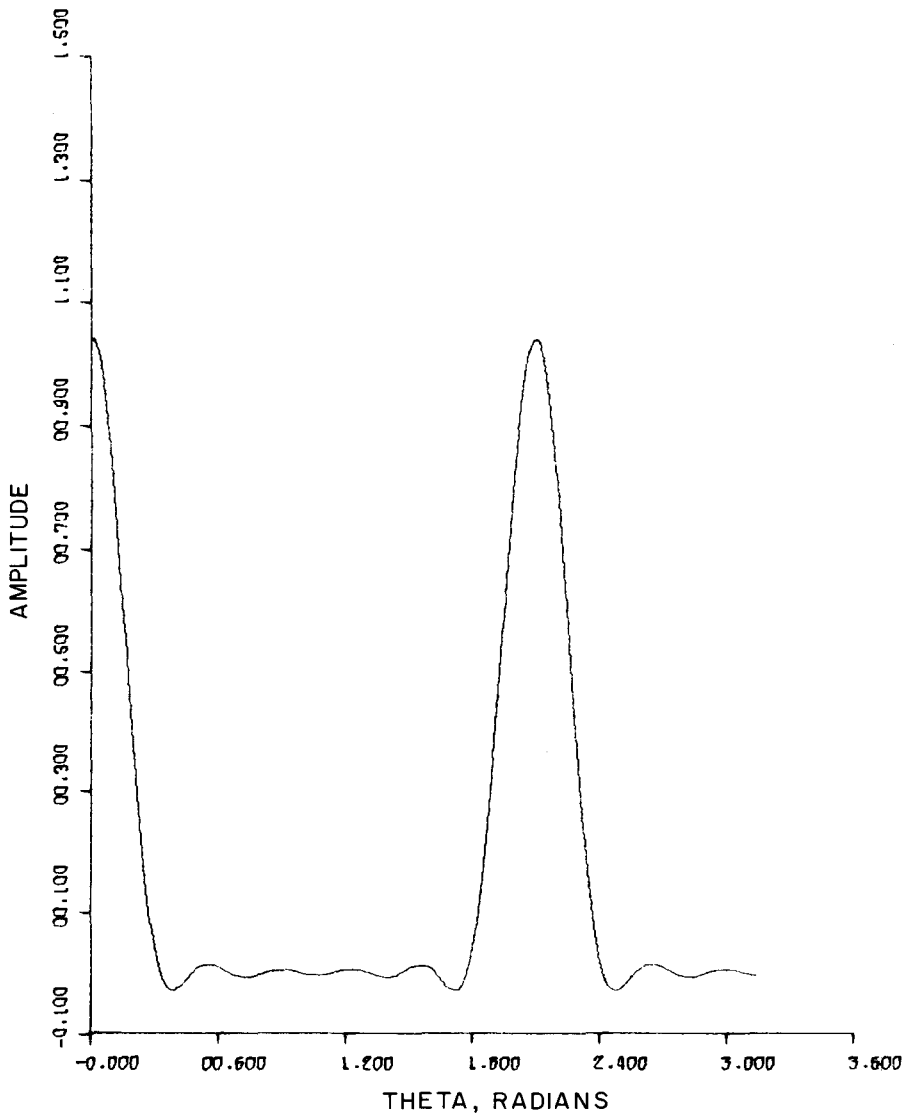

FIGURE 25. LOAD APPROXIMATION, 7 TERMS n = 0,3,6,9,12,15

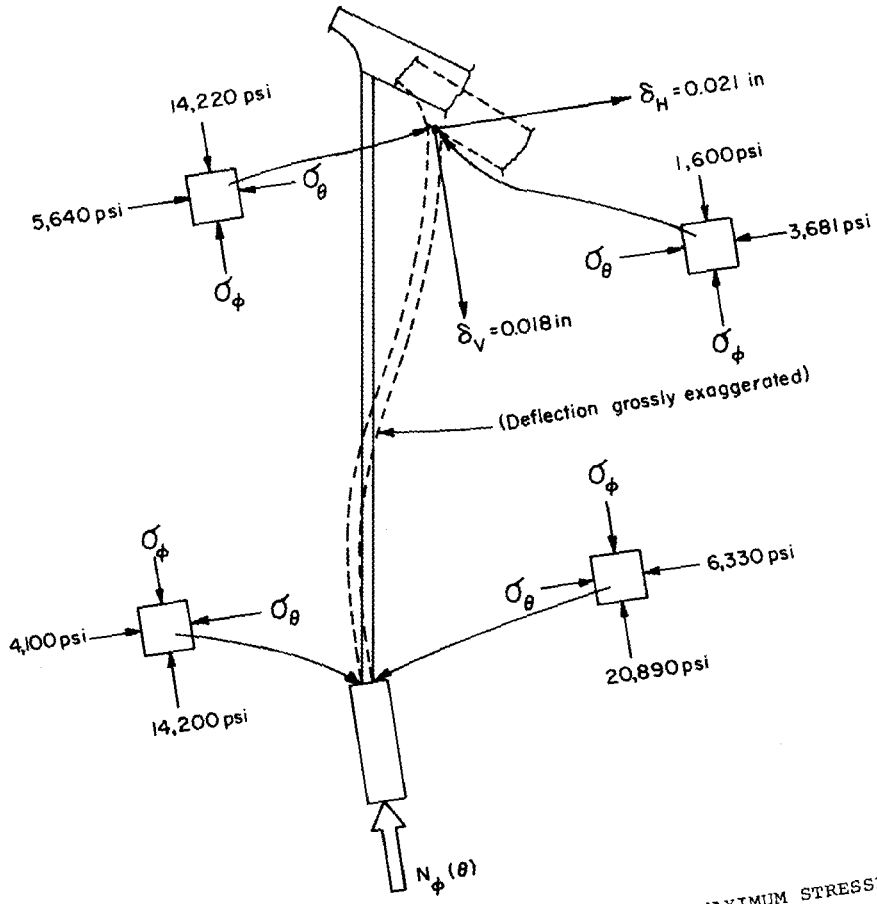

FIGURE 26. RELATIVE DEFLECTION PATTERN AND MAXIMUM STRESSES IN SUPPORT CONE UNDER ASSUMED LOAD

decayed rapidly. This validates the use of the model shown in Figure 19 for the determination of stresses other than in the cone.

The cone does not form part of the pressure boundary of the vessel and thus does not come under the jurisdiction of Section VIII - Division 2. The stresses induced in this structure are well below the yield stress of the material.

The maximum equivalent fully reversed bending fatigue stress in this structure is determined as follows:

$$\sigma_{eq} = \frac{\sigma_r/2}{1-\sigma_m/\sigma_{ul}}$$

where σ_{eq} = Equivalent fully reversed bending fatigue stress

σ_r = Stress range; maximum stress minus minimum stress

σ_m = Mean stress; maximum stress plus minimum stress divided by 2

σ_{ul} = Ultimate stress of the material.

From Figure 26, σ_{max} = 28,000 psi. Assume for conservative purposes,that σ_{min} = 0 psi (neglecting dead weight); thus, σ_r = 28,000 psi, σ_m = 14,000 psi, and taking σ_{ul} as 70,000 (at 72° F) then the σ_{eq} equals

$$\sigma_{eq} = \frac{14,000}{1 - \frac{14,000}{70,000}} = 17,500 \text{ psi}$$

The minimum unnotched fully reversed bending fatigue limit for 316L at 72° F is approximately 35,000 psi. Thus, if local stress concentrations in this structure are kept to 2.0 or less this component is structurally adequate for more than 10^7 cycles of operation at the maximum anticipated load condition. This last statement is predicated upon the absence of any large stress concentration factor that would considerably alter the results. Thus, the welds forming the transitions from the cone to the support ring and from the cone to the main weldment body must be sound and generously filleted and ground smooth.

This analysis has also generated data to allow the design of the attachment of the cone-support ring to the supporting leg structure.

Whatever means of attachment is employed it must be capable of sustaining a shearing-thrust force which reaches a maximum of 9,620 pounds per inch at the midpoint between the two legs in each set.

Flange-Spacer

Well into the design stage of the chamber a need arose to employ a spacer between the main flange of the chamber weldment and the upper flange of the "Z" section. The configuration and dimensions of this spacer are shown in Figure 27. The inclusion of this item in the overall design was a late addition and occurred after most of the analysis was completed. Rather than redo a great deal of analytic work a brief approximate analysis was carried out that was quite sufficient to establish the adequacy of the spacer design.

It was assumed that the inclusion of this spacer did not basically change the moment distribution in the immediate area. Examination of the moments induced in this region, (as determined in the analysis of the lower half of the main chamber), under a loading condition of 200 psi in the "Z" section and 70 psi in the chamber showed a maximum moment of less than 7,000-inch-pounds per inch occurring there. The bending stress in the spacer can then be approximated by

$$\sigma_b = \frac{6M_{max}}{t^2}$$

where, σ_b = bending stress

M_{max} = bending moment assumed

t = effective wall thickness of spacer.

Thus if t is taken as 2.5 inches

$$\sigma_b = \frac{(6)(7,000)}{(2.5)^2} = 6,720 \text{ psi.}$$

This basic stress is so low that the moment assumed could be off by a factor as great as 7.0 and the nominal stress would still be acceptable. Further, if the recommendation made previously as to the

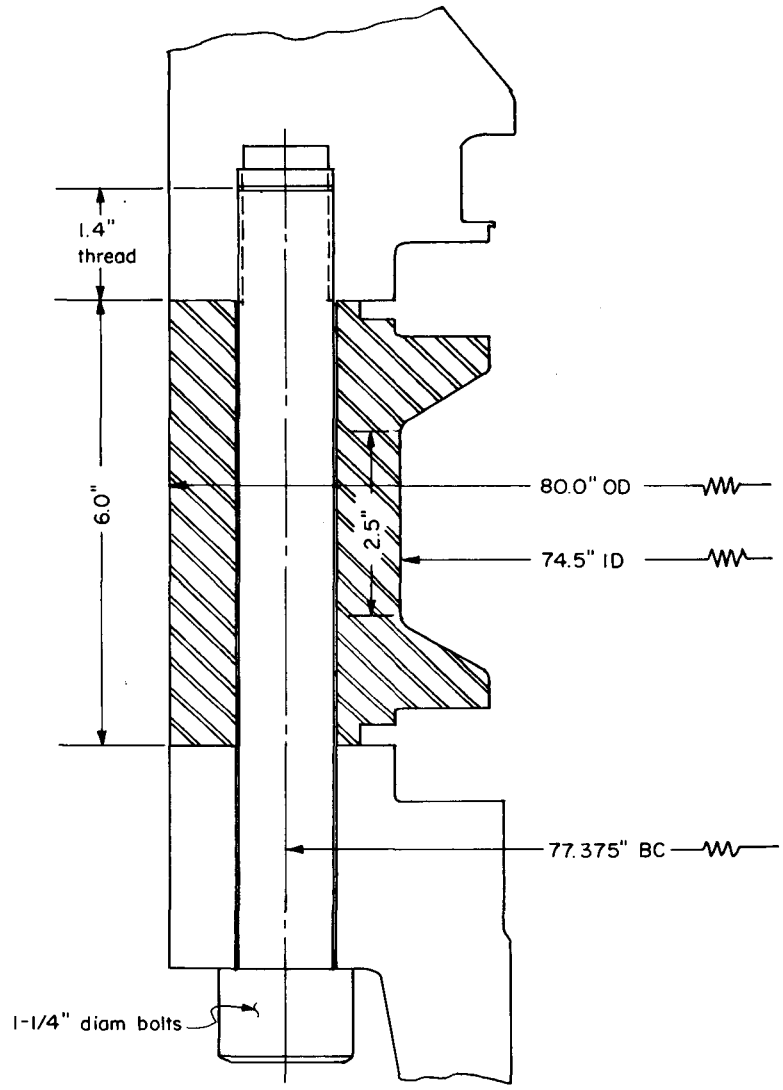

FIGURE 27. BASIC CONFIGURATION OF MAIN FLANGE SPACER

required preload on the bolts is followed, then the spacer is loaded in sufficient compression as to prevent flange separation or fatigue in the bolts.

Beam Window and Beam Window Protuberance

The chamber beam window structural analysis was conducted utilizing the finite element method. In this method, the continuum is separated by imaginary lines or surfaces into a number of "finite or discrete elements". These elements are assumed to be interconnected at a discrete number of nodal points situated on their boundaries. The displacements of these nodal points are then the basic unknown parameters of the problem. The form that these discrete elements take depend on the type of structural behavior assumed and the form of the approximation to that behavior.

Once the nodal points and the form of the elements have been defined, this approximate solution of the continuum static problem becomes the solution of a system of simultaneous linear equations. These equations can be written in matrix form as

$$[K] \{\Delta\} = \{F\} ,$$

where $[K]$ = stiffness matrix determined by the form of the individual finite elements and the geometry of the system

$\{\Delta\}$ = generalized nodal displacements

$\{F\}$ = generalized nodal forces.

This requires that only concentrated or point loads be applied to the model at the nodal locations. However, a very accurate transition from distributed forces to concentrated forces can be obtained in most practical applications.

Once the applied nodal forces are known, the nodal displacements can be solved by solving the above matrix equation through the inversion of the stiffness matrix to give

$$\{\Delta\} = [K]^{-1} \{F\} ,$$

where $[K]^{-1}$ = inverse of $[K]$.

Following the determination of the nodal displacements, the stresses and strains in the individual elements can be determined from the assumed behavior pattern of the elements.

In concept, this method produces the exact mathematical solution to the assumed problem. In general, this solution is not the solution to the real problem but converges to the continuum solution under the same basic assumptions as the number of elements increases.

The finite element model of the beam window protuberance as detailed in NAL drawing No. 2621.ME-25305 (included in this report) is shown in Figure 28. Only one-half of the assembly was modeled due to the symmetry of the structure and loading with regard to the vertical center plane of the assembly. The basic element employed for this model is a flat plate triangular shell element. This element has both an inplane (membrane) and out-of-plane (bending) solution and is a constant stress element. The outer two most circumferential rows of elements model a part of the spherical shell portion of the bubble chamber. They were proportioned to model the spherical shell critical length to help remove the model boundary effects on the beam window protuberance solution. The outer row of nodal points was fixed in space for this model.

The beam window flange was modeled by three or four rows of elements. Three rows were used on the top and side portion while four rows were used on the lower portion. Figure 29 shows a front view of the model. The nose cone section of the protuberance assembly was modeled by twelve rows of elements. Figure 30 shows a two-dimensional true length plot of the nose cone section of the model. Throughout the model, elements of different thicknesses were employed to account for the varying thicknesses of the actual structure. Thus, for example, the elements along the top of the nose cone were modeled with considerably thicker elements than are found in the center rows of this structure. These elements represent the heavy reinforcing boss located in this region.

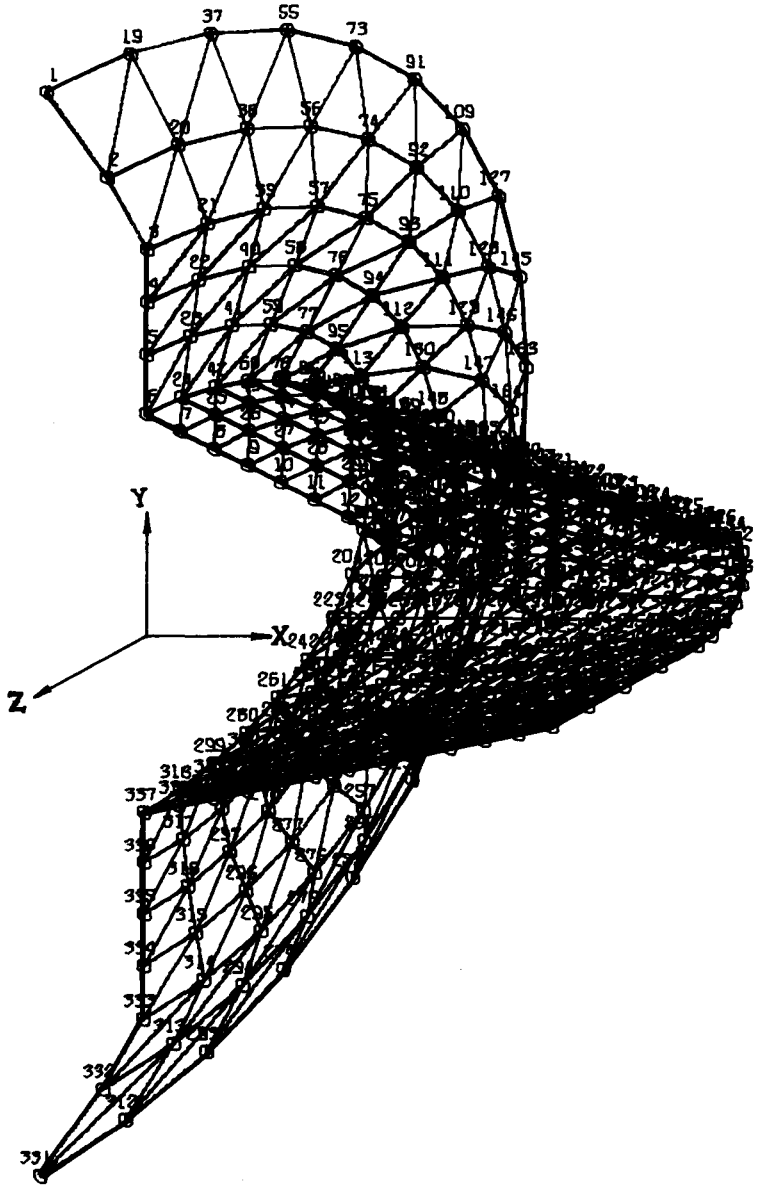

FIGURE 28. FINITE ELEMENT MODEL OF CHAMBER BEAM WINDOW ASSEMBLY

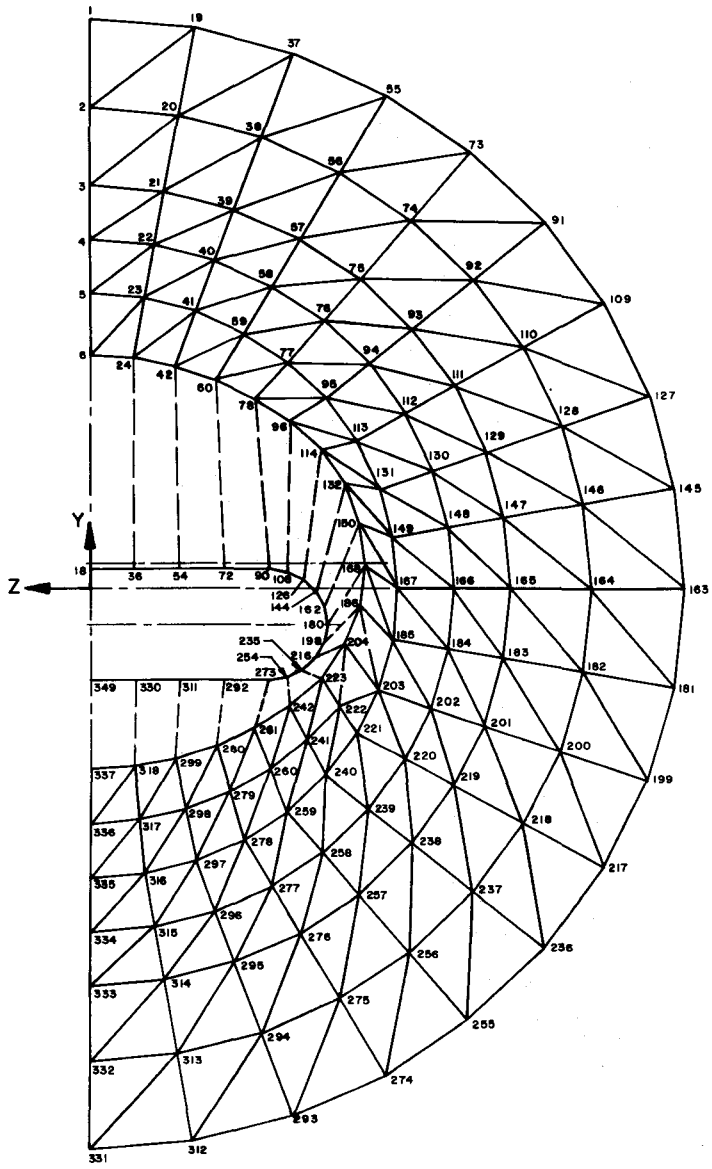

FIGURE 29. FRONT VIEW OF FINITE ELEMENT MODEL

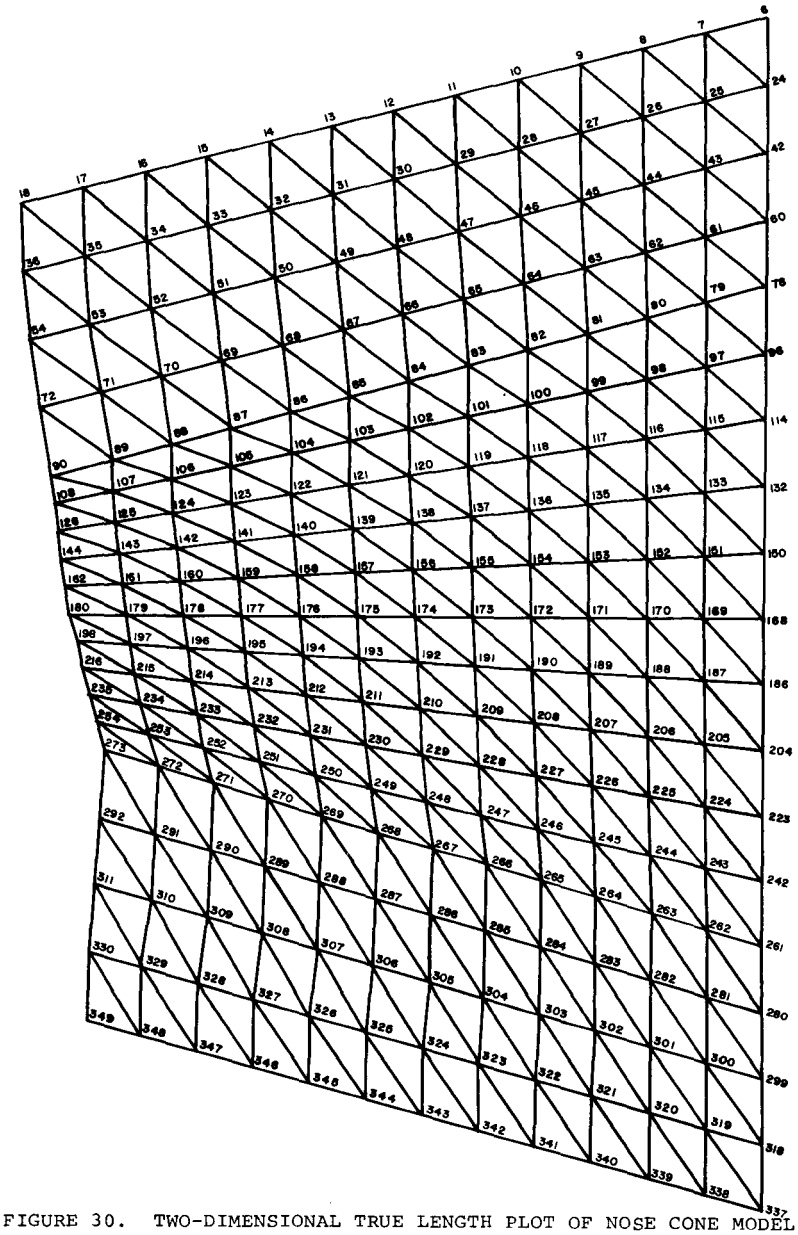

FIGURE 30. TWO-DIMENSIONAL TRUE LENGTH PLOT OF NOSE CONE MODEL

The actual beam window was not included in the beam window protuberance model. Due to the small thickness (as compared to the thicknesses of the nose cone and reinforcing boss) of the beam window, it was assumed that it would "ride along" with the nose cone. Therefore, a finite element model of the beam window alone was generated. This model, illustrated in Figure 31, utilizes the same plate triangular shell element as did the beam window protuberance model. In addition, a flat plate rectangular shell element was also incorporated in this model. This element has a linearly varying stress field. Once the displacement pattern of the beam window protuberance model was determined, then those displacements common with the beam window model were applied to this latter model together with the internal pressure to determine the stress state in the 1/8-inch-thick beam window.

Figures 32 and 33 show the displacements and maximum stresses respectively, along the edge of the protuberance model cut by the centerline symmetry plane, and induced by the 150 psi internal pressure. Figures 34 and 35 show the displacements and maximum stresses, respectively, around the beam window end of the nose cone. Figures 36 and 37 show the displacements and stresses, respectively, along the approximate horizontal center plane of the model.

The maximum stress predicted by this analysis of the protuberance model is 30,500 psi. This is primarily a discontinuity bending stress occurring at the flange-nose cone intersection on the horizontal centerline of the assembly. This stress and its location is shown in Figure 37. This stress, at this location, is the maximum stress intensity and meets the code requirement that

$$\sigma_i = P_L + P_b + Q = 30{,}500 \text{ psi} < 49{,}800 \text{ psi} = 3.0S_m.$$

The maximum stress not including a discontinuity effect is 23,000 psi and occurs at the beam window end of the nose cone at the horizontal centerline of the beam window opening. Thus, here

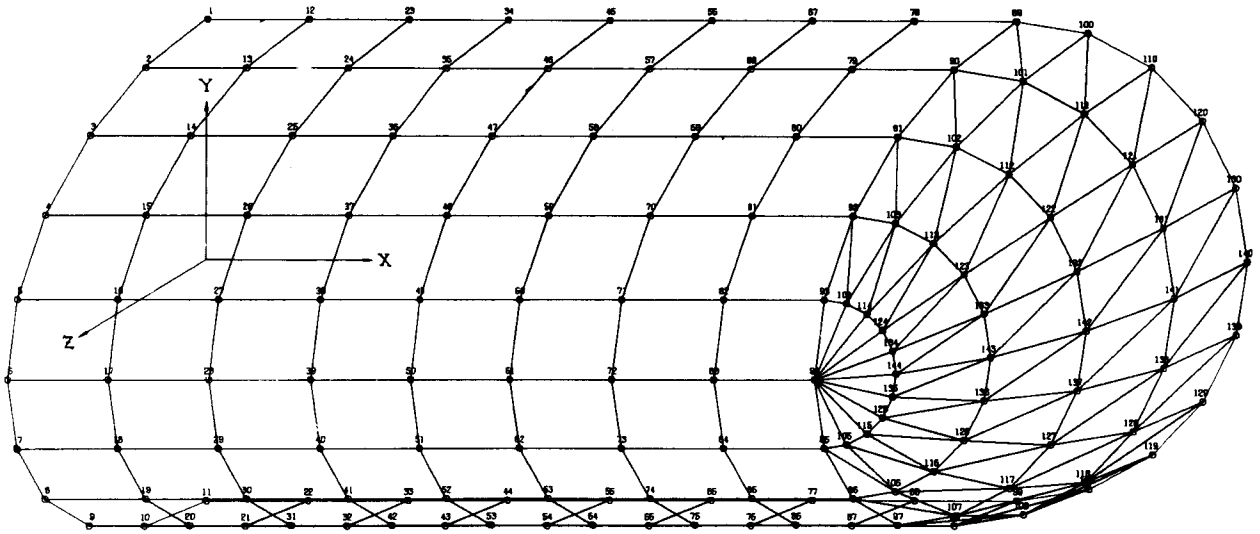

FIGURE 31. FINITE ELEMENT MODEL OF BEAM WINDOW

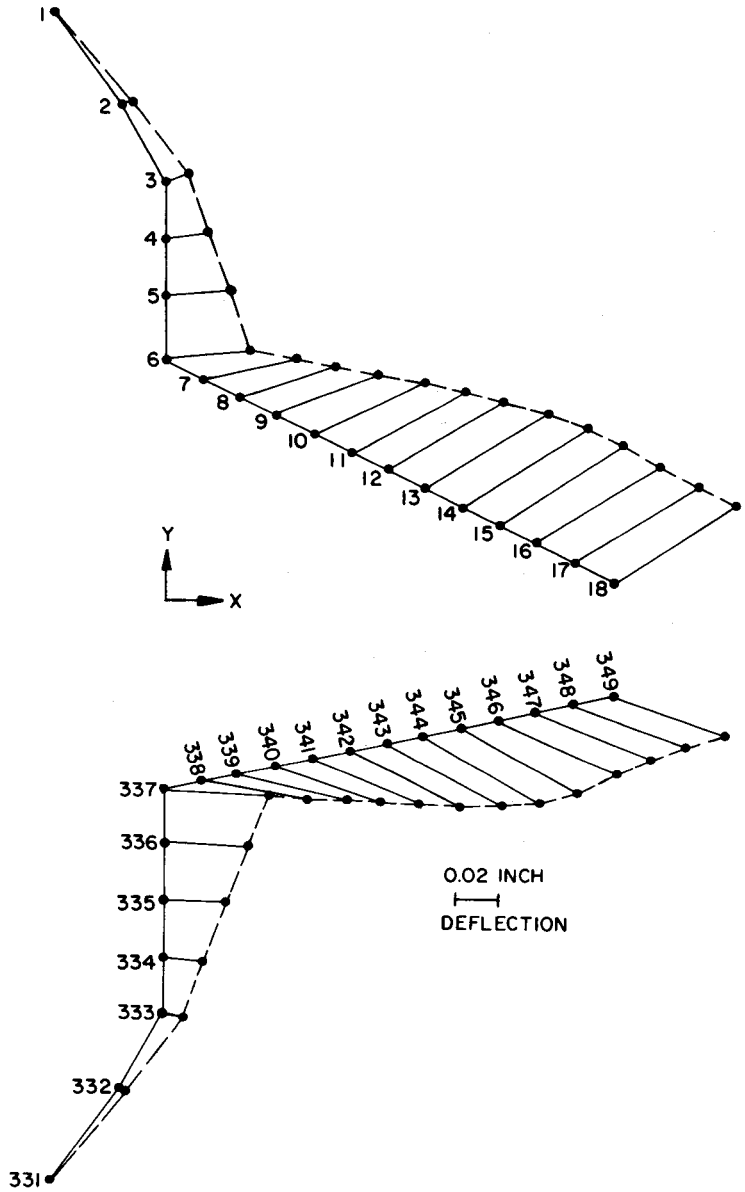

FIGURE 32. DISPLACEMENT OF NODES ALONG VERTICAL CENTERLINE OF MODEL UNDER 150 PSI INTERNAL PRESSURE

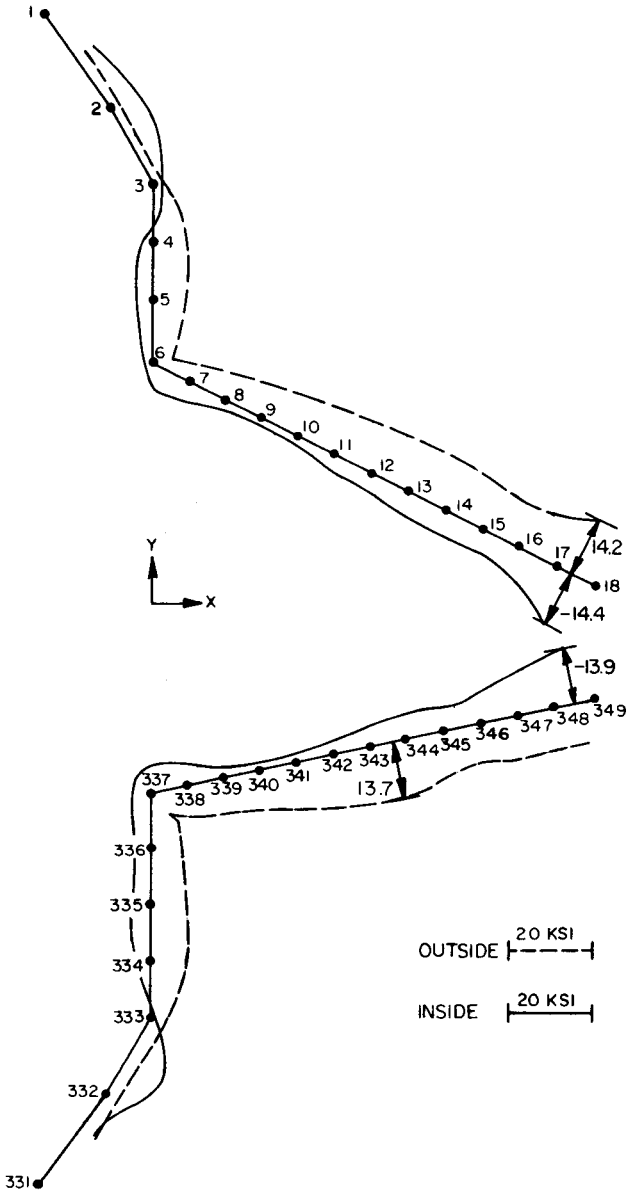

FIGURE 33. MAXIMUM STRESSES IN MODEL ALONG VERTICAL CENTERLINE

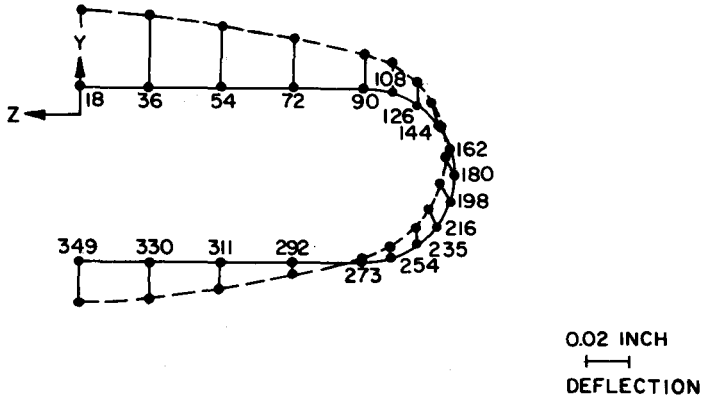

FIGURE 34. DISPLACEMENT OF NODES ALONG BEAM WINDOW END OF MODEL UNDER 150 PSI INTERNAL PRESSURE

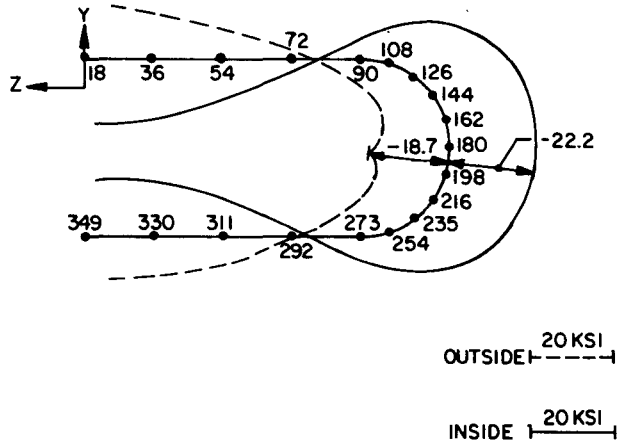

FIGURE 35. MAXIMUM STRESSES ALONG BEAM WINDOW END OF MODEL

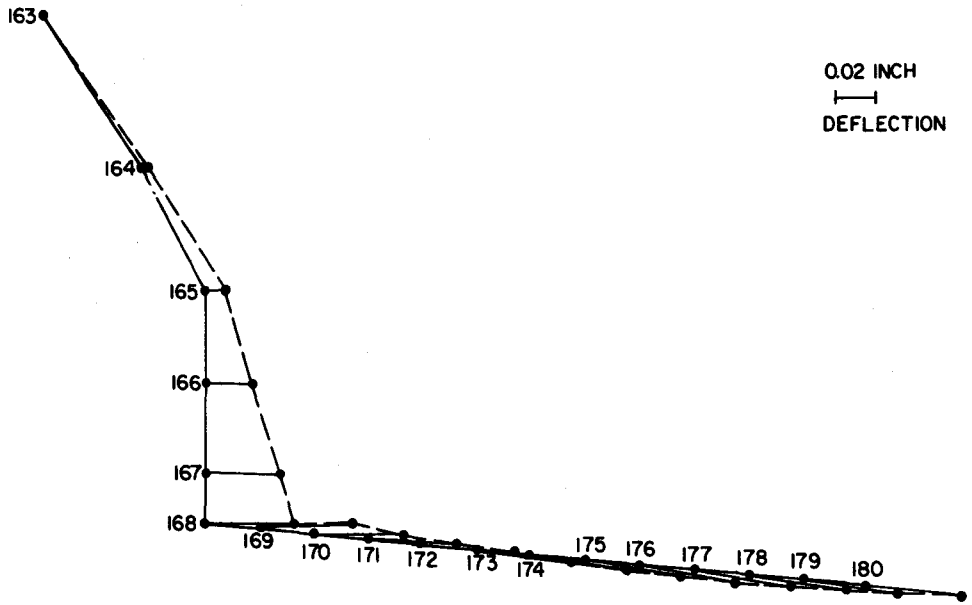

FIGURE 36. DISPLACEMENT OF NODES ALONG APPROXIMATE HORIZONTAL CENTERLINE OF MODEL UNDER 150 PSI INTERNAL PRESSURE

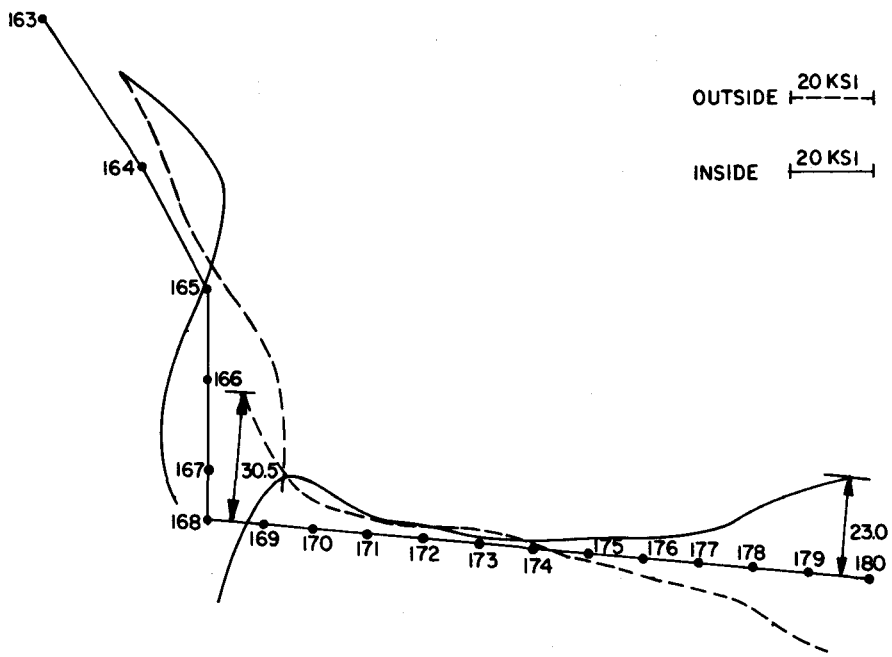

FIGURE 37. MAXIMUM STRESSES ALONG APPROXIMATE HORIZONTAL CENTERLINE OF MODEL

$\sigma_i = |23,000 - (-150)| = 23,150 = P_m(\text{or } P_L) + P_b < 24,900 = 1.5S_m$

and again the code specifications are satisfied. If the generous weld fillet radii as shown in the above mentioned NAL drawing are employed no significant stress concentration factors should be encountered in the structure and the stress intensities quoted above can be interpreted as the peak stress intensities as well. These figures meet the $2S_a$ limit of 52,000 psi imposed by the code.

Once the analysis of the chamber beam window assembly or protuberance was complete, the resulting displacements were applied to the beam window model along with an internal pressure of 150 psi. The maximum stress occurred at the vertical centerline of the beam window at the lower window-nose cone intersection. This stress, which is almost a pure bending stress, is 28,000 psi. If the junction of the window and the protuberance reinforcement boss were generously filleted with weld metal no fatigue problems in this area should occur.

Based on the above analysis the beam window assembly is judged to be structurally adequate to sustain the anticipated loadings, and meets the intent of Section VIII - Division 2. To exactly meet some of the specifications of this code an experimental evaluation of the stresses at certain geometric discontinuities is required.

A detailed presentation of the acceptable beam window protuberance geometry is given in NAL drawing No. 2621.ME-25305, titled "Chamber Beam Window Ass'y".

(6) DYNAMIC ANALYSIS OF THE BUBBLE CHAMBER COMPLEX

The static analysis of the bubble chamber components, as described in detail in the above sections of this report, show that the bubble chamber is structurally adequate to sustain the assumed loading conditions for the anticipated life of the structure. This finding is completely dependent upon the loads being as described.

The actual loads to be applied to the structure are impulsive in nature. They take the form of a pressure drop in the main chamber and

a pressure increase in the "Z" section, both pressure variations in the form of a versine wave shape. The period of these pressure variations are dependent upon the type of liquid in the chamber, and range from 0.040 to 0.130 seconds per pressure pulse. The entire loading sequences consist of several of these pulses occurring during an approximate 1.0 second time span followed by a 3.0 second dwell period at maximum chamber pressure. The anticipated pressure cycles are shown for hydrogen, deuterium, and neon in Figures 38 through 40, respectively.

If the chamber complex responds to these loads with no significant dynamic effects then the stresses induced in the structure are as those calculated for the static loading condition. If on the other hand appreciable dynamic reaction is encountered then the stresses induced in the structure can be considerably greater than those previously calculated. Thus the purpose of the study described in the following sections was to determine the structural response of the bubble chamber to the dynamically imposed loads, and to ensure that no significant dynamic amplification of statically calculated stresses will occur in the structure during operation.

Axisymmetric Shell Analysis

A finite-element model of the entire bubble chamber, support legs, vacuum tank, and cryostat was the principal tool used for the dynamic analysis. However, additional analyses were made using a continuum shell model of only the bubble chamber. The shell analyses were used to aid the development of the finite-element representation of shell sections, such as the conical support skirt, and to verify that the natural frequencies of the spherical sections of the bubble chamber pressure vessel were sufficiently high to justify the "rigid-body" assumption which was made for these components. These analyses were carried out using the programs MONSA-S and MONSA-V, which were described in some detail in the section of this report titled "Static Stress Analysis of Chamber Components".

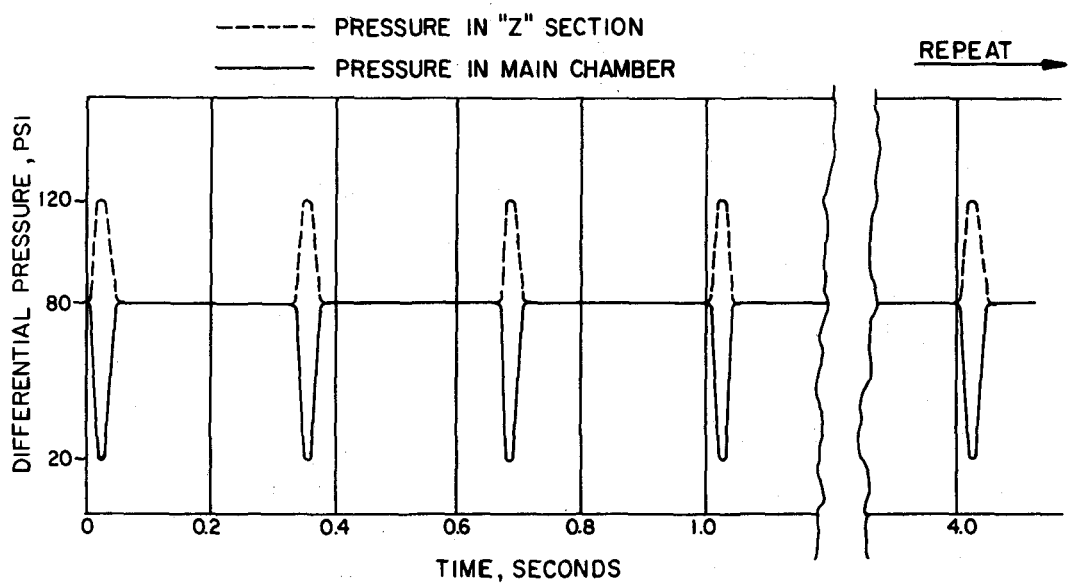

FIGURE 38. PRESSURE-TIME HISTORY FOR HYDROGEN OPERATION

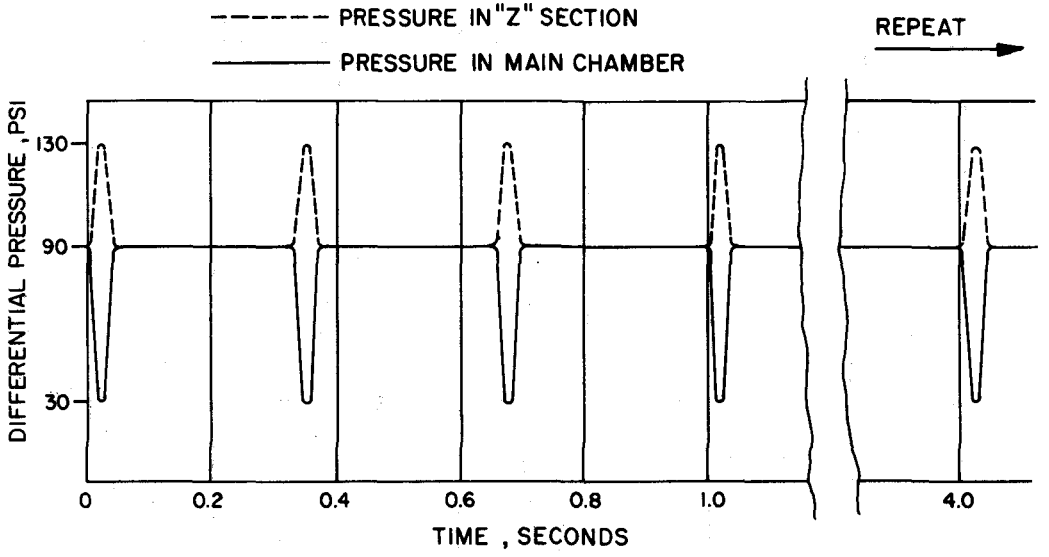

FIGURE 39. PRESSURE-TIME HISTORY FOR DEUTERIUM OPERATION

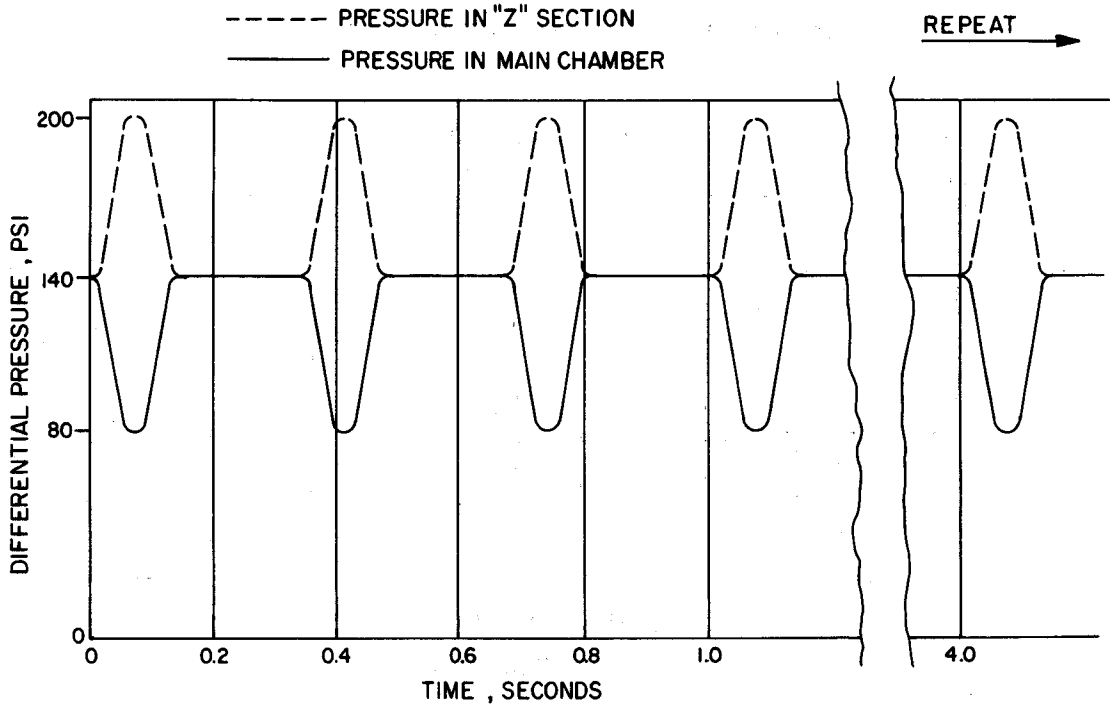

FIGURE 40. PRESSURE-TIME HISTORY FOR NEON OPERATION

The initial step in using the MONSA program is to divide the shell structure into a number of parts and to describe a continuous reference surface for each part. Figure 41 shows a sketch of the bubble chamber and the location of the 11 parts used for the analysis model. The input data describing the geometry of these parts are listed in Table 2.

Because the program is limited to the analysis of shells of revolution, it was necessary to rotate the bubble chamber head ("beanie") to a symmetrical position and to eliminate the beam window protuberance. The only other major artifact introduced was the use of a continuous boundary restraint instead of three pairs of support columns at the initial edge of part 1. However, the effect of the load distribution from the support columns was evaluated by the application of a Fourier series representation of this non-symmetrical load in a set of static analysis runs.

The MONSA model permits a very detailed description of the actual structure, including significant changes in wall thickness in each part. The provision for multilayer orthotropic shells was utilized to represent the inner and outer conical sections in Part 3 by 3 layers. The material properties of the center layer were set to zero to represent the cooling chamber between the two shells.

In order to check the finite element representation of the bubble chamber, the MONSA model was used to calculate the effective stiffness in the vertical and horizontal directions at the bottom of the cylinder and rod guide hub (bottom of Part 9 in Figure 41). Table 3 lists the deflections at the ends of each shell part for horizontal and vertical loads sufficient to produce a 1.0 inch deflection, and the calculated horizontal and vertical stiffnesses were 5.83×10^5 lb/in. and 126.16×10^5 lb/in., respectively. Here W represents a deflection normal to the reference surface of the shell, while U represents a deflection tangential to this plane. In the case of the horizontal load,

TABLE 2. DATA FOR MONSA SHELL ANALYSIS MODEL OF BUBBLE CHAMBER

Part	Type	Radius of Reference Surface, in.	Length, in.	Number of Layers	Wall Thickness, in.
1	Cylindrical	68.23	4.00	1	1.5
2	Conical	68.23	28.30	1	0.5
3	Toroidal	70.97	6.75(1)	1	1.0
4	Conical	65.18	11.04	1	Variable
5	Conical	58.36	36.63	3	Variable
6	Cylindrical	35.69	7.75	1	4.6875
7	Varicylinder	35.69	68.25	1	Variable
8	Conical	35.69	57.50	1	Variable
9	Varicylinder	6.63	43.75	1	Variable
10	Spheroidal	76.0	--	1	1.0
11	Spheroidal	55.0	--	1	1.0

(1) Minor radius of toroidal section.

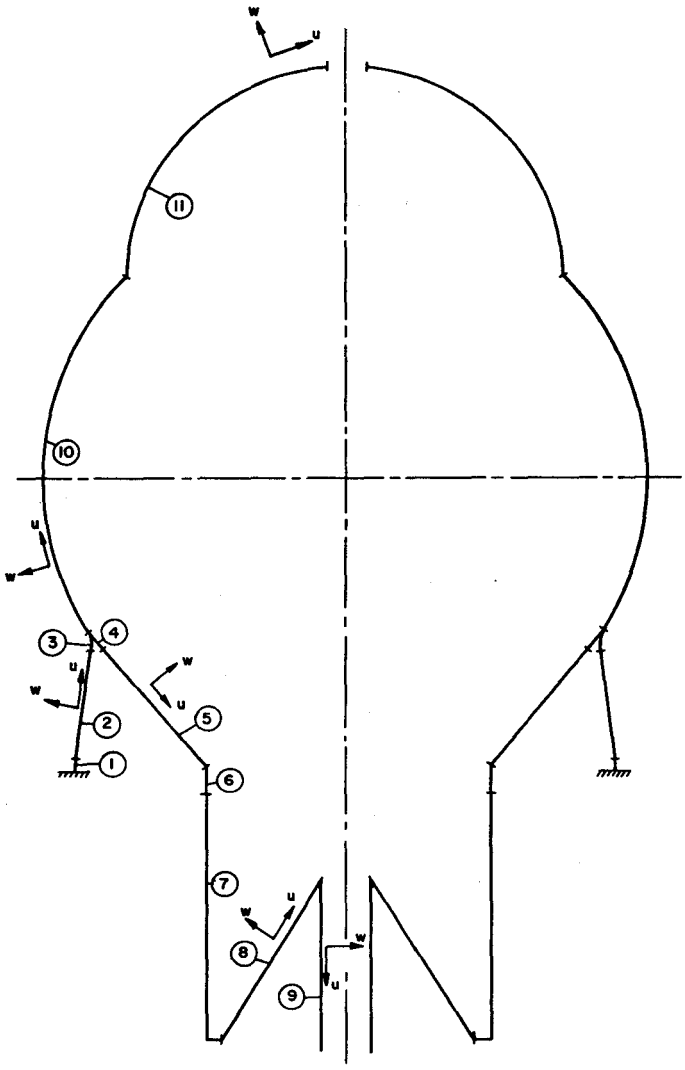

FIGURE 41. AXISYMMETRIC MODEL FOR MONSA-V SHELL DYNAMIC STUDY

TABLE 3. STATIC DEFLECTION OF BUBBLE CHAMBER STRUCTURE RESULTING FROM VERTICAL AND HORIZONTAL LOADS AT THE BOTTOM OF THE ROD AND CYLINDER GUIDE HUB

Part	Deflection from 583,000 lb. Horizontal Load		Deflection from 12,616,000 lb. Vertical Load	
	W,in.	U,in.	W,in.	U,in.
9 (Load Position)	1.000	0.139	-0.011	1.000
9	0.189	0.054	0.039	0.669
8	-0.190	0.049	-0.372	-0.558
8	-0.203	0.074	-0.123	-0.390
7	0.213	0.039	-0.090	0.399
7	0.111	0.031	-0.012	0.271
6	0.111	0.031	-0.009	0.271
6	0.103	0.030	-0.019	0.625
5	0.062	0.087	-0.179	0.197
5	0.054	0.085	-0.053	0.180
4	0.054	0.085	-0.053	0.180
4	0.069	0.083	0.095	0.174
3	-0.078	-0.074	-0.114	-0.158
3	-0.103	-0.008	-0.146	-0.060
2	-0.103	-0.008	-0.146	-0.060
2	-0.0048	-0.0004	0.011	-0.005
1	-0.0046	-0.001	0.011	-0.003
1	0	0	0	0

approximately 80 percent of the total deflection results from a bending deformation of the conical shell (Part 8) supporting the hub. The vertical deformation is distributed through a greater part of the bubble chamber structure.

The results from the shell vibration analysis (employing MONSA-V) are listed in Table 4. The lowest predicted frequency for the chamber with no fluid is 95 Hertz, and this mode was characterized by an axisymmetric deflection of the "beanie" with some bending in the chamber body and the conical support skirt. The calculation of the axisymmetric modes was completed successfully by dividing the 11 main shell parts into a total of 60 segments. The number of segments, along with an adjustable error criterion governs the accuracy of the numerical integration subroutine.

TABLE 4. RESULTS OF SHELL VIBRATION ANALYSIS OF BUBBLE CHAMBER STRUCTURE (No Liquid in Chamber)

Mode	Natural Frequency, Hz.	Description of Mode Shape
1	95	Vertical, axisymmetric deflection with maximum deflection at the top of chamber head and some bending in conical support skirt and chamber body.
2	137	Lateral bending of the cylinder and rod guide hub with local bending at the top of the cylinder and rod guide hub. Negligible deflection of main chamber and head.
3	163	Vertical, axisymmetric deflection with maximum deflection at the top of chamber head.

The lowest frequency vibration mode with significant lateral motion occurred at a frequency of 137 Hertz, and this mode consisted of local bending of the rod and cylinder guide hub and cone. The analytical prediction of lateral modes (nonsymmetric) for this complex structure

was made particularly difficult by numerical accuracy problems inherent in MONSA-V for the solutions of such conditions. In order to achieve reasonable results for nonsymmetric, lateral modes, it was necessary to increase the number of segments to 200. Even with this increase, it is suspected that there may still be some error in the 137 Hertz predicted frequency. However, since all of the shell modes have much higher natural frequencies than those predicted using the finite element model (to be discussed later) which includes an accurate representation of the chamber support legs, it was concluded that no additional effort on the shell analysis was warranted.

Weight and Moment of Inertia Data

The development of a mathematical model for the finite element dynamic analysis of the bubble chamber required a detailed description of the mass and moments of inertia of those components which were considered "structurally flexible". In the bubble chamber, all the structure above the conical support skirt was assumed rigid and represented by a single concentrated mass with appropriate moments of inertia at its center of gravity. The mass and inertia components of the chamber support and cylinder and rod guide assemblies were distributed at local mass points in the model.

The entire vacuum tank and cryostat assembly was represented as a single rigid body on flexible supports with mass and moments of inertia concentrated at its center of gravity. Table 5 summarizes all of the data used for both the bubble chamber assembly and the vacuum tank and cryostat. The center of the coordinate axes coincides with the center of the bubble chamber and the vacuum tank at Elevation 745 ft-3 inches (from DUSAF drawings). The z-axis is vertical with the positive direction up. The x-axis is horizontal with the positive direction coinciding with the beam direction. The y-axis is oriented according to the conventional "right-hand" rule for coordinate systems, and is normal

TABLE 5. SUMMARY OF WEIGHT AND MOMENT OF INERTIA DATA FOR BUBBLE CHAMBER, VACUUM TANK, AND CRYOSTAT

Description	Weight, lb.	Mass lb-sec^2/in.	CG Coordinates[a], in. X	CG Coordinates[a], in. Z	Moments of Inertia, lb-in-sec^2 I_{xx}	Moments of Inertia, lb-in-sec^2 I_{yy}	Moments of Inertia, lb-in-sec^2 I_{zz}
Chamber Vessel Above Conical Support Skirt							
With Hydrogen	40,320	104.5	-8.1	+39.5	257,070	358,410	303,330
With Neon	109,950	284.8	-2.1	+25.0	408,200	538,450	332,230
Chamber Support							
Upper Ring	3,290	8.53	0	-43.0	15,350	15,350	30,710
Support Skirt	1,860	4.82	0	-59.0	10,500	10,500	21,000
Support Skirt Ring	770	2.99	0	-73.5	4,740	4,740	9,470
Inner Cone	2,770	7.18	0	-56.0	9,330	9,330	18,670
Outer Cone	4,450	11.53	0	-56.0	14,990	14,990	29,980
Expansion Cylinder Flange	1,700	4.40	0	-75.0	3,180	3,180	6,350
Hydrogen Weight	735	1.90	0	-53.4	0	0	0
Neon Weight	12,650	32.77	0	-53.4	0	0	0
Chamber Cylinder & Rod Guide Spacer Ring	1,290	3.34	0	-79.5	2,410	2,410	4,820
Chamber Cylinder & Rod Guide							
Flange	1,540	3.99	0	-84.5	2,880	2,880	5,760
Cylinder	3,520	9.12	0	-115.9	5,910	5,910	11,820
Ring	880	2.28	0	-146.0	1,480	1,480	2,960
Cone	2,600	6.74	0	-133.0	1,790	1,790	3,570
Hub	1,420	3.69	0	-124.0	90	90	180
Hydrogen Weight	160	0.40	0	-120.0	0	0	0
Neon Weight	2,690	6.97	0	-120.0	0	0	0
Total Weight Supported on Chamber Legs	62,120						
With Hydrogen	67,310						
With Neon	151,390						
Vacuum Tank & Cryostat	310,000	803.1	0	-6.6	4,160,000	4,160,000	7,020,000

(a) Coordinate axes center coincides with bubble chamber and vacuum tank center at EL 745 ft 3 in. Z axis is vertical (positive up) and x axis is horizontal with positive direction coinciding with the beam direction.

to the plane of symmetry for the bubble chamber vessel. Therefore the centers-of-gravity of all components lie in the x-z plane.

Finite-Element Model Analyses

The finite-element, or as it is sometimes called, the lumped parameter model, as generated for this study is given in Figure 42. Figure 43 shows only the model above the caisson for clarity of viewing. Nodes 1 through 5 represent the prestressed concrete caisson supporting the bubble chamber legs. The caisson was taken to be 41 feet deep and 20 feet in diameter. The elastic modulus of the concrete was taken as 3.6×10^6 psi and having a Poisson's ratio of 1/8. Node 1 was assumed to be fixed in space at the bottom of the caisson, representing the caisson-rock interface. The mass and rotary inertia of the caisson was then lumped at Nodes 1 through 5. The elastic elements representing the caisson were assumed to be straight uniform beam and bar elements having response properties normally associated with small-deflection linear elastic theory. The effect of the soil restraint on the caisson was not included in the model. This was due to several reasons: it is difficult to predict the soil behavior after many applications of small cyclic vibrations; it was assumed that the caisson's lateral motions would not be large enough to create significant lateral restraining forces; and that the vertical and torsional restraint of the caisson due to the lateral earth pressure was not significant.

The bubble and vacuum chambers are supported by three groups of legs. Each leg group consists of two supporting legs for the bubble chamber and one for the vacuum chamber. These groups of legs are spaced 120 degrees apart. The bubble chamber supporting legs are steel rods with one cross-sectional change. The elastic modulus of the steel was taken as 29×10^6 psi and having a Poisson's ratio of 3/10. Each vacuum chamber supporting leg consists of a vertical isolator unit with the concrete column on top of it and with a steel column on top of the concrete. The

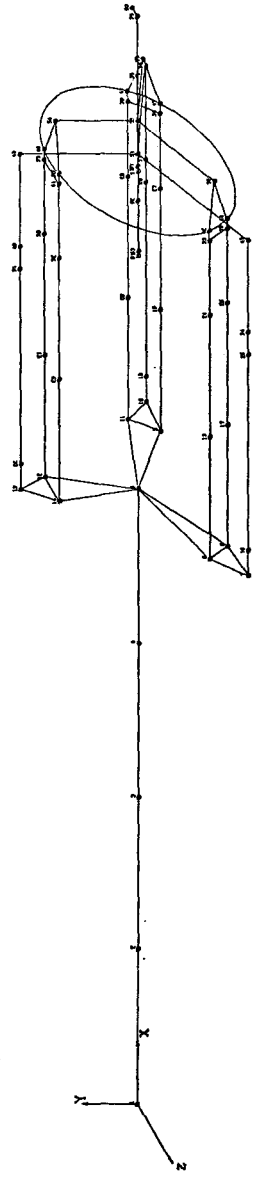

FIGURE 42. FINITE ELEMENT MODEL OF BUBBLE CHAMBER, SUPPORT LEGS, VACUUM TANK, AND CAISSON

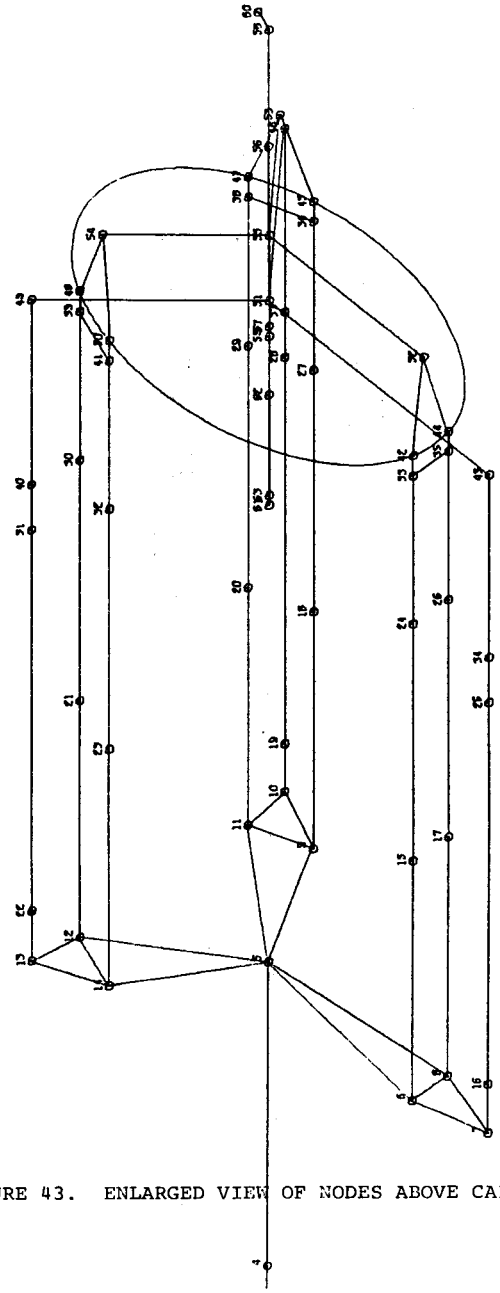

FIGURE 43. ENLARGED VIEW OF NODES ABOVE CAISSON

vertical isolator unit is a Barry Control air bag system. Using design data furnished by Barry Control, the vertical isolation unit was modeled by a spring-mass system such that it gave a vertical natural frequency of the isolator unit of 7/10 Hz. Elastic elements of the legs consisted of straight uniform beam and bar elements.

Each group of legs is connected to the top of the caisson by rigid elements, thus, the three supporting legs of each group and the top of the caisson work as a rigid unit. On the top of each adjacent pair of bubble chamber support legs is a flat plate tie member. Above this tie member is the support for the conical support skirt of the bubble chamber. The conical supporting skirt lower ring was modeled as a circularly curved beam element.

The bubble chamber above the conical supporting skirt-bubble chamber intersection was assumed to act as a rigid body in the dynamic environment of this study. This assumption was based on the natural frequency data generated for the bubble chamber by use of the axisymmetric model of the chamber and MONSA-V as discussed previously. This data, in addition to a finite element vibration analysis of the beam window protuberance which showed that this component's lowest natural frequency is approximately 157 Hz, established that the bubble chamber components above the chamber-support skirt intersection have a response, to forcing function frequencies similar to those employed in this study, which are almost completely as if the loads were applied slowly. Thus, for the purposes of this phase of the study these components can be modeled as rigid bodies with no introduction of error. The bubble chamber components below this intersection were assumed to behave elastically. The mass center of that portion of the bubble chamber above the conical skirt-chamber intersection which was assumed to be rigid was lumped at Node 60. This mass center was not located on the vertical centerline of the bubble chamber. This was due to the existence of the beam window

protuberance, "beanie", and cameras, which are all nonsymmetrically placed about the vertical centerline.

The calculation of the elastic properties of the supporting skirt and the portion of the bubble chamber below the skirt-chamber intersection were determined by use of the program MONSA-S and a symmetric model of the chamber. This effort consisted of applying symmetric and non-symmetric loads to the symmetric model of the chamber and establishing influence coefficients for the distinct parts of the bubble chamber modeled with finite elements. The parts so analyzed were the conical support skirt, the conical portion of the bubble chamber, and the outer cylinder, cone and inner cylinder of the "Z" section. Influence coefficients were generated for a horizontal and vertical load applied to the bottom of the inner cylinder of the "Z" section, and horizontal (radial) and vertical loads acting on the support cone at the position of the support legs. From these influence coefficients, equivalent elastic elements were generated to represent the portions of the bubble chamber discussed. The conical support skirt was represented by six elements; as an example the lines connecting Nodes 42-52 and 44-52 are two of those six elements. The conical portion of the bubble chamber was represented by the elastic element connecting Nodes 55-57; the heavy ring by element connecting Nodes 57-59, the outer cylinder of the "Z" section by element 59-61, the conical "Z" section by element 61-62 and the inner cylinder by element 62-63. The elastic elements used to model the shell structure were beam and bar elements. The elastic properties of those "artificial" members are given in Table 6.

The vacuum chamber above the cryostat was assumed to act as a rigid member. This assumption was based upon the judgment that the vibration isolators would screen all forcing functions with frequencies greater than 0.7 Hz from reaching the vacuum tank, and that the fundamental frequencies of the shell components comprising the vacuum tank are many

TABLE 6. ELASTIC PROPERTIES OF EQUIVALENT BEAM ELEMENTS

Connecting Nodes	Bubble Chamber Component	Moment of Inertial in^4	Area in^2
42-52 44-52 45-53 47-53 48-54 50-54	Conical Supporting Shirt	30.0	6.7
55-57	Conical Portion Bubble Chamber	1.2×10^5	83.4
57-59	Heavy Ring	7.8×10^5	1074.4
59-61	Outer Cylinder, Lower Chamber	9.0×10^4	217.6
61-62	Conical Section, Z-Section	3.0×10^3	70.8
62-63	Inner Cylinder, Lower Chamber	75.0	52.6

$E = 2.9 \times 10^7$ lbs/in^2

times greater than 0.7 Hz. The center of mass of the vacuum tank, including the mass of the cryostat, was located at Node 56. This center of mass is located on the vertical geometric centerline of the tank. Both the translational mass and the rotary inertia of the vacuum tank were included at this node.

The stiffness model of the lumped parameter model was now complete. However, the mass model depends upon the fluid inside the chamber. The location of the mass center of the chamber, Node 60, is also dependent on the type of fluid employed. Therefore, two distinct mass models were generated, one for hydrogen and one for neon.

Dynamic Forcing Function

The dynamic forcing function used in this study is derived from two sources: the inertial force due to the acceleration of the piston and the change of chamber pressure above and below the piston.

It was assumed that the displacement of the piston could be represented by the function,

$$\delta = \frac{X_o}{2}\left(1 - \cos\left\{\frac{2\pi t}{T_p}\right\}\right), \quad 0 \leq t \leq T_p$$

$$\delta = 0, \quad T_p < t \leq T_{PS}$$

where δ = the piston displacement as a function of time

X_o = stroke of the piston, inches

T_p = period of piston stroke

T_{PS} = period of multipulsing.

The displacement functions used in this study are shown in Figure 44.

The inertial force of the piston is therefore the mass of the piston multiplied by its acceleration. This required inertial force is supplied by the actuator and reacted by the caisson. Therefore, this inertial force, which is applied at the top of the caisson (Node 5 in the model), is given by

$$F_{IF} = \frac{M_p X_o}{2}\left\{\frac{2\pi}{T_p}\right\}^2 \cos\left\{\frac{2\pi}{T_p}\right\}, \quad 0 \leq t \leq T_p$$

$$F_{IF} = 0, \qquad T_p \leq t \leq T_{PS}$$

where F_{IP} = piston inertial force as a function of time

M_p = mass of the piston.

The pressure force for the pressure change above the piston is given by:

$$F_{PU} = \frac{\Delta P_c}{2} A_{pT}\left(1 - \cos\frac{2\pi t}{T_p}\right), \quad 0 \leq t \leq T_p$$

$$F_{PU} = 0, \qquad T_p < t \leq T_{PS}.$$

where F_{PU} = force generated in upper chamber due to the piston displacement

ΔP_c = pressure change in bubble chamber

A_{pT} = area of the top of the piston.

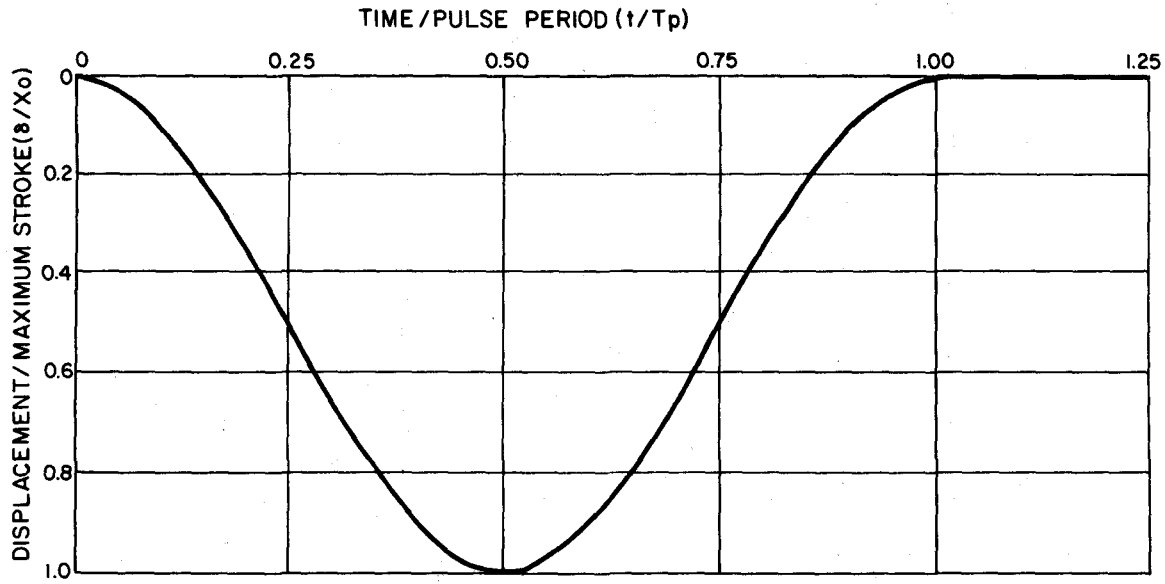

FIGURE 44. NON-DIMENSIONAL PLOT OF DISPLACEMENT FUNCTION

The pressure force for the pressure change below the piston is given by:

$$F_{PL} = \alpha \frac{\Delta P_c}{2} A_{PB} \left(1 - \cos \frac{2\pi t}{T_p}\right), \quad 0 \leq t \leq T_p$$

$$F_{PL} = 0 \quad , \qquad T_p \leq t \leq T_{PS}$$

where F_{PL} = force generated in lower chamber due to the piston displacement

α = correction factor for pressure change in lower chamber

A_{PB} = area of the bottom of the piston.

The sum of the three forces given above were assumed to act through the piston actuator and reacted on the top of the caisson. This was applied to the model in the positive x-axis (vertical) at Node 3. The two pressure forces were applied to the chamber. The negative of the upper chamber force was applied at Node 55 while the negative of the lower chamber force was applied at Node 61. (The upper force represents a decrease in the chamber pressure while the lower force represents an increase in the pressure in the "Z" section. The equilibrium pressure was taken as the equilibrium force configuration for the chamber for dynamic analysis purposes.) Table 7 gives the values for the above parameters for the two fluids considered, hydrogen and neon, and for both single and multipulse operation.

Solution Technique

Once the lumped parameter model and the forcing function on that model have been defined, the dynamic response of the system is characterized by the multi-degree-of-freedom matrix equation given below:

$$[M]\{\ddot{\Delta}\} + [C]\{\dot{\Delta}\} + [K]\{\Delta\} = \{f(t)\}, \qquad (1)$$

where $[M]$ = mass matrix

$[C]$ = damping matrix

$[K]$ = stiffness matrix

$\{f(t)\}$ = generalized coordinates time-dependent forcing function

$\{\Delta\}$ = generalized coordinates displacements

$\{\dot{\Delta}\}$ = generalized coordinates velocities

$\{\ddot{\Delta}\}$ = generalized coordinates accelerations.

For this study velocity dependent damping was assumed.

TABLE 7. FORCING FUNCTION PARAMETERS

Parameter	Hydrogen	Neon
X_o, inches	4.0	4.0
T_p, seconds	0.040	0.100
T_{PS}, seconds	0.250	0.333
Number of Pulses	4	3
M_p, $\frac{\text{pounds-second}^2}{\text{inch}}$	8.193	8.193
P_c, psi	60	65
$_{PT}$, inch^2	3940	3940
$_{PB}$, inch^2	3831	3831
	0.75	0.85

Once the continuum elastic dynamic problem has reduced to the form given in the matrix equation (1), the solution can proceed along several paths. The method used here is known as the normal mode method for proportional damping and is explained briefly in Appendix A.

The normal mode method makes it possible to solve matrix equation (1), with certain constraints on the form of the damping matrix, by using the appropriate linear transformation to reduce the matrix equation of order N to the solution of a system of N single-degree-of-freedom equations of the form given in Equation (2):

$$M_i\ddot{y}_i + C_i\dot{y}_i + K_iy_i = F_i(t), \quad i = 1 \rightarrow N, \tag{2}$$

where M_i = i^{th} modal mass

C_i = i^{th} modal damping coefficient

K_i = i^{th} modal stiffness coefficient

$F_i(t)$ = i^{th} modal force

$\ddot{y}_i$ = i^{th} modal acceleration

$\dot{y}_i$ = i^{th} modal velocity

y_i = i^{th} modal displacement.

When the i^{th} modal force, $F_i(t)$, which is obtained from the applied dynamic forces, is known at a discrete number of points and is assumed to be linear between those points, a closed form solution of Equation (2) is used to determine the modal response parameter, y_i, ($i = 1 \rightarrow N$). Once the modal response parameters are known, the response of the original system, $\{\Delta\}$, can be obtained by applying the same linear transformation to the y_i's that was used to transform Matrix Equation (1) to Equation (2). This linear transformation involves the determination of the undamped natural frequencies of the system. Although, for completeness, knowledge of all the natural frequencies and their corresponding mode shapes are required, in practice usually only a few of the frequencies are needed to obtain very accurate results. The nature of the dynamic force determines how many and which of the modes are critical for a proper evaluation of the dynamic response of the system.

Another assumption critical to the proper evaluation of the dynamic response of the system is the value of the damping matrix. This matrix is reduced to a proportion of critical damping in each normal mode employed. The value of this damping is usually 0.5 percent to 1.0 percent of critical damping for welded steel structures and 2.0 percent to 5 percent for concrete structures. Because it was anticipated that most of the response of the structure would occur in the supporting legs, which are steel, a value of 1.0 percent of critical damping was assumed for all modes of response.

For this study, only the displacement response was calculated. These displacements were compared to the corresponding static displacements to obtain a dynamic amplification factor. This dynamic amplification factor

was then applied to the static results to determine the acceptability of the chamber components.

Natural Frequencies

Once both the mass and stiffness models had been generated, the next step was the determination of the natural frequencies and their corresponding mode shapes. For this study, these natural frequencies and mode shapes were determined by the well-known power method. The basic forcing functions were vertical in nature with frequencies ranging from 25 Hz for hydrogen to 10 Hz for neon. Therefore all natural frequencies of the system up to slightly above the forcing frequencies were determined. In addition, the first two purely vertical response frequencies were also generated for each model.

Table 8 gives the natural frequencies of the system as determined for both the hydrogen and neon models. Frequencies up to 35.4 Hz and up to 23.4 Hz were generated for the hydrogen and neon models, respectively. The two vertical frequencies for the hydrogen model were 51.3 and 67.3 Hz and 36.4 and 63.7 Hz for the neon model. Table 8 also gives a description of the type of modal response by which each frequency is characterized. In this table the modes where movement of the vacuum tank characterizes the mode shape is so identified. All other modes pertain to primary motion of the bubble chamber.

For the frequencies determined only three made a significant contribution to the response of the structure when acted upon by the basic forcing functions. These three were the vertical mode, 51.3 Hz for the hydrogen and 36.4 Hz for the neon, and a radial mode of the conical support skirt and bubble chamber legs, mode number 13 for both the hydrogen and neon models at approximately 20 Hz.

Single-Pulse Response

The dynamic responses of both the hydrogen and neon models were obtained for the single pulse dynamic loading. Table 9 summarizes the

TABLE 8. NATURAL FREQUENCIES AND MODE TYPE

Mode	Frequency, Hz			
	H_2		N_e	
Vert. 1	51.3		36.4	
Vert. 2	67.5		63.7	
1	0.7	Vacuum Chamber Vertical	0.7	Vacuum Chamber Vertical
2	1.4	Vacuum Chamber Vertical	1.4	Vacuum Chamber Vertical
3	1.4	Vacuum Chamber Vertical	1.4	Vacuum Chamber Vertical
4	3.5	Lateral	2.4	Lateral
5	3.5	Lateral	2.4	Lateral
6	5.5	Torsional	5.4	Torsional
7	6.2	Vacuum Chamber Torsional	5.7	Torsional
8	6.6	Vacuum Chamber Lateral	6.6	Vacuum Chamber Lateral
9	6.6	Vacuum Chamber Lateral	6.6	Vacuum Chamber Lateral
10	13.3	Lateral	13.2	Lateral
11	13.3	Lateral	13.2	Lateral
12	20.4	Lateral	20.1	Lateral
13	20.1	Radial	20.0	Radial
14	20.4	Lateral	20.1	Lateral
15	23.4	Vacuum Chamber Lateral	23.4	Vacuum Chamber Lateral
16	22.8	Vacuum Chamber Radial	22.8	Vacuum Chamber Radial
17	23.4	Vacuum Chamber Radial		
18	29.0	Lateral		
19	29.0	Lateral		
20	30.9			
21	32.2			
22	32.5			
23	33.8			
24	32.5			
25	35.4			

Coupled Vacuum Chamber and Bubble Chamber

TABLE 9. MAXIMUM DISPLACEMENTS IN SINGLE PULSE OPERATION

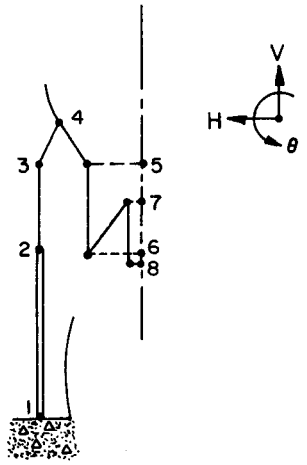

Node	H_2, 0.0195 sec.			H_2, 0.0320 sec.			N_e, 0.0525 sec.		
	H	V	θ	H	V	θ	H	V	θ
1	0.0	-4.3	0.00	0.0	-0.4	0.00	0.0	-0.5	0.00
2	13.3	-7.4	0.21	32.3	-0.6	0.51	38.3	-3.8	0.65
3	9.7	-8.8	-1.13	23.6	-0.6	-2.74	28.4	-5.6	-3.19
4	0.0	-22.7	-0.02	0.0	-23.9	0.00	0.0	-25.7	0.00
5	-1.8	-24.5	-0.28	0.0	-24.0	0.01	-1.1	-27.2	-0.15
6	-4.3	-25.0	-0.33	0.1	-24.0	0.01	-2.4	-27.6	-0.16
7	-3.5	-25.4	-0.23	0.1	-24.0	0.01	-2.3	-28.0	0.03
8	-5.7	-25.5	-0.69	0.1	-24.0	0.02	-2.3	-28.2	-0.01

H = horizontal displacement in mils

V = vertical displacement in mils

θ = rotation in radians x 10^{-4}

maximum response of the bubble chamber supporting legs and the lower portion of the bubble chamber proper.

The response of the vacuum tank was essentially zero. Therefore the points of interest are all concerned with the portion of the bubble chamber and legs just mentioned. Also included in this table is the response of the top of the caisson.

The maximum vertical response of the bubble chamber occurs at the bottom of the inner cylinder of the "Z" section (Node 63) and is 28.2 mils at 0.0525 second after the initiation of the pulse for the neon model. The maximum lateral (horizontal) response is 38.3 mils and occurs at the change in cross section in the bubble chamber support legs. This motion is radial from the vertical line of the chamber. All six legs experienced this same radial action. The maximum lateral response of the bottom of the lower chamber inner cylinder was 5.7 mils, occurring at 0.0195 second after the initiation of the hydrogen pulse.

The bubble chamber above the mass center was assumed to act as a rigid body. Thus, the motion of the "beanie" at the camera penetration locations was determined by utilizing the displacements and rotations of the mass center. The maximum displacements of the cameras for the hydrogen model were 23 mils in a vertical direction and 1 mil in a lateral direction, while for the neon model these displacements were 26 mils and 1.5 mils, respectively. These displacements are due solely to the dynamic loads. For the total movement of the cameras during operation the static deflection of the bubble chamber shell, under internal pressure, must be added to the above figures.

Multi-Pulse Response

For this part of the study the full, anticipated, pulsing sequences where applied to both the hydrogen and neon models. The multi-pulse response of the neon model showed no significant increase in the maximum displacements as generated by the single pulse study. The total increase

in displacements for the neon multi-pulse response as compared to the single pulse response was approximately 6 percent. The maximum displacements for the multi-pulse neon response occurred immediately after the fourth (final) pulse was completed.

The maximum displacements in the hydrogen model, as determined by multi-pulse response, showed an unacceptable increase over those displacements generated by the single pulse study. In the multi-pulse response, the maximum radial deflection of the bubble chamber support legs and the conical support skirt increased 286 percent above that calculated for the single pulse response. The resulting maximum radial deflection of the conical support skirt at the leg intersections thus calculated was 55 mils. The maximum radial deflection at this location as calculated from the static loading condition was 21 mils. A 21 mil deflection of this type results in stresses in the support cone which are acceptable from the viewpoint of fatigue. A 55 mil deflection of the same type would induce stresses in the bottom of the conical support skirt, at the support leg positions, that would be high enough to cause fairly rapid fatigue failure. A plot of the radial displacement of the conical support skirt ring, at the critical location, for the final pulse of the four pulse in the hydrogen cycle is given in Figure 45. The start of the final pulse occurred at 1.0 second.

From the results of the above work it became apparent that some form of cross-bracing of the support legs would be required. A bracing system as depicted in NAL drawing No. 2621.ME-25486, titled "30K Liter Hydrogen B.C. Chamber Support Ass'y" (included in this report), was developed and included in the stiffness model for both the hydrogen and neon models. The location of this bracing is shown in Figure 47. The response of the multi-pulse hydrogen model, which now included the cross-bracing, was determined and the maximum displacement of the conical support skirt in the critical location was shown to be reduced to approximately 18 mils,

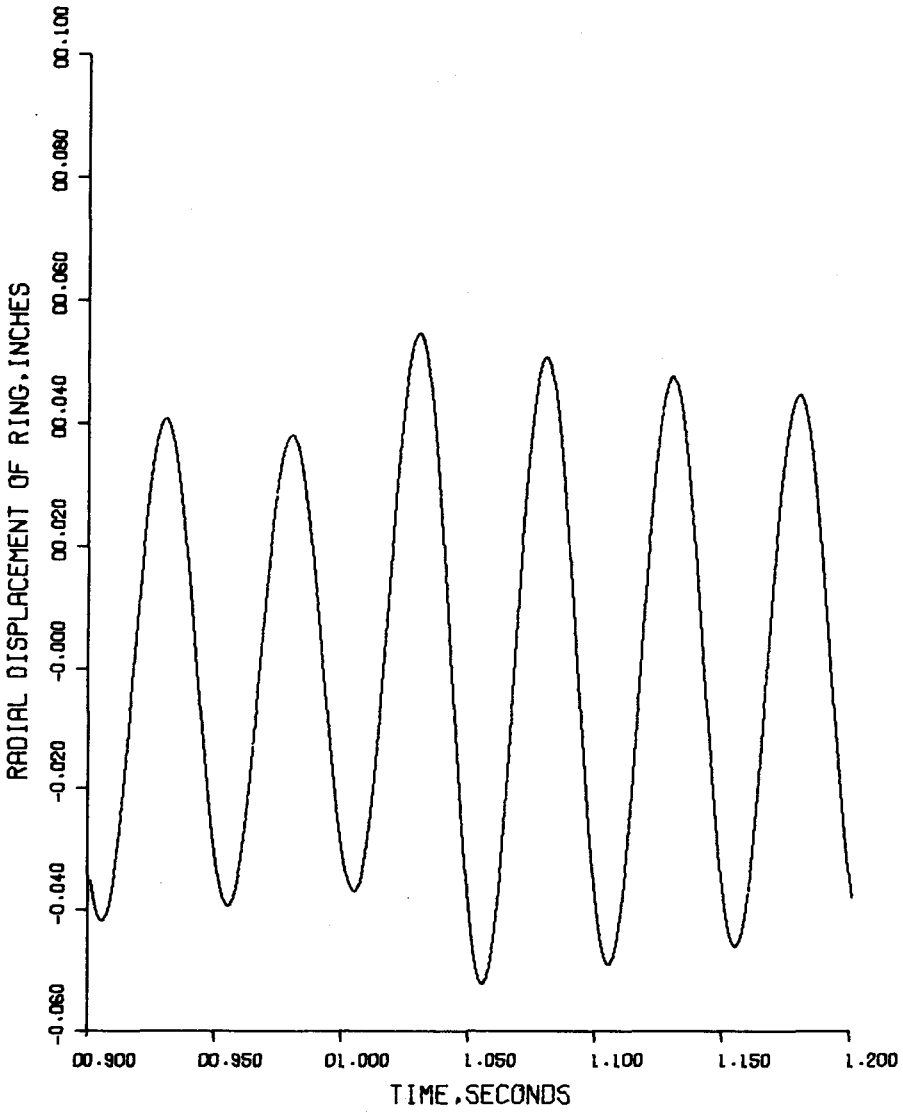

FIGURE 45. RADIAL DISPLACEMENT DURING MULTI-PULSING OF UNBRACED MODEL

thus reducing the resultant stresses in this region to slightly below those calculated for the static case. A plot of the radial displacement of the conical support skirt ring for the model incorporating the cross-bracing is shown in Figure 46.

Incorporation of the 33-Ton Target

One of the planned missions for the bubble chamber is the use of a large, stainless steel plate for muon identification. This plate which will weigh approximately 66,000 pounds will be placed off center, towards the rear of the chamber, while the remainder of the chamber volume will be filled with liquid neon. The off-center emplacement of such a large mass caused concern as to its effect upon the dynamic response of the structure. To resolve this concern a complete dynamic response study of this configuration was carried out.

The lumped parameter model generated for this study is shown in Figure 47. This view is of the model only above the caisson. The major changes in this new neon model are the value and location of the mass center for the bubble chamber, and the inclusion of the cross-bracing as previously discussed. The 33-ton target was assumed to act as a rigid body. The center of mass moved to a position 10.87 inches from the vertical centerline of the chamber on the hadron beam line, away from the window and 14.85 inches above the horizontal centerline of the chamber. The dynamic forcing function remained the same. It was assumed that the presence of the large plate target added no new forces (other than gravity loads) to the system. This is a reasonable assumption so long as the support system connecting the target to the chamber (to be designed at some future date) is sufficiently stiff so as to be considered rigid from the dynamic viewpoint. Any significant flexibility in this support system, say below approximately 5×10^6 pounds per inch in the bending mode, may invalidate the findings of this study.

Table 10 gives the natural frequencies determined for this model. Also given in this table is the maximum modal response of each of these

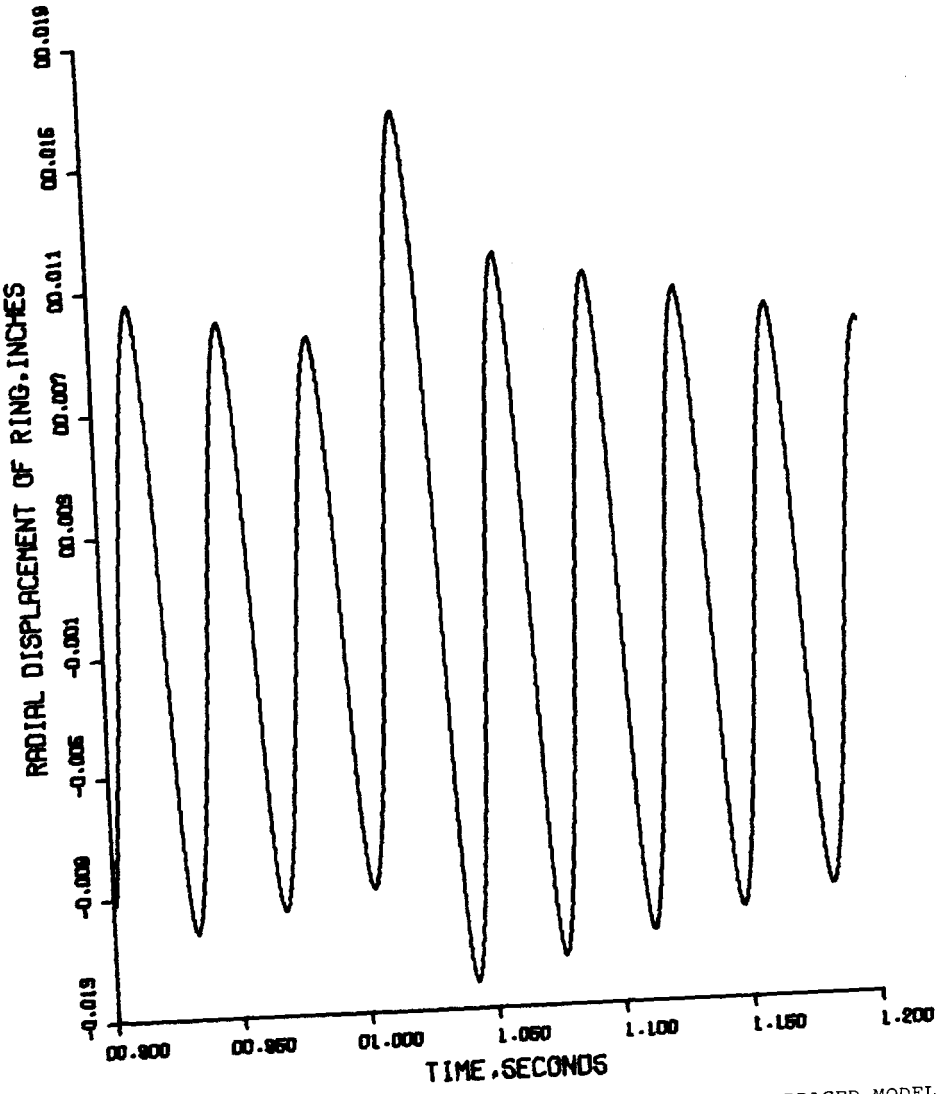

FIGURE 46. RADIAL DISPLACEMENT DURING MULTI-PULSING OF BRACED MODEL

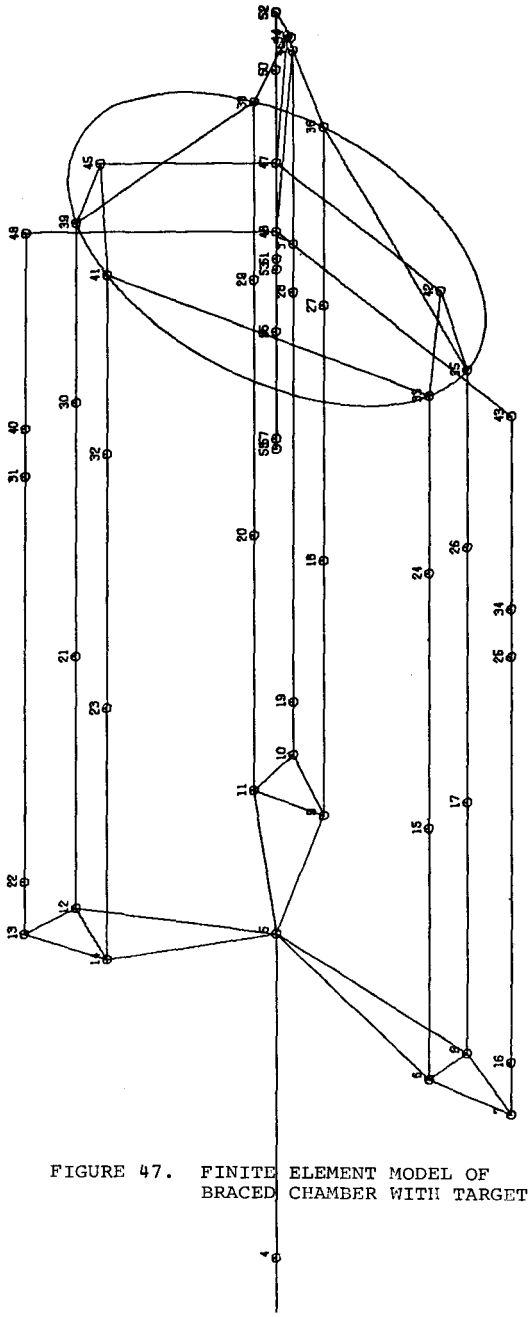

FIGURE 47. FINITE ELEMENT MODEL OF BRACED CHAMBER WITH TARGET

TABLE 10. NATURAL FREQUENCIES OF THE NEON MODEL WITH 33-TON TARGET

Mode	f. Hz		$\delta_{max.}$ inches	Time, second
Vert. 7	32.44		2.5225×10^{-2}	0.0555
Vert. 10	63.34		-3.1217×10^{-3}	0.0545
1	0.70	Vacuum Chamber Vertical	1.8627×10^{-6}	0.049
2	1.38	Vacuum Chamber Vertical	-5.6609×10^{-7}*	0.200
3	1.38	Vacuum Chamber Vertical	5.9103×10^{-7}*	0.200
4	2.16	Lateral	-1.7376×10^{-6}	0.165
5	2.17	Lateral	1.6524×10^{-6}	0.1645
6	4.79	Torsional	-9.5417×10^{-8}	0.102
7	6.17	Vacuum Chamber Torsional	2.6853×10^{-8}	0.090
8	6.56	Vacuum Chamber Lateral	8.6183×10^{-5}	0.0875
9	6.56	Vacuum Chamber Lateral	3.9689×10^{-5}	0.0875
10	13.25	Lateral	1.5695×10^{-4}	0.062
11	13.26	Lateral	1.5794×10^{-4}	0.062
12	22.89	Lateral	-1.9680×10^{-3}	0.047
13	23.61	Lateral	-3.5792×10^{-3}	0.0465
14	22.87	Lateral	2.2015×10^{-3}	0.047
15	25.10	Lateral	5.0548×10^{-3}	0.045
16	23.81	Lateral	-1.4129×10^{-2}	0.046
17	22.82	Lateral	1.1757×10^{-3}	0.047
18	23.61	Vacuum Chamber Lateral		
19	26.54	Radial	4.2533×10^{-3}	0.0445
20	28.90	Lateral	8.6435×10^{-3}	0.044
21	29.03	Lateral	5.0278×10^{-3}	0.044
22	29.11	Lateral	5.4412×10^{-5}	0.044
23	30.89			

* not true max.

modes for the single-pulse forcing function (neon). The combined dynamic response of Node 57 (the bottom of the inner cylinder of the "Z" section) is given in Figure 48 through 50. It should be pointed out that numerous lateral modal responses tend to cancel the large lateral response of the vertical mode. This indicates that the system, as modeled, is dynamically "tuned" to minimize the lateral response of the system, and that such response is highly dependent upon the modal frequency of the constituent modes.

Due to the possibility of modeling errors and the possibility of variation of piston displacement period from that used in this study, additional work was carried out to determine the true effect of this "tuning" phenomenon. First the frequencies of the predominant vertical modes were increased by 10 percent while the frequencies of the predominant lateral modes were reduced by 10 percent. The resultant combined response of Node 57 is shown in Figures 51 through 53. For this case the maximum lateral response changed from +6 mils to -10 mils. The frequencies of the modes described above were then changed in the other direction by 10 percent each. In this case the effect was to narrow the gap between frequencies while in the former action the effect was to increase the gap between frequencies. For this latter case the maximum lateral displacement at Node 57 changed from +6 mils to +13 mils. This effect is shown in Figures 54 through 56.

From the above it can be seen that the lateral response of the bubble chamber structure, with neon in the chamber and with the incorporation of the 33-ton target is strongly dependent upon relatively small changes in the constituent part frequencies. It is therefore recommended that for seal design purposes (at Node 57) that the maximum lateral deflection of the bottom end of the inner cylinder of the "Z" section be estimated as 15 mils.

The multi-pulse response of the system showed very little magnification of the single pulse response. The maximum multi-pulse response

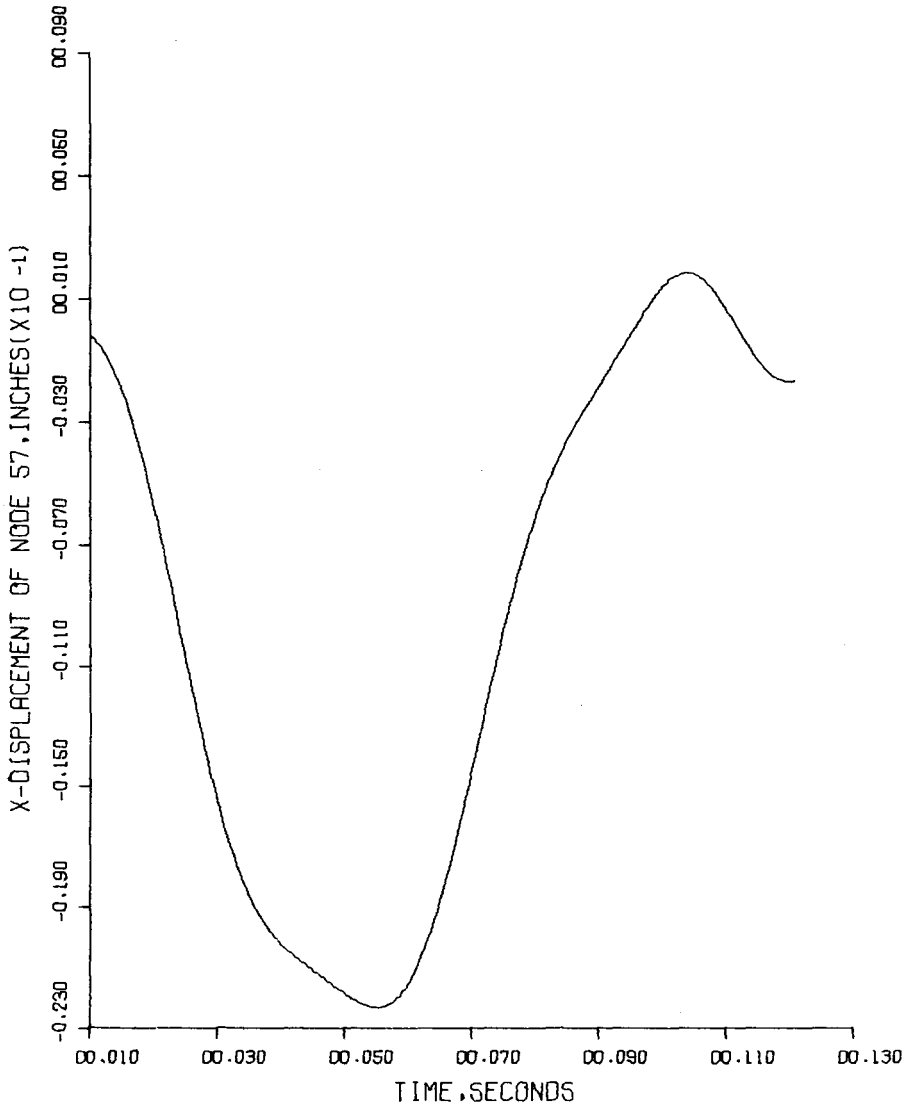

FIGURE 48. VERTICAL DISPLACEMENT AT SPOOL END FOR TARGET MODEL

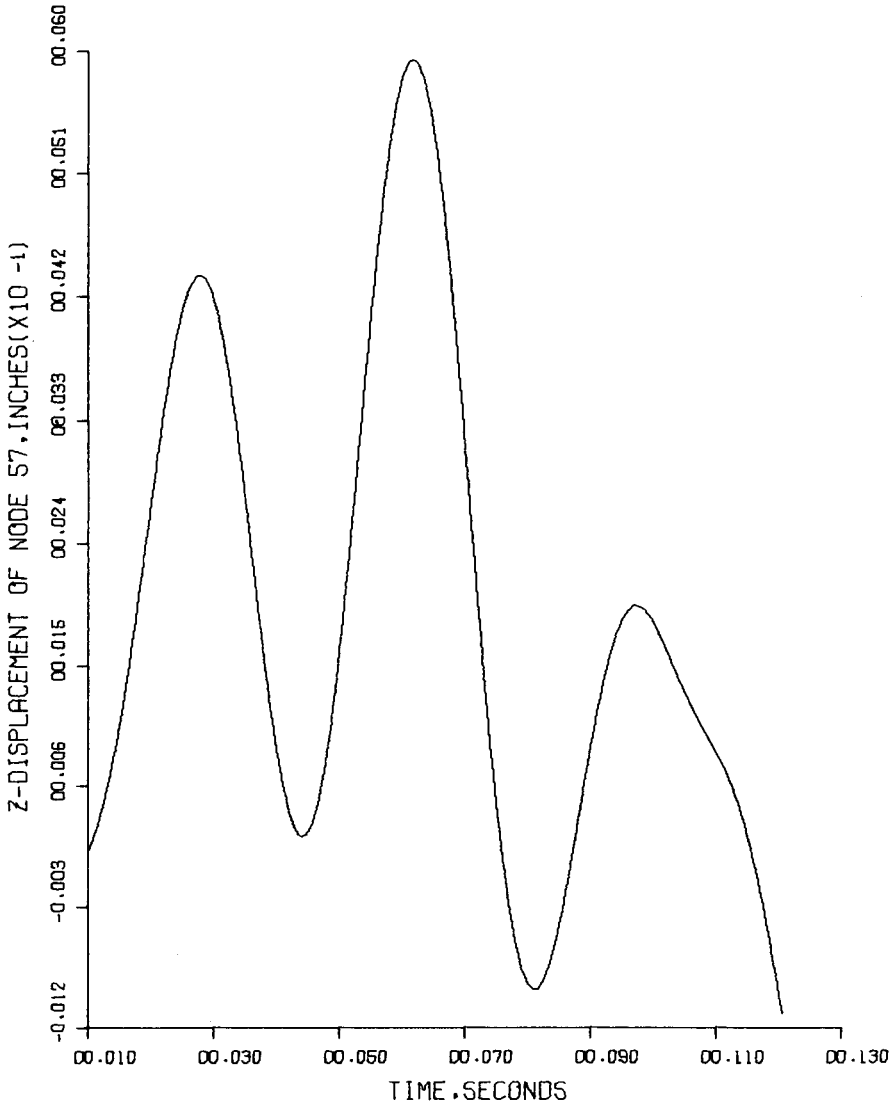

FIGURE 49. PRINCIPAL LATERAL DISPLACEMENT AT SPOOL END FOR TARGET MODEL

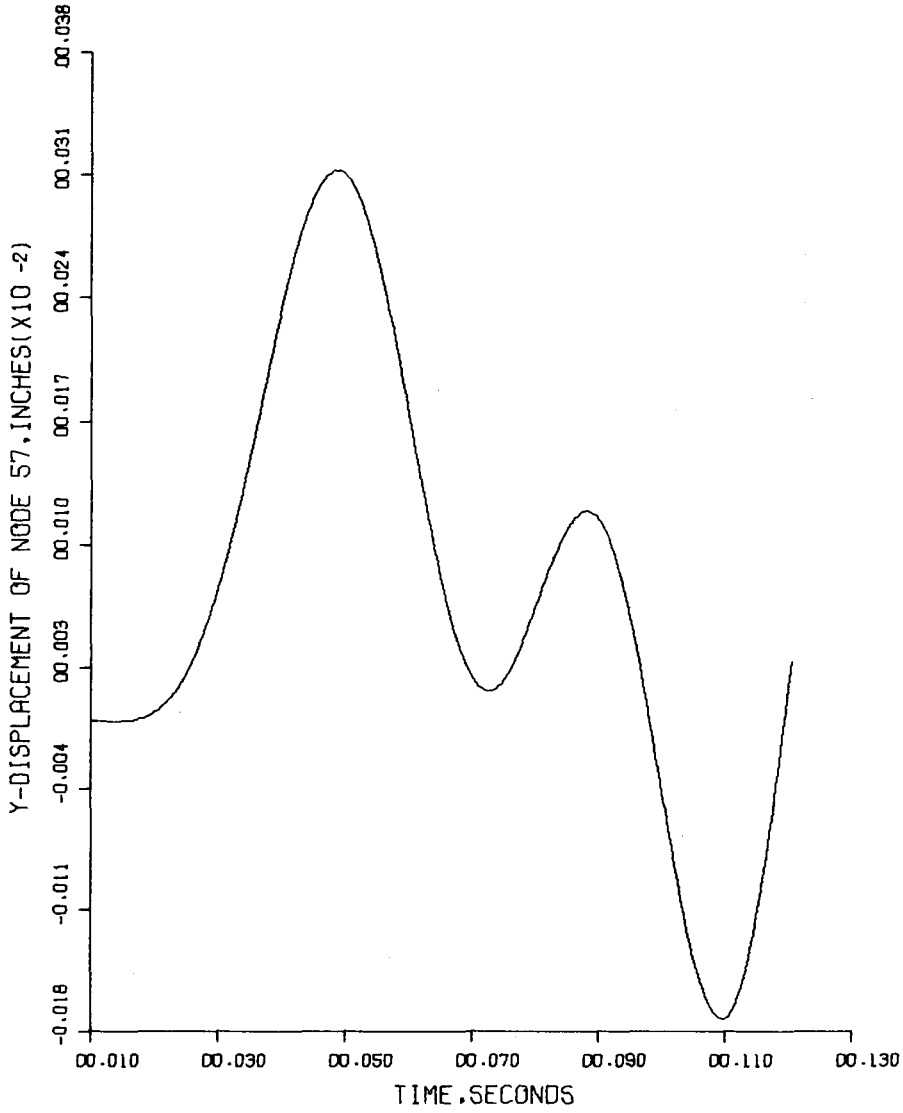

FIGURE 50. SECONDARY COMPONENT OF LATERAL DISPLACEMENT AT SPOOL END FOR TARGET MODEL

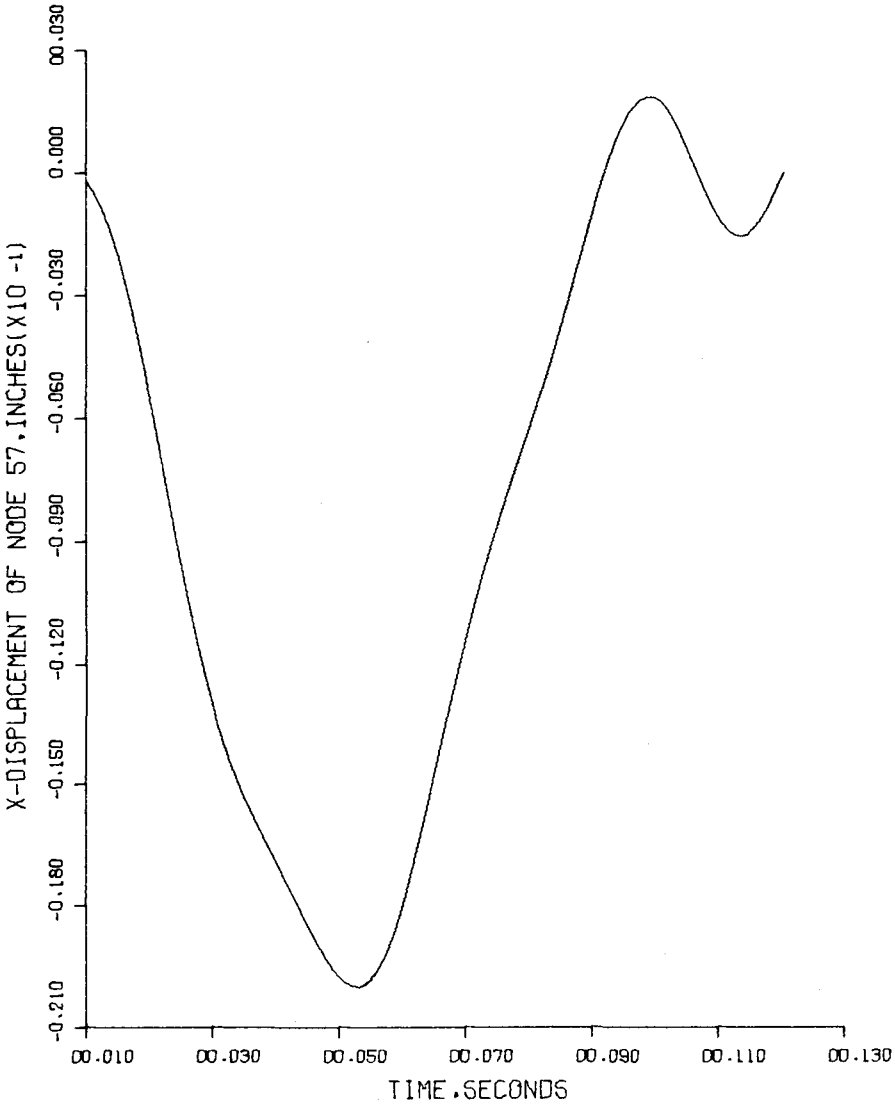

FIGURE 51. VERTICAL DISPLACEMENT AT SPOOL END FOR "FREQUENCY-APART" TARGET MODEL

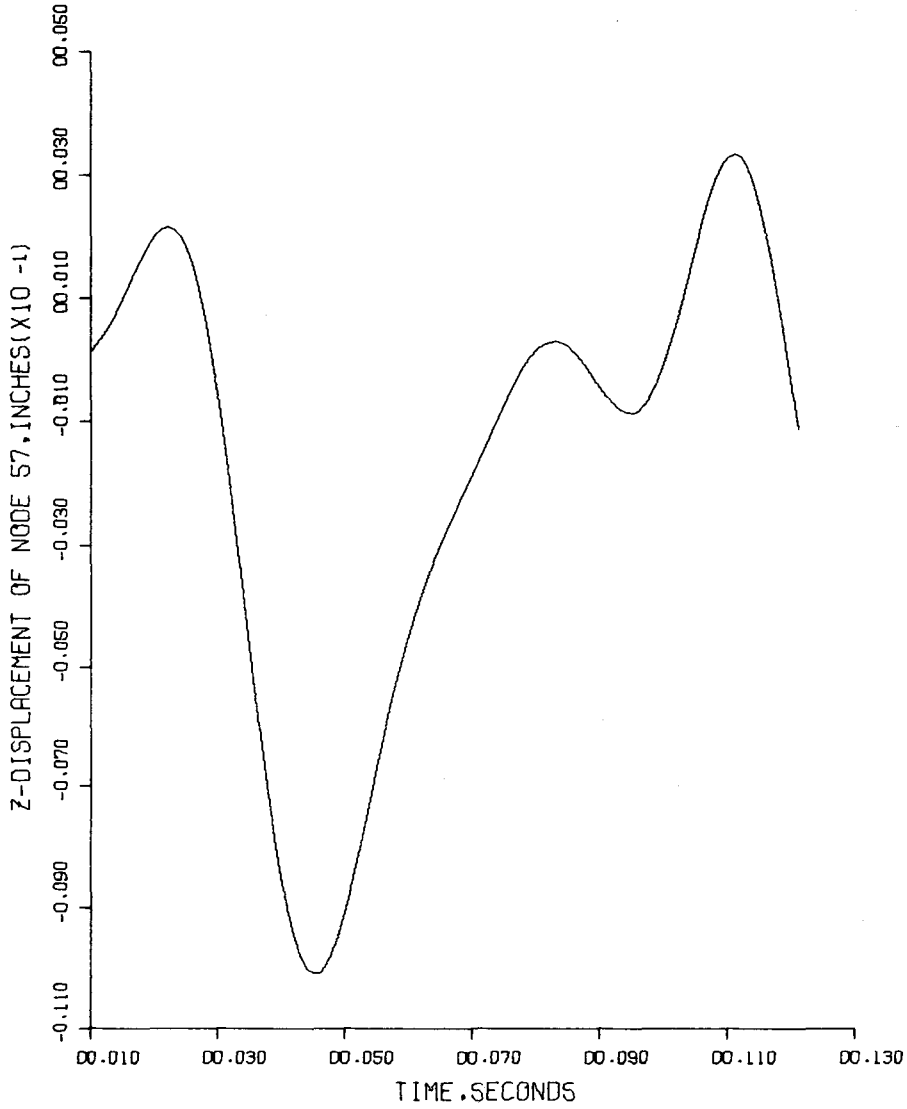

FIGURE 52. PRINCIPAL LATERAL DISPLACEMENT AT SPOOL END FOR "FREQUENCY-APART" TARGET MODEL

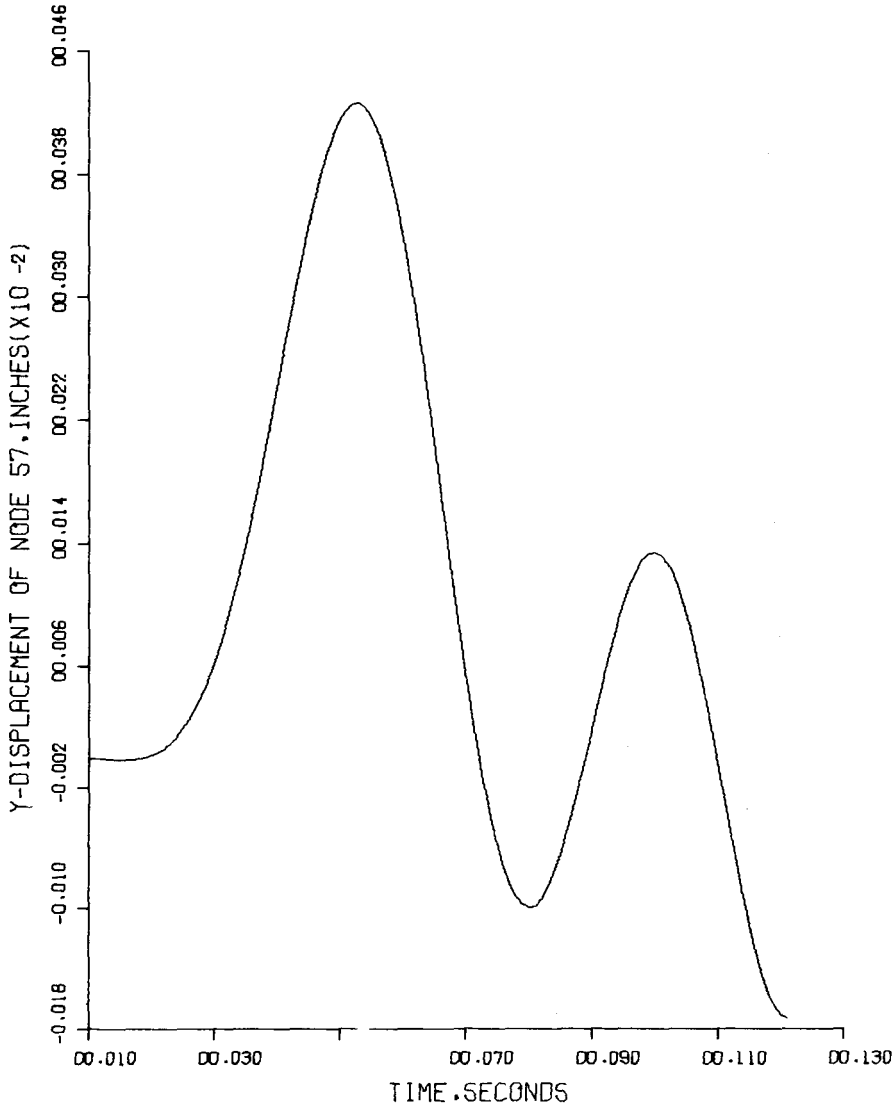

FIGURE 53. SECONDARY COMPONENT OF LATERAL DISPLACEMENT AT SPOOL END FOR "FREQUENCY-APART" TARGET MODEL

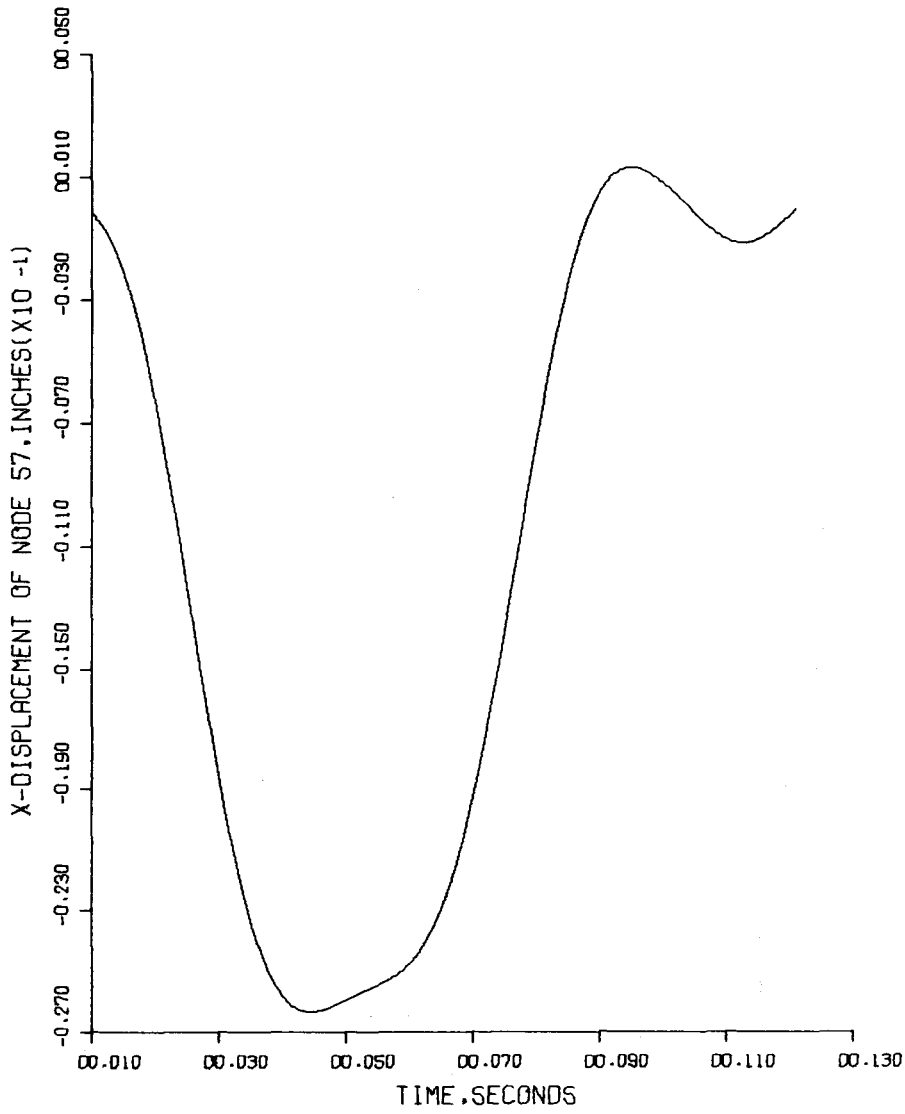

FIGURE 54. VERTICAL DISPLACEMENT AT SPOOL END FOR "FREQUENCY-TOGETHER" TARGET MODEL

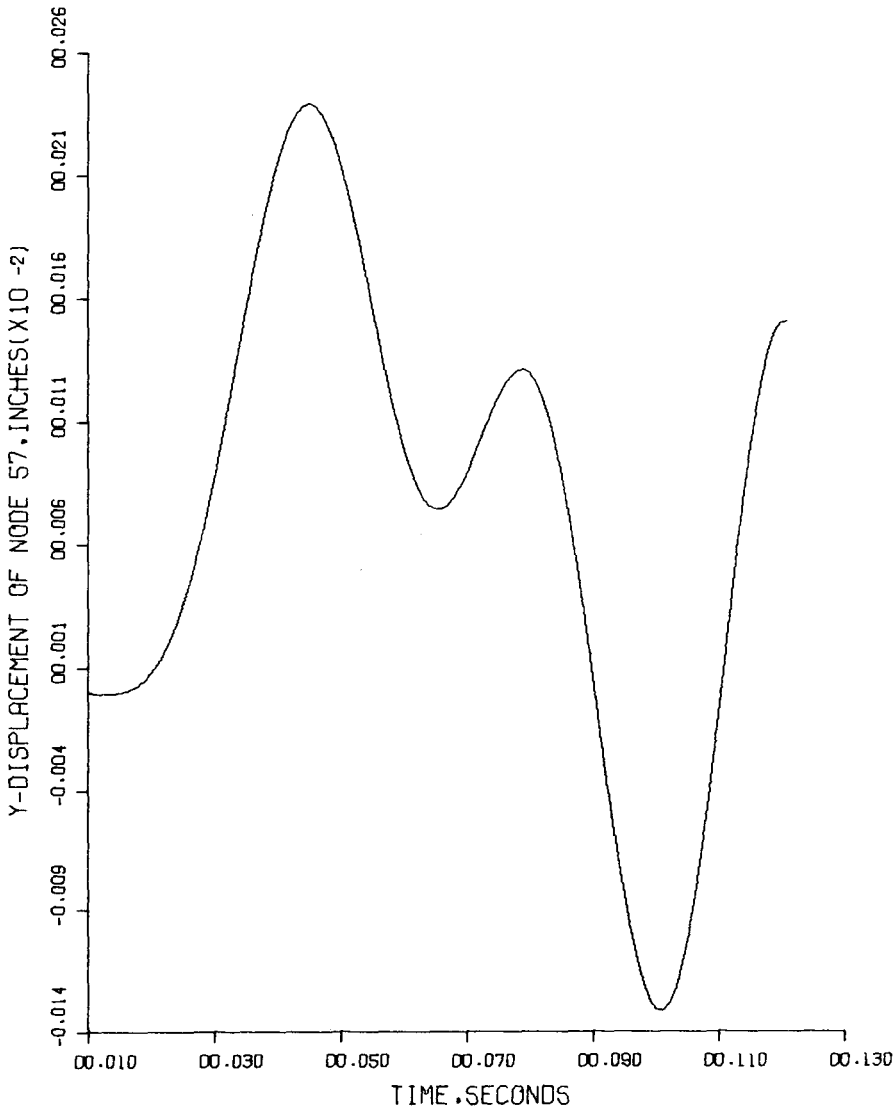

FIGURE 55. PRINCIPAL LATERAL DISPLACEMENT AT SPOOL END FOR "FREQUENCY-TOGETHER" TARGET MODEL

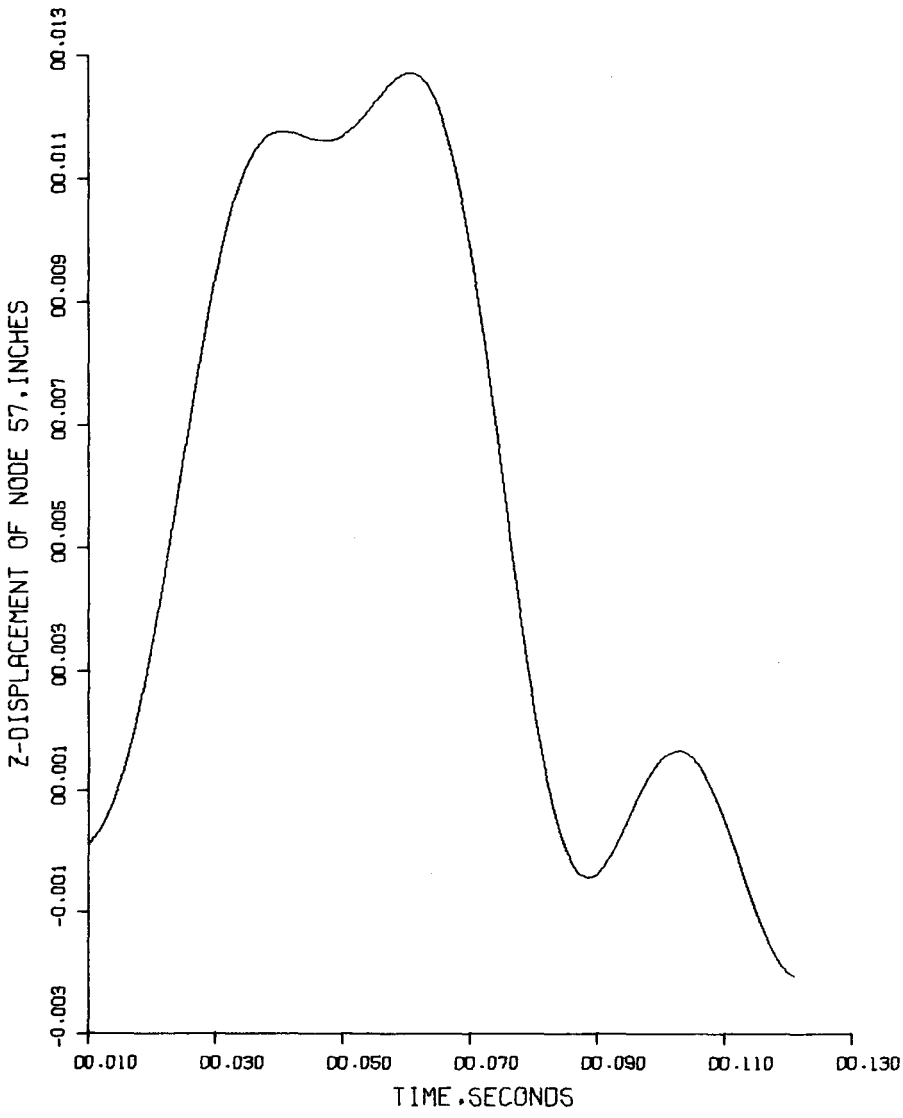

FIGURE 56. SECONDARY COMPONENT OF LATERAL DISPLACEMENT AT SPOOL END FOR "FREQUENCY-TOGETHER" TARGET MODEL

increased approximately 10 percent over the single pulse results.

(7) SUMMARY AND MISCELLANEOUS

From all of the results generated by the dynamic analysis described in the preceding sections of this report it is determined that no significant dynamic amplification of the statically calculated stresses will occur. Thus the bubble chamber, including its support configuration is judged adequate to sustain the anticipated load conditions for an operational life in excess of 10^7 cycles of operation. Further, the design of the bubble chamber and its components are judged to meet the intent of the specifications and requirements of the ASME Boiler and Pressure Vessel Code, Section VIII, Pressure Vessels - Division 2, Alternative Rules. However, for strict compliance with some of these specifications an experimental evaluation of the stress occurring in certain locations in the bubble chamber must be carried out. These locations are:

- At the "beanie"-nozzle intersections
- At the beam window-flange-chamber spherical shell intersection
- At the welds in the outer wall of the multi-wall region of the conical portion of the upper chamber
- In the beam window protuberance at the flange-nose cone intersection on the horizontal centerline of the assembly and at the beam window end of the nose cone at the horizontal centerline location.

"G" Loadings

In order to properly design accessory components to the bubble chamber, such as camera optic parts and piping, it is necessary to know both the displacements and the accelerations that are expected to occur in the bubble chamber at the locations at which they are emplaced or attached. The regions of primary importance are at the camera nozzles, at the main flange position, midway down the outer cylinder in the "Z"

section, and at the bottom of the inner cylinder or "spool" of the "Z" section.

The methods of analyses used in this overall study particularly the sectioning and analysis of individual parts of the chamber and the assumed rigidity of certain components during the dynamic response study, makes the "exact" determination of the displacements and accelerations most difficult. However a good approximation of these values can be attained by superposition of the results obtained in the various segments of the study. For instance, during the hydrogen cycle it has been determined that the change in deflection of the camera nozzles, due to the dynamic application of load, as taken from the equilibrium or maximum pressure condition, and neglecting the elastic expansion of the bubble chamber wall, is approximately 23 mils in the vertical direction. From the static analysis of the "beanie"-chamber intersection, plus the static analysis of the lower section of the chamber it is determined that the static vertical deflection of the camera nozzles for this same cycle and again taken from the equilibrium or maximum pressure condition is 14 mils. Thus the total vertical deflection of the camera nozzles during hydrogen operation is 37 mils. The maximum acceleration can be estimated by

$$g_{max} = \delta_{max}(2\pi f_f)^2/386$$

where g = acceleration ratio, i.e., number of gravities

δ_{max} = maximum displacement, inches

f_f = forcing function frequency, Hz.

For the hydrogen cycle and at the cammera nozzle position then

$$g_{max} = 0.037(2\pi \cdot 25)^2/386 \approx 2.4$$

Following the same reasoning as above, the change in displacements as taken from the equilibrium positions and the maximum "g" loadings

predicted to occur at certain locations in the bubble chamber have been calculated and are presented in Table 11.

TABLE 11. DISPLACEMENT AND ACCELERATION DATA

	Change in Vertical Displ. inches	Change in Horizontal Displ. inches	Maximum g's 1/1
At Bottom of Spool			
Hydrogen	0.0255	0.006	1.63
Neon	0.0283	0.015	0.3
At "Z" Outer Cylinder Midpoint			
Hydrogen	0.0248	0.002(radial)	1.76
Neon	0.0275	0.003(radial)	0.28
At Main Flange			
Hydrogen	0.0245	0.004(radial)	1.57
Neon	0.0272	0.003(radial)	0.28
At Camera Nozzles			
Hydrogen	0.037	0.001	2.4
Neon	0.040	0.0015	0.41

It must be emphasized that the "g" loadings as shown in Table 11 are dependent upon the displacement functions for the piston being basically as shown in Figure 44, that is in the form of versine waves. If the motion of the piston differs in shape (not necessarily period), particularly if there is any residual movement or ringing of the piston upon completion of the versine pulse then the "g" loadings actually occurring at the locations indicated could be many times greater than the figures shown. All care should be taken to ensure that the piston motion does conform to as nearly a pure versine form as possible.

APPENDIX A

NORMAL MODE METHOD FOR PROPORTIONAL DAMPING

APPENDIX A

NORMAL MODE METHOD FOR PROPORTIONAL DAMPING

Consider the differential equations of motion for a structural system having N generalized coordinates written in matrix form:

$$[M]\{\ddot{\Delta}\} + [C]\{\dot{\Delta}\} + [K]\{\Delta\} = \{F(t)\} \tag{A-1}$$

where $[M]$ = mass matrix

$[C]$ = damping matrix

$[K]$ = stiffness matrix

$\{F(t)\}$ = generalized coordinate time dependent forces

$\{\Delta\}$ = generalized coordinate displacements

$\{\dot{\Delta}\}$ = generalized coordinate velocities

$\{\ddot{\Delta}\}$ = generalized coordinate accelerations.

Now, if $[C] = \alpha_1[M] + \alpha_2[K]$ (that is, if the damping matrix is a linear combination of the mass matrix and the stiffness matrix) the equations of motion can be uncoupled using the normal mode method for proportional damping.

First, assume that the response $\{\ddot{\Delta}\}$ can be expressed as the sum of the series of products of the undamped free-vibration-mode shape and a time-dependent scalar:

$$\{\Delta\} = \sum_{j=1}^{n} \{\Phi\}_j y_j(t) \tag{A-2}$$

where $\{\Phi\}_j$ = undamped free-vibration-mode shape for the j^{th} normal mode

$y_j(t)$ = time-dependent scalar.

Consider the undamped free-vibration portion of Equation (A-1):

$$[M]\{\ddot{\Delta}\} + [K]\{\Delta\} = \{o\} \tag{A-3}$$

where $\{o\}$ = null vector.

Assume that a normal mode exists such that in free vibration:

$$\{\Delta\} = A\{\Phi\}e^{i\omega t} \tag{A-4}$$

where $\{\Phi\}$ = undamped free-vibration-mode shape

A = amplitude constant

ω = oscillatory frequency

$i^2 = -1$.

Now, differentiating this expression for $\{\Delta\}$ with respect to time twice, yields

$$\ddot{\{\Delta\}} = -\omega^2 A\{\Phi\}e^{i\omega t} . \tag{A-5}$$

Using Equations (A-4) and (A-5) in Equation (A-3) results in

$$-\omega^2 A[M]\{\Phi\}e^{i\omega t} + A[K]\{\Phi\}e^{i\omega t} = \{o\} . \tag{A-6}$$

Dividing through by $Ae^{i\omega t}$ and factoring out $\{\Phi\}$ yields:

$$\left[-\omega^2[M] + [K]\right]\{\Phi\} = \{o\}\Big]. \tag{A-7}$$

Equation (A-7) is one form of the classical eigenvalue problem, which, for [M] positive definite and symmetry and [K] symmetry, there are N solutions of ω^2. Corresponding to each ω_j^2 there exists a $\{\Phi\}$ that is orthogonal to all other $\{\Phi\}_\ell$, $\ell = 1 \to n$, $\ell \neq j$. Therefore the $\{\Phi\}_j$, $j = 1 \to n$, forms the basic vectors for a space of dimension N, and any vector in that space is a linear combination of the basis vectors, $\{\Phi\}_j$, $j = 1 \to n$, or

$$\{\Delta\} = \sum_{j=1}^{n} \beta_j\{\Phi\}_j . \tag{A-8}$$

Now, the β_j's in Equation (A-8) can be associated with the $y_j(t)$'s in Equation (A-2). This proves that the undamped-free-vibration solution is a linear combination of the normal modes under the assumptions stated. Equation (A-2) can be written in matrix form as:

$$\{\Delta\} = [\Phi]\{y(t)\} \tag{A-9}$$

where $[\Phi]$ = modal matrix, which, by repeated differentiation with respect to time, yields

$$\dot{\{\Delta\}} = [\Phi]\dot{\{y(t)\}} \tag{A-10}$$

and

$$\ddot{\{\Delta\}} = [\Phi]\ddot{\{y(t)\}} . \tag{A-11}$$

Now, using Equations (A-9), (A-10), and (A-11) in Equation (A-1) yields:

$$[M][\Phi]\ddot{\{y(t)\}} + [C][\Phi]\dot{\{y(t)\}} + [K][\Phi]\{y(t)\} = \{F(t)\} . \tag{A-12}$$

Premultiplying Equation (A-12) by the matrix transpose of the modal matrix yields the uncoupled equations of motion in the scalars $y_j(t)$:

$$[\Phi]^T[M][\Phi]\{\ddot{y}(t)\} + [\Phi]^T[C][\Phi]\{\dot{y}(t)\} + [\Phi]^T[K][\Phi]\{y(t)\} = [\Phi]^T\{F(t)\} \tag{A-13}$$

where $[\Phi]^T$ = matrix transpose of $[\Phi]$.

It can be shown that, under the assumptions of the formulation of the procedure, the three matrices $[\Phi]^T[M][\Phi]$, $[\Phi]^T[C][\Phi]$, and $[\Phi]^T[K][\Phi]$ are now diagonalized by the transformation. Therefore, the j^{th} equation in Matrix Equation (A-13) is:

$$M_j\ddot{y}_j(t) + C_j\dot{y}_j(t) + K_jy_j(t) = \{\Phi\}_j^T\{F(t)\} \tag{A-14}$$

where $M_j = \{\Phi\}_j^T[M]\{\Phi\}_j$

$C_j = \{\Phi\}_j^T[C]\{\Phi\}_j = \alpha_1M_j + \alpha_2K_j$

$K_j = \{\Phi\}_j^T[K]\{\Phi\}_j$.

Now the N uncoupled equations can be integrated numerically or in closed form independently to give $y_j(t)$, $\dot{y}_j(t)$, and $\ddot{y}_j(t)$. Then, by use of the transformations given in Equations (A-9), (A-10), and (A-11), the displacements, velocities, and accelerations of the generalized coordinates to the given forcing functions can be obtained.

CHICAGO BRIDGE & IRON COMPANY
901 WEST 22ND STREET, OAK BROOK, ILLINOIS 60521

Area Code: 312 654-1700

150 ø 30 K Liter Weldment
for
National Accelerator Laboratory
Batavia Weldment

STRESS REPORT CERTIFICATION

As a professional engineer experienced in pressure vessel design and registered in the State of Illinois with License No. 62-25201, I do hereby certify that I have reviewed the portions of the stress report prepared by the Battelle Memorial Institute which pertain to the design and analysis of the weldment supplied by Chicago Bridge and Iron Company, under CB&I contract 71-2025 and the contract drawings prepared by CB&I, Revision numbers as shown on attached. I further certify that the reviewed sections of the Battelle stress report meet the design requirements of the ASME Code, Section VIII, Division 2; Addenda through Summer 1970, and the NAL user's Design Specification with the following limitations and exceptions:

Limitations:

1. This certification applies to the stainless weldment supplied by CB&I only. The configuration is as shown on Revision 6 of the General Plan except that the dimple plate shown attached has not been considered in this review and certification.

2. The design and operational loadings are not specifically defined in the design specification. This certification is based on the assumption that the loading conditions as defined in the Battelle stress report are correct. Of particular concern is the combination of pressures that can occur in the chamber and cooling space. The stress report assumes a

Limitations (continued)

2. maximum net external pressure of 80 psi acting on the inner wall of the cone section while the CB&I General Plan indicates a design pressure between cones of 65 psi. It has been assumed that the 80 psi used in the analysis is a conservative analysis value and that the differential external pressure will not exceed 65 psi.

3. The number of design cycles for this chamber is not specified. It is indicated in the stress report that the number of cycles is in excess of 10^7. The fatigue curves of Section VIII, Division 2 give stress values for up to 10^6 cycles only, and strictly speaking the data does not cover the specified design conditions. However, the approach used in the Battelle stress report, in treating the stress amplitude at 10^6 cycles as given in Section VIII, Division 2 as an endurance limit, is in accordance with Code rules for fatigue exemption. Therefore, the Battelle procedures are in accordance with the intent of the fatigue requirements of Section VIII, Division 2.

4. In making this certification it has been assumed that there will be no amplification of the statically calculated stresses due to dynamic interaction between the loads, the chamber and the support structure. The portions of the Battelle stress report which treat the dynamic interaction have not been reviewed.

5. In making this certification it has been assumed that the cooldown and warmup of the chamber will be slow enough so that the resulting temperature gradients in the support skirt will not produce stresses which are significantly greater than the steady state stresses. It is also assumed that no significant temperature gradients exist in the chamber except for the support skirt.

6. It is assumed that experimental stress investigation as described in the Battelle stress report confirm the assumptions made in the report.

Exceptions:

1. The socket weld couplings attached to the outer cone of the chamber are not attached with Code acceptable weld details, and the stress report does not treat the as-built detail.

2. The primary local membrane stress intensity in the knuckle joining the chamber and beanie does not meet the requirements of Paragraph 4-111(i) of Section VIII, Division 2 when the stresses are calculated for the 1 inch thickness shown on Drawing 1, Revision 6. When the 1-1/16 inch order thickness is used, the primary local membrane stress intensity requirements are met.

Signed Jon Hagstrom

Jon Hagstrom, P.E.
Illinois No. 62-25201

CHICAGO BRIDGE & IRON COMPANY

CONTRACT NO. 71-2025

	Drawing No.	Revision No.
General Plan	1	6
Detail & Shell	2	6
Shell Plate Det.	2A	0
Reinforcing Cone	2B	1
In Outer Cone	2C	0
Expansion Cylinder Flange	3	8
Beam Window Flange	4	3
Dome and Knuckle Det.	5	2
Camera Mount	6	1
Drilling Templet For Camera Mount Noz.	6A	1
Camera Mounts 2 and 3	7	2
Camera Mounts 1 and 4	8	3
Camera Mounts 5 and 6	9	2
Condenser Port	10	2
Reinf. Calculation and Proposed Construction for 48" Forging	L0-2	0
Proposed Dimensions and Tolerances	L0-3	0
Orientation Lift Lugs	11	1
Details for Lifting Lugs	11A	1

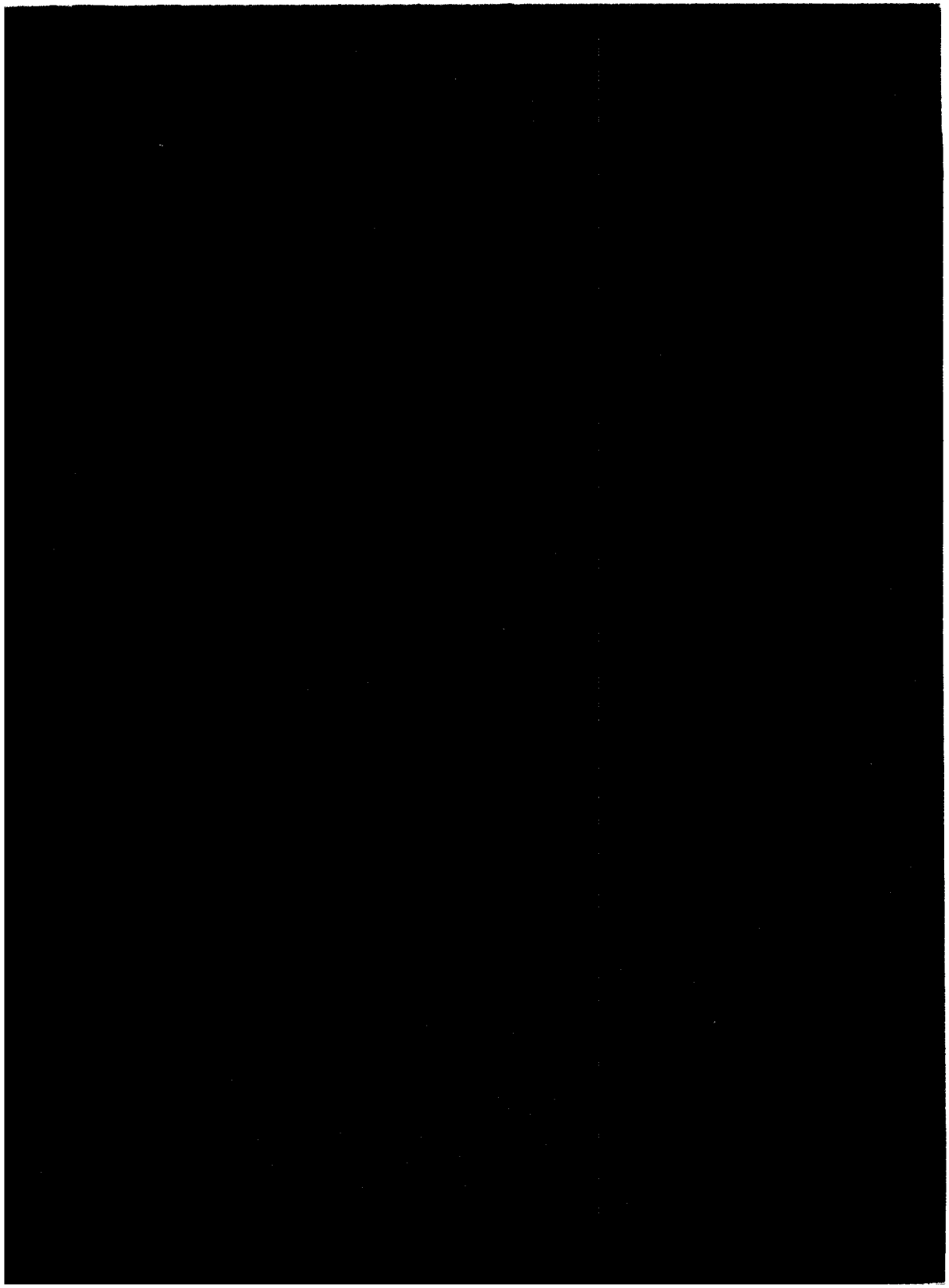

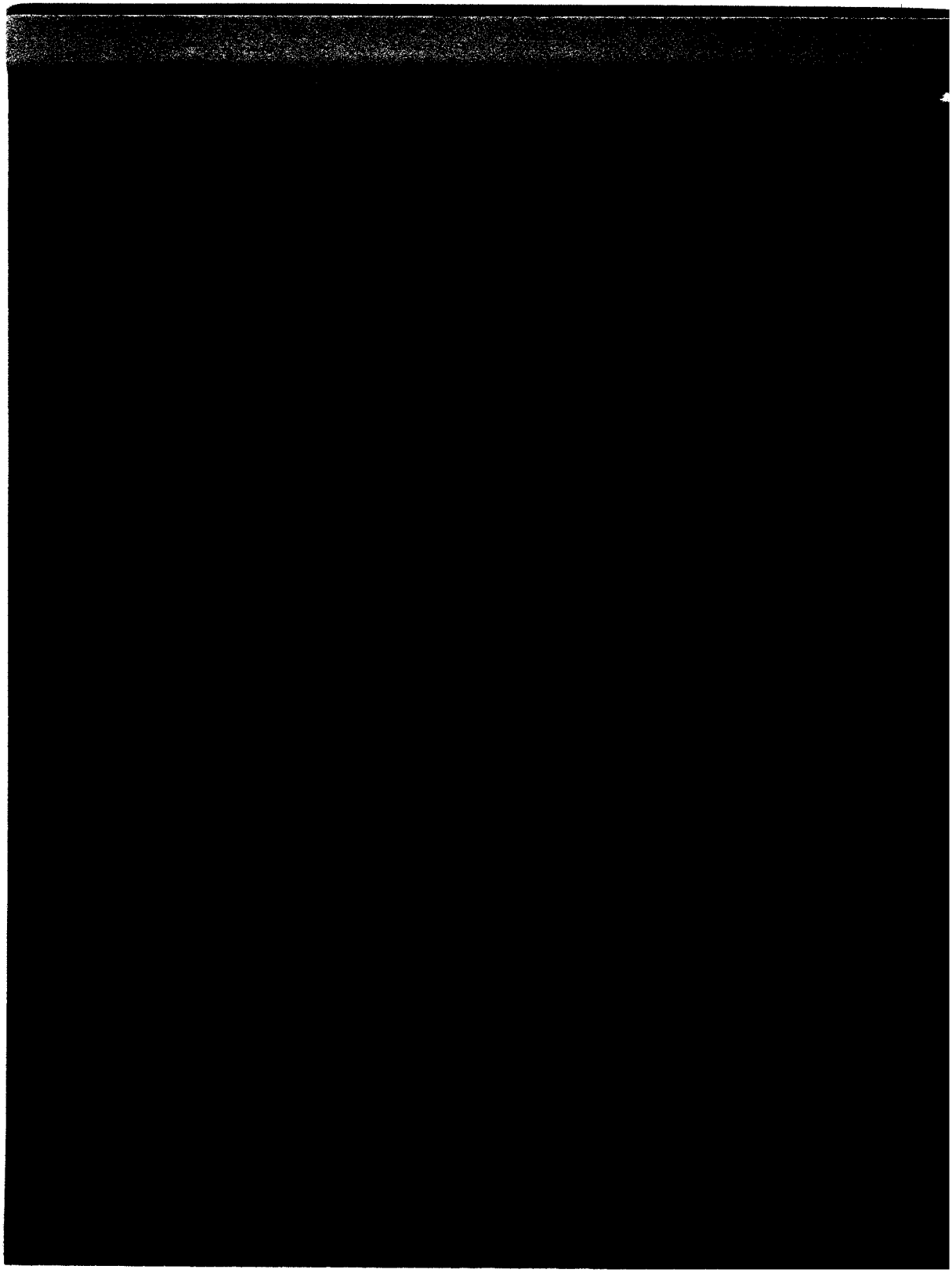

IV. EQUIPMENT

C. Chamber Vessel

3. National Accelerator Laboratory Specification for Stainless Steel Weldment for the NAL 30,000 Liter Hydrogen Bubble Chamber

Prepared by

W. B. Fowler

TABLE OF CONTENTS

IV. EQUIPMENT

C. Chamber Vessel

3. National Accelerator Laboratory Specification for Stainless Steel Weldment for the NAL 30,000 Liter Hydrogen Bubble Chamber

		Page
1.0	General	231
2.0	Stainless Steel Weldment	231
3.0	Scope	232
4.0	Materials	234
5.0	Welding	234
6.0	Non-Destructive Testing	236
7.0	Removal and Repair of Defects	237
8.0	Inspection, General	238
9.0	Leak Checking and Hydrostatic Test	240
10.0	Machining and Finishing	240
11.0	Shipping	241
	NAL BILL OF MATERIAL	243

IV. C. Chamber Vessel

3. SPECIFICATION FOR STAINLESS STEEL WELDMENT FOR THE NAL 30,000 LITER HYDROGEN BUBBLE CHAMBER

1.0 GENERAL

1.1 This specification covers fabrication and delivery of a stainless steel weldment for the National Accelerator Laboratory's 30,000 liter hydrogen bubble chamber as shown on assembly drawing 2621.ME-25172, Rev. G and the NAL Bill of Material, "Stainless Steel Weldment for NAL 30,000-liter Hydrogen Bubble Chamber". A final stress analysis check prior to fabrication is also the responsibility of the SELLER.

1.2 It is the SELLER's responsibility that the weldment is produced within tolerances as shown on the assembly drawing. Location of penetrations on the drawings are tentative. Final locations will be given the SELLER within 10 days after contract is signed.

2.0 STAINLESS STEEL WELDMENT

2.1 This weldment serves as the major portion of the liquid hydrogen container for the bubble chamber. Its purpose is to provide a tight vessel which contains the liquid hydrogen under normal operating pressures of up to 150 psi. It is to be fabricated from Type 316L stainless steel. All welds are to be full-penetration and 100% radiographed in accordance with Class A vessels, Section III of the ASME Boiler and Pressure Vessel Code.

2.2 A 108" diameter opening in the top of weldment will be closed by welding on at a later time a hemispherical head. This dome, which is furnished by NAL contains the optic mounting.

2.3 A particle beam entry window located with respect to the weldment as shown on the assembly drawing will be furnished and inserted by NAL at a later time. This window has an obround section with a thickness of 1/8-inch suitably reinforced and flanged. NAL will supply the vendor with a template for locating the bolt holes in the flange.

2.4 At the bottom of the weldment there is a heavy flange of ~71" ID. This opening will be closed by NAL at a later time by bolting on the expansion cylinder which is also furnished by NAL. NAL will supply the vendor with a template for locating the bolt holes in the flange.

2.5 The weldment is supported by a cone which flares out to a ring of 137-1/2" O.D. This design is to reduce the heat leak to the weldment.

2.6 The lower section of the weldment is double-walled to provide a cooling channel.

2.7 The weldment shall satisfactorily pass a helium mass spectrometer leak test when evacuated and sprayed externally with helium. The helium leak test procedure shall conform to Section 9.0. A hydrostatic test in accordance with ASME Pressure Vessel Code will be performed.

3.0 SCOPE

3.1 The SELLER shall perform a check stress analysis prior to ordering material. The results of this analysis shall be presented to NAL in report form. The report shall consist of the stress calculations as well as any recommendations or comments on the design. The contractor's recommendations shall be presented in a separate section of the report which shall also include a summary of any design change or addition that, in the SELLER's opinion, may be required. If necessary, the

SELLER shall investigate alternate design configurations to determine a more economical method of fabrication. Proposed design changes thus submitted to NAL for approval, if accepted, will be incorporated on the drawings by NAL. This will form the basis for any appropriate adjustment in price and delivery.

3.2 Loading Conditions

3.2.1 Under normal operating conditions, the weldment operates at a maximum internal pressure of 150 psi. During pump and purge the weldment will be evacuated while the outside surface is exposed to atmospheric pressure. The double wall cone may contain a maximum internal pressure of 150 psi while the inside of the vessel is evacuated and/or the outside of the vessel is exposed to vacuum.

3.2.2 In addition to the pressure loads a dynamic load of 700,000 pounds is carried through the lower 71" diameter flange through the double wall cone into the support cone. Thermal stresses are the responsibility of NAL.

3.3 Stress Analysis

3.3.1 Examine adequacy of spherical shell thickness under loading conditions in Paragraph 3.2. Verify the adequacy of material thicknesses and analyze the two flanges and their proposed bolts. Determine adequacy of cone support design including interface with six legs. Determine value of permissible side load.

3.4 The SELLER shall furnish all labor, materials, supplies, tools, plant, machinery, and equipment, engage sub-contractors (subject to NAL approval), and shall perform all work necessary to fabricate and complete the weldment according to NAL Bill of Material, "Stainless Steel Weldment for NAL 30,000 Liter Hydrogen Bubble Chamber" and these specifications.

3.5 The SELLER shall design and provide all temporary and permanent fixtures which are required for handling the various components during fabrication, assembly and shipping. The design of all such fixtures, as well as all alterations to components to accommodate these fixtures, shall be submitted to NAL for approval.

3.6 The fabricator shall ship all components to the designated loading site at NAL in finished form.

3.7 No part of this specification may be changed or disregarded without written approval of NAL.

3.8 The SELLER shall complete the weldment covered by this specification and shall verify positional tolerances indicated on the assembly drawing.

4.0 MATERIALS

4.1 Where required, corrosion-resisting Chromium-nickel steel Type 316L shall conform to the following ASTM specifications of the issue in effect:

4.1.1 Plate: ASTM A240, Type 316L

4.1.2 Forging: ASTM A182, Grade 316L

4.2 Weld filler metal shall conform to ASTM A371, Type ER308L. Coated electrodes shall correspond to ASTM A298, Type E308L.

5.0 WELDING

5.1 Welding performance and procedure qualifications shall be in compliance with Paragraph A, "Requirements for Ferrous Materials", of Section IX of the ASME Boiler and Pressure Vessel Code.

5.2 Fabrication procedures shall comply with the following paragraphs of Section VIII of the above Code:

UW-26 "General"

UW-28 "Qualification of Welding Procedure"

UW-29 "Tests of Welders and Welding Operators"

UW-31 "Cutting, Fitting, and Alignment"

UW-32 "Cleaning Surfaces to be Welded"

UW-33 and 34 "--------- Alignment Tolerances"

UW-35 "Finished Longitudinal and Circumferential Joints"
Except that the reinforcement on the interior of the vessel shall be removed.

UW-36 "Fillet Welds"

UW-37 "Miscellaneous Welding Requirements"

The following paragraphs of Section III of the above Code shall also apply:

N516 "Tolerance for Shells"

N517 "Tolerance for Formed Heads"

N518 "Attachments"

5.3 The welding processes that may be used on all construction covered by these specifications are restricted to:

a. Shielded metal arc.

b. Submerged arc.

c. Inert-gas metal arc.

5.4 The type of joint required is indicated on the drawings. If the SELLER wishes to employ an alternate joint design, a drawing showing the proposed alternate design shall be submitted to NAL for approval prior to fabrication.

5.5 Appearance of Welds

5.5.1 Each weld shall be smooth and without undercutting. Any undercutting shall be removed or faired in by grinding. Each weld bead shall be uniform in width and shall be smooth and splatter-free.

5.6 Cleaning

5.6.1 Weld craters shall be ground out prior to proceeding with the weld. All wire brushing shall be done using

stainless steel wire brushes which have not been previously used on any material other than stainless steel.

5.7 Radiographic Examination

5.7.1 All welded joints shall be examined radiographically for their full length in the manner prescribed in Paragraph 6.2.

5.8 Liquid Penetrant Examination

5.8.1 Welded joints shall also be examined on the face or faces of the completed weld after grinding smooth.

6.0 NON-DESTRUCTIVE TESTING

6.1 This specification covers the performance and evaluation of non-destructive tests and gives acceptance standards for the amount of surface and internal discontinuities permitted in weld areas and on machined sealing surfaces. The following types of test methods are specified:

a. Radiography

b. Liquid penetrant

6.2 Procedures and Standards

6.2.1 Radiography: Radiographic examination shall be performed in accordance with Section III of the ASME Boiler and Pressure Vessel Code.

6.2.2 Liquid Penetrant: The liquid penetrant test shall be performed in accordance with Section III of the ASME Boiler and Pressure Vessel Code.

6.3 Acceptability Requirements

6.3.1 Radiographic Examination Acceptability: Porosity acceptance standards shall be in accordance with Appendix IV of Section III of the above Code.

6.3.2 Liquid Penetrant Examination Acceptability Requirement: Acceptance standards shall be in accordance with

Section N-627 of the above Code.

6.3.3 Sealing Surfaces: All machined sealing surfaces as designated on the drawing shall meet the requirements in 6.3.2 and, in addition, shall be free of all cracks, tears, and uninterrupted linear indications greater than 1/16-inch.

7.0 REMOVAL AND REPAIR OF DEFECTS

7.1 Unacceptable defects in the weldment as supplied by the vendor and revealed by the hydrostatic test, leak test, visual examination, the liquid penetrant tests, and those in excess of radiographic standards shall be removed and repaired as follows:

7.1.1 Areas to be repair welded shall be prepared by grinding. All defects shall be completely removed and removal confirmed by liquid penetrant and/or radiographic inspection. Areas to be repair welded shall be angled or flared out to provide proper welding acceptability. The bottom of any groove shall have a minimum 1/8-inch radius. All grinding shall be done by using rubber or resin-bonded aluminum oxide and/or silicon carbide wheels, and/or carbide burrs. Areas to be welded shall be cleaned of all dirt, grease, or other foreign matter by scrubbing with new or redistilled acetone or alcohol followed by rinsing with clean water and drying with lint-free cloths.

7.1.2 Any defects requiring removal of metal completely through the wall section shall have a 3/16-inch-thick backing plate tack-welded in place. This plate shall be formed to the contour of the wall at the location of the hole and shall be Type 316L stainless steel. The

plate shall be of such size to extend at least 1/8-inch beyond the hole in all directions. In addition to the inspection required in Paragraph 5.7 and 5.8, after the plate has been removed by grinding or machining and the weld repair has been completed, the reverse side of the root layer shall be ground and liquid penetrant inspected.

8.0 INSPECTION, GENERAL

8.1 Materials and workmanship at all times shall be subject to the inspection of NAL representatives.

8.2 Inspections shall be made to insure that all materials used conform in all respects to that which is specified on drawings, bills of material, and elsewhere within these specifications.

8.3 All workmanship shall be equal to the best practice in modern shops or in field fabrication.

8.4 All components which are purchased by the SELLER will be inspected by the SELLER, and if required, the SELLER shall test any purchased item to insure that the quality of merchandise complies with that specified.

8.5 All inspections will be made at the place of manufacture. The SELLER will cooperate with the NAL representative and will permit him free entry, at all times while work on the contract is being performed, to all parts of the SELLER's works which concern this contract.

8.6 The SELLER will afford the NAL representative, without charge, all reasonable facilities to satisfy him that all parts are being manufactured and will be supplied according to the drawings and specifications.

8.7 Where NAL personnel are required to inspect components, they will, as far as is practicable, conduct their inspections so

as not to interfere with the SELLER's operation. Any work in progress which is being, or appears to be, executed contrary to drawings and/or specifications will be required to be discontinued.

8.8 Items which have been rejected by the NAL representative will not be used in the construction of any part associated with this contract. However, defective parts that have been reworked may be used providing they comply in all respects to the drawings and specifications, or to the satisfaction of the NAL representative.

8.9 The SELLER shall be notified within 24 hours of the rejection of any part.

8.10 The SELLER will advise NAL the specific time and date all tests and inspections are to be conducted and will permit authorized NAL representatives to witness them. Such notification shall be given at least 48 hours in advance of all such tests and inspections.

8.11 All methods that the SELLER proposes to use in conducting all tests and inspections shall be detailed in writing and submitted to NAL for approval, prior to the conduction of such tests and inspections. Tests and inspections conducted in a manner not conforming to the authorized procedure, unless otherwise approved, will be re-run.

8.12 The SELLER will give NAL the opportunity of conducting any non-destructive testing it deems advisable and which is not covered by this specification during fabrication or erection of component assemblies. Such testing shall in no way deleteriously affect any component part, nor adversely interfere with the SELLER's operation. NAL will provide all equipment and will bear all expenses for such tests. These additional tests are for information and will not be used as a cause for rejection.

9.0 LEAK CHECKING AND HYDROSTATIC TEST

9.1 The components covered by this specification shall be hydrostatic tested by the SELLER and leak tested by NAL. The SELLER will have complete responsibility for furnishing cover-closures required for hydrostatic testing; however, should NAL elect to furnish the top 108-inch diameter hemispherical head and beam window and cylindrical piston housing, the $10,450 price for hydrostatic testing incorporated in the total subcontract #40106 price will be subject to renegotiation at a later date during the time period called for in this stated subcontract #40106. The assembly will be considered satisfactory (vacuum tight) only if a repeatable helium response is not obtained on the maximum sensitivity scale of a high sensitivity helium leak detector, such as Veeco MS-9 or Consolidated 24-110. The sensitivity of the helium mass spectrometer is to be recalibrated before and after each test run or after four (4) hours of running time. The minimum allowable sensitivity is to be 2.2×10^{-7} micro liters per second for helium.

9.2 All gaskets and sealing materials will be supplied by NAL.

9.3 The leak check equipment shall be provided by NAL and operated by NAL. The SELLER may observe the tests.

9.4 Any defect or leak indicated by the above tests shall be repaired by the SELLER. NAL shall approve, in writing all such repairs. Gasket leaks, or leaks in welds or components not supplied by the vendor, unless due to non-compliance with these specifications by the SELLER, shall be excepted.

10.0 MACHINING AND FINISHING

10.1 Finish machining and grinding operations shall be performed only after all welding operations have been completed.

10.2 Finish surfaces shall be made on machine tools and shall conform to the best machine shop practices. The type of machine tool used shall be determined by the tolerance and finish required as stated on the drawings and specifications.

10.3 Machine finishes shall be determined by the American Standard Associations's method and symbols. A General Electric Surface Roughness Scale Catalogue No. 342X60 and Catalogue No. 342X61 or its equivalent shall be used for comparison.

10.4 Finishes on surfaces shall be protected during fabrication and shipping by whatever means are necessary to preserve that finish.

10.5 It is imperative that where sealing surfaces with a micro-inch finish are specified, this finish shall cover the full required area without nicks or scratches.

10.6 It is important that the final assembled complex contain linear dimension squareness and parallelism tolerances as per the assembly drawing. In certain cases dimensions out of tolerance may be compensated for.

10.7 The weldment shall be cleaned of dirt, metal, chips, grease, oil, paint, etc., by alkaline cleaners, emulsion or solvent cleaners, vapor degreasing or other suitable means.

10.8 Interior surfaces of the weldment shall be shot-blasted prior to use in fabrication. After fabrication and before final testing the interior surfaces of the weldment will be finished by wire brushing in order to obtain a surface free of entrapped dirt.

10.9 All machined surfaces shall be protected during wire brushing.

11.0 SHIPPING

11.1 The SELLER shall be responsible for shipping all components covered in this specification from their place of manufacture

to the point of unloading on the NAL site.

11.2 All machined surfaces, particularly those surfaces which are ultimately to accept gaskets, are to be thoroughly protected from weather and shipping damage.

11.3 All components are to be internally supported, where necessary, so as to prevent damage.

11.4 All components are to be secured so that they will in no way be damaged or distorted as a result of transportation.

11.5 The SELLER shall prepare the specification for safe transport of this equipment as recommended by the Loading Committee of the American Railroad Association or the American Trucking Association. Loading specifications shall be forwarded to NAL for approval prior to loading.

NAL BILL OF MATERIAL

Spec. No. 2621-ES-7019

STAINLESS STEEL WELDMENT FOR 30,000 LITER HYDROGEN BUBBLE CHAMBER

Description	Drawing No.	No.Req.	Rev.
Stainless Steel Weldment	2621.ME-25172	1	
All material, Type 316L Stainless Steel and all welds full penetration.			
Spherical Shell 12'6" ID x 1" min. thick wall 100" total height 61" above equator 39" below equator			
Support Ring 137 1/2" OD x 4" height - 1 1/2" thick		1	
Support Cone 136 1/2" max. OD x 129" min. OD 25" height - 1/2" min. thick wall		1	
Reinforcing Ring 131" OD x 8" height - 3" thick		1	
Cooling Cones			
Outer Cone -		1	
125" max. OD x 83" min. OD - 28" height - 1" min. wall thickness			
Inner Cone -		1	
125" max. OD x 80" min. OD - 29" height - 1" min. wall thickness			
Exp. Cyl. Flange - Machined from ring of 81" OD x 71" ID x 6 1/2" height		1	
Beam Window Flange - Machined from ring of 74" OD x 47 1/2" ID - 7" height		1	
Note: Beam Window and Exp. Cyl. Flanges require drilling and blind tapping for bolt pattern as called out on drawing.			
Bolts and cover plates are to be supplied by NAL.			
Prepared by: W.B.Fowler 11/18/70			

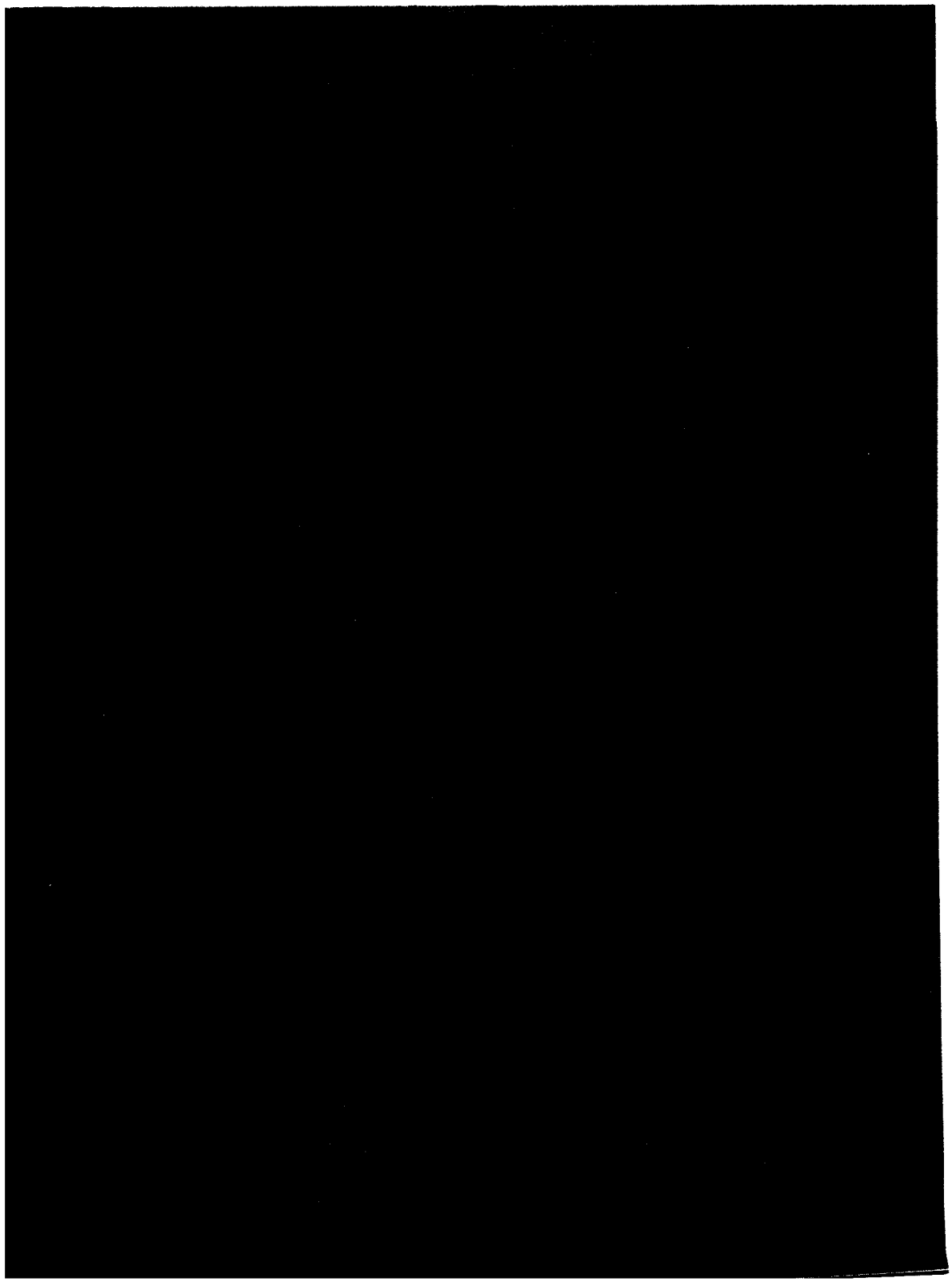

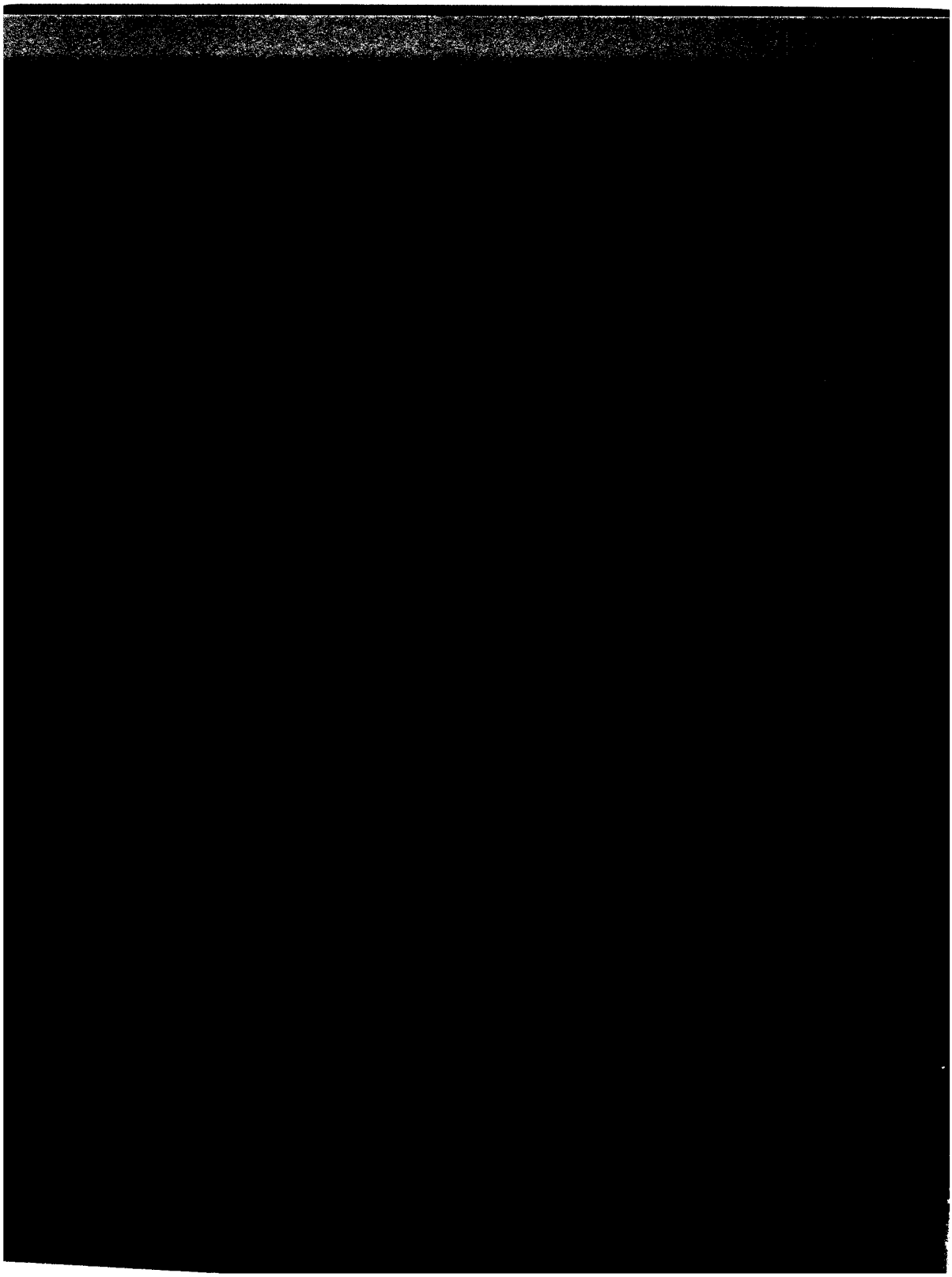

IV. EQUIPMENT

C. Chamber Vessel

4. Chicago Bridge & Iron Company Quality Assurance Program

TABLE OF CONTENTS

IV. EQUIPMENT

C. Chamber Vessel

4. Chicago Bridge & Iron Company Quality Assurance Program

		Page
(a)	Specification for Chromium Nickel Stainless Steel Plate	245
(b)	Inspection Instructions	248
(c)	Special Instructions and Notes	250
(d)	Fabrication Instructions	257
(e)	Welding Procedure Specifications	276

IV. C. 4. CHICAGO BRIDGE & IRON COMPANY

QUALITY ASSURANCE PROGRAM

(a) SPECIFICATION FOR CHROMIUM NICKEL STAINLESS STEEL PLATE

1.0 SCOPE

1.1 This specification covers 18% chromium-10% nickel-2% molybdenum stainless steel plates for use in pressure vessel built in accordance with Section VIII, Division 2 of the ASME Boiler and Pressure Vessel Code. Fabrication of the plates will include cold forming, machining and welding.

2.0 MATERIAL AND MANUFACTURE

2.1 The plate shall conform with all requirements of SA 240 Type 316L plus the additional provisions contained in the specification.

2.2 The plate shall be furnished hot rolled, annealed and pickled.

2.3 The ferrite content shall not exceed a 2% maximum. Ferrite content is to be reported by use of a Schaeffler Diagram.

3.0 TEST

3.1 One set of three Charpy V-notch impact test specimens from each plate as rolled (see paragraph 8.2) shall be tested at minus 423 degrees F.

3.1.1 Test procedure shall be in accordance with Paragraph AM204.1 of Section VIII, Division 2 of the ASME Boiler and Pressure Vessel Code.

3.1.2 Test specimens shall be in accordance with Paragraph AM204.2 of Section VIII, Division 2 of the ASME Boiler and Pressure Vessel Code.

3.1.3 Acceptance criteria for impact tests shall be in accordance with Paragraph AM211 of Section VIII, Division 2 of the ASME Boiler and Pressure Vessel Code (see paragraph 8.3).

4.0 HEAT TREATMENT OF TEST SPECIMENS

4.1 The material for tension, bend and impact test shall be annealed with, but not necessarily attached to, the plate.

5.0 ULTRASONIC INSPECTION

5.1 Plates 3-inches and over in thickness shall be ultrasonically inspected in accordance with the requirements of ASTM A435 with the exception that a 100% search shall be made.

5.2 Results of the ultrasonic inspection for each plate shall be reported on a grid chart.

6.0 REPAIR OF PLATE

6.1 Surface defects may be removed by grinding. All grinding shall be done by using rubber or resin bonded aluminum oxide and/or silicon carbide wheels, and/or carbide burrs.

6.2 The removal of defects beyond the minimum thickness of the plate must have the approval of CB&I.

6.3 Any defect requiring weld repair must be welded by CB&I, with the cost of such repairs charged to the plate manufacturer or supplier.

7.0 MILL TEST REPORT

7.1 The mill test reports shall include at least the following information:

7.1.1 The results of all mechanical and chemical analysis.

7.1.2 All heat treatments given to plates and test specimens including the actual time and temperatures.

7.1.3 A grid chart showing the results of ultrasonic inspection.

7.2 The mill test reports including ultrasonic grid chart shall be submitted on or before shipment of the plates. It is important that they be received and the plates identified before fabrication is started.

8.0 SPECIFICATION REFERENCES

8.1 Unless otherwise indicated, the latest revision of all ASTM and ASME Specifications at date of order are applicable.

8.2 The term "as rolled" as used herein is defined in ASTM Specification A300-68 (Note 3).

8.3 In paragraph 3.1.3 the reference to Paragraph AM211 of Section VIII, Division 2 of the ASME Boiler and Pressure Vessel Code shall be used as follows:

8.3.1 Paragraph AM211.1 and AM211.2 are not applicable.

8.3.2 Paragraph AM211.3 - Criterion for lateral expansion in this paragraph applies.

8.3.3 Paragraph AM211.4, AM211.5 and AM211.6 - Requirements are applicable.

(b) INSPECTION INSTRUCTIONS

1.0 INSPECTION, GENERAL

1.1 Materials and workmanship at all times shall be subject to the inspection of NAL representatives.

1.2 Inspections shall be made to insure that all materials used conform in all respects to that which is specified on drawings, bills of materials, and elsewhere within these specifications.

1.3 All workmanship shall be equal to the best practice in modern shops or in field fabrication.

1.4 All components which are purchased by the SELLER will be inspected by the SELLER, and if required, the SELLER shall test any purchased item to insure that the quality of merchandise complies with that specified.

1.5 All inspections will be made at the place of manufacture. The SELLER will cooperate with the NAL representative and will permit him free entry, at all times while work on the contract is being performed, to all parts of the SELLER's works which concern this contract.

1.6 The SELLER will afford the NAL representative, without charge, all reasonable facilities to satisfy him that all parts are being manufactured and will be supplied according to the drawings and specifications.

1.7 Where NAL personnel are required to inspect components, they will, as far as is practicable, conduct their inspections so as not to interfere with the SELLER's operation. Any work in progress which is being, or appears to be, executed contrary to drawings and/or specifications will be required to be discontinued.

1.8 Items which have been rejected by the NAL representative will not be used in the construction of any part associated with

this contract. However, defective parts that have been re-worked may be used providing they comply in all respects to the drawings and specifications, or to the satisfaction of the NAL representative.

1.9 The SELLER shall be notified within 24 hours of the rejection of any part.

1.10 The SELLER will advise NAL the specific time and date all tests and inspection are to be conducted and will permit authorized NAL representatives to witness them. Such notification shall be given at least 48 hours in advance of all such tests and inspections.

1.11 All methods that the SELLER proposes to use in conducting all tests and inspections shall be detailed in writing and submitted to NAL for approval, prior to the conduction of such tests and inspections. Tests and inspections conducted in a manner not conforming to the authorized procedure, unless otherwise approved, will be re-run.

1.12 The SELLER will give NAL the opportunity of conducting any non-destructive testing it deems advisable and which is not covered by this specification during fabrication or erection of component assemblies. Such testing shall in no way deleteriously affect any component part, nor adversely interfere with the SELLER's operation. NAL will provide all equipment and will bear all expenses for such tests. These additional tests are for information and will not be used as a cause for rejection.

(c) SPECIAL INSTRUCTIONS AND NOTES

	Reference* Para. No.
1.0 MATERIAL OWNERSHIP	
1.1 Scrap material is the property of the customer but CB&I may sell all scrap and credit the proceeds to customer as a reduction in contract cost.	
1.2 Any special tooling, nondurable tools, jigs, dies, fixtures, molds, patterns, taps, gauges, test equipment and other similar manufacturing aids not considered special tooling, charged to this contract shall become the property of the customer.	
2.0 CODE REQUIREMENT	
2.1 Vessel is to be fabricated in accordance with ASME Code Section VIII, Division 2 and addenda through Summer 1970. Vessel cannot be stamped. (Limited to fabrication methods; i.e. welding, forming, NDT, and Q.A. program.)	
3.0 FABRICATION	
3.1 Welding: Welding performance and procedure qualifications shall be in accordance with Paragraph A, "Requirements for Ferrous Materials", of Section IX of the ASME Code.	5.1
3.2 The welding processes that may be used on all construction are restricted to:	5.3 Except Heliarc
- shielded metal arc - inert gas metal arc	
- submerged arc - heliarc (inert-gas tungsten arc)	

*Reference: (1) Specification for Stainless Steel Weldment for the NAL 30,000 Liter Hydrogen Bubble Chamber

	Para. No.
3.3 Weld filler metal shall conform to ASTM 371, Type ER308L. Coated electrodes shall correspond to ASTM A298, Type E308L.	4.2
3.4 Each weld shall be smooth and without undercutting. Any undercutting shall be removed or faired in by grinding. Each weld bead shall be smooth and splatter free.	5.5
3.5 Unacceptable defects in the weldment as supplied by CB&I and revealed by the hydrostatic test, helium leak test, visual examination, the liquid penetrant tests, and those in excess of radiographic or ultrasonic examination standards shall be removed and repaired as follows:	7.0
3.5.1 Areas to be repair welded shall be prepared by grinding. All defects shall be completely removed and removal confirmed by liquid penetrant and/or radiographic inspection. Areas to be repair welded shall be angled or flared out to provide proper welding acceptability. The bottom of any groove shall have a minimum 1/8-inch radius.	
3.5.2 Any defects requiring removal of metal completely through the wall section shall have 3/16-inch thick backing plate tack-welded in place. This plate shall be formed to the contour of the wall at the location of the hole and shall be type 316L stainless steel. The plate	

	Para. No.
shall be of such size to extend at least 1/8-inch beyond the hole in all directions. Plate shall be ground off weld 100% radiographed and dye penetrant examined on both sides.	
4.0 MACHINING AND FINISHING	
4.1 Finish machining and grinding operations shall be performed only after attachment welds have been made.	10.1
4.2 Finish surfaces shall be made with machine tools and shall conform to the best machine shop practices. The type of machine tool used shall be determined by the tolerance and finish required.	10.2
4.3 Machine finishes shall be determined by the American Standard Association's method and symbols. A General Electric surface roughness scale (catalogue #342X60 and 342X61) or its equivalent shall be used for comparison.	10.3
4.4 Finishes on surfaces shall be protected during fabrication and shipping by whatever means are necessary to preserve that finish.	10.4
4.5 It is imperative that where sealing surfaces with a micro-inch finish are specified, this finish shall cover the full required area without nicks or scratches.	10.5
4.6 It is important that the final assembled complex contain linear dimension squareness and parallelism tolerances as per the contract drawings.	10.6

		Para. No.
4.7	The weldment shall be cleaned of dirt, metal, chips, grease, oil, paint, etc., by alkaline cleaners, emulsion or solvent cleaners, vapor degreasing or other suitable means.	10.7
4.8	After fabrication and before final testing, the interior surfaces of the weldment will be finished by wire brushing in order to obtain a surface free of entrapped dirt. All wire brushing shall be done using stainless steel wire brushes which have not been previously used on any material other than stainless steel.	10.8 & 5.6.1
4.9	All machined surfaces shall be protected during wire brushing.	10.9
5.0	NON-DESTRUCTIVE TESTING	
5.1	Radiography: Radiographic examination shall be performed in accordance with Section VIII, Division 2 of the ASME Code. CB&I standard procedure for radiographic examination.	
5.2	Liquid Penetrant: The liquid penetrant test shall be performed in accordance with Section VIII, Division 2 of the ASME Code. CB&I standard procedure for liquid penetrant examination	
6.0	INSPECTION	
6.1	See Inspection Instruction (b)	8.0
7.0	LEAK CHECK AND HYDROSTATIC TEST	
7.1	Weldment shall be hydrostatic tested by CB&I in accordance with test instructions.	9.0

		Para. No.
	CB&I shall have the responsibility of furnishing all gaskets and sealing material and blind flanges required for hydro test. NAL shall furnish any sealing material for leak tests.	
7.2	Weldment shall be helium leak tested by NAL after hydrostatic testing. The assembly will be considered satisfactory (vacuum tight) only if a repeatable helium response is not obtained on the maximum sensitivity scale of a high sensitivity helium leak, such as Veeco MS-9 or Consolidated 24-110. The sensitivity of the helium mass spectrometer is to be recalibrated before and after each test run or after four (4) hours of running time. The minimum allowable sensitivity is to be 2.7×10^{-7} micro-liters per second for helium. NAL is to furnish equipment and manpower required for test.	9.0
7.3	Any defect or leak indicated by the hydrostatic or helium leak test shall be repaired by CB&I. NAL shall approve, in writing, all such repairs. Gasket leaks are excepted.	9.0
8.0	SHIPPING	
8.1	All machined surfaces, particularly those for gaskets, are to be thoroughly protected from weather and shipping damage.	11.2
8.2	All components are to be internally supported, where necessary, so as to prevent damage.	11.3

	Para. No.
8.3 All components are to be secured so that they will in no way be damaged or distorted as a result of transportation.	11.4

9.0 GENERAL

9.1 See (d) Fabrication Instructions.

9.2 The following information shall be available to the NAL inspector:

9.2.1 Mill test certification.

9.2.2 Evidence of examination of all materials before fabrication to make certain it has the required thickness, for detection of unacceptable defects, and that identification traceable to the mill test report or material certification has been maintained.

9.2.3 Documentation of impact test.

9.2.4 Examination of the vessel components to confirm that they are properly formed or machined to specified shapes within permissible tolerances.

9.2.5 Qualification of welding.

9.2.6 Qualification of all welders.

9.2.7 Examination of all parts prior to joining to make certain they have been properly fitted for welding and that surfaces to be joined have been cleaned and alignment tolerances maintained.

9.2.8 Examination of parts as fabrication progresses for material identification,

that surface defects are not evident, and that dimensional geometrics are maintained.

9.2.9 Records of NDT examinations performed.

9.2.10 Hydrostatic test chart.

9.2.11 Schaeffler diagram for production welds.

(d) FABRICATION INSTRUCTIONS

LEGEND: R.T. = Radiographic Inspection
P.T. = Dye Penetrant Inspection

12'-6 ID Spherical Section - Drawing 2 and 2A, Plate 2-1/3^{R}L:

1. Dish plates.
2. Layout.
3. Cut and bevel edges.
4. Weld 2-1/3^{R}L together with E308L. P.T. Root weld and backchip surfaces.
5. Grind inside surface of welds smooth and flush so as to remove any defects.*
   Grind outside surface of welds smooth.
6. R.T. Welds.
7. P.T. Welds on both surfaces.

3" Reinforcing Cone - Drawing 2 and 2B, Plate 2-4:

1. Layout and cut plate in flat as shown on drawing 2B.
2. Form.
3. Cut and bevel ends per seam "A" P.T. plate edges.
4. Weld 2-4 together with E308L. P.T. root weld and backchip surface.
5. Grind inside surface of welds smooth and flush so as to remove any defects.*
   Grind outside surface of welds smooth.
6. R.T. Welds.
7. P.T. Welds on both surfaces.
8. Machine finished cone on lower end.
9. P.T. finished surfaces and plate edges.

*See Testing Instructions

TESTING INSTRUCTIONS

1. Production test plates are required in accordance with Section VIII, Division 2 of ASME Code Article T-2. Material for the test plates is billed on bill sheet 6.

On 1" Plate:

One set on horizontal position - Manual welding

One set on vertical position - Manual welding

One set on horizontal position - Combine manual and TIG welding

On 3" Plate:

One set on vertical position - Manual welding

2. Ferrite range in the production welds shall be reported on a Schaeffler diagram. Ferrite range is to be determined by use of chemistries. Ferrite MUST be in 4 to 10 percent range.

1" Inner Cone - Drawing 2, Plate 2-5:

1. Layout, cut, and bevel plate edges as shown on Drawing 2.
2. Form.
3. Weld 2-5 together with E308L. P.T. root weld and backchip surface.
4. Grind inside surface of welds smooth and flush so as to remove any defects.
   Grind outside surface of welds smooth.
5. R.T. welds.
6. P.T. welds on both surfaces.

1" Outer Cone - Drawing 2, Plate 2-6:

1. Layout, cut, and bevel plate edges as shown on Drawing 2.
2. Form.
3. Weld 2-6 together with E308L. P.T. root weld and backchip surface.
   Grind inside surface of welds smooth and flush so as to remove any defects.
4. Grind outside surface of welds smooth.
5. R. T. welds.
6. P.T. welds on both surfaces.

Expansion Cylinder Flange - Drawing 3, Plate 3-1:

1. Set-up and rough machine flange as shown on Drawing 3.
2. P.T. machined surfaces.

Beam Window Flange - Drawing 4, Plate 4-1, 4-2, 4-3:

1. Set-up and rough machine flange as shown on Drawing 4. (Except tapped holes.)
2. P.T. machined surfaces.
3. Set-up drill and tap bolt holes in flange. CB&I is to make templates 4-2 and 4-3 by match drilling with flange.

Sphere Assembly 1-A - Drawings 1, 2, 2A, 2B, 2C, 3 and 4:

1. a. Fit 1" inner cone to 3" reinforcing cone.
   b. Fit expansion cylinder flange to 1" inner cone.
   c. Weld together with E308L. P.T. root weld and backchip surface.
   d. Grind inside surface of welds smooth and flush so as to remove any defects. Grind outside surface of welds smooth.
   e. R.T. welds.
   f. P.T. welds on both inside and outside surface of welds.

2. a. Slip 1" outer cone over expansion cylinder flange. Remove cone, layout, weld, and P.T. couplings on Drawing 2C. LOX clean cooling space.
   b. Weld outer cone to 3" reinforcing cone and expansion cylinder flange. Heliarc root pass with ER308L. P.T. root pass. Weld remainder of seam with E308L. P.T. weld at every 1/4" of depth. NOTE: Purge back side of weld with argon; close opening after root weld is complete.
   c. Grind welds smooth.
   d. P.T. finished surface of welds.

3. a. Machine upper end of 3" cone.
   b. P.T. finished surfaces and plate edges.

4. a. Fit 12'-6"ID spherical section to 3" reinforcing cone.
   b. Weld together with E308L. P.T. root weld and backchip surface.
   c. Grind inside surface of weld smooth and flush so as to remove any defects. Grind outside surface of weld smooth.
   d. R.T. weld.
   e. P.T. weld on both surfaces.

5. a. Fit beam window flange to 12'-6"ID spherical section.
   b. Weld together with E308L. P.T. root weld and backchip surface.

c. Grind inside surface of welds smooth and flush so as to remove any defects. Grind outside surface of welds smooth.

d. R.T. welds.

e. P.T. welds on both surfaces.

1/2" Skirt - Drawing 2, Plate 2-7:

1. Layout, cut, and bevel plate edges as shown on drawing 2.
2. Form.
3. Weld 2-7 together with E308L.
   P.T. root weld and backchip surfaces.
4. Grind welds smooth on both surfaces.
5. R.T. welds.
6. P.T. welds on both surfaces.

1-1/2" Base - Drawing 2, Plate 2-8:

1. Layout, cut, and bevel plate edges as shown in drawing 2.
   Plane bottom edge. P.T. plate edges.
2. Roll.
3. Weld 2-8 together with E308L.
   P.T. root weld and backchip surfaces.
4. Grind welds smooth on both surfaces.
5. R.T. welds.
6. P.T. welds on both surfaces.

Skirt Assembly 2-A - Drawing 2:

1. Fit skirt to base.
2. Weld together with E308L. P.T. root weld and backchip surfaces.
3. Grind weld smooth on both surfaces.
4. R.T. weld.
5. P.T. weld on both surfaces.

1" Knuckle Drawing 5, Plate 5-2:

1. Form knuckle.
2. Layout and cut.
3. Bevel top edge and ends.
4. Weld 5-2 together with E308L. P.T. root weld and backchip surface.
5. Grind inside surface of welds smooth and flush so as to remove any defects. Grind outside surface of welds smooth.
6. R.T. welds.
7. P.T. welds on both surfaces.

Camera Nozzles - Drawing 6 (nozzles furnished by NAL):

1. Layout, drill and tap bolt holes.

Beanie Fabrication - Drawing 5-10 (head furnished by NAL):

1. Knuckle to head.
   a. Make cutback on hemispherical head.
   b. Fit knuckle assembly to head. Weld together with E308L. P.T. root weld and backchip surface.
   c. Grind inside surface of welds smooth and flush so as to remove any defects. Grind outside surface of welds smooth.
   d. R.T. weld.
   e. P.T. weld on both surfaces.
2. Weld on lift lugs, grind welds smooth, P.T.
3. Nozzles to head.
   a. Layout cutouts for nozzles. Layout must be accurate to $\pm$1/8" of arc length from W.P. to centerline of cutout. NOTE: When all cutouts are laid out NAL inspector must approve before cutting.
   b. After NAL inspects and okays layout, make all nozzle cutouts.
   c. Fit up and aim nozzles as shown on detail Drawings 7 through

10. Nozzles must be within 1° of aim shown.

NOTE: When all nozzles are fit up NAL inspector must approve layout before any welding is done. After the NAL inspector has approved layout NAL has agreed to accept the position of the nozzles with no further inspection rights. CB&I will report final aim for NAL's use.

d. After NAL inspector has accepted fit up of all nozzles weld nozzles to head with E308L. P.T. root weld and backchip surface. Weld nozzle ⟨7⟩ into head first.

e. Grind inside surface of weld smooth and flush so as to remove any defects. Grind outside surface of weld smooth.

f. P.T. weld on both surfaces.

g. R.T. Nozzles 1 through 7.

4. Set up and final machine all beanie nozzles.

5. Dye check all machined surfaces.

Expansion Cylinder Flange - Drawing 3, Plate 3-1:

1. Set-up and final machine flange as shown on drawing 3.

NOTE: Holes in flange shall be located and drilled using template furnished by NAL.

2. P.T. all final machined surfaces.

Beam Window Flange - Drawing 4, Plate 4-1:

1. Set-up and final machine flange as shown on drawing 4.

2. P.T. all final machined surfaces.

Main Sphere to Beanie and Skirt - Drawing 2 and 5:

1. a. Set-up and cut edge prep on 1-A for beanie attachment.

b. Set-up and cut edge prep on 5-A.

c. Weld 1-A to 5-A with E308L. P.T. root weld and backchip surface.

d. Grind inside surface of weld smooth and flush so as to remove any defects. Grind outside surface of welds smooth.

e. R.T. weld.

f. P.T. weld on both surfaces.

2. a. Trial fit and trim skirt to fit 3" reinforced cone.

b. Weld 2-A to 1-A with E308L. P.T. root weld and backchip surface.

c. Grind both surfaces of weld smooth.

d. P.T. weld.

e. R.T.

GENERAL

1. Wire brush inside of completed vessel.
2. Complete tabulation of as-built dimensions.
3. Hydro test vessel.
4. Helium leak check shall be performed by NAL and witnessed by CB&I.
5. Final acceptance.

RADIOGRAPHIC EXAMINATION PROCEDURE

1.0 SCOPE

1.1 This Radiographic Examination Procedure is to be used for the examination of welded joints or as otherwise required on heavy wall pressure vessels.

2.0 REFERENCE

2.1 This procedure meets the requirements of Chicago Bridge & Iron Company and applicable 1968 Pressure Vessel Code.

3.0 TYPE OF RADIATION SOURCE

3.1 Isotopes of the following types may, at fabricator's option, be used for the thicknesses of material indicated:

Cobalt 60	Thickness Range 1.5" - 11"
Iridium 192	Thickness Range 1/4" - 3"

In addition to isotopes, X-ray machines may, at fabricator's option, be used for the thicknesses of material indicated:

150-300 KVP X-Ray Machines	Thickness Range 1/4" - 1-3/4"
2 MEV Van de Graf	Thickness Range 1" - 7"
25 MEV Betatron	Thickness Range 1" - 14"

4.0 SIZE OF RADIATION SOURCES

4.1 Isotopes

200 Curies Cobalt 60	Focal Spot Size .25"Ø x .25" long
100 Curies Cobalt 60	Focal Spot Size .25"Ø x .25" long
100 Curies Iridium 192	Focal Spot Size .16"Ø x .15" long

4.2 X-ray Equipment

150-300 KVP Machines	Focal Spot Size 2.0-5.0 MM
2 MEV Van de Graf	Focal Spot Size 0.75 MM
25 MEV Betatron	Focal Spot Size 0.2 MM

5.0 TYPE OF FILM

5.1 Film types manufactured by the following companies may be used for radiography:

Eastman Kodak	AA	T	M	R
Ansco	A		B	HD
DuPont	506		510	
Gevaert	D7		D4	D2

5.2 Choice of film will be determined by CB&I considering radiation source and thickness of material to be radiographed.

5.3 Film techniques with two or more film of equal or different speeds may be used to meet the job conditions in order to provide radiographs which will meet the quality level as required.

6.0 TYPE OF SCREEN

6.1 Lead screens will be used in each holder.

7.0 BLOCKING AND MASKING TECHNIQUE

7.1 Lead filters will be used, if necessary, to improve the quality of the radiograph.

7.2 Whenever necessary to eliminate back radiation, 1/8" lead sheet will be placed behind the film holder.

8.0 TYPE OF MATERIAL RADIOGRAPHED

8.1 All types of material.

9.0 EXPOSURE

9.1 Approximate exposure times will be determined from the developed technique charts for the thickness of material involved and source size used. Adjustments in the exposure will be made to obtain the proper density and quality level.

10.0 RANGE OF FILM DENSITIES

10.1 Film densities at the penetrameter shall be as required by applicable code.

11.0 OVERLAP OF FILM

11.1 The length of film exposed in an individual film holder on straight joints will be 17" with a minimum overlap of 1" at each end of the film when multiple exposures are made.

11.2 Whenever circular joints are radiographed, the length of film used will be determined by the job conditions; however, an equivalent of a 1" overlap of film will be provided.

12.0 TYPE OF PENETRAMETERS

12.1 Penetrameter with 2T, 3T and 4T holes, or according to applicable code.

13.0 NUMBER AND LOCATION OF PENETRAMETERS

13.1 On single film exposures one penetrameter will be placed so that the penetrameter is normal to the radiation beam.

13.2 On multiple film exposures circumferential and longitudinal joints, penetrameters will be placed as required by applicable code.

13.3 The penetrameters will be placed on the source side adjacent to the welded joint. If the filler metal is not radiographically similar to the base metal, the penetrameter shall be placed over the filler metal or as otherwise permitted by applicable code.

14.0 USE OF SHIMS UNDER PENETRAMETERS

14.1 If the weld reinforcement and/or backing strip is not completely removed, a shim of radiographically similar material

to the filler metal shall be placed under the penetrameter. The shim thickness shall be selected so that the total thickness being radiographed under the penetrameter is the same as the total weld thickness. The penetrameter thickness shall be based on the total metal thickness under the penetrameter including the shim.

15.0 IMAGE QUALITY LEVEL

15.1 The images of the identifying numbers of the penetrameters outline, and the 2T hole are all essential indexes of image quality on the radiograph, and they shall appear clearly on the radiograph except that for penetrameters 5, 7 and 10 the slit shall appear clearly and the hole need not appear.

16.0 FILM PROCESSING

16.1 Automatic machine processing will normally be used. The temperature of the solutions, the degree of agitation and the type of solutions will be according to the recommendations of the manufacturer.

16.2 Manual developing may be used as an alternate method.

16.3 Developing time of exposed film will be based on recommended time and temperature charts, using a standard of 5 minutes at 68°F.

16.4 Short Stop Time-minimum of 1.2 minute.

16.5 Fixing Time-minimum of 2 times the clearing time.

16.6 Washing Time-minimum of 30 minutes in running water

16.7 Renewal of Chemicals-Whenever the chemicals have been used to the extent of the recommended life of the chemical manufacturer, the chemicals shall be replaced and new chemicals provided. (Normally about 600-4-1/2" x 17" film can be processed per 5 gallons of solution.)

16.8 During the processing of film, the film hangers shall be agitated periodically in order to obtain uniform development over the entire film.

17.0 VIEWING CONDITIONS

17.1 Viewing apparatus using photo flood bulbs or a high intensity bulb with a variable diaphragm, and a rheostat for varying the light intensity will be provided which will be capable of reading radiographs with up to 3.6 density.

17.2 Means of providing reduced lighting for viewing radiographs will be provided, when necessary, to properly interpret the radiographs.

18.0 IDENTIFICATION OF FILMS

18.1 Each film will be permanently marked with the following information:

a. Contract number

b. Seam number

c. Film interval number

d. Whether film is an initial, or repair shot

18.2 The structure will be marked to provide a method of correlating the film with the structure. Lead markers will be placed adjacent to these marks to record the area on the radiographs.

18.3 An expanded layout will be provided to show the location and identification of all radiographed joints on the vessel which can be used as a progress chart.

19.0 ACCEPTANCE CRITERIA

19.1 Acceptability Standards-Sections of weld that are shown by radiography to have any of the following types of defects are

unacceptable unless the defects are removed and the weld is repaired as provided in ASME Boiler & Pressure Vessel Code, Section VIII, Div. 2.

19.1.1 Any type of crack or zone of incomplete fusion or penetration.

19.1.2 Any elongated inclusion such as slag, which has a length greater than:

1/4 in. for t up to 3/4 in.
1/3 t for t from 3/4 in. to 2-1/4 in.
3/4 in. for t over 2-1/4 in.

Where t is the thickness of the thinner part being welded.

19.1.3 Any group of inclusions in line that have an aggregate length greater than t in a length of 12t, except when the distance between the successive imperfections exceeds 6L, where L is the length of the longest imperfection in the group.

19.1.4 Porosity in excess of that shown as acceptable by the porosity standards given in ASME Boiler & Pressure Vessel Code, Section VIII, Div. 2, Appendix 8.

20.0 REPAIRS

20.1 Welds showing unacceptable defects shall be repaired in accordance with ASME Boiler & Pressure Vessel Code, Section VIII, Div. 2.

20.2 All portions of weld which have been repaired shall be radiographed using the techniques prescribed herein and the customary amount of film overlap. The welds shall also be examined by all other means that were specified for the original weld and all examination shall meet the acceptability standards originally required.

21.0 DOCUMENTATION REQUIRED

21.1 A signed written report shall be made of all radiographic examination.

21.2 Reports shall show the type and length of any defect found in a particular film, or section of the vessel.

LIQUID PENETRANT EXAMINATION PROCEDURE

1.0 SCOPE

1.1 This Liquid Penetrant procedure shall be used when liquid penetrant examination is required on all work other than Nuclear Class "A" vessels.

2.0 REFERENCE

2.1 This procedure fulfills the requirements of Chicago Bridge & Iron Company Standards and applicable 1968 Pressure Vessel Codes.

3.0 APPARATUS

3.1 Water washable or solvent removable visible liquid penetrant.

3.2 Liquid developer.

4.0 PROCEDURE

4.1 A liquid penetrant is applied to the surface to be examined and allowed to enter any discontinuities open to the surface, after which, excess liquid is removed. A developer is then applied which is wetted or otherwise affected by the penetrant entrapped in the discontinuities. This increases the evidence of the discontinuities so that they may be seen directly.

4.2 Cleaning: It is essential that the part or surface to be examined be clean. Since the success of the method depends upon entry of the penetrant into any defects present, the requirement for cleanliness is paramount. Cleanliness in this application shall be interpreted to include the removal of all rust, scale, welding flux, spatter, grease, oily films, water, dirt, etc., not only from the surface but, more

particularly, from any defects present.

Typical cleaning facilities applicable for this purpose are detergents, organic solvents, descaling solutions or paint removers, and vapor degreasing, or ultrasonic cleaning methods.

4.3 Drying: It is essential that the part or surface to be examined be sufficiently dried prior to application of penetrant so that no trace of water or cleaning agent remains in any defects that are present.

4.4 Penetrant Application: The penetrant is applied by dipping, brushing, or spraying. Penetration time is critical. In general, the finer and tighter the discontinuity, the longer the penetration time should be. The penetration time shall be at least ten minutes but this minimum time may have to be extended under certain conditions such as when the temperature is below 60°F. At 40°F, for example, twice the time required above 60°F is suggested.

As a standard technique, the temperature of the surface or part to be examined, the liquid penetrant, the rinse, and the developer shall not be below 40°F, nor above 125°F throughout the examination period. Local heating or cooling is permitted provided temperatures remain in the range of 40°-125°F during examination. Where it is impractical to comply with the foregoing temperature limitations, other temperatures and times may be used providing that the procedure is qualified by use of a liquid penetrant comparator prepared and used as described in Paragraph UA-99.

4.5 Excess Penetrant Removal: After suitable penetration time has elapsed, any penetrant remaining on the surface shall be removed. Insufficient removal will leave a background which will interfere with subsequent indication of defects. Care

must be exercised that the penetrant in any defects is not removed.

4.5.1 With water-washable penetrants, it is recommended that the excess be removed with a water spray. Water pressures over 50 psi or water temperatures over 110°F should not be employed.

4.5.2 With solvent removable penetrants, excess penetrant will be removed from the surface by wiping with rags or cloths moistened with the solvent. Care shall be employed not to use an excess of the solvent in order to avoid removing penetrant from defects. On smooth surfaces it may be possible sometimes to remove excess penetrant merely by wiping the surface with clean dry rags or cloth.

4.6 Developing: The liquid developer is a suspension of powder in water or a volatile solvent. It is applied by dipping, spraying, or brushing. In any case, when the developer dries, a film of powder is left on the surface. Where a water suspension developer is used, drying time may be decreased by the use of warm air.

5.0 EXAMINATION

5.1 The true size and type of defect are difficult to appraise if the dye diffuses excessively in the developer. The examination shall be conducted starting at a minimum of seven minutes after applying the developer. In no case shall the examination be made later than thirty minutes after the developer has dried.

5.1.1 With Visible Penetrants, the developer forms a more or less even white coating. Surface defects are indicated by bleeding out of the penetrant, which is

normally of a deep red color. Adequate illumination shall be provided since otherwise sensitivity will be diminished.

6.0 EVALUATION OF INDICATIONS

6.1 Linear Indications are those indications in which the length is more than twice the width.

6.2 Rounded Indications are indications which are circular or elliptical with the length less than twice the width.

6.3 Any questionable or doubtful indications shall be retested to verify whether or not actual defects are present.

6.4 General broad areas of pigment penetration shall be interpreted as indicative of improper processing. Such areas shall be retested with a suitably modified procedure.

7.0 ACCEPTANCE STANDARDS

7.1 All surfaces required to be examined shall be free of linear defects (cracks, laps, fissures) and of four or more rounded defects in a line separated by 1/16-inch or less (edge to edge).

8.0 DOCUMENTATION

8.1 A signed written report shall be made covering those areas examined and the repairs to be made. In addition areas to be repaired shall be marked on the part of vessel examined.

(e) WELDING PROCEDURE SPECIFICATIONS

150" ROUND STAINLESS BUBBLE CHAMBER

PART I GENERAL

1.0 PROCESS

The welding shall be accomplished by the Shielded Metal Arc Process.

2.0 BASE METAL, FILLER METAL AND WELDING SPECIFICATION NUMBERS

The base metal and filler metal shall be in accordance with the Table.

BASE METAL	FILLER METAL	CB&I WELDING SPECIFICATION
SA240--Type 316L S.S.	E308-L	1419

3.0 POSITION

The welding shall be performed in the horizontal, vertical or flat position.

4.0 PREPARATION OF BASE METAL

The edges or surfaces of parts to be joined by welding shall be prepared by shearing, chipping, grinding, machining, plaining, arc gouging and grinding, flame powder burning or plasma burning.

5.0 WELDING TECHNIQUE

The welding technique such as electrode sizes, mean voltages, etc., shall be substantially as shown on the attached sketches and data sheets.

6.0 CLEANING AND DEFECTS

All slag or flux remaining on any bead of welding shall be removed before depositing the next successive bead of welding. Any

defects that appear on any bead of welding shall be removed by chipping, grinding or arc gouging before depositing the next successive bead of welding.

7.0 PEENING

In general, light peening shall be used as an aid to cleaning the weld beads.

8.0 TREATMENT OF BACKSIDE OF WELDING GROOVE

When required, in order to obtain complete fusion, the backside of the welding groove shall be prepared by chipping, grinding, or arc gouging to sound metal.

9.0 WELDING CURRENT

The welding current shall be direct current, reversed polarity.

10.0 INSPECTION OF WELDS

All root passes, back gouged areas and finished welds will be dye penetrant examined.

Radiography will be performed where required and practical.

See Engineering drawings for additional special instructions.

RECORD OF WELDING PROCEDURE QUALIFICATION SPECIFICATION
TO A.S.M.E. SECTION IX LATEST EDITION

PART II ESSENTIAL VARIABLES

Specification No. 1419

Date: 4/19/71

Welding Process: Shielded Metal Arc

Manual or Machine: Manual

Material Specification: A 240 Type 316L

ASME P. No. 8 To ASME P. No. 8

Thickness(if pipe, diameter and wall thickness): 2"

Thickness Range This Test Qualifies: 3/16" - 4"

Filler Metal Group No. F 5

Weld Metal Analysis No. A 7

ASTM Specification No.: SFA 5.4

FLUX OR ATMOSPHERE: Is Backing Strip Used? No

WELDING PROCEDURE

Single or Multiple Pass: Multiple

Single or Multiple Arc: Single

Position of Groove: Horizontal

WELDING TECHNIQUE (For Information Only)

Electrode: E 308L Type of Backing: None

Filler Wire Diameter: 5/32 and 3/16

Welding Current: D.C. R.P.

Consult Part III Non-Essential Variables for joint dimensions and welding current setting.

TEST RESULTS

Reduced Section Tensile Results:

SPECIMEN NUMBER	DIMENSIONS WIDTH	THICKNESS	AREA	ULTIMATE TOTAL LOAD,LB.	ULTIMATE UNIT STRESS, PSI	CHARACTER OF FAILURE AND LOCATION
1	1.054	1.905	2.050	173,100	86,400	Weld
2	1.047	1.907	1.991	172,600	86,600	Weld

Guided Bend Test:

TYPE	RESULT
4 Side Bends	All OK

Laboratory Test No. P.T 282 Al , original signed by Rick Boone, 4/19/71.

RECORD OF WELDING PROCEDURE QUALIFICATION SPECIFICATION
TO A.S.M.E SECTION IX LATEST EDITION

PART II ESSENTIAL VARIABLES

Specification No.: 1419 Date: 4/19/71

Welding Process: Shielded Metal Arc

Manual or Machine: Manual

Material Specification: A 240 Type 316L

ASME P. No. 8 to ASME P. No. 8

Thickness (If pipe, diameter and wall thickness): 2"

Thickness Range This Test Qualifies: 3/16" - 4"

Filler Metal Group No. F 5

Weld Metal Analysis No. A 7

ASTM Specification No: SFA 5.4

FLUX OR ATMOSPHERE: Is Backing Strip Used? No

WELDING PROCEDURE

Single or Multiple Pass: Multiple

Single or Multiple Arc: Single

Position of Groove: Vertical

WELDING TECHNIQUE (For Information Only)

Electrode: E 308L

Type of Backing; None

Filler Wire Diameter: 1/8, 5/32 and 3/16

Welding Current: D.C. R.P.

Consult Part III Non-Essential Variables for joint dimensions and welding current settings.

TEST RESULTS

Reduced Section Tensile Results:

SPECIMEN NUMBER	DIMENSIONS WIDTH	DIMENSIONS THICKNESS	AREA	ULTIMATE TOTAL LOAD,LB.	ULTIMATE UNIT STRESS, PSI	CHARACTER OF FAILURE AND LOCATION
1	1.053	1.907	2.010	173,600	86,400	Weld
2	1.055	1.907	2.010	173,400	86,400	Weld

Guided Bend Test:

TYPE	RESULT
4 Side Bends	All OK

Laboratory Test No. P.T 282 A2, original signed by Rick Boone, 4/19/71.

WELDING PROCEDURE SPECIFICATION
TO A.S.M.E. SECTION IX LATEST EDITION

PART III NON-ESSENTIAL VARIABLES

	LAYER NUMBER	WIRE SIZE	AMPS	VOLTS
First Side Welded	1-20	5/32" ø	120-190	21-25
First Side Welded	21-41	3/16" ø	150-225	21-25
First Side Welded	42-51	5/32" ø	120-190	21-25
Second Side Welded	1-22	5/32" ø	120-190	21-25

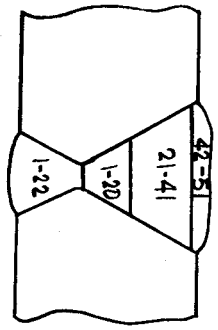

HORIZONTAL

	LAYER NUMBER	WIRE SIZE	AMPS	VOLTS
Both Sides	1-3	1/8" ø	90-150	21-25
Both Sides	4-6 and Cap Off	5/32" ø	120-190	21-25
Both Sides	7	3/16" ø	150-190	21-25
Second Side Welded	4-5	5/32" ø	120-190	21-25

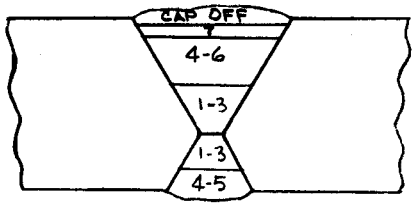

VERTICAL

IMPACT TEST DATA

Type of Notch: V

SPEC. NO.	SPEC. ORIENT	SPEC. SIZE	NOTCH LOCATION	TEST TEMP. DEG. F	ENERGY FT-LBS	LATERAL EXPANSION MILS
H-1	Trans	Full	Weld	-423°	18	21
H-2	"	Full	"	-423°	18	25
H-3	"	Full	"	-423°	16	27
H-4	"	Full	"	-423°	15	23
H-5	"	Full	"	-423°	21	24
H-6	"	Full	"	-423°	17	24
V-1	Trans	Full	Weld	-423°	29.5	23
V-2	"	Full	"	-423°	35.5	29
V-3	"	Full	"	-423°	32.0	28
V-4	"	Full	"	-423°	28	28
V-5	"	Full	"	-423°	35.5	26
V-6	"	Full	"	-423°	29.5	23

WELDING PROCEDURE SPECIFICATIONS
150" ROUND STAINLESS BUBBLE CHAMBER

PART I GENERAL

1.0 PROCESS

The welding shall be accomplished by the Shielded Metal Arc and Tungsten Inert Gas Processes

2.0 BASE METAL, FILLER METAL AND WELDING SPECIFICATION NUMBERS

The base metal and filler metal shall be in accordance with the Table.

BASE METAL	FILLER METAL	CB&I WELDING SPECIFICATION
SA 240 Type 316L S.S.	E 308L	1420
	ER 308L	

3.0 POSITION

The welding shall be performed in the Flat or Vertical Position.

4.0 PREPARATION OF BASE METAL

The edges or surfaces of parts to be joined by welding shall be prepared by shearing, chipping, grinding, machining, planning, arc gouging, and grinding, flame power burning or plasma cutting.

5.0 WELDING TECHNIQUE

The welding technique such as electrode sizes, mean voltages, etc, shall be substantially as shown on the attached sketches and data sheets.

6.0 CLEANING AND DEFECTS

All slag or flux remaining on any bead of welding shall be removed before depositing the next successive bead of welding. Any

defects that appear on any bead of welding shall be removed by chipping, grinding, or arc gouging before depositing the next successive bead of welding.

7.0 PEENING

In general, light peening shall be used as an aid to cleaning the weld beads.

8.0 TREATMENT OF BACKSIDE OF WELDING GROOVE

When required, in order to obtain complete fusion, the backside of the welding groove shall be prepared by chipping, grinding, or arc gouging to sound metal. Purging shall be used when necessary.

9.0 WELDING CURRENT

The welding current shall be direct current, reversed polarity for S.M.A. welding and straight polarity for T.I.G. welding.

10.0 INSPECTION OF WELDS

All root passes, back gouged areas and finished welds will be dye penetrant examined.

Radiography will be performed where required and practical.

See Engineering Drawings for Additional Special Instructions.

RECORD OF WELDING PROCEDURE QUALIFICATION SPECIFICATION
TO A.S.M.E. SECTION IX LATEST EDITION

PART II ESSENTIAL VARIABLES

Specification No.: 1420

Date: 4/19/71

Welding Process: S.M.A. w T.I.G. Root Pass

Material Specification: A240 Type 316L

ASME P. No. 8 to ASME P. No. 8

Thickness (if pipe, diameter and wall thickness): 3/4"

Thickness Range This Test Qualifies: 3/16" - 1-1/2

Filler Metal Group No. F 5 and F 7

Weld Metal Analysis No. A 7

ASTM Specification No.: SFA 5.4 and 5.9

Manual or Machine: Manual

FLUX OR ATMOSPHERE

Inert Gas Composition: Argon for T.I.G.

Trade Name: Airco

Flow Rate: 25 cfh

Is Backing Strip Used? No

WELDING PROCEDURE

Single or Multiple Pass: Multiple

Single or Multiple Arc: Single

Position of Groove: Vertical

WELDING TECHNIQUE (For Information Only)

Electrode: Root Pass ER-308L Remainder E 308L

Type of Backing: None

Filler Wire Diameter: 3/32 and 1/8

Welding Current: T.I.G. - D.C. S.P. - SMA-DC R.P.

Consult Part III Non-Essential Variables for joint dimensions and welding current settings.

TEST RESULTS

Reduced Section Tensile Results:

SPECIMEN NUMBER	DIMENSIONS WIDTH	THICKNESS	AREA	ULTIMATE TOTAL LOAD,LB.	ULTIMATE UNIT STRESS, PSI	CHARACTER OF FAILURE AND LOCATION
1	1.321	.759	1.003	78,400	78,000	Plate
2	1.307	.753	.983	77,800	79,100	Plate

Guided Bend Test:

TYPE	RESULT
4 Side Bends	All OK

Laboratory Test No. P.T 282 B, original signed by Rick Boone, 4/19/71.

WELDING PROCEDURE SPECIFICATION
TO A.S.M.E. SECTION IX LATEST EDITION

PART III NON-ESSENTIAL VARIABLES

LAYER NUMBER	WIRE SIZE	AMPS	VOLTS
1-3 & 9	3/32	140-235	13-15
4-8	1/8	90-150	21-25

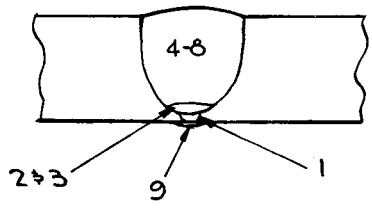

IMPACT TEST DATA

Type of Notch: V

SPEC. NO.	SPEC. ORIENT	SPEC. SIZE	NOTCH LOCATION	TEST TEMP. DEG. F	ENERGY FT-LBS	LATERAL EXPANSION MILS
1	Trans.	Full	Weld	-423°	31	24
2	"	Full	Weld	-423°	22.5	17
3	"	Full	Weld	-423°	26.5	19
4	"	Full	Weld	-423°	28	20
5	"	Full	Weld	-423°	27.5	20
6	"	Full	Weld	-423°	24	21

WELDING PROCEDURE SPECIFICATIONS
150" ROUND STAINLESS BUBBLE CHAMBER

PART I GENERAL

1.0 PROCESS

The welding shall be accomplished by the Tungsten Inert Gas Process.

2.0 BASE METAL, FILLER METAL AND WELDING SPECIFICATION NUMBERS

The base metal and filler metal shall be in accordance with the Table.

BASE METAL	FILLER METAL	CB&I WELDING SPECIFICATION
SA240 Type 316L S.S.	ER 308L	1421

3.0 POSITION

The welding shall be performed in the flat or vertical position.

4.0 PREPARATION OF BASE METAL

The edges or surfaces of parts to be joined by welding shall be prepared by shearing, chipping, grinding, machining, plaining, arc gouging and grinding, flame powder burning, or plasma burning.

5.0 WELDING TECHNIQUE

The welding technique such as electrode sizes, mean voltages, etc. shall be substantially as shown on the attached sketches and data sheets.

6.0 CLEANING AND DEFECTS

All slag or flux remaining on any bead of welding shall be removed before depositing the next successive bead of welding. Any defects that appear on any bead of welding shall be removed by chipping,

grinding or arc gouging before depositing the next successive bead of welding.

7.0 PEENING

In general, light peening shall be used as an aid to cleaning the weld beads.

8.0 TREATMENT OF BACKSIDE OF WELDING GROOVE

When required, in order to obtain complete fusion, the backside of the welding groove shall be prepared by chipping, grinding, or arc gouging to sound metal. Purging will be used when necessary.

9.0 WELDING CURRENT

The welding current shall be direct current, straight polarity.

10.0 INSPECTION OF WELDS

All root passes, back gouged areas and finished welds will be dye penetrant examined.

Radiography will be performed where required and practical.

See Engineering drawings for additional special instructions.

RECORD OF WELDING PROCEDURE QUALIFICATION SPECIFICATION
TO A.S.M.E. SECTION IX LATEST EDITION

PART II ESSENTIAL VARIABLES

Specification No.: 1421 Date: 4/19/71

Welding Process: Tungsten Inert Gas

Material Specification: A 240 Type 316L

ASME P. No 8 to ASME P. No. 8

Thickness (if pipe, diameter and wall thickness): 3/4"

Thickness Range This Test Qualifies: 3/16" to 1-1/2"

Filler Metal Group No. F 7

Weld Metal Analysis No. A 7

ASTM Specification No.: SFA 5.9

Manual or Machine: Manual

FLUX OR ATMOSPHERE

Inert Gas Composition: Argon

Trade Name: Airco

Flow Rate: 25 cfh

Is Backing Strip Used? No

WELDING PROCEDURE

Single or Multiple Pass: Multiple

Single or Multiple Arc: Single

Position of Groove: Vertical

WELDING TECHNIQUE (For Information Only)

Electrode: ER 308L

Type of Backing: None

Filler Wire Diameter: 3/32

Welding Current: D.C. S.P.

Consult Part III Non-Essential Variables for joint dimensions and welding current settings.

TEST RESULTS

Reduced Section Tensile Results

SPECIMEN NUMBER	DIMENSIONS WIDTH	THICKNESS	AREA	ULTIMATE TOTAL LOAD,LB.	ULTIMATE UNIT STRESS, PSI	CHARACTER OF FAILURE AND LOCATION
1	1.305	.781	1.020	87,000	85,100	Weld
2	1.316	.785	1.032	87,600	84,800	Weld

Guided Bend Test:

TYPE	RESULT
4 Side Bands	All OK

Laboratory Test No. P.T. 282 C, original signed by Rick Boone, 4/19/71.

WELDING PROCEDURE SPECIFICATION
TO A.S.M.E. SECTION IX LATEST EDITION

PART III NON-ESSENTIAL VARIABLES

LAYER NUMBER	WIRE SIZE	AMPS	VOLTS
All	3/32" Ø	140-235	13-15

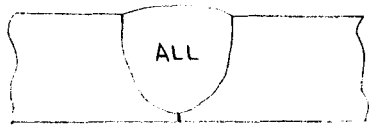

VERTICAL

IMPACT TEST DATA

Type of Notch: V

SPEC. NO.	SPEC. ORIENT	SPEC. SIZE	NOTCH LOCATION	TEST TEMP. DEG. F	ENERGY FT-LBS	LATERAL EXPANSION MILS
1	Trans.	Full	Weld	-423°	56	30
2	"	Full	Weld	-423°	47	30
3	"	Full	Weld	-423°	44	23
4	"	Full	Weld	-423°	52.5	29
5	"	Full	Weld	-423°	45	25
6	"	Full	Weld	-423°	35	31

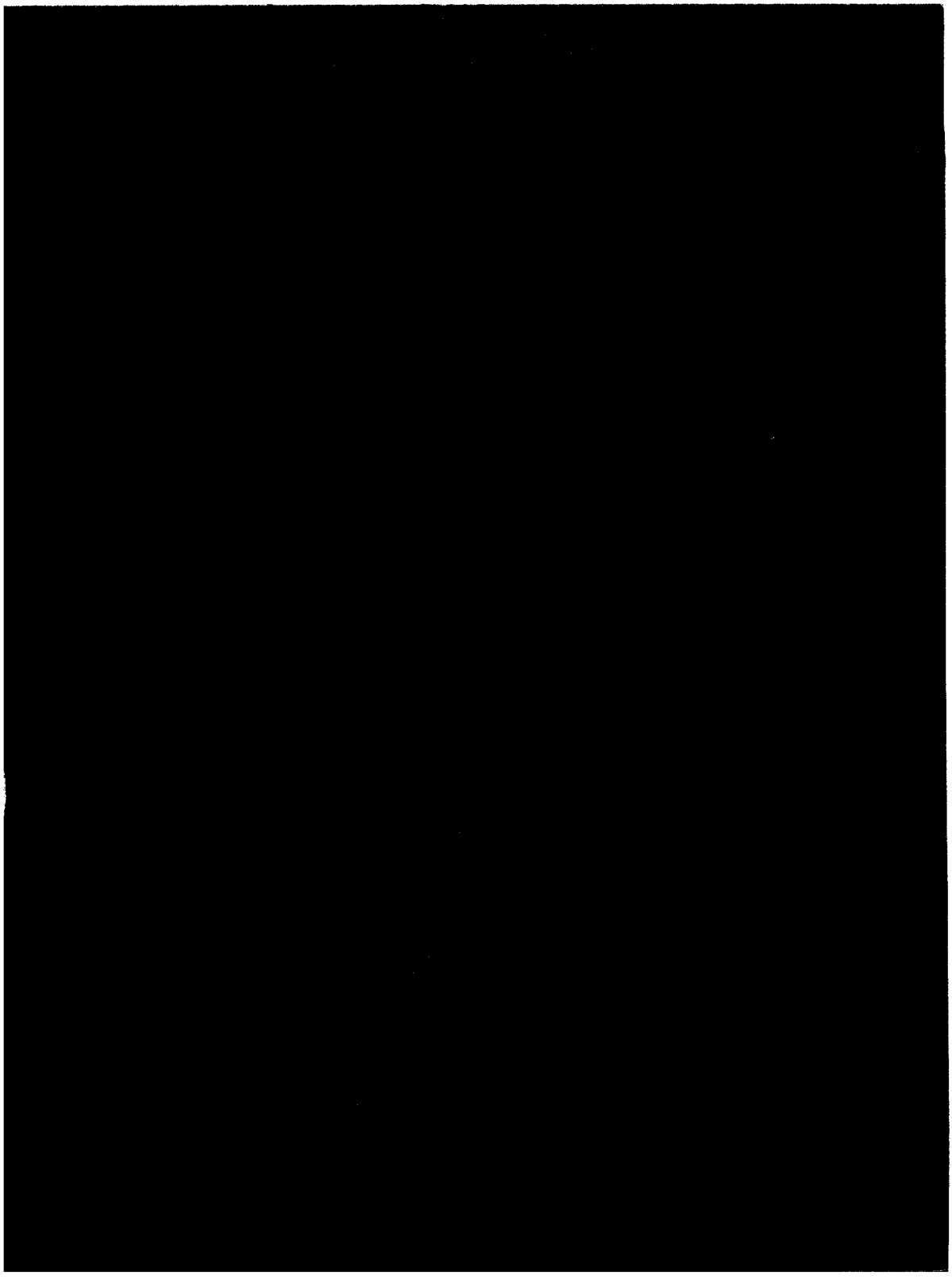

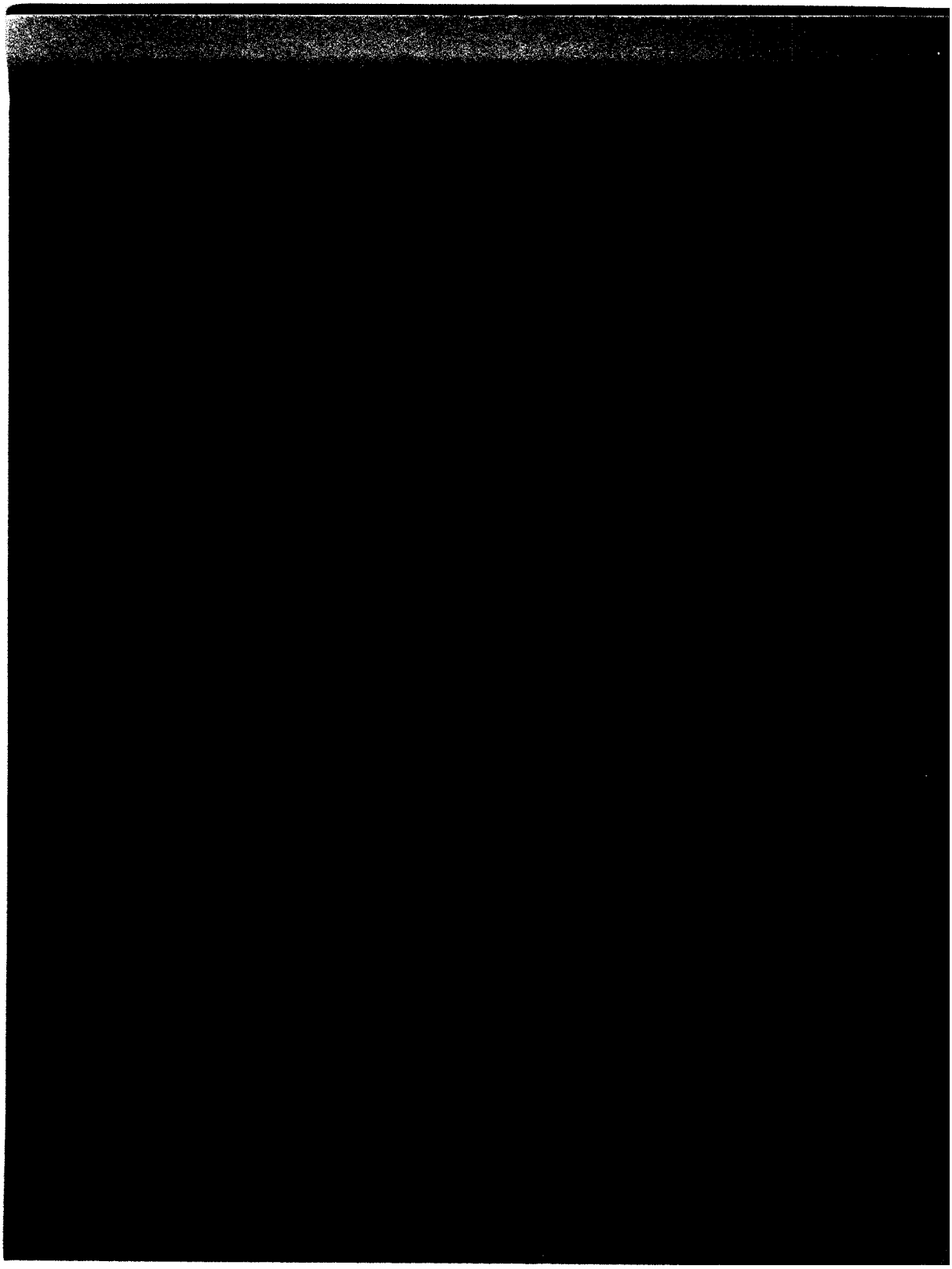

IV. EQUIPMENT

C. Chamber Vessel

5. Report of Inspection Trip to Fabricator's Plant

Prepared by

C.L.Goodzeit
Brookhaven National Laboratory

IV. C. 5. REPORT OF INSPECTION TRIP TO FABRICATOR'S PLANT

(1) INTRODUCTION

The 150-inch, 30,000ℓ NAL Bubble Chamber vessel was inspected at the Chicago Bridge & Iron plant in Birmingham, Alabama on October 6 and October 7, 1971. Verification of fabrication procedures for Section VIII, Division 2 of the ASME Pressure Vessel Code was carried out, a general inspection was made and the hydrostatic test was witnessed. The results are summarized as follows.

(2) MATERIALS CERTIFICATION AND TESTS

Chemistry, tensile and impact tests results were reviewed for the plate material and weld rod used in the fabrication and found to conform to specification SA240 Type 316L in the plate and E308L and ER308L for the weld rod. In addition a ferrite content of 4-10% was specified for the weld rod and the actual values fell between 4% and 9% as determined by the Schaeffler Diagram.

An exception was that impact tests had not been performed on the 3/4-inch plate material used for the fabrication of the condenser head. In addition, tensile and impact test results for the camera nozzle material supplied by NAL were not available in Birmingham.

(3) GENERAL INSPECTION

The vessel was clean and the inside surfaces, not covered by dimple plate, had been polished to receive Scotchlite. The dimple jacket was welded to the inside of the "beanie", the plug welds appeared to be scaled with oxide.

Welded seams on the inside and outside had been ground smooth and flush with the surfaces. Visual inspection showed good fit up between the plate segments, knuckle piece and rings. The fit between the support

cone and transition ring was good with only about 1/8-inch variation around the circumference. The bottom seal surface appeared in good condition; other seal surfaces were not visible because of blank-off plates attached for the hydrostatic test.

(4) WELDING PROCEDURES AND QUALIFICATIONS

Spot checks were made of the weld seam records kept for this job to ascertain welder's qualifications and type of electrode used for the specific seam. For example, it was verified that nozzle penetrations welds were made with ER308L electrode for the first passes, as specified. Remainder of these welds was made with E308L. Welding operators used for the joints, had been qualified for the welding procedures involved in the fabrication according to the procedure qualification in Section IX of the ASME Code. Spot checks of the welder qualification records showed that they had been qualified using two bend tests.

(5) NDT

Qualification of NDT technicians were reviewed with the CB&I Safety Coordinator who described their training program and level of proficiency required. Individual records of NDT qualification were spot checked.

Liquid penetrant records of individual weld seams were reviewed. Such records indicated that almost all seams examined passed this type of inspection without requiring repair. Repaired areas were noted to have been rechecked and the records were consistent. It was specifically noted that all of the first passes on the camera nozzle penetration welds had been tested.

Radiographs were spot checked for various seams. In addition, the NAL representative reviewed the entire film set for the final "beanie" to chamber weld seam. Although not required under Section VIII, Division 2, the camera nozzle penetration welds had been completely radiographed.

These joints were not readily radiographable;however, some defects were revealed by this method and repairs had been made.

Ultrasonic testing had been performed on the flange and ring material by G. O. Carlson.

(6) DIMENSIONAL CHECKS

Certain dimensional checks had been made by CB&I. Detailed dimensional information had been given to the NAL representative which indicated that there were no significant deviations. The procedure for the alignment of the camera nozzles was reviewed. This consisted of optical alignment of the nozzles in the "beanie" which was tilted at 10°. It was pointed out that welding had been done while alignment was being checked to ensure that the welding procedures did not cause misalignment. The installation of the camera nozzle was completed prior to the assembly of the "beanie" onto the spherical shell. It was felt that the final weld of the "beanie" to the shell did not cause any loss of alignment accuracy.

(7) HYDROSTATIC TEST

The hydrostatic test was performed on October 7. The procedure was to blank off the flanges with carbon steel cover plates using impregnated asbestos flat gaskets. The vessel (with the exception of the cone cooling jacket and dimple jacket) was filled with 85°F water. An effort was made to remove excess air from the camera nozzles with U-tubes; however, this was not entirely satisfactory. Nevertheless, the vessel was sealed and pressurized to about 195 psig in a period of about 3 hours. At that time leakage was observed from the 74-inch I.D. cover plate gasket on the expansion flange. This was apparently caused by excessive deflection of the 3-3/4-inch thick flat cover plate. The pressure was immediately reduced to 150 psig and the leakage stopped. A careful inspection was made of the surface of the vessel

and the weld seams and no other leakage was observed at this pressure. The pressure was maintained for about 15 minutes, then the vessel was dumped.

(8) OTHER REMARKS

1) Camera Nozzles. It was reported that the camera nozzles were centrifugally cast of SA351, Type CF3M material with the chemistry adjusted to produce about 10% ferrite. In this case, there may be some tendency for this material to undergo martensite transformation during low temperature operation. It would be advisable to record magnetic permeability measurements for these nozzles and recheck them from time to time after the chamber has been operated.

2) Dimple Jacket. Inspection of the dimpled refrigeration jacket welded to the inside of the "beanie" has verified that plug welds were used to attach it to the shell. These are incomplete penetration welds made from the outside. Sections of this type of dimple jacket weld made at BNL have shown that a sharp crack-like defect exists around the periphery of the weld at the point where fusion has terminated. There is some possibility in this case, that the crack could propagate during cyclic loading. It has been stated that test results on sample panels have indicated that this type of joint is adequate for the expected service condition. However, it would be advisable to use caution in applying new loading conditions that may be in excess of the present ones and it would be advisable to continue testing this type of welded configuration under fatigue loading to determine the limitations of this assembly.

E. T. Goodzeit

SIGNATURE

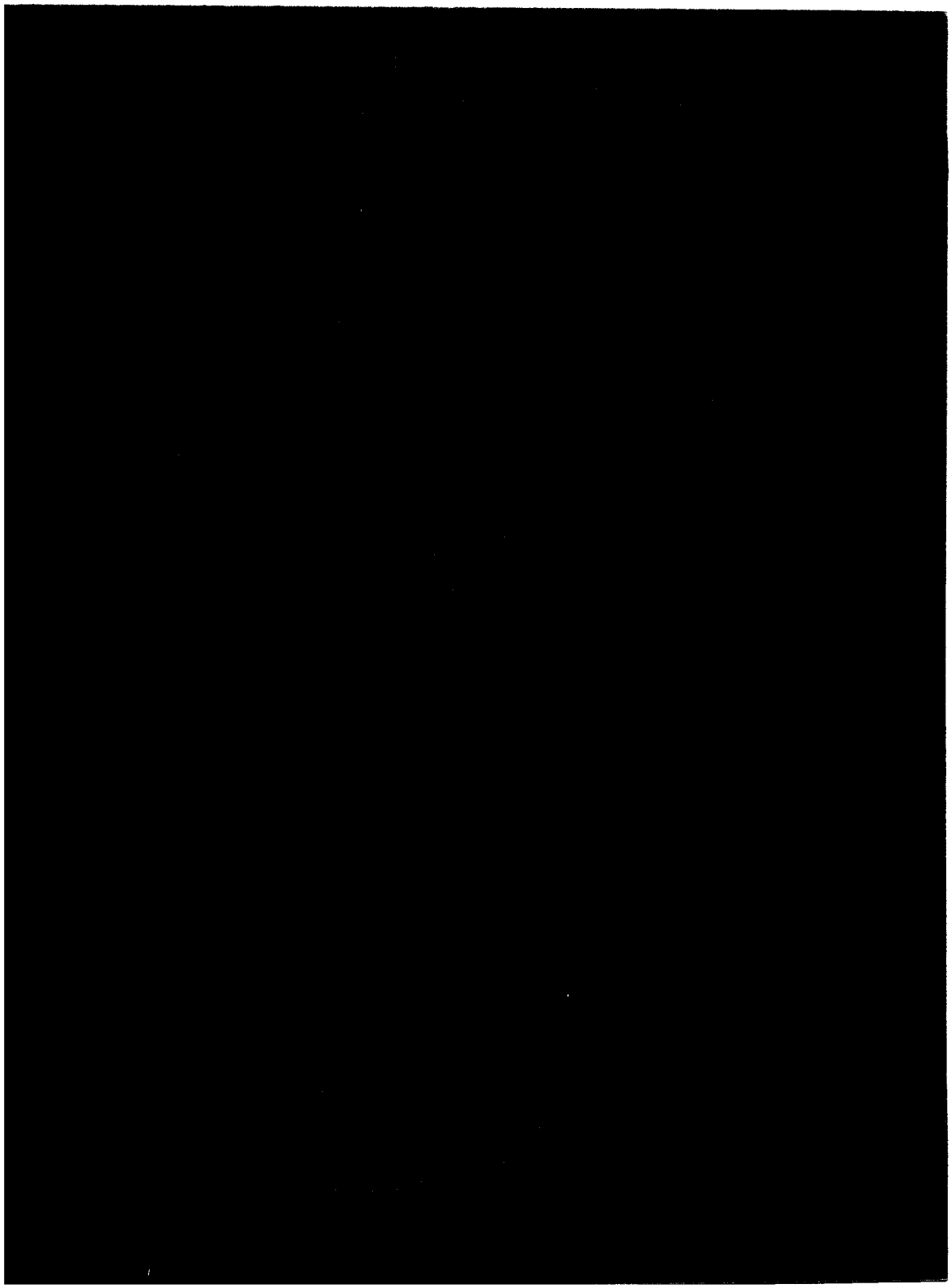

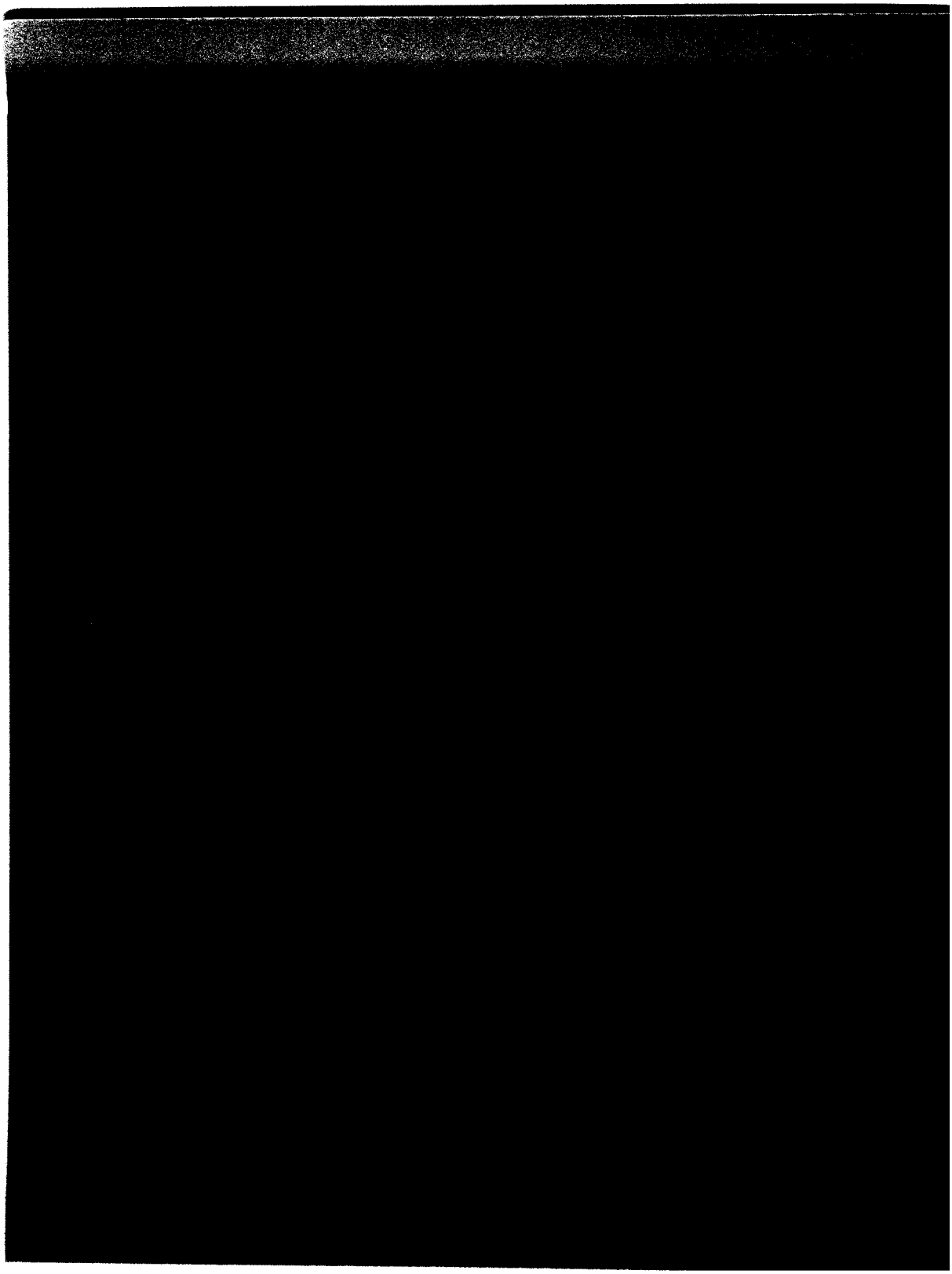

IV. EQUIPMENT

C. Chamber Vessel

6. Special Report by Battelle Memorial Institute on Charpy Impact Testing

Prepared by

H. W. Mishler

TABLE OF CONTENTS

IV. EQUIPMENT

C. Chamber Vessel

6. Special Report by Battelle Memorial Institute on Charpy Impact Testing — Page

(1) Introduction 299

(2) Specimens 299

(3) Evaluation 303

(4) Test Results 304

(5) Ferrite Determination 310

(6) Conclusions 311

LIST OF FIGURES

FIGURE 1: TYPICAL LOCATION OF IMPACT SPECIMENS 302

FIGURE 2: LOCATION OF IMPACT SPECIMENS IN "BAR" WELDS 307

LIST OF TABLES

TABLE 1: SPECIMENS RECEIVED FOR IMPACT EVALUATION 300

TABLE 2: IMPACT PROPERTIES OF STAINLESS STEEL WELDS AT -421°F 305

IV. C

6. SPECIAL REPORT BY BATTELLE MEMORIAL INSTITUTE ON CHARPY IMPACT TESTING

(1) INTRODUCTION

This is a report on the results that have been obtained to date on the evaluation of the impact properties at -421°F of various components of the bubble chamber.

The requirements of the ASME Boiler and Pressure Vessel Code, Section VIII, Division 2, are being followed in the fabrication of the 316-L stainless steel bubble chamber. Paragraph AM-213 of this code (Summer 1969 Addenda) requires impact testing of all materials operating below -325°F. The operating temperature of the bubble chamber is -421°F. Charpy V-notch impact specimens are required; the test temperature must be the service temperature of the completed weldment. Various specimens of base metal and of weld joints were sent to Battelle-Columbus by NAL and subcontractors. The impact properties of these joints were evaluated by Battelle-Columbus in accordance with the requirements of the Code.

(2) SPECIMENS

The weld and base metal specimens that were received by Battelle are listed in Table 1. Any identifying numbers appearing on the specimens are noted. In the table, the terms Lockport and Lenape Forge stand, respectively, for Lockport Manufacturing Company, Division of Universal Head Company, and Lenape Forge Division, Gulf Western Industrial Products Company. Charpy V-notch specimens were cut from the welds following the requirements of Paragraph AT-201 which specifies positioning of the impact specimens. If the material thickness was large enough, one specimen would be taken from the top of the piece and one from the bottom as shown in Figure 1. If the piece was too thin for this specimen orientation, the specimens were cut side-by-side. In the first few welds evaluated, heat-affected-zone (HAZ) and base metal specimens also were

TABLE 1 SPECIMENS RECEIVED FOR IMPACT EVALUATION

Sample Number	Date Received	Source	Identification
1	2-21-71	NAL	Weld made with 316-L electrodes between two bars of 316-L base metal.
2	2-21-71	NAL	316-L base metal.
3	2-21-71	CB&I	Weld deposited with 308-L electrode in 2-inch thick 316-L base metal. Procedure qualification.
4	3-10-71	NAL	316-L base metal from chamber head, marked: A24069/316L/50032L-1B.
5	3-10-71	NAL	Weld made with 308-L electrodes between two bars of 316-L base metal.
6	3-10-71	NAL	316-L centrifugal cast 7th camera nozzle, as-cast condition.
7	3-11-71	Lockport	Weld deposited with 316-L electrodes in 1-inch thick 316-L base metal.
8	3-26-71	Canadian Lukens	Weld deposited with 316-L electrodes in 1-inch thick 316-L base metal.
9	4-8-71	Lockport	Weld deposited with Stoody 308-L electrodes in 1-inch thick 316-L base metal. Hand carried to Battelle by NAL.
10	4-6-71	NAL	316-L centrifugal casting, Heat P519, heat treated.
11	4-6-71	NAL	316-L centrifugal casting, Heat P567, heat treated.
12	4-6-71	NAL	316-L centrifugal casting, Heat P590, heat treated.
13	4-20-71	CB&I	Weld deposited with 308-L electrodes in 2-inch thick 316-L base metal. Weld No. PT282-2A. Welder and position qualification.
14	4-20-71	CB&I	Weld deposited with 308-L electrodes in 7/8-inch thick 316-L base metal. Weld No. PT282-2B. Welder and position qualification.
15	4-20-71	CB&I	Weld deposited with 308-L electrodes in 7/8-inch thick 316-L base metal. Weld No. PT282-2C. Welder and position qualification.
16	4-27-71	Lasker Boiler	Weld deposited with 308-L electrodes in 1-11/16-inch thick 316-L base metal.

TABLE 1 SPECIMENS RECEIVED FOR IMPACT EVALUATION (continued)

Sample Number	Date Received	Source	Identification
17	5-19-71	Lenape Forge	Weld deposited with 308-L electrodes in 1-1/4-inch thick 316-L base metal. Weld No. 4.
18	5-19-71	Lockport	Weld deposited with 308-L electrodes in 1-1/4-inch thick 316-L base metal. Weld No. SA240-68/692674.
19	5-20-71	Canadian Lukens	Weld deposited with 308-L electrodes in 1-inch thick 316-L base metal.

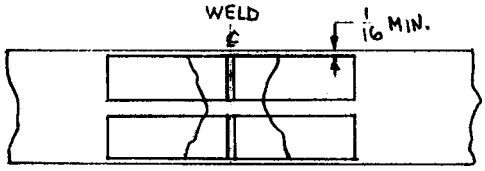

A. WELD-METAL SPECIMENS

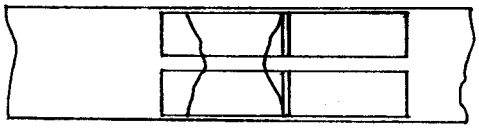

B. HAZ SPECIMENS

FIGURE 1. TYPICAL LOCATION OF IMPACT SPECIMENS

tested. It soon became obvious, however, that the properties of these specimens so far exceeded the Code requirements that further testing of such specimens would not be necessary. Therefore, only weld metal specimens were taken for the subsequent welds.

(3) EVALUATION PROCEDURE

The procedures for cooling and testing the specimens have been developed previously at Battelle. The specimens first are cooled in liquid nitrogen for a minimum of 15 minutes. They then are transferred to liquid hydrogen (-421°F) for 5 minutes. Each specimen is cradled in a paper boat throughout the cooling and testing operation. By using this boat, the specimen can be lifted and transferred without direct contact between the tongs and the specimen. Direct contact with the tongs could change the temperature of the specimen. The boat also retains some of the liquid hydrogen which helps to keep the specimen at the correct temperature. The specimen is transferred from the liquid hydrogen to the impact testing machine in the paper boat; the boat is not removed during testing. Thus, some of the liquid hydrogen is retained around the specimen up to the moment of impact.

Both the impact strength and the lateral expansion of the specimen were recorded. The acceptance requirement is based on lateral expansion only. In Paragraph AM-211.3 (Summer 1969 Addenda) the requirement is stated that the minimum acceptable lateral expansion shall be 0.015-inch. In addition (Paragraph AM-211.6), if the lateral expansion for one specimen in a group of three specimens (the required number) is below 0.015-inch but not below 0.010-inch, and if the average value exceeds 0.015-inch, a retest of three additional specimens may be made. Each of the retest specimens, however, must have a lateral expansion of 0.015-inch or greater. Although impact energy is no longer a measure of acceptance, the impact energies were recorded for information purposes.

Lateral expansion was measured with micrometers and by using the dial-gage system specified by ASTM A370. Micrometer measurement is

faster but may give low readings. This is because the fracture path seldom bisects the point of maximum expansion on both halves of the broken specimen. A given specimen half may include the maximum expansion for both halves, one half only or neither half. Micrometer measurement does not distinguish this effect and if each broken half contains the maximum expansion for that half, the micrometer measurement will be low. If the initial micrometer measurement indicated that the lateral expansion was below 0.017-inch, the specimens were remeasured using the dial-gage technique to obtain a more accurate reading.

(4) TEST RESULTS

The test results are presented in Table 2. In certain welds, results are noted as being from Side A or Side B. These were welds that were thick enough that impact specimens could be machined from both sides of the specimen. These two sides are designated A or B.

A discussion of the results of each weld or base metal piece follows:

Specimen 1

The weld was made between two 1-inch-square bars of base metal with the bars being oriented so that a double-V joint was formed. The weld metal and HAZ specimens had to be oriented in such a manner that the cross section of each specimen contained some weld metal and some HAZ (Figure 2). Therefore, the results from the weld metal and HAZ specimens are not valid for Code acceptance but must be considered of the "information only" category.

Specimen 2

The 316-L base metal far exceeds the Code requirement for lateral expansion.

Specimen 3

This weld was made to qualify the welding procedure at CB&I. The weld metal, HAZ, and base metal exceeded the Code requirements.

TABLE 2. IMPACT PROPERTIES OF STAINLESS STEEL WELDS AT -421°F

Specimen No.	Description		Lateral Expansion inch			Impact Strength foot-pounds		
			Weld	HAZ	Base Metal	Weld	HAZ	Base Metal
1	316-L "bar weld" from NAL		0.025	0.016	0.066	28	27	110
			0.027	--	0.092	38	--	170
			0.034	--	--	33	--	--
2	316-L base metal from NAL		--	--	0.059	--	--	87
			--	--	0.056	--	--	86
			--	--	0.060	--	--	95
			--	--	0.064	--	--	98
			--	--	0.067	--	--	102
			--	--	0.059	--	--	99
			--	--	0.064	--	--	98
			--	--	0.057	--	--	87
3	308-L weld from CB&I	Side A	0.021	0.049	0.060	30	94	94
			0.027	0.052	0.066	41	85	103
			0.026	0.058	0.061	33	92	90
		Side B	0.024	0.047	0.061	40	75	109
			0.023	0.050	0.057	43	85	92
			0.026	0.049	0.057	38	70	97
4	316-L chamber head base metal from NAL		--	--	0.045	--	--	63
			--	--	0.040	--	--	57
			--	--	0.037	--	--	62
			--	--	0.045	--	--	67
			--	--	0.042	--	--	68
			--	--	0.050	--	--	79
			--	--	0.045	--	--	69
			--	--	0.043	--	--	59
5	308-L "bar weld" from NAL		0.020	0.080	--	23	146	--
			0.019	0.078	--	22	143	--
			0.017	0.082	--	17	159	--
			0.019	0.077	--	20	146	--
			0.028	--	--	32	--	--
			0.014	--	--	15	--	--
			0.029	--	--	34	--	--
			0.015	--	--	18	--	--
6	316-L centrifugal casting, 7th camera nozzle, from NAL		--	--	0.006	--	--	5.5
			--	--	0.004	--	--	5
			--	--	0.003	--	--	5.5
			--	--	0.009	--	--	6
7	316-L weld from Lockport	Side A	0.010	0.059	0.055	18	91	87
			0.012	0.048	0.060	20	88	106
			0.011	0.055	0.060	18	87	102
		Side B	0.013	0.047	0.058	15	91	95
			0.019	0.049	0.057	20	86	92
			0.012	0.052	0.061	18	89	98
8	316-L weld from Canadian Lukens	Side A	0.014	0.067	0.082	18	129	150
			0.014	0.068	0.088	18	129	150
			0.017	0.075	0.088	21	133	158
		Side B	0.011	0.058	0.073	16	106	141
			0.012	0.060	0.073	15	106	132
			0.011	0.064	0.085	17	111	145
9	308-L weld from Lockport	Side A	0.015	--	--	15.5	--	--
			0.012	--	--	14.0	--	--
			0.014	--	--	15.5	--	--

(cont.)

TABLE 2. IMPACT PROPERTIES OF STAINLESS STEEL WELDS AT -421°F (cont.)

Specimen No.	Description		Lateral Expansion inch			Impact Strength foot-pounds		
			Weld	HAZ	Base Metal	Weld	HAZ	Base Metal
		Side B	0.020	--	--	22.5	--	--
			0.017	--	--	20.0	--	--
			0.017	--	--	19.5	--	--
10	316-L centrifugal casting, heat treated, from NAL, Heat P519		--	--	0.068	--	--	93
			--	--	0.044	--	--	84
11	Ditto, Heat P567		--	--	0.031	--	--	49
			--	--	0.028	--	--	39
12	Ditto, Heat 590		--	--	0.034	--	--	52
			--	--	0.035	--	--	58
13	308-L, weld, from CB&I, weld number PT282-2A	Side A	0.023	--	--	30	--	--
			0.028	--	--	32	--	--
			0.026	--	--	36	--	--
		Side B	0.029	--	--	36	--	--
			0.023	--	--	28	--	--
			0.021	--	--	30	--	--
14	Ditto, weld number PT282-2B		0.024	--	--	31	--	--
			0.016	--	--	23	--	--
			0.019	--	--	27	--	--
			0.020	--	--	28	--	--
			0.019	--	--	28	--	--
			0.021	--	--	24	--	--
15	Ditto, weld number PT282-2C		0.030	--	--	56	--	--
			0.030	--	--	47	--	--
			0.022	--	--	45	--	--
			0.028	--	--	53	--	--
			0.025	--	--	45	--	--
			0.023	--	--	35	--	--
16	Weld from Lasker Boiler	Side A	0.024	--	--	28	--	--
			0.017	--	--	21	--	--
			0.020	--	--	23	--	--
		Side B	0.023	--	--	25	--	--
			0.024	--	--	25	--	--
			0.017	--	--	25	--	--
17	Weld from Lenape Forge	Side A	0.012	--	--	14	--	--
			0.010	--	--	11.5	--	--
			0.012	--	--	14.5	--	--
		Side B	0.019	--	--	15	--	--
			0.014	--	--	14.5	--	--
			0.015	--	--	17	--	--
18	Weld from Lockport	Side A	0.015	--	--	14	--	--
			0.015	--	--	13	--	--
			0.015	--	--	15	--	--
		Side B	0.016	--	--	15	--	--
			0.017	--	--	17.5	--	--
			0.015	--	--	15.5	--	--
19	Weld from Canadian Lukens	Side A	0.018	--	--	20	--	--
			0.017	--	--	18	--	--
			0.019	--	--	19.5	--	--
		Side B	0.015	--	--	15	--	--
			0.012	--	--	13	--	--
			0.011	--	--	14.5	--	--

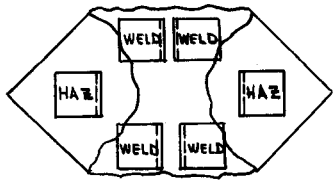

FIGURE 2

LOCATION OF IMPACT SPECIMENS IN "BAR" WELDS

Specimen 4:

The chamber-head base metal exceeds the Code requirements.

Specimen 5:

This weld was similar to Specimen 1 except that 308-L electrodes were used instead of 316-L electrodes. As with Specimen 1, the weld metal specimens contained varying portions of the HAZ. As a result, the lateral expansions of the weld metal specimen were rather erratic and should be treated as information only. The HAZ specimens were oriented differently than in Specimen 1 and did not contain any weld metal. The HAZ exceeded the Code requirements.

Specimen 6:

The impact specimens were oriented so that the notch was perpendicular to the casting surface. The lateral expansion of these specimens was far below the Code required minimum. This material was in the as-cast condition.

Specimen 7:

This weld was made with 316-L electrodes to qualify the procedure. (The brand of electrode was not known but presumed to be a Stoody electrode as subsequent Lockport welds were made with Stoody electrodes.) The HAZ and base metal lateral expansions were acceptable but the weld metal failed to pass the Code requirements. Only one specimen of the six exceeded 0.015-inch lateral expansion. Therefore, this weld and procedure were not acceptable.

Specimen 8:

This weld, also made with 316-L electrodes but by Canadian Lukens, failed to pass the Code requirements. Only one of the six weld-metal specimens exceeded 0.015-inch lateral expansion.

Specimen 9:

This was the second weld from Lockport but was made with 308-L electrodes

instead of 316-L electrodes (Specimen 7). Side B had better impact properties than Side A. The reason for this is not known since the welding procedures used were not available for examination. Several factors could contribute to this difference such as the sequence of weld passes, heat input, or fixturing of the pieces. If the weld was made by first welding one side and then the other, the two sides would experience different amounts of restraint that might influence the impact properties. The operator might have used a different heat input or technique on one side than the other. In any case, the weld from one side passed while the other side failed. This is a borderline situation that should be resolved by making another weld with more careful consideration to welding technique and procedures.

Specimens 10, 11, and 12

This casting was similar to that of Specimen 6 except that the casting had been heat treated (exact heat treatment unknown). Apparently, the heat treatment used is satisfactory as the impact properties improved significantly and are acceptable by the Code. Sufficient material was available from each piece to make only two impact specimens. As with Specimen 6, the notches were oriented perpendicular to the casting surface.

Specimens 13, 14, and 15

These welds were made with 308-L electrodes as part of qualifications of welders and welding positions. All three welds were acceptable.

Specimen 16

This weld, made with 308-L electrodes, was part of a procedure qualification. This weld was acceptable.

Specimen 17

This weld, made with 308-L electrodes, was part of a procedure qualification. The weld is not considered acceptable since four of the six impact specimens had lateral expansions less than 0.015-inch. The

performance of this weld was similar to that of the second Lockport weld (Specimen 9) in that one side of the weld had better impact properties than did the other. As with the Lockport weld, the reason for this is not known.

Specimen 18

This is the third weld from Lockport, the second weld that was made with 308-L electrodes. This weld has better properties than the other Lockport 308-L weld. The properties were improved to the point where this weld is acceptable.

Specimen 19

This second weld from Canadian Lukens was made from 308-L electrodes. This is a borderline weld since one side of the weld passed and the other failed (as the second Lockport weld). The welding procedures should be reviewed to determine what might be the cause of the different results.

(5) FERRITE DETERMINATION

Several of the welds were examined with a Severn Ferrite Indicator to determine the amount of ferrite in the weld and to see if the impact results might be correlated with ferrite content. Ferrite determinations were not made on all of the specimens as the Severn gage was not available until recently. The welds that were examined were those that initially were large enough that a portion of the joint remained after the specimens were machined. Valid ferrite determinations cannot be made on broken impact specimens as the act of fracturing the specimen causes some ferrite to form as a result of straining the specimen. The welds that were examined were:

Specimen	3	CB&I
	13	CB&I
	14	CB&I
	15	CB&I
	16	Lasker Boiler

Specimen 17	Lenape Forge
18	Lockport

The Severn Ferrite Indicator Measures ranges of ferrite content rather than an exact quantity. This is done by comparing the ferrite content of the specimen to that of a known standard by magnetic means. The standards that are used are 0.5, 1.0, 1.5, 2.5, 3.5, 5.0, 7.5, 10.0, and 15.0 percent ferrite.

The thick CB&I welds, Specimens 3 and 13, had ferrite contents between 7.5 and 10.0 percent near the surface and between 3.5 and 5.0 percent ferrite near the center. This is as expected since the dilution from the ferrite-free base metal is greater near the center of the joint where the weld is thinner. The weld metal ferrite content near the surface more closely represents the ferrite content designed into the welding electrodes. The thinner CB&I welds, Specimens 15 and 14, had ferrite contents between 10.0 and 15.0 percent. Presumably, a higher ferrite content electrode was used for these thinner welds.

The thick welds made by Lasker Boiler, Lenape Forge, and Lockport had ferrite contents between 10 and 15 percent throughout the weld. This indicates that these welds must have been made with higher ferrite content electrodes than were the CB&I thick welds.

Previous data from CB&I that was obtained by Mr. Kula of NAL show that optimum impact strengths are expected with ferrite contents around 5 percent. As the ferrite content increases to 12 percent, impact strenghts decrease. The thick CB&I welds generally had better impact properties than the thick welds produced by Lasker Boiler, Lenape Forge, and Lockport. Considering the ferrite contents of these welds, these results would be expected. This is probably one of the reasons that the CB&I welds were better than the other welds.

(6) CONCLUSIONS

On the basis of these evaluations, the welds made with 308-L electrodes generally had better impact properties than did those welds

made with 316-L electrodes. The welds produced by CB&I had better impact properties than the welds made by other fabricators. This probably is a result of several factors. Ferrite content of those few welds examined was lower in two of the CB&I welds. CB&I apparently has more experience in welding 316-L stainless steel for critical applications than do the other fabricators. This is reflected in the impact data previously developed by CB&I and the fact that they have established welding procedures that they are using in this fabrication. If possible, the welding procedures of the various fabricators should be reviewed or observed so that any differences could be noted. On the basis of the impact property evaluations, CB&I procedures should be followed if possible.

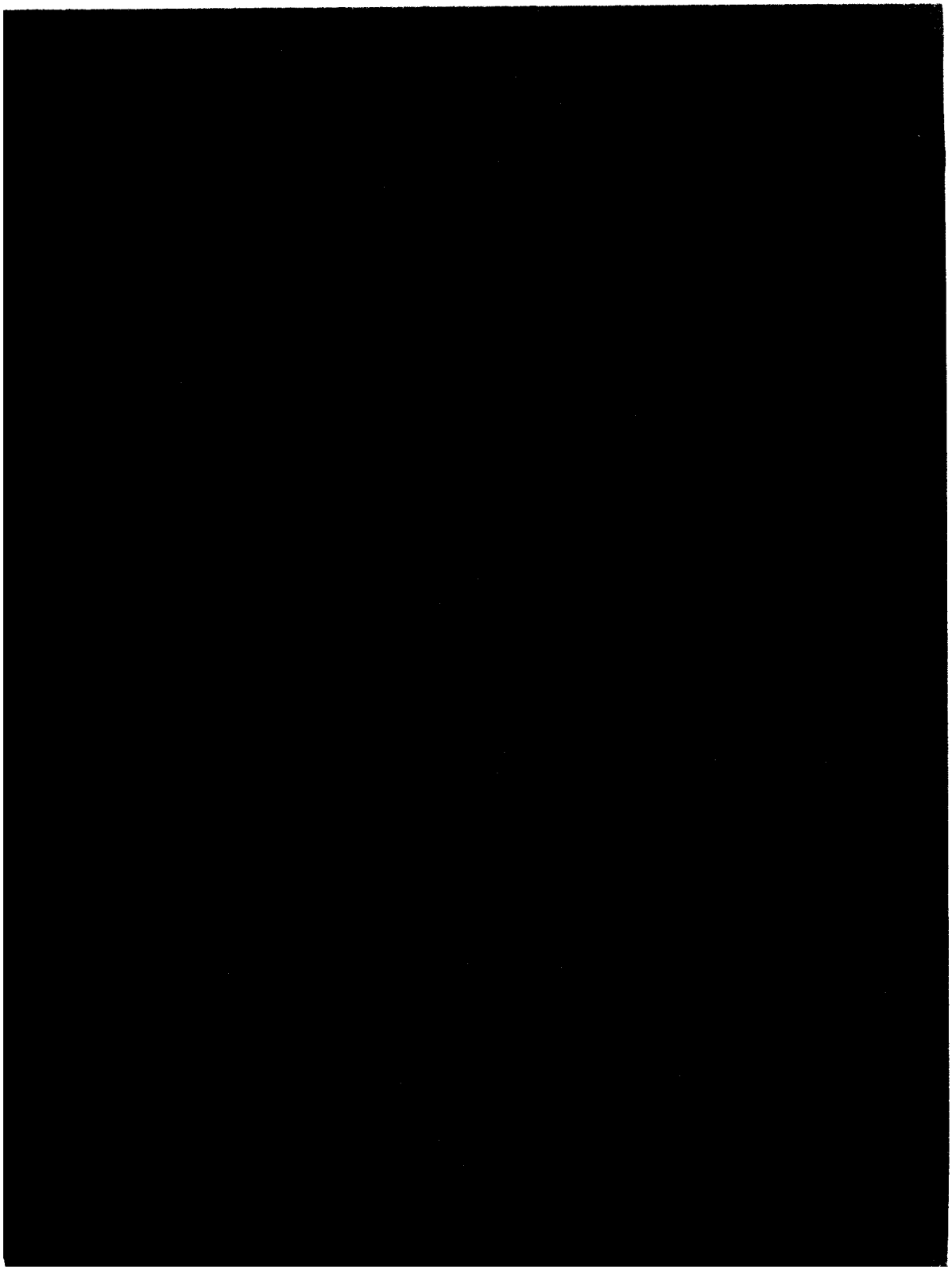

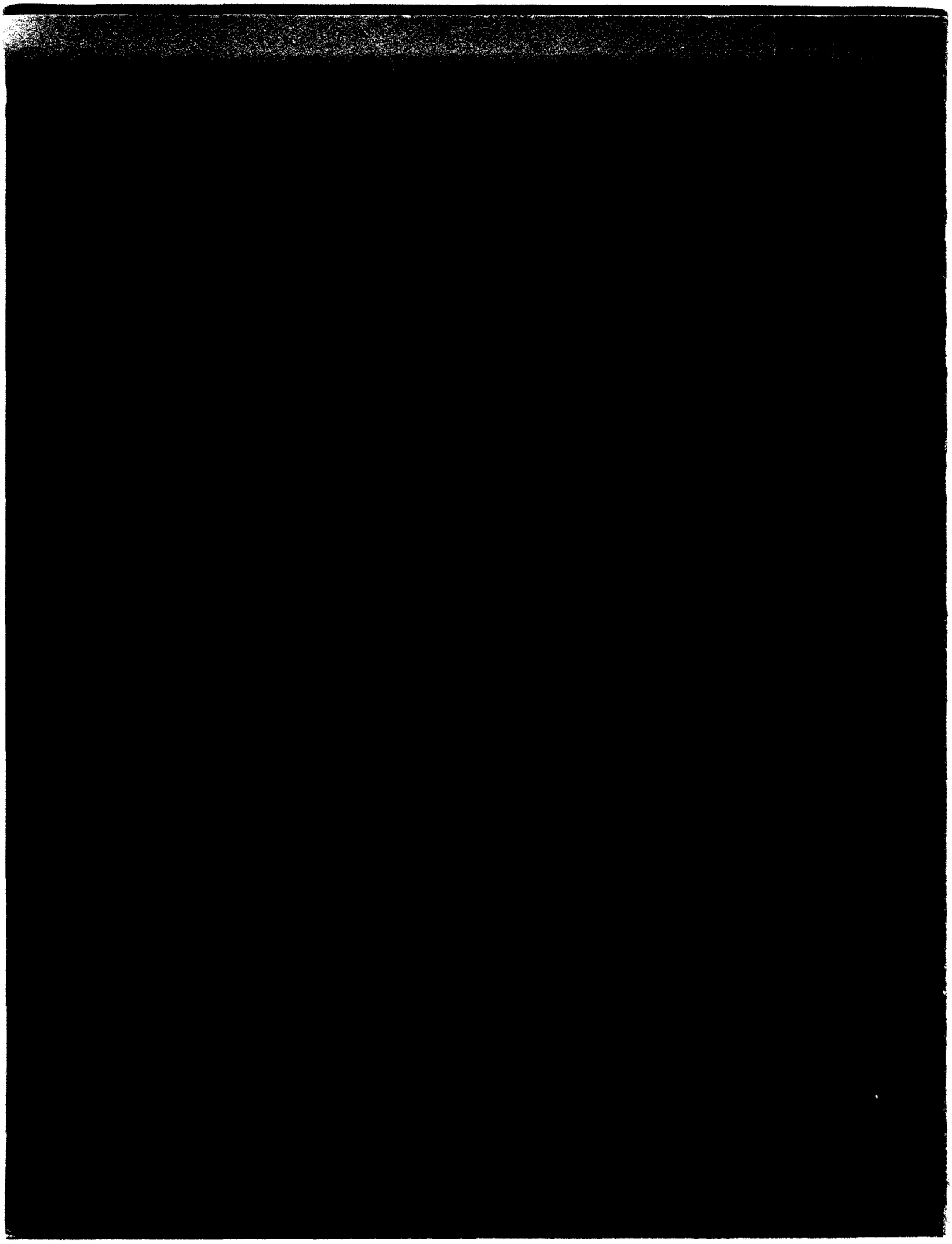

IV. EQUIPMENT

C. Chamber Vessel

7. Chemical Analysis of Component Parts

Prepared by

L.Kula
National Accelerator Laboratory

CHEMICAL ANALYSIS
LIST OF COMPONENT PARTS

PART	HEAT NO.	C	Mn	Si	Cr	Ni	S	P	Mo
Camera Nozzles (Total of 6)	P519	.03	.62	0.70	19.00	9.40	.014	.013	2.45
	P551	.03	.76	1.18	19.40	9.30	.013	.014	2.40
	P567	.03	.78	0.87	19.80	9.70	.013	.014	2.50
	P580	.03	.83	1.00	20.40	9.60	.016	.014	2.55
	P590	.03	.82	0.92	19.50	9.60	.012	.012	2.50
	P615	.03	.69	1.10	20.40	9.40	.013	.013	2.40
Hemispherical Optics Head (108" Inside Diameter)	500321	.024	1.64	0.60	16.70	13.08	.016	.019	2.28
Knuckle	500407-1B	.024	1.60	0.52	16.28	13.04	.013	.016	2.32
Spherical Shell (150" Inside Diameter)	500407-1B	.024	1.60	0.013	16.28	13.04	.013	.016	2.32
	500407-1	.024	1.60	0.52	16.28	13.04	.013	.016	2.32
	50040 -1A	.024	1.60	0.52	16.28	13.04	.013	.016	2.32
Beam Window Flange	500427-1	.027	1.66	0.66	16.96	12.88	.014	.017	2.28
Reinforcing Cone (3" Thick)	600408-1	.030	1.61	0.55	16.38	13.06	.015	.016	2.30
Expansion Cylinder Flange	500427-1	.027	1.66	0.66	16.96	12.88	.014	.017	2.28

CHEMICAL ANALYSIS
LIST OF COMPONENT PARTS (continued)

PART	HEAT NO.	C	Mn	Si	Cr	Ni	S	P	Mo
Inner Cooling Cone	500426-1B	.025	1.39	0.52	16.70	12.98	.012	.015	2.28
Outer Cooling Cone	500334-1	.023	1.55	0.59	16.75	12.95	.012	.017	2.29
Support Skirt	500334-1A	.023	1.55	0.59	16.75	12.95	.012	.017	2.29
Support Ring	600293-1A	.028	1.52	0.61	17.06	13.22	.016	.016	2.34
Cylinder and Rod Guide Flange	139527	.025	1.70	0.45	17.48	13.15	.017	.015	2.25
Cylinder	500322	.027	1.64	0.65	16.68	13.06	.016	.018	2.41
Ring	139527	.025	1.70	0.45	17.48	13.15	.017	.015	2.25
Cone	335309	.22	1.80	0.55	17.68	13.26	.007	.015	2.23
Hub	P-61S	.024	1.42	0.58	16.69	13.32	.011	.018	2.24

CHEMICAL ANSLYSIS
LIST OF COMPONENT PARTS (continued)

PART	HEAT NO.	C	Mn	Si	Cr	Ni	S	P	Mo
Nose Cone									
4 5/8" thick plate	610026-1	.025	1.59	0.54	16.40	12.82	.015	.013	2.26
1" thick plate	613280-1	.020	1.22	0.53	16.53	12.70	.014	.017	2.21
1 1/2" thick plate	616265-1B	.022	1.64	0.46	16.46	13.06	.011	.021	2.26
8 1/4" thick plate	616377-1	.023	1.58	0.66	16.53	13.13	.015	.025	2.34
Beam Window	690811	.029	1.50	0.71	17.28	13.65	.014	.020	2.30
Plug Ring	CT	.020	1.79	0.45	17.25	13.93	.015	.014	2.34
Plug Dome	34513	.025	1.81	0.56	16.50	11.60	.013	.024	2.32
Bubble Condenser	2P2295	.021	1.47	0.42	17.28	13.48	.017	.017	2.10

PART	HEAT NO.	Ni	Cu	Fe	Mn	S	Si	C	Cr	P
Optical Fisheye Flanges	841	36.1	0.08	Rest	0.50	0.009	0.22	0.037	0.01	0.006
	843	36.1	0.05	Rest	0.49	0.009	0.20	0.035	0.01	0.006
	844	36.3	0.06	Rest	0.47	0.010	0.19	0.035	0.02	0.005
	847	36.05	0.09	Rest	0.47	0.008	0.21	0.034	0.02	0.006
	838	35.95	0.05	Rest	0.41	0.008	0.18	0.020	0.02	0.007
	840	36.00	0.04	Rest	0.48	0.007	0.24	0.036	0.02	0.005
	898	36.00	0.08	Rest	0.45	0.008	0.24	0.038	0.02	0.009
	899	36.00	0.06	Rest	0.49	0.007	0.21	0.038	0.01	0.009
	908	36.00	0.14	Rest	0.41	0.007	0.22	0.027	0.02	0.008
	909	36.50	0.06	Rest	0.45	0.007	0.26	0.035	0.01	0.009
	849	42.45	0.06	Rest	0.63	0.009	0.17	0.032	0.01	0.003
	850	42.60	0.05	Rest	0.64	0.008	0.26	0.032	0.01	0.006
	851	42.65	0.06	Rest	0.56	0.010	0.27	0.026	0.01	0.007
	852	42.50	0.06	Rest	0.62	0.009	0.25	0.032	0.01	0.006
	1058	36.00	0.05	Rest	0.36	0.008	0.24	0.046	0.01	0.009
	1072	36.00	0.04	Rest	0.40	0.008	0.11	0.043	0.01	0.006
	1016	42.60	0.10	Rest	0.63	0.009	0.40	0.040	0.02	0.003

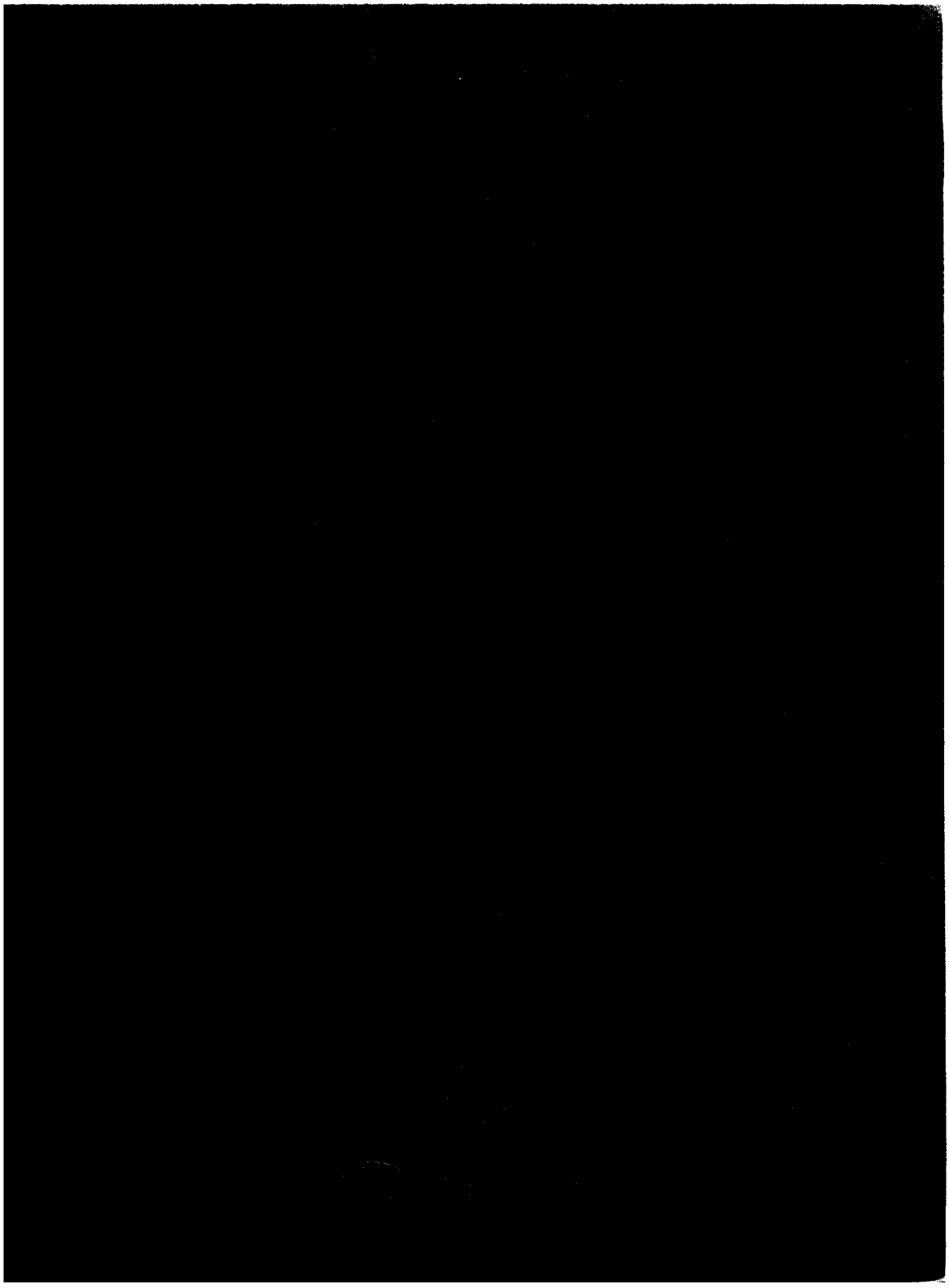

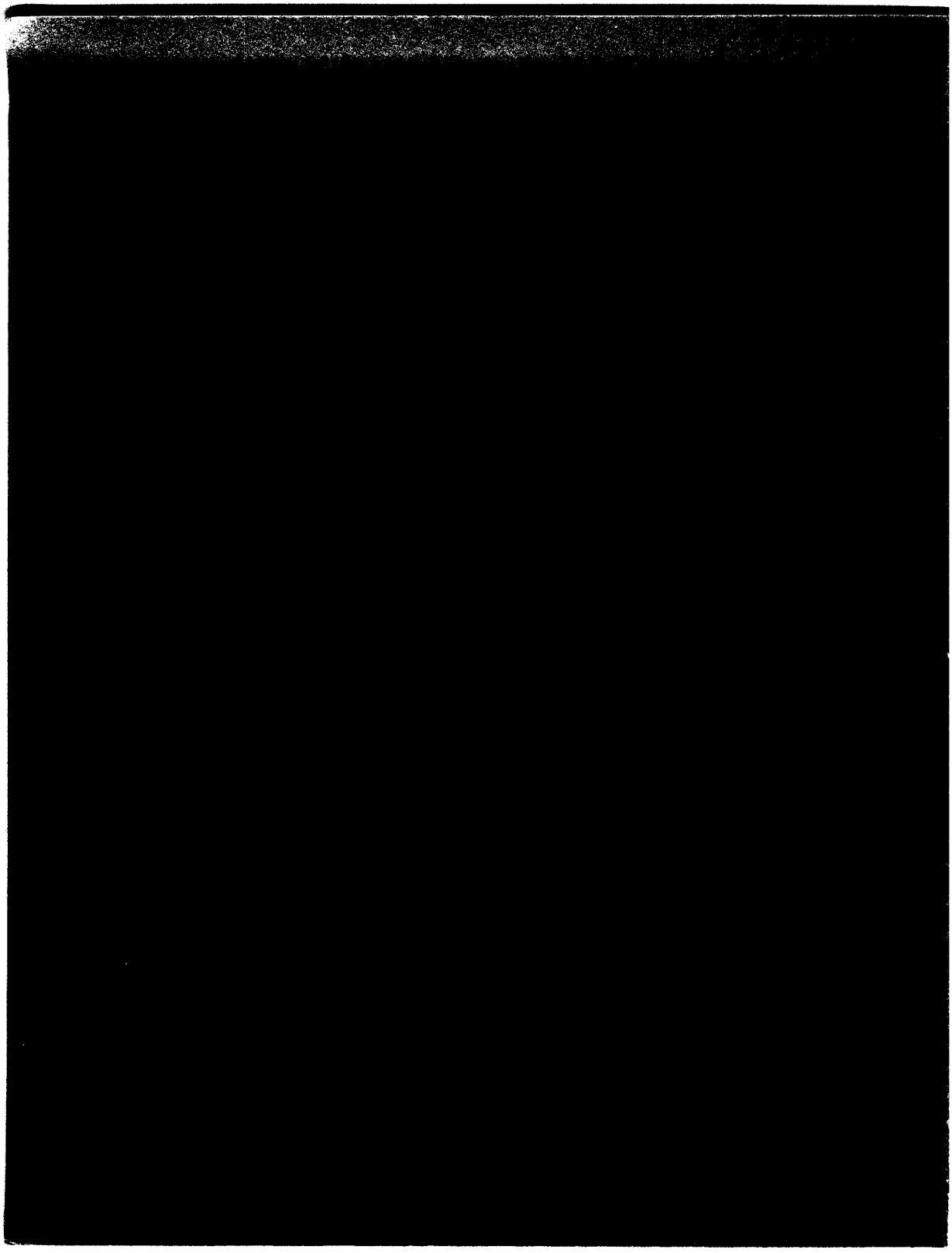

IV. EQUIPMENT

D. Failure Mode Analysis: CHAMBER AND CHAMBER PIPING

Prepared by

P. C. Vander Arend

IV. D. Failure Mode Analysis: CHAMBER AND CHAMBER PIPING

(1) LARGE BREAK FROM CHAMBER INTO THE VACUUM SPACE

The Safety Report of the 15 Foot Bubble Chamber (November, 1970) assumes a flow rate of 1,000 liters per second of liquid hydrogen spilling from the beam window and spraying onto the warm wall of the vacuum chamber. The rate of vapor generation from flashing of the liquid in the vacuum space will be the dominating factor, since rate of vapor generation from heat transfer is a function of wetted surface area. A first approximation is that the rate of vapor generation will be proportional to the rate of spillage. In order to maintain a constant pressure in the system, the rate of venting must be the same as the rate of vapor generation. The vent system of the vacuum chamber of the bubble chamber consists of a 19 inch manway which narrows to a 12 inch IPS, Schedule 5 pipe. A rupture disc set to go at 30 psig is located between two 150 pound flanges. Downstream of the rupture disc, a 12 inch IPS, Schedule 5 pipe leads through a single 90° ell into a vent stack. The vent stack is equipped with a 1 inch thick loose plate and rubber O-ring at at elevation of 794 feet, 9 inches. This plate is protected from weather through an inverted metal "hat" of 30 inches diameter, equipped with 4 x 4 stainless wire screening. Drawing No. 2625.MD-33445 shows the details of the stack design. The stack will be maintained under an inert atmosphere through a nitrogen gas purge.

In case of a large spill of liquid into the vacuum chamber, pressure will rise to 30 psig. The rupture disc will break and the gas will flow into the warm stack.

The impedance to flow will change with time. Initially the stack is warm and some warming of the gas occurs, before it reaches the atmosphere. With a postulated flow rate of 175,000 pounds/hour of

hydrogen gas, this gas will reach a temperature of approximately 75°K at time zero (burst disc breaks) at the end of the stack. The estimated pressure drop at time zero is 25 psig, which drops to less than 20 psig in a matter of 10 seconds. From this time on, liquid air is formed on the outside of the stack which runs down and will flow into the gravel at the base of the stack.

In order to determine that the vent system is adequate in size for all potential rates of spillage, the upper limit of vapor generation and/or pressure should be determined.

It is obvious that when the pressure in the vacuum chamber approaches the vapor pressure of the liquid previously stored in the bubble chamber, vapor generation by flashing of liquid disappears and only heat transfer from the warm walls of the vacuum chamber and magnet vessel will generate gas. In order to vaporize liquid at a pressure of 4 atm, 8,600 KW are required to generate 175,000 pounds/hour of gas. With film boiling, a flux of approximately 2 W/cm^2 may be expected and the wetted warm surface area needs to be 4.3×10^6 cm^2 (460 $feet^2$). This is a very large part of the vacuum chamber and magnet reservoir wall and it is not likely that this much warm surface area is wetted under the worst of conditions.

It appears that the postulated rate of vapor generation covers all potential accidents and that higher rates are not to be expected.

In order to reduce the rate of heat transfer to liquid spilled through a break in the beam window or any other part of the chamber, beam window and chamber have been insulated and are enclosed by super-insulation. The complete chamber is enclosed in a superinsulated warm vessel and it is difficult to spray liquid hydrogen directly on the warm walls of the vacuum chamber and generate high rates of gas generation.

When a break with liquid hydrogen spilling into the vacuum chamber occurs, it is possible that the vacuum pumps maintaining the chamber

insulation vacuum are in open connection with the vacuum chamber. The pumping system discharges into a 4 inch stack. As soon as the vacuum is broken, hydrogen gas will flow through this system to the atmosphere. A valve between diffusion pump and chamber vacuum vessel will close at a pressure of 500 microns through an interlock triggered by the vacuum gauge.

Ignition of the hydrogen venting from the stack is initially prevented through the presence of an inert nitrogen atmosphere. Once the gas is venting, ignition may take place outside the stack, if charged particles are carried by the hydrogen gas into the atmosphere. The nitrogen atmosphere in the stack is interlocked to prevent operation of the chamber without it.

The helium cryostat located in the vacuum space of the chamber is protected by a rupture disc set to go at a differential of 20 psig. This means that at 5 psig, the vacuum space of the magnet will be connected to the vacuum space of the chamber. Liquid helium in the magnet system will vaporize rapidly and vent through the rupture disc, RD-403.

(2) BREAK OF HYDROGEN PIPING IN THE VACUUM SPACE

All liquid and gaseous piping in the chamber vacuum space, with the exception of part of the 4 inch vent line from valve PV-190 to knockout drum A-A, is located between superinsulation and chamber. A break in this piping will not result in spraying liquid or gaseous hydrogen directly on the warm wall of the vacuum vessel.

a. Cooling Loop Pipe Break

The maximum rate of flow is that flow which can be supplied by A tank through line LH-2214. If the break occurs between the point where line LH-2214 enters the vacuum space of valve box R and the chamber-valve box vacuum barrier, pressure in valve box R will rise

to A tank pressure. The vacuum shell of valve box R is rated at 94 psig. As long as A tank pressure is below this pressure, the situation is safe. Valve box R is protected by a rupture disc, RD-267, the discharge of which is connected to the vent system.

b. Cooling Loop Pipe Break Downstream of Valves PV-162, PV-163, PV-164, PV-166, PV-167, and PV-168

The line may break in the valve box R vacuum space or in the chamber vacuum vessel. The break in the valve box R vacuum space is a less severe case of the Cooling Loop Pipe Break described above. A break in the vacuum space of the chamber will flow liquid hydrogen at a rate determined by pressure in A tank and flow coefficients of valve PV-109 with a cooling loop control valve in series. The flow rate which can be supplied is considerably less than the flow rate postulated under Section (1).

c. Cooling Loop Pipe Break Downstream of Cooling Loop Heat Exchangers

This case is a less severe case of b) above.

d. Break in 3 Inch Liquid Line LH-2247

Flow is determined by C_v of valve PV-189 and that of valve PV-180. The highest flow rate will be obtained when liquid is being transferred between A tank and the chamber. At all other times the line is closed off at the chamber. The flow rate which may be obtained is considerably less than the 1,000 liters per second postulated under Section (1).

e. Break in 4 Inch Chamber Vent Line Between Valve PV-190 and Vacuum Vessel Wall

The flow rate is governed by the C_v of valve PV-190. The maximum possible flow rate is less than 1,000 liters per second, and after a few seconds, the line will flow gas rather than liquid. It should be noted that the line is partially located outside the superinsulation and that spraying of liquid or gas on a warm wall is possible.

f. Break in 1 Inch and 3/4 Inch Lines from Chamber to Hydrogen Pump and Valves PV-194 and PV-195

The maximum attainable flow rate is considerably less than 1,000 liters per second and conditions are less severe than those under Section (1).

g. Break in Target Lines

Same as f) above.

(3) BREAK IN HEAT EXCHANGERS OF THE VARIOUS COOLING LOOPS

Breaks fall in the same category as those discussed under Section (2). The total inventory of liquid in any of these heat exchangers is small compared to the liquid available from a 1,000 liter/second spill.

(4) MALFUNCTION OF THERMAL RELIEF VALVES OF THE COLD LIQUID AND GAS LINES

Failure of a relief valve to open at high pressure implies closed valves at both ends of the cold line. The line may break and a limited amount of gas or liquid will spill into the vacuum space.

(5) AIR LEAK INTO VACUUM SPACE

It is conceivable that an air leak exists during steady state operation of the bubble chamber. Some of this air may be pumped by the pumping system of the bubble chamber. Some of it may freeze out on the cold surface of the bubble chamber proper.

A large leak rate would be the addition of .1 cc/second (NTP) of air to the vacuum system. In 100 days, a total of 864 liters of air would be present in the form of snow on the cold surface. The total oxygen content is 170 liters or 240 grams.

When hydrogen breaks into the vacuum space, the cold surfaces holding the solid air will not warm immediately and the vapor pressure of the solid will not change. Without ignition source, nothing will happen. Once the solid air starts to warm, vapor will be generated.

The vacuum space of the chamber contains at least 400,000 liters (NTP) of hydrogen gas. The mixture of 1,000 liters of air and 400,000 liters of hydrogen gas is not flammable. The slow release of air will also prevent the formation of flammable mixtures in the immediate vicinity of the solid.

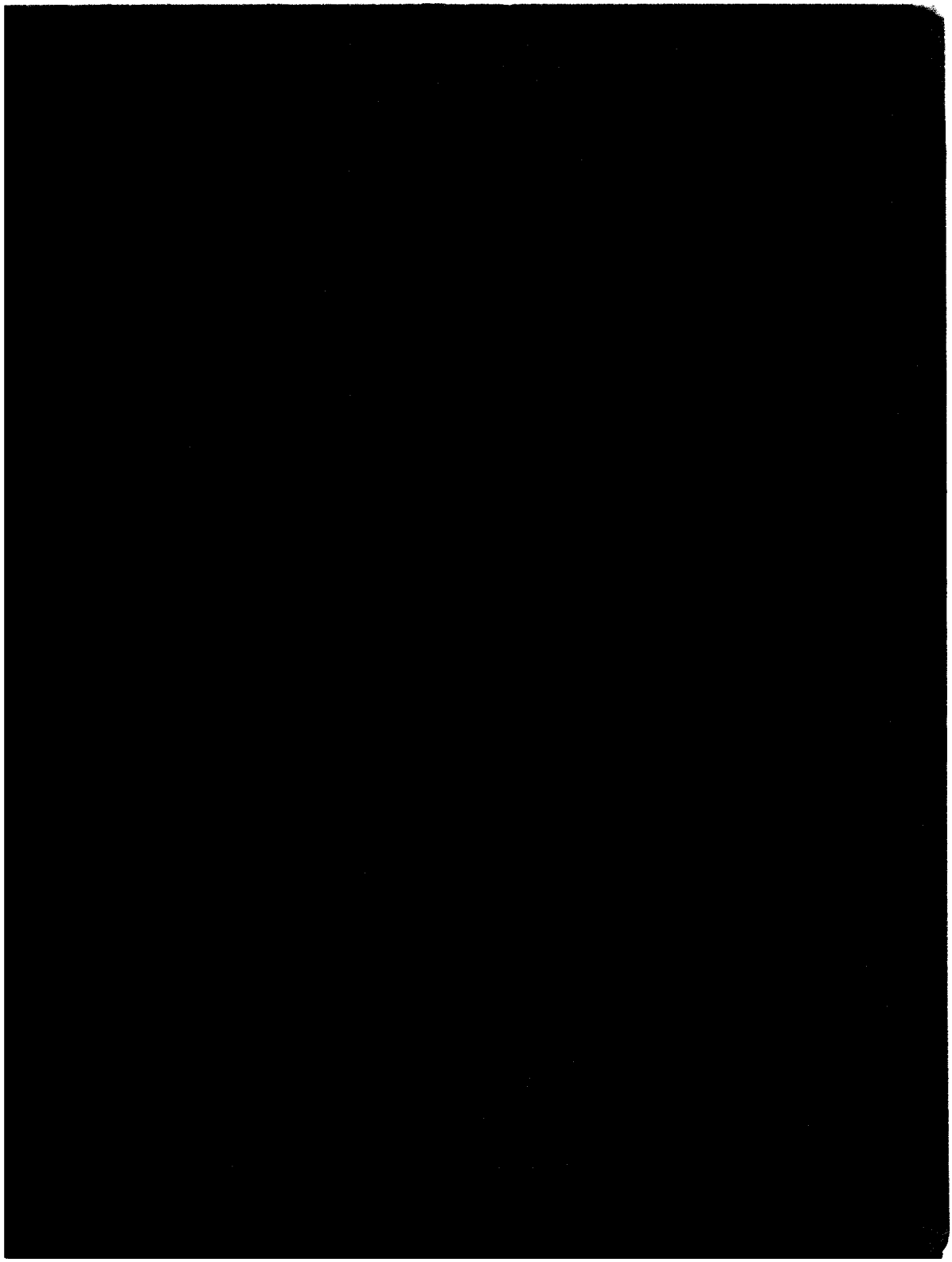

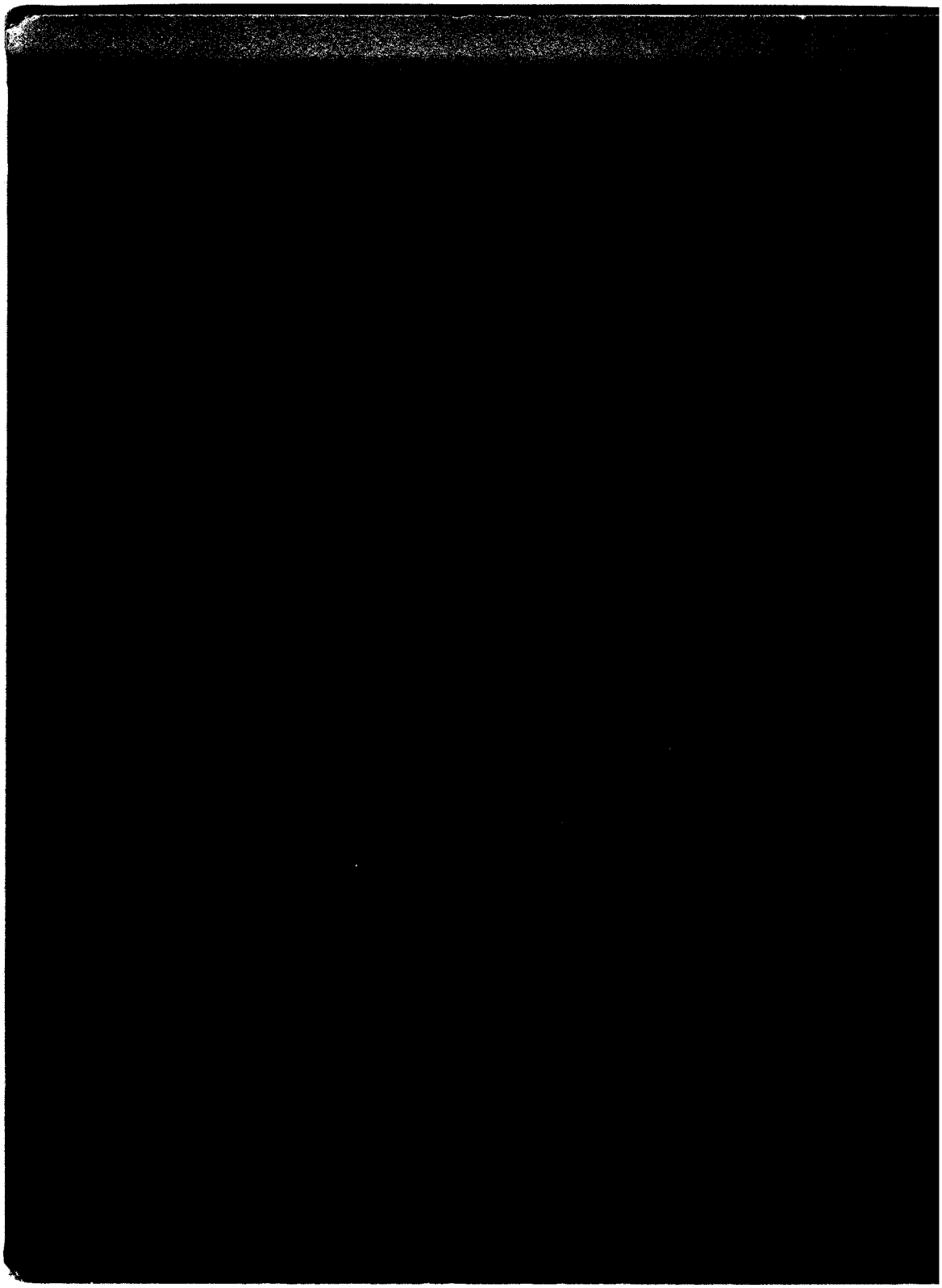

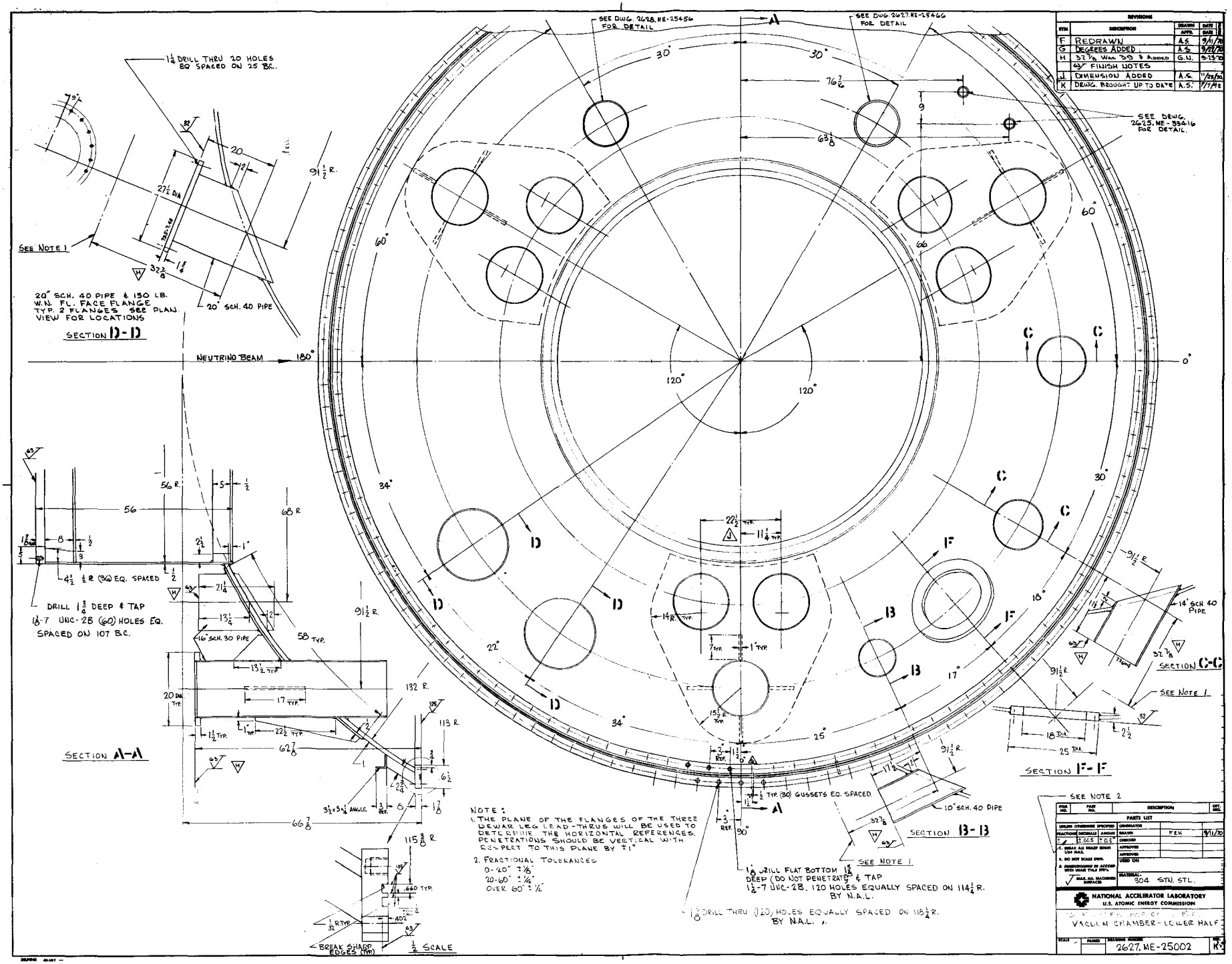

ITEM	DESCRIPTION	DRAWN APPR.	DATE
F	REDRAWN	A.S.	9/11/70
G	DEGREES ADDED	A.S.	9/21/70
H	32⅜ WAS 32⅝ & ADDED	G.W.	9-25-70
	63 FINISH NOTES		
J	DIMENSION ADDED	A.S.	11/23/70
K	DRWG. BROUGHT UP TO DATE	A.S.	7/7/72

ITEM NO.	PART NO.	DESCRIPTION	QTY. REQ.
		PARTS LIST	

UNLESS OTHERWISE SPECIFIED: FRACTIONS ±1/64, DECIMALS ±.005, ANGLES ±0.5°. BREAK ALL SHARP EDGES 1/64 MAX. DO NOT SCALE DWG. DIMENSIONING IN ACCORD WITH USAS Y14.5 1973. MAX. ALL MACHINING SURFACES

DESIGNED: F.R.H. 9/11/70 | DRAWN | CHECKED | APPROVED | APPROVED | ISSUED ON

MATERIAL: 304 STN. STL.

NATIONAL ACCELERATOR LABORATORY
U.S. ATOMIC ENERGY COMMISSION

VACUUM CHAMBER - LOWER HALF

SCALE: ¼ | DRAWING NUMBER: 2627.ME-25002 | REV. K

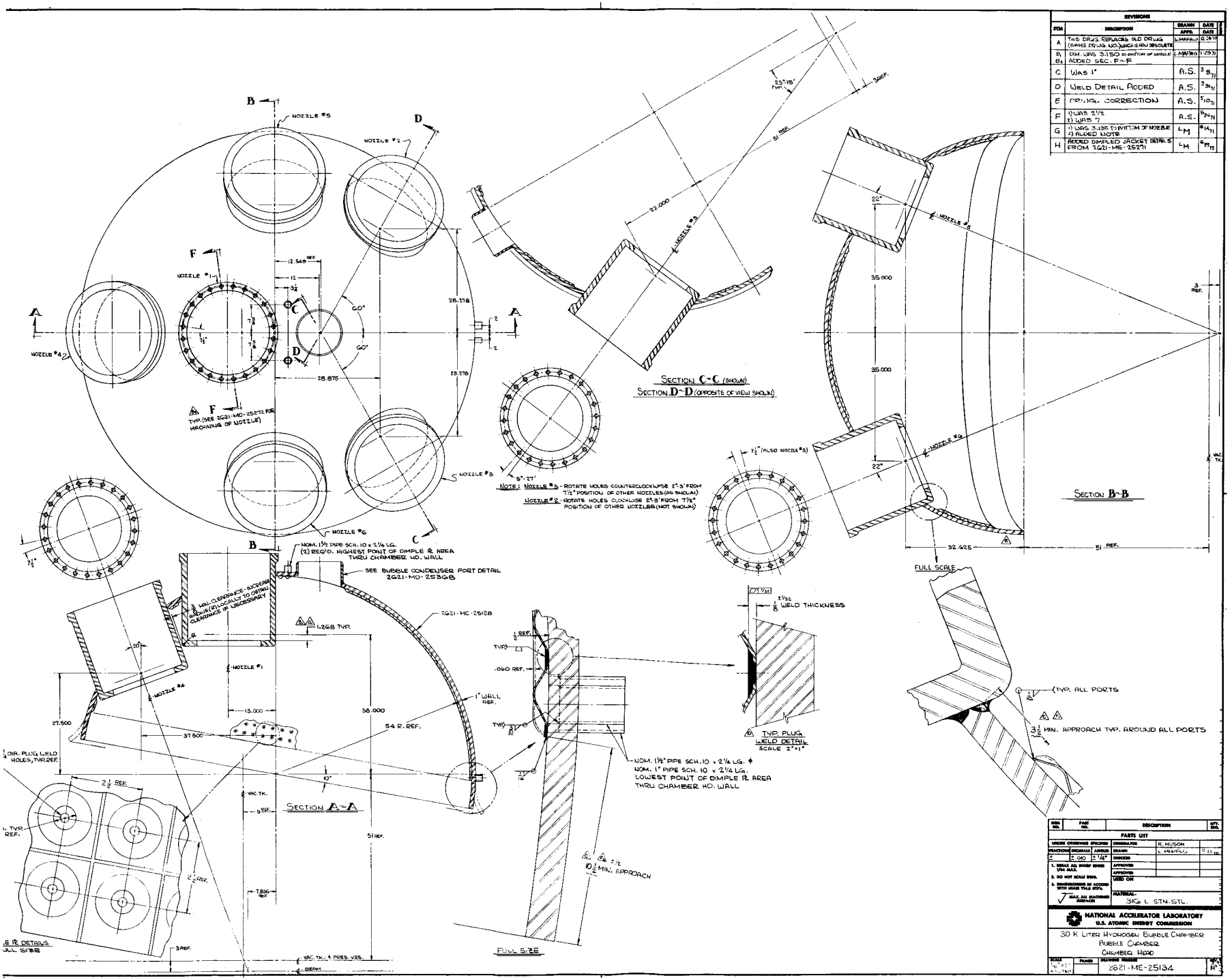

REVISIONS			
SYM	DESCRIPTION	DRAWN APPR.	DATE DATE
A	THIS DRWG. REPLACES OLD DRWG (SAME DRWG. NO.) WHICH IS NOW OBSOLETE	L.MARIANO	12-28-70
B, B_1	DIM. WAS 3.150 TO BOTTOM OF NOZZLE; ADDED SEC. F-F	L.MARIANO	1-29-71
C	WAS 1"	A.S.	$3_{3/71}$
D	WELD DETAIL ADDED	A.S.	$3_{3/71}$
E	DIM'L. CORRECTION	A.S.	$5_{10/71}$
F	1) WAS 2½ 2) WAS 7	A.S.	$5_{24/71}$
G	1) WAS 3.135 TO BOTTOM OF NOZZLE 2) ADDED NOTE	L.M.	$6_{14/71}$
H	ADDED DIMPLED JACKET DETAILS FROM 2621-ME-25271	L.M.	$6_{29/72}$

ITEM NO.	PART NO.	DESCRIPTION	QTY. REQ.
		PARTS LIST	

UNLESS OTHERWISE SPECIFIED			DESIGNATION	R. HUSON	
FRACTIONS	DECIMALS	ANGLES	DRAWN	L. MARIANO	12-22-70
±	± .010	± 1/4°	CHECKED		
1. BREAK ALL SHARP EDGES .016 MAX.			APPROVED		
2. DO NOT SCALE DWG.			APPROVED		
3. DIMENSIONS IN ACCORD WITH ASAB 1946 STD.			USED ON		
√ MAX. ALL MACHINED SURFACES			MATERIAL 316 L STN. STL.		

NATIONAL ACCELERATOR LABORATORY
U.S. ATOMIC ENERGY COMMISSION

30 K LITER HYDROGEN BUBBLE CHAMBER
BUBBLE CHAMBER
CHAMBER HEAD

SCALE	PROJECT	DRAWING NUMBER	REV. NO.
1"=1" UNLESS NOTED		2621-ME-25134	H

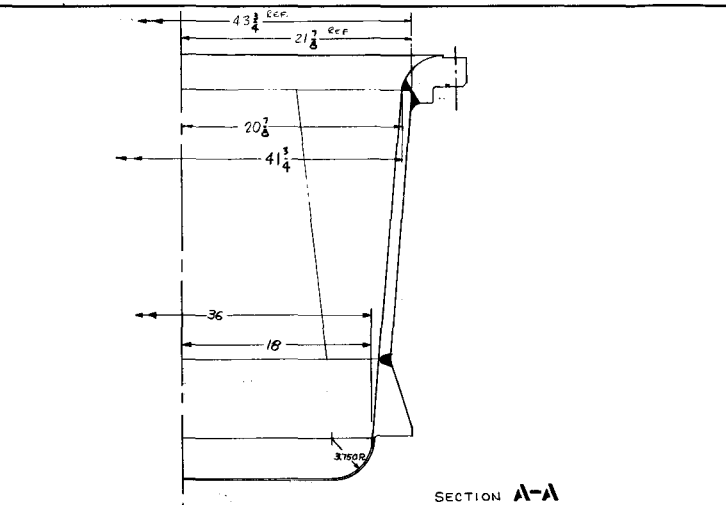

SECTION A-A

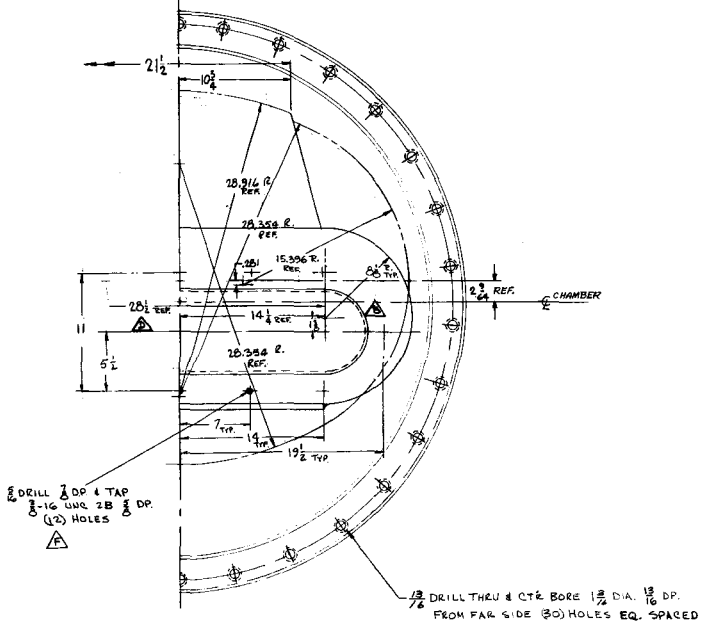

5/8 DRILL 7/8 DP & TAP 3/8-16 UNC 2B 5/8 DP. (12) HOLES

13/16 DRILL THRU & CTR BORE 1 3/8 DIA. 13/16 DP. FROM FAR SIDE (30) HOLES EQ. SPACED ON 51 3/4 B.C.

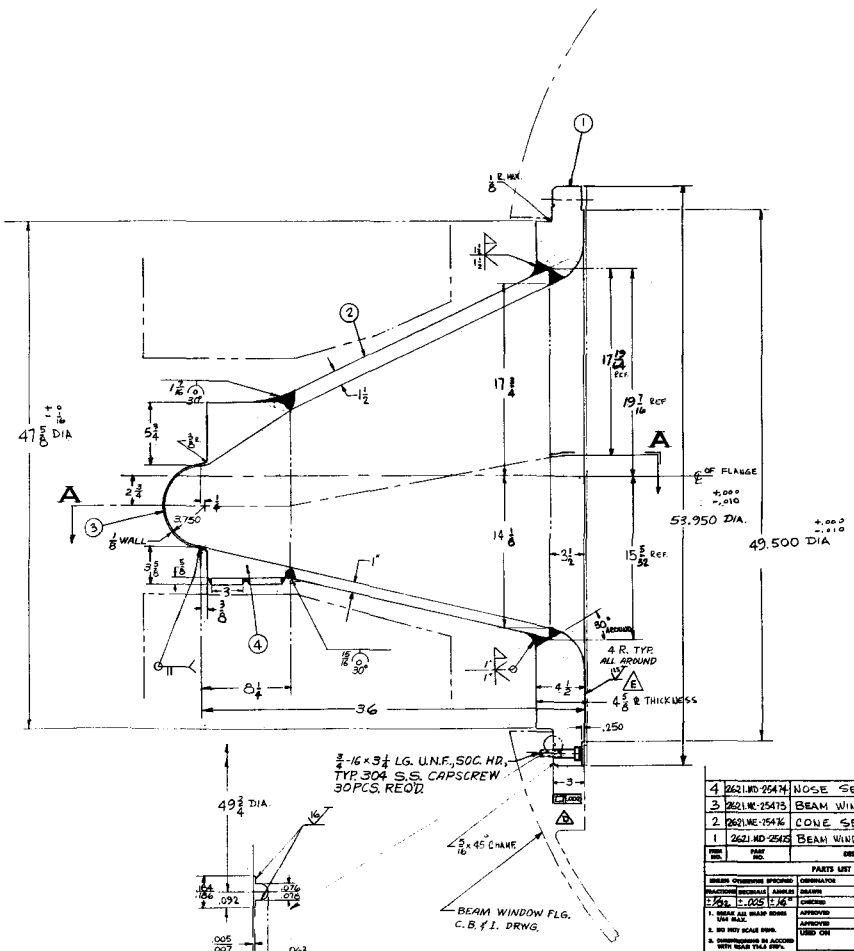

APPROX. WT 3100 LBS

REVISIONS			
STN	DESCRIPTION	DRAWN APPD.	DATE
A	REVISED	A.S.	11/1/71
B	WAS 7 3/8 R.	A.S.	11/29/71
C	ELLIPSE RADII CHANGE	A.S.	1/10/72
D	FINALIZED	A.S.	3/24/72
E	FINISH ADDED	A.S.	5/30/72
F	(12) 5/8-16 TAP HOLES ADDED	A.S.	4/19/74

PARTS LIST			
ITEM NO.	PART NO.	DESCRIPTION	REQ'D.
4	2621.MD-25474	NOSE SECTION	1
3	2621.ME-25473	BEAM WINDOW	1
2	2621.ME-25476	CONE SECTION	1
1	2621.MD-25475	BEAM WINDOW MTG. FLANGE	1

UNLESS OTHERWISE SPECIFIED: FRACTIONS ±1/64, DECIMALS .XX ±.025, .XXX ±.010
1. BREAK ALL SHARP EDGES MAX.
2. DO NOT SCALE DWG.
3. DIMENSIONING IS ACCORD WITH MAB 1963 SPEC.
125 MAX. ALL MACHINED SURFACE

DESIGNATOR: J.A. MOULDER 9-13-71
CHECKED
APPROVED
APPROVED
USED ON
MATERIAL: 316 L STN. STEEL

NATIONAL ACCELERATOR LABORATORY
U.S. ATOMIC ENERGY COMMISSION

30 K LITER HYDROGEN B.C.
BEAM WINDOW ASS'Y.

SCALE 1/2"=1" | DRAWING NUMBER 2621.ME-25305 | SHT. NO. 1 OF 1

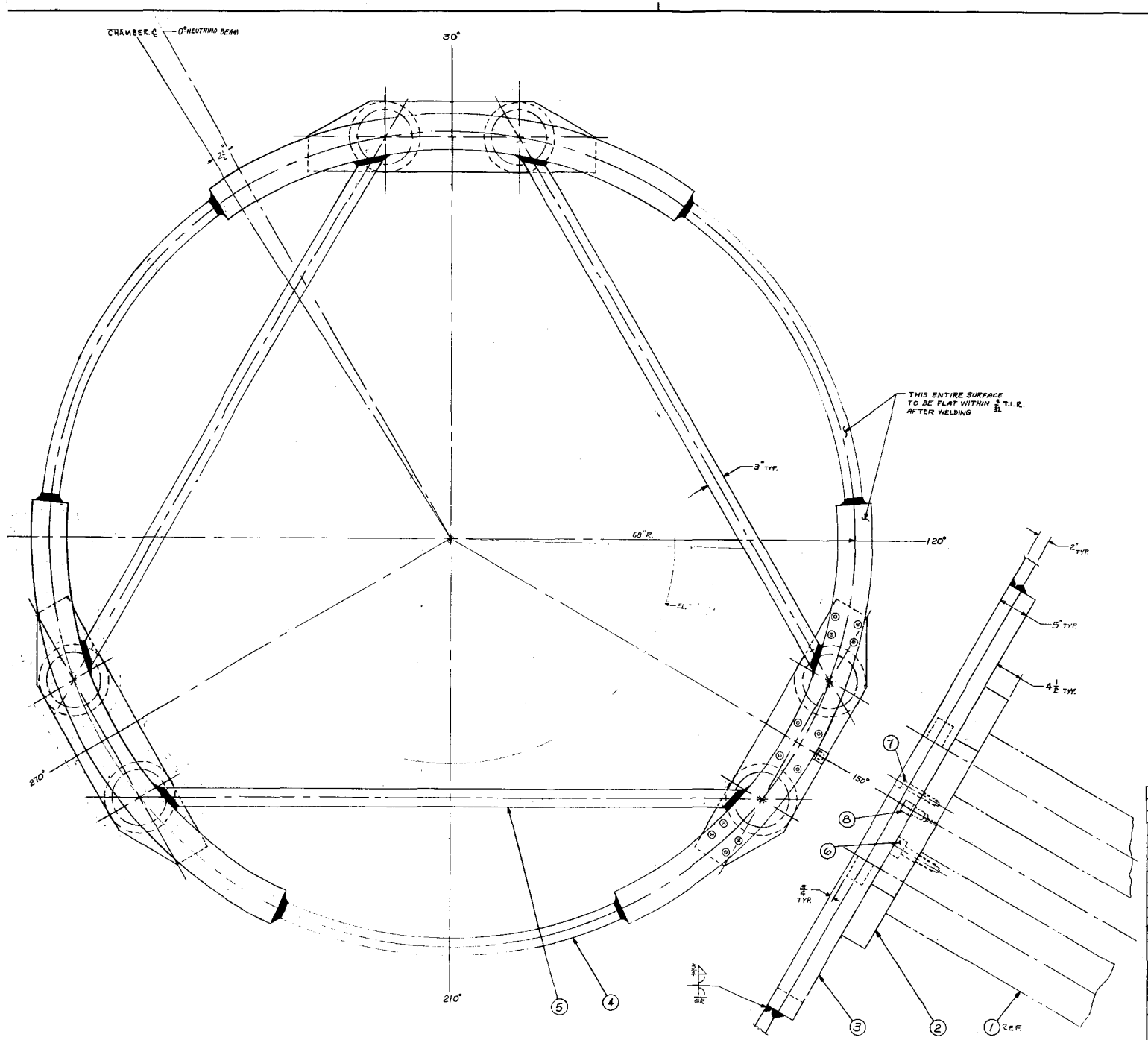

REVISIONS				
ITEM	DESCRIPTION	DRAWN APPD.	DATE	
A	REVISED		10/1/71	

ITEM NO.	PART NO.	DESCRIPTION	QTY. REQ'D
8	2621.MB-25525	CAM PIN	3
7		SCR. ½-13 UNC 2A x 3 LG. SOC. HD.	36
6		SCR. ½-13 UNC 2A x 4½ LG. SOC. HD.	24
5	2621.MB-25485	COLUMN CROSS BRACE	3
4	2621.MC-25484	SUPPORT SEGMENT	3
3	2621.MC-25483	SUPPORT PLATE	3
2	2621.MC-25482	COLUMN TOP PLATE	3
1	2621.MC-25605	COLUMN	6

PARTS LIST

UNLESS OTHERWISE SPECIFIED: DIMENSIONS ARE IN INCHES; FRACTIONS ±1/64; DECIMALS ±.01; ANGLES ±1°

1. BREAK ALL SHARP EDGES 1/64 RAD.
2. DO NOT SCALE DWG.
3. DIMENSIONS TO BE ACCORD WITH DRAW THIS DWG.
4. 125 RMS ALL MACHINED SURFACE

DESIGNED FOR
DRAWN J.A. MOULDER 7-28-71
CHECKED
APPROVED
APPROVED
USED ON

MATERIAL: 304 STN. STEEL

NATIONAL ACCELERATOR LABORATORY
U.S. ATOMIC ENERGY COMMISSION

30 K LITER HYDROGEN B.C.
CHAMBER SUPPORT ASS'Y.

SCALE 3/4"/1" | DRAWING NUMBER 2621.ME-25486 | REV. A

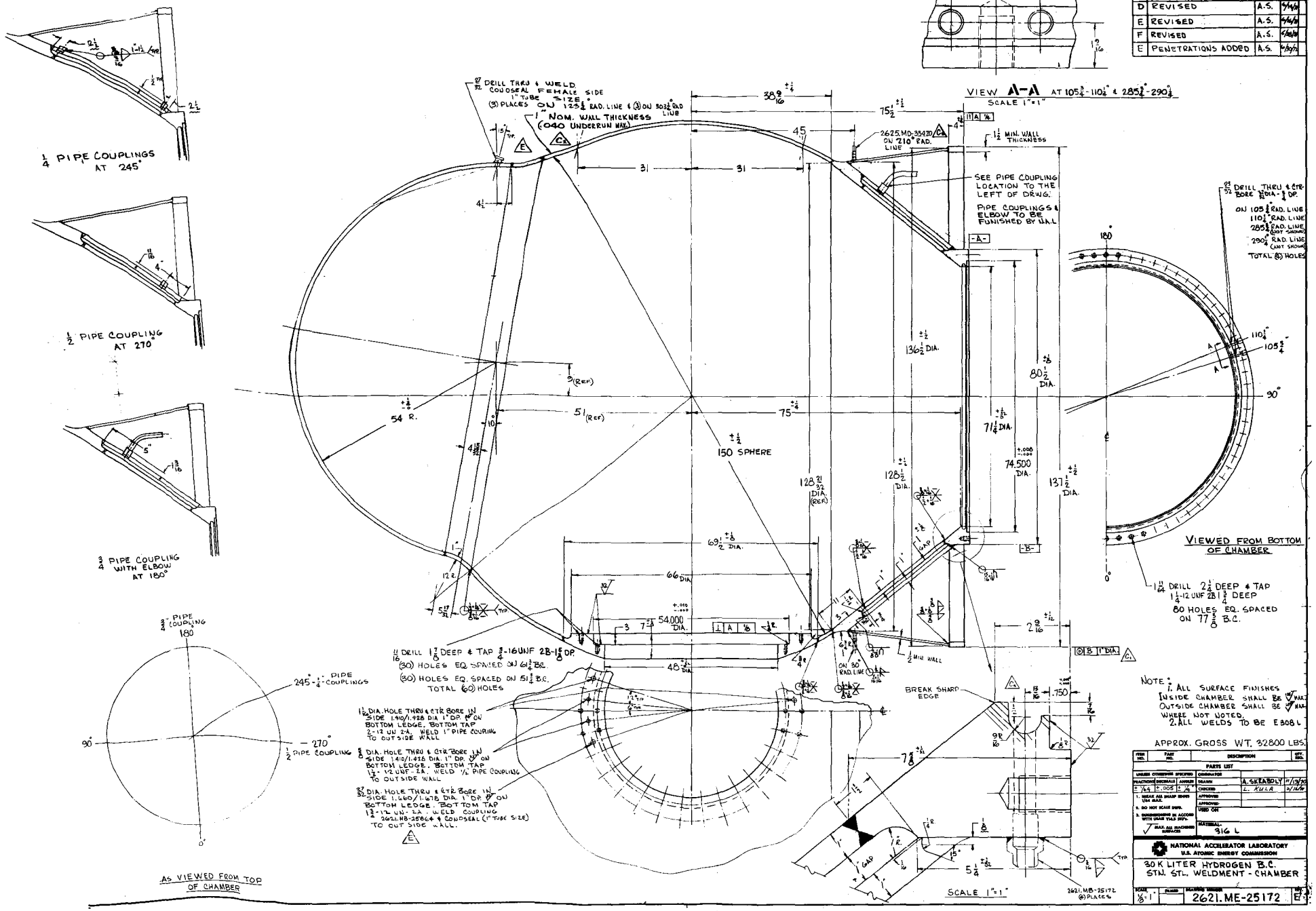

REVISIONS			
SYM	DESCRIPTION	DRAWN APPD.	DATE
B	REVISED	A.S.	3/1/76
C	(1) WAS 1" DIA. (2) WAS 1" MIN. (3) WAS 4 HOLES (4) REVISED COOLING LOOP	A.S.	4/6/76
D	REVISED	A.S.	5/4/76
E	REVISED	A.S.	6/16/76
F	REVISED	A.S.	6/16/76
E	PENETRATIONS ADDED	A.S.	6/29/76

PARTS LIST			
ITEM NO.	PART NO.	DESCRIPTION	QTY. REQ.
UNLESS OTHERWISE SPECIFIED: FRACTIONS ± 1/64, DECIMALS ± .005, ANGLES ± 1/2°			
1. BREAK ALL SHARP EDGES .015 MAX.			
2. DO NOT SCALE DWG.			
3. DIMENSIONING & ACCORD WITH USAS Y14.5M-1966			
MAX. ALL MACHINED SURFACES			

DRAWN	A. SKRABOLY 11/19/76
CHECKED	L. KULA 12/14/76
APPROVED	
APPROVED	
USED ON	
MATERIAL	316 L

NATIONAL ACCELERATOR LABORATORY
U.S. ATOMIC ENERGY COMMISSION

30 K LITER HYDROGEN B.C.
STN. STL. WELDMENT - CHAMBER

SCALE	FINISH	DRAWING NUMBER	REV.
1/8" = 1"		2621.ME-25172	E

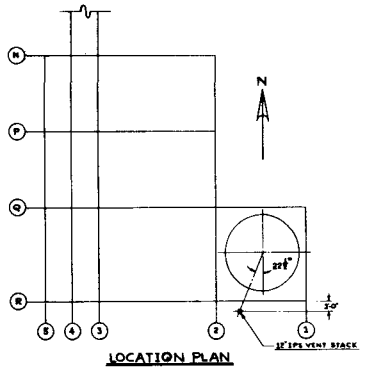

LOCATION PLAN

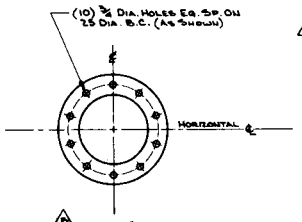

ITEM # 11
BOLT HOLE LOCATION
N.T.S.

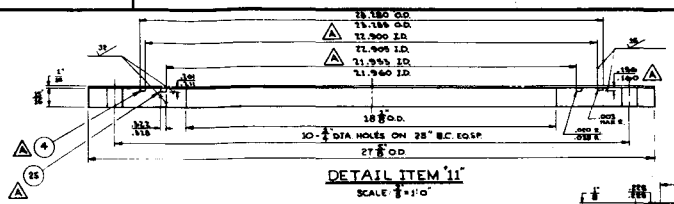

DETAIL ITEM "11"
SCALE: ½"=1'0"

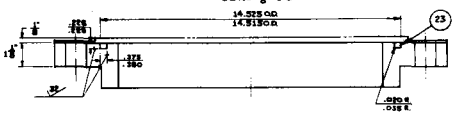

DETAIL ITEM "8"
SCALE: ½"=1'0"

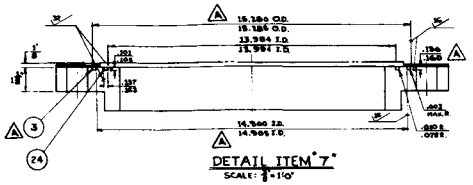

DETAIL ITEM "7"
SCALE: ½"=1'0"

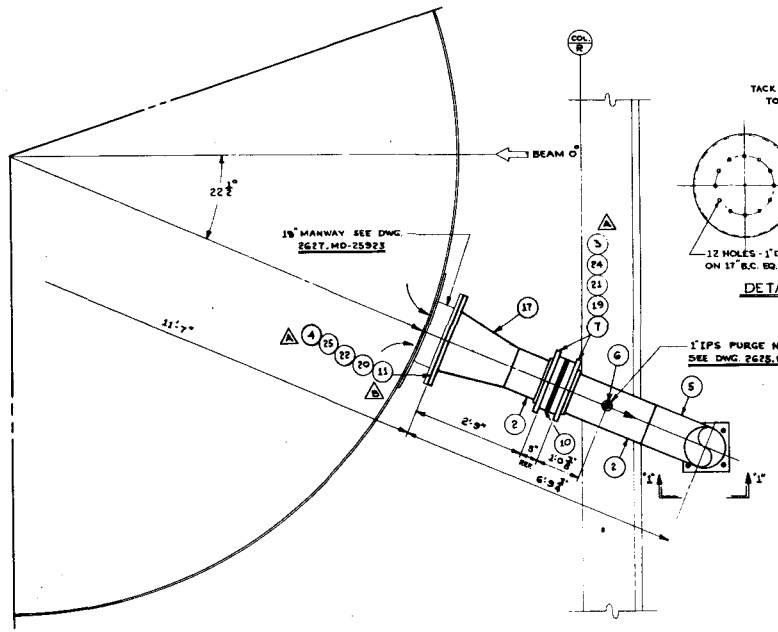

PARTIAL PLAN VIEW

NOTE:
1. WELD FLANGES TO PIPE BEFORE MACHINING O-RING GROOVES.

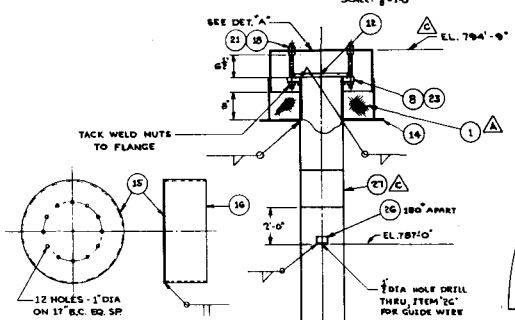

DETAIL "A"

DETAIL ITEM "13"

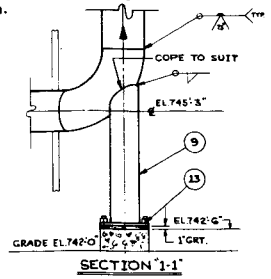

SECTION "1-1"

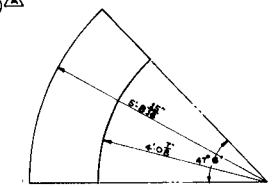

ITEM "17" DEVELOPMENT

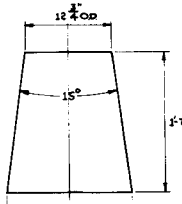

DETAIL ITEM "17"
SCALE: 1½"=1'0"

REVISIONS			
SYM	DESCRIPTION	DRAWN / APPD.	DATE
A	GENERAL REVISION	HOBAL	4-7-72
B	ADDED ITEM #11 DETAILS	HOBAL	5-1-72
C	ADDED ITEM #27	HOBAL	6-30-72

C	27	PIPE, 12" I.P.S. SCH.SS (.156 WL) A312-TP304 WLD.	3'-1½"
	26	ANGLE, 2"X2"X ¼" THK X 2" LG. A276-TP304	2
A	25	O-RING, MAT'L. BUNA-N, # 2-471 PARKER OR EQUAL	1
A	24	O-RING, MAT'L. BUNA-N, # 2-280 PARKER OR EQUAL	2
A	23	O-RING, MAT'L. BUNA-N, # 2-457 PARKER OR EQUAL	1
	22	NUT, HEX. HD ⅝" NOM. A194-8T-TP316	80
	21	NUT, HEX. HD ⅜" NOM. A194-8T-TP316	48
	20	BOLT, STUD ⅜" DIA. X 6" LG. A320-B8-TP304	10
	19	BOLT, STUD ⅜" DIA. X 5" LG. A320-B8-TP304	12
	18	BOLT, STUD ⅝" DIA. X 12" LG. A320-B8-TP304	12
	17	SHEET, 12GA (.105) X 38"W. X 53"LG. A240-TP304	1
	16	SHEET, 11 GA. (.120) X 38"W. X 7'-9 ⅜"LG., ROLL TO 30" O.D. A240-TP304	1
	15	SHEET, 11GA. (.120) X 30" O.D. A240-TP304	1
	14	SHEET, 11 GA (.120) X 36" O.D. X 12 ⅜" I.D. A240-TP304	1
	13	PLATE, 14"X 14"X 1" THK. A240-TP304 P(A. H.R.	1
	12	PLATE, 18" O.D. X 1" THK. A240-TP304 P(A H.R.	1
B	11	PLATE, 27 ⅜" O.D. X 1" THK. A240-TP304 P(A. H.R.	1
	10	DISC, RUPTURE 12" IPS, 150# ASS'Y "G" - RKB INVERT TYPE WITH O-RING SEAL SET @ 30 PSIG PTKE OR EQUAL	1
	9	PIPE, 8" IPS SCH 40S A312-TP304 WLD.	4'-0"
	8	FLANGE, 150#, W/F S/O, R/S A182-F304	1
	7	FLANGE, 150#, R/F S/O F/S A182-F304	2
	6	SOCKOLET, 12"X 1" S.W. 3000# A182-F304	1
	5	ELBOW, 90° LR, B/W, SCH.SS (.156W) A403-WP304	1
A	4	O-RING, 28" I.D. x ¾" O.D.T. = .026 W.L. S.STL. 304 BUTT WELD ENDS, COAT WITH INDIUM .002 THK.	1
A	3	O-RING, 18" I.D. x ¾" O.D.T. = .020 W.L. S.STL. 304 BUTT WELD ENDS, COAT WITH INDIUM .002 THK.	2
	2	PIPE, 12" IPS SCH.SS (.156W) A312-TP304 WLD.	50'-0"
A	1	SCREEN, WIRE MESH, 4x4 (.91 STL. 304, 1'-0" WIDE x 8'-0" LG., ROLL TO DIA. I.D. & TACK TOGETHER	1

ITEM NO.	PART NO.	DESCRIPTION	QTY. REQ.

PARTS LIST

UNLESS OTHERWISE SPECIFIED			ORIGINATOR		
FRACTIONS	DECIMALS	ANGLES	DRAWN		
±	±	±	CHECKED		
1. BREAK ALL SHARP EDGES 1/64 MAX.			APPROVED		
2. DO NOT SCALE DWG.			APPROVED		
3. DIMENSIONING IN ACCORD WITH USAS Y14.5 1994.			USED ON		
√ MAX. ALL MACHINED SURFACES			MATERIAL- STSTL TP 304 UNLESS OTHERWISE SPECIFIED		

NATIONAL ACCELERATOR LABORATORY
U.S. ATOMIC ENERGY COMMISSION

VACUUM SPHERE
12" VENT STACK & 18" MANWAY

SCALE	FILMED	DRAWING NUMBER	REV.
1"=1'-0"		2625-MD-33445	C

E RISHKO 2-15-72 P.V 2-23-72
P.V 2-23-72